MESA+
Institute for Nanotechnology

University of Twente
Enschede - The Netherlands

LAB-ON-A-CHIP SURFACE PLASMON RESONANCE BIOSENSOR FOR MULTIPLEX BIOASSAYS

BIOS
lab on chip group

stw

The described research was performed at the BIOS/Lab-on-a-Chip group of the MESA+ Institute for Nanotechnology at the University of Twente, Enschede, The Netherlands. This research was financially supported by the Dutch technology foundation STW project 06635 titled “Multi-analyte food screening with μfluidic biochips”.

Committee members:

Chairman

Prof. Dr. Ir. G. van der Steenhoven	University of Twente

Promotor

Prof. Dr. Ir. A. van den Berg	University of Twente

Assistant Promotor

Dr. E. T. Carlen	University of Twente
Dr. R. B. M. Schasfoort	University of Twente

Members

Prof. Dr. Ir. A. Manz	KIST Europe
Prof. Dr. Ir. V. Subramaniam	University of Twente
Prof. Dr. Ir. H. T. Soh	University of California
Prof. Dr. Ir. W. Norde	University of Wageningen
Prof. Dr. Ir. J. G. E. Gardeniers	University of Twente

Title: Lab-on-a-Chip Surface Plasmon Resonance Biosensor for Multiplex Bioassays
Cover: Surface plasmon resonance imaging schematic illustration (front); fabricated chips (back)
Author: Ganeshram Krishnamoorthy
Publisher: Wohrmann Print Service, Zutphen, the Netherlands.
ISBN: 978-90-365-2995-2
DOI: 10.3990./1.9789036529952

LAB-ON-A-CHIP SURFACE PLASMON RESONANCE BIOSENSOR FOR MULTIPLEX BIOASSAYS

DISSERTATION

to obtain
the degree of doctor at the University of Twente,
on the authority of the rector magnificus,
prof. dr. H. Brinksma,
on account of the decision of the graduation committee,
to be publicly defended
on Friday the 12th of March 2010 at 16.45 hrs

by

Ganeshram Krishnamoorthy

born on the 10th of January 1978
in Mayiladudurai, India

Dit proefschrift is goedgekeurd door

Promotor: Prof. Dr. Ir. Albert van den Berg

Assistant promotor: Dr. Ir. Edwin T. Carlen

Assistant promotor: Dr. Ir. Richard B. M. Schasfoort

Dedicated to my Parents, Karthika & my lovely Daughter Nirupa

Table of Content

1

Introduction

This chapter briefly introduces the newly designed and developed integrated microarray – microfluidics – surface plasmon resonance imaging (iSPR) device for biomolecular screening applications. The aim of this research work is to design and develop an electrokinetic lab-on-a-chip to simultaneously measure the multiple biomolecular interactions using an iSPR-based biosensor. A brief insight into every chapter that this thesis is composed of, is given here.

1.1 Introduction: Integrated Microarray, Microfluidics, and iSPR system

iSPR[1] is a surface-sensitive optical technique that detects the binding affinity of unlabeled biological molecules onto arrays of molecules, attached to chemically-modified gold surfaces. It is a rapidly developing technique for monitoring biomolecular interactions in various application fields such as genomics,[2,3] proteomics,[4,5] and cellomics,[6,7] where the affinity and binding kinetics can be estimated directly from the measured responses.[8] For high-throughput applications, there is a need for another technique (microarray) that has to be integrated into iSPR. iSPR measurements of microarrays fabricated on gold surfaces were reported for various application areas varying from DNA-DNA,[9] RNA-DNA,[10] protein-DNA,[11] protein-protein,[12] protein-peptide,[13,14] and drugs-protein[15] interactions, down to nanomolar concentrations. One of the problems in this kind of experiment is that the availability of the sample is very less and it is necessary to perform the whole assay with the limited sample. There is a need for another technique to use a significantly smaller sample volume. One way to achieve this is to employ microfluidic networks. Microfluidic devices provide a convenient means for manipulating very small amounts of sample

and have been utilized in a variety of bioanalytical applications such as genetic analysis,[16,17] clinical analysis,[18,19] and immunoassays.[20] Microfluidic devices can be fabricated in a wide variety of materials such as glass, silica, and polymers, by the patterning techniques of either photolithography,[21] wet chemical etching,[22] or soft lithography.[23,24] Recently, microchip devices, formed in poly(dimethylsiloxane) (PDMS) and then attached to either glass or gold surfaces, have received an increased amount of interest as a simple, rapid, and low-cost fabrication methodology.[16,23,25-33] Microfluidic channels created in PDMS have been used in conjunction with a number of different detection methods such as fluorescence microscopy,[16,20,33] laser induced fluorescence,[30] mass spectroscopy,[32] electrochemical detection,[28] and SPR-mass spectroscopy,[34] as well as with SPR imaging[35-37]. The combination of SPR with microarray and lab-on-a-chip (LOC) technology, is particularly compelling for bioanlytical systems[38,39] because the three techniques can be integrated relatively easily and it has the potential for fast and automated biomolecular analysis with ultra-small sample volumes.[37,40]

Commercial systems, such as Biacore's Flexchip[41] and the IBIS-iSPR (IBIS Technologies, b.v. Hengelo, Netherlands)[12-14] use a microarray approach together with an iSPR-LOC system. One of the major advantages of these new systems is that they are completely automated. However, the conventional systems use syringe pumps for sample transport, which requires a complex matrix of valves and connectors for multiple analyte analysis (> 10) and it is not currently possible to handle it efficiently. There is a need for an alternate flow technique for handling a large number of samples in parallel without complex plumbing. In this thesis, we explore not only the integrated device (microarray + microfluidics + iSPR) system, but also the electrokinetic flow technique for the operation of the biochip. This project is funded by the Dutch Technology Foundation STW for the project titled "Multi-analyte food screening with microfluidic biochips".

1.2 Main Objective of the Project

The main aim of the project is to design and develop a lab-on-a-chip for simultaneous measurement of multiple ligand-multiple analyte interaction using the iSPR system. In other words, the goal is to design a high-throughput multiplex device for biomolecular screening applications. In the first step, we have developed microarray based conventional assays with the conventional iSPR systems (reference measurements) and transferred the measurement procedures to the lab-on-a-chip based measurements. We have started the design of the chip with the existing electrokinetic focusing chip design[42] and modified it for our use with the iSPR system for the biomolecular interaction measurements.[36] Later, the chip design was simplified and implemented together with iSPR for multi-ligand/multi-analyte detection.[37] Finally, the chip was further modified in the direction of realization of drug screening applications.

1.3 Thesis Outline

Besides the introduction chapter, the thesis contains state of the art and motivation chapter, as well as, a chapter about technical background of the main aspects that are mainly discussed in the thesis. Apart from these chapters, there are five experimental chapters, which mainly focus on the development of a new method for multi-ligand/multi-analyte measurements using iSPR. The main focus is on the development of electrokinetic lab-on-a-chip for such multi-ligand/multi-analyte measurements based on iSPR system. A brief summary of the chapters of this thesis follows.

Chapter 2: The chapter "*A Powerful Combination – High-Throughput Surface Plasmon Resonance Based Multiplex Bioassays*" gives the detailed literature review of the technology that leads to high-throughput multiplex bioassay by integrating microarray, microfluidics and iSPR system. This chapter also explains the motivation behind the development of the new integrated chip described in this thesis, as well as the advantages and disadvantages of such an integrated system.

Chapter 3: "*Technical Background*", describes the basics of iSPR system instrumentation and the principles, surface modification techniques, biomolecular interactions and the kinetics as well as electrokinetics, which are the core components of this thesis in the development of new electrokinetic lab-on-a-chip for high-throughput multiplex detection device.

Chapter 4: "*Single Injection Microarray-based Biosensor Kinetics*", describes the new biomolecular interaction kinetics estimation method, where a single concentration of the analyte is injected over the array of ligands with varying density. This new approach was demonstrated with two well-known biomolecular interactant pairs. This measurement acts as the reference measurement for the new chip-based biomolecular binding measurements.[12]

Chapter 5: "*Multiplexed Biosensor: Parallel Kinetics Screening Assay for Multiple Biomolecular Interactions*", describes another miniaturized approach for measuring biomolecular interaction kinetics of multiple biomolecular interactant pairs in parallel. This is also known as "kinetic screening". We have demonstrated this approach with five well-known interactant pairs, where various ligands were immobilized on the sensor surface in duplicates, and mixtures of analytes were injected over the sensor surface with immobilized biomolecules. Kinetics and affinity parameters were extracted for all the biomolecular interactant pairs at the same time. This reduces the time consumption of the experiments drastically.[43]

Chapter 6: "*Integrated Electrokinetic Sample Focusing and Surface Plasmon Resonance Imaging System for Measuring Biomolecular Interactions*", describes the first integrated electrokinetic lab-on-a-chip for iSPR-based biomolecular interactions. The major advantages and disadvantages of this newly-developed chip, as well as the necessary improvements to make such an integrated system user friendly, are discussed.[36]

Chapter 7: The chapter "*Electrokinetic Lab-on-a-BioChip for Multi-Ligand/Multi-Analyte Biosensing*", deals with a more simplified biochip when compared to the chip described in chapter 6. The chip is demonstrated with multiple ligands and multiple

analytes with the known multiple biomolecular interactant pairs.[37]

Chapter 8: The chapter "*Electrokinetic Drug Screening Chip*", demonstrates the extended version of the electrokinetic chip described in chapter 7, for up to 10-12 well-known biomolecular interactant pairs. We also propose a new way to realize the drug screening assay in such an integrated system.

Chapter 9: "*Concluding Remarks and Recommendations for Future Work*", describes the major conclusion extracted from the experiments conducted to realize the project described in this thesis. It also outlines future recommendations to improve the chip quality as well as the reproducibility of extracted results, which is important to put the chip to use in real biological applications.

1.4 References

(1) Piscevic D., Knoll W., and Tarlov MJ.; Supramolecular Science, 2 (1995) 99-106.
(2) Baldrich E., Restrepo A., and O'Sullivan CK.; Anal. Chem., 76 (2004) 7053-7063.
(3) Ehlers I., Horke S., Reumann K., Rang A., Grosse F., Will H., and Heise T.; J. Biol. Chem., 279 (2004) 43437-43447.
(4) Ikeda Y., Imai Y., Kumagai H., Nosaka T., Morikawa Y., Hisaoka T., Manabe I., Maemura K., Nakaoka T., Imamura T., Miyazono K., Komuro I., Nagai R., and Kitamura T.; Proc. Natl. Acad. Sci. USA, 101 (2004) 10732-10737.
(5) Yamaguchi S., Mannen T., and Nagamune T.; Biotechnol. Lett., 26 (2004) 1081-1086.
(6) Sadamoto R., Niikura K., Ueda T., Monde K., Fukuhara N., and Nishimura S-I.; J. Am. Chem. Soc., 126 (2004) 3755-3761.
(7) Verdonck F., Cox E., Vancaeneghem S., and Goddeeris BM.; FEMS Immunol. Med. Mic., 41 (2004) 243-248.
(8) Doyle ML., Myszka DG., and Chaiken IM.; J. Mol. Recognit., 9 (1996) 65-74.
(9) Nelson BP., Grimsrud TE., Liles MR., Goodman RM., and Corn RM.; Anal. Chem., 73 (2001) 1-7.
(10) Brockman JM., Nelson BP., and Corn RM.; Annu. Rev. Phys. Chem., 51 (2000) 41-63.
(11) Brockman JM., Frutos AG., and Corn RM.; J. Am. Chem. Soc., 121 (1999) 8044-8051.
(12) Krishnamoorthy G., Carlen ET., Beusink JB., Schasfoort RBM., and van den Berg A.; Anal. Methods, 1 (2009) 162-169
(13) Lokate AMC., Beusink JB., Besselink GAJ., Pruijn GJM., and Schasfoort RBM.; J. Am. Chem. Soc., 129 (2007) 14013-14018.
(14) Beusink JB., Lokate AMC., Besselink GAJ., Pruijn GJM., and Schasfoort RBM.; Biosens Bioelectron., 23 (2008) 839-844.
(15) Myszka DG., and Rich RL.; Pharm. Sci. Technol. To., 3 (2000) 310-317
(16) Esch MB., Locascio LE., Tarlov MJ., and Durst RA.; Anal. Chem., 73 (2001) 2952-2958
(17) Woolley AT., Sensabaugh GF., and Mathies RA.; Anal. Chem., 69 (1997) 2181-2186
(18) Deng Y., Zhang H., and Henion J.; Anal. Chem., 73 (2001) 1432-1439
(19) Deng Y., Henion J., Li J., Thibault P., Wang C., and Harrison DJ.; Anal. Chem., 73 (2001) 639-646
(20) Yang T., Jung, S., Mao H., and Cremer PS.; Anal. Chem., 73 (2001) 165-169

(21) Rai-Choudhury P.; Handbook of microlithography, micromachining and microfabricarion; SPIE Opt. Engineer Press: Bellingham, WA (1997).
(22) Wang J., Chatrathi MP., Tian B., and Polsky R.; Anal. Chem., 72 (2000) 2514-2518
(23) Deng T., Wu H., Brittain ST., and Whitesides GM.; Anal. Chem., 72 (2000) 3176-3180
(24) Xia Y., and Whitesides GM.; Annu. Rev. Mater. Sci., 28 (1998) 153-184
(25) Jo BH., Van Lerberghe LM., Motsegood KM., and Beebe DJJ.; J. Microelectromech. Syst., 9 (2000) 76-81
(26) Yang T., Simanek EE., and Cremer P.; Anal. Chem., 72 (2000) 2587-2589
(27) Anderson, JR., Chiu DT., Jackman RJ., Cherniavskaya O., McDonald JC., Wu H., Whitesides SH., and Whitesides GM.; Anal. Chem., 72 (2000) 3158-3164
(28) Martin RS., Gawron AJ., and Lunte SM.; Anal. Chem., 72 (2000) 3196-3202
(29) Turner JS., and Cheng YL; Macromolecules, 33 (2000) 3714-3718
(30) Duffy DC., McDonald JC., Schueller OJA., and Whitesides GM.; Anal. Chem., 70 (1998) 4974-4984
(31) Jackman RJ., Duffy DC., Ostuni E., Willmore ND., and Whitesides GM.; Anal. Chem., 70 (1998) 2280-2287
(32) Effenhauser CS., Bruin GJM., Paulus A., and Ehrat M.; Anal. Chem., 69 (1997) 3451-3457
(33) Delamarche E., Bernard A., Schmid H., Bietsch A., Michel B., and Biebuyck H.; J. Am. Chem. Soc., 120 (1998) 500-508
(34) Lenigk R., Carles M., Ip NY., and Sucher NJ.; Langmuir, 17 (2001) 2497-2501
(35) Lee HJ., Goodrich TT., and Corn RM., Anal. Chem., 73 (2001) 5525-5531
(36) Krishnamoorthy G, Carlen ET, Kohlheyer D., Schasfoort RBM., and van den Berg A.; Anal. Chem., 81 (2009) 1957-1963
(37) Krishnamoorthy G, Carlen ET., deBoer HL. van den Berg A., and Schasfoort RBM.; (2010) Manuscript submitted.
(38) Brockman JM., Frutos AG., and Corn RM., J. Am. Chem. Soc., 121 ((1999) 8044-8051
(39) Lee HJ., Goodrich TT., and Corn RM., Anal. chem., 73 (2001) 5525-5531
(40) Lew HS., and Fung YC., J. Biomech., 2 (1969) 105-119
(41) Rich RL., Cannon MJ., Jenkins J., Pandian P., Sundaram S., Magyar R., Brockman J., Lambert J., and Myszka DG., Anal. Biochem., 373 (2008) 112-120
(42) Besselink GAJ., Vulto P., Lammertink RGH., Schlautmann S., van den Berg A., Olthuis W., Engbers GHM., and Schasfoort RBM.; Electrophoresis, 25 (2004) 3705-3711.
(43) Krishnamoorthy G., Carlen ET., van den Berg A., and Schasfoort RBM.; (2010) Manuscript submitted.

2

A Powerful Combination – High-Throughput Surface Plasmon Resonance Based Multiplex Bioassays

Multiplex bioassays implemented by integrating surface plasmon resonance imaging (iSPR), protein microarrays and microfluidics is a powerful label-free combination for the real-time and simultaneous detection of multiple ligand – ligate pairs. The surface plasmon resonance (SPR) technique is a well established label-free approach for measuring real-time biomolecular interactions, from which kinetics of the biomolecular interactant pairs can be directly extracted by fitting the SPR response data (sensorgrams) to the appropriate model functions. A microarray is an assay technique that consists of an array of biomolecular regions, or spots, where each spot acts as an individual sensing region in a highly parallel fashion and can be configured with any type of molecule, such as nucleic acids, proteins, antibody, cells, virus, phages, as well as drugs and small molecules. Microfluidics provides the ability to analyze small sample volumes and reagents, which leads to lower assay costs as well as sample preparation automation. The integration of these existing techniques provides a number of advantages and challenges when combined with an optical detection platform, such as SPR. In this chapter, a review of recent advances in combining biomolecular microarrays, microfluidics and SPR biosensing is presented and its advantages and disadvantages are discussed. The motivation for the work in this thesis is also explained. This lays a foundation for future work. A part of this chapter has been submitted as review paper (2010).

2.1 Introduction

Bioassays are typically developed to measure or detect organic molecules and their effects on the other substances and can be broadly classified as qualitative or quantitative. Qualitative bioassays are used for assessing the physical effects of a substance. For example, a fly bioassay is a quantitative assay that screens toxic

substances and is based on filter paper impregnated with an autoclaved culture supernatant. Most fly bioassays are performed by mixing autoclaved culture supernatant with diet ingredients that are added to support larval growth and development.[1] Quantitative bioassays involve the estimation of the potency, such as concentration, of a substance by measurement of a biological response that it produces. Qualitative and quantitative bioassays are important techniques for extracting as much information as possible for applications such as disease diagnostics and drug discovery. Bioassays are based on a technology platform, such as optical,[2] electrical[3] or electrochemical[4]. The duration of each and every assay depends on the nature of the assay. When multiple samples have to be tested, a lot of time is typically required for measuring all samples. Therefore, multiplexing of such assays is very important.

A multiplex assay is capable of simultaneously measuring multiple analyte samples in a single assay[5] and often requires specialized technologies or miniaturization to achieve a high degree of parallelization.[6] Multiplex assays are widely used in functional genomics experiments to detect the state of all biomolecules of a given class (e.g., mRNAs and proteins) within a biological sample, to determine the effect of an experimental treatment or the effect of a DNA mutation over all of the biomolecules or pathways in the sample.[7] For example, multiplex assays for the detection of respiratory pathogens where many different pathogens present similar symptoms; accurate pathogen identification and fingerprinting are important for patient recovery and public health monitoring.[8] Multiplex assays are also important for cancer diagnostics.[9,10] The ability to perform such multiplex assays has been established by the use of microarrays.

The microarray was first reported as the Southern Blotting assay where fragmented DNA is attached to a substrate and then probed with a known gene or fragment.[11] A very nice example of using microarrays is for experiments measuring large number of biomolecular analytes in the human genome sequence and many other model organisms.[12]

Multiplex assays are often used in high-throughput screening applications,

where many specimens can be analyzed simultaneously.[13] The main advantages of bioassay multiplexing are related to experimental time reduction and reduced cost since assays are performed simultaneously. When the execution of a single multiplex assay generates data for a large number of analytes (e.g., gene expression levels for all genes in the human genome, drug screening), it is considered high-throughput. However, it is more the ability to rapidly process multiple specimens in an automated fashion that characterizes high-throughput techniques. Massive parallelization of assays is one way to achieve "high-throughput" status. Another way is via automating a manual laboratory procedure. However, it is not necessary that all the multiplex assays are high throughput (eg. enzyme linked immunosorbant assays, or ELISA).

Multiplex assays can be classified into two categories based on the detection technique used: labeled and label-free. Labeled-based detection requires the conjugation of a molecular label for detection purposes. Common labels are fluorophores, chemophores,[14] nanoparticles,[15] microbead,[14] radioactive probes,[16] magnetic particles,[17] and quantum dots[6], for example. Label-free multiplex assays are commonly reported in literature and important examples include the metallic barcode assay,[18] quartz crystal microbalance,[19] and SPR[20].

In this discussion, we limit our discussion to label-free SPR based multiplexing in combination with microarrays and microfluidics and how it can be improved to make use of such an integrated platform effectively.

2.2 Components of Label-Free Multiplex Bioassays

Ever since Otto[21] introduced a method for generating surface plasmon polaritons (SPP), which was later modified by Kretschmann,[22] SPR has become an important biosensing technique and has been reported for many different applications. Another breakthrough in the SPR technique was reported by Knoll[23] with the development of imaging SPR (iSPR). SPR is considered to be a mature biosensing technology and is ideally suited for the integration with microarrays[11,24] and microfluidics.[25]

The microarray, introduced in the early 70's by Southern[11] for genomics and later in 2000 for proteomics by McBeath,[24] is a method for high throughput discrimination of multiple targets from a sample. A microarray is simply an array of biomolecular spots that are immobilized on a solid support. When a sample is introduced to the microarray surface, target molecules in the sample (analytes/ligates) will bind with the appropriate probe molecule on the surface (ligands) forming a ligand-ligate pair. For labeled detection, this ligate typically has a molecular signaling label attached that is used to detect the binding event. Many types of biomolecules have been used in microarrays, including nucleic acids,[26] proteins,[24] antibodies,[27] cells,[28] virus,[29] phages,[30] tissues,[31] enzymes,[32] and small molecules.[33]

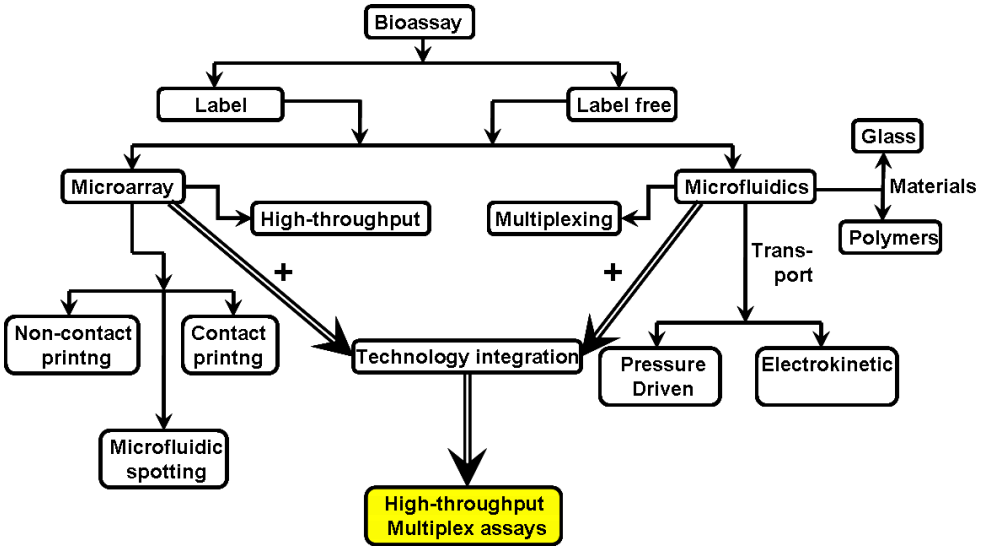

Figure 2.1 Schematic illustration of bioassay classification showing the integration of detection, microarray and microfluidics.

Another powerful tool used for miniaturized multiplex assays is microfluidics. After the introduction of microfluidics for capillary electrophoresis in microchannels,[25] various applications have been reported and have been critically reviewed.[34,35] Microfluidics provides the ability to analyze small volumes (micro-, nano- or even

pico-liters) of samples and reagents and can minimize assay costs, as well as, automate sample preparation and reduce sample processing time.

High throughput and multiplexing are the major benefits offered by microarrays and microfluidics, respectively. When these two methods are integrated with any of the label-free detection techniques, then a high throughput multiplex detection platform can be realized. Miniaturized multiplex bioassays are further improved by integrating microarrays and microfluidics such that both the ligand immobilization and analytes can be used for multi-ligand and multi-analyte detection (in other words – high-throughput multiplex detection). The combination of microarrays and microfluidics has been previously reported.[36] The integration of such methods provides a number of advantages and challenges when it is used in combination with an optical detection platform, such as iSPR. However, the integration with iSPR still requires significant improvements, which is the core importance of this thesis and is discussed further in section 2.5. Further suggestions for improving such high-throughput multiplex devices are discussed in section 2.6. Multiplex label-free bioassays have been previously reported.[17, 18, 37, 38]

2.3 Combined Microarray and iSPR

There are a few reviews which describe the combination of microarrays and iSPR, which have been reported for various application areas including micro RNA expression,[37] affinity biosensing,[38] high throughput screening,[39, 40] drug discovery[41] and small molecules.[42] This integration leads to multiple ligands on the surface and with the injection of single analyte (ligates/analytes are the biomolecule in the flow) or series of analytes, one after the other, for the purpose of detection or diagnostics, termed as high-throughput.

Most of the iSPR systems use a sensor surface immobilized with multiple ligands and serial injection of analytes using a flow-cell specific for a particular system with regeneration steps between each sample injection (Fig. 2.2a). Currently, this is the most common way of performing multiplex bioassays. This kind of approach is

especially useful for fast diagnostics (e.g. allergy or cancer diagnostics)[43] where human serum is reactive to various ligands. In addition, "hit identification" in drug discovery for screening for the successful targets is another important application.

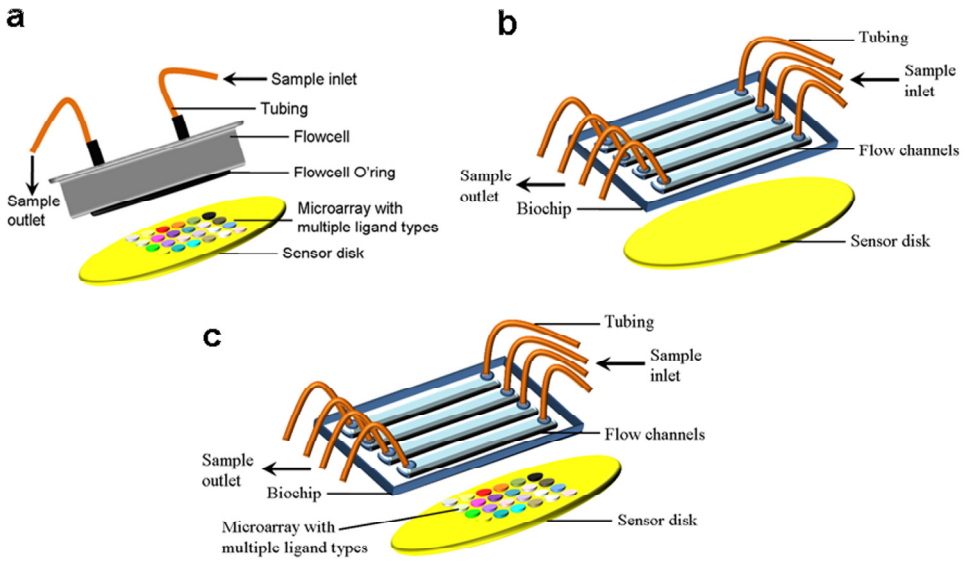

Figure 2.2 (a) High-throughput system: Conventional microarray based iSPR with fluid handling system. Microarrays fabricated from different proteins/antibodies or the same proteins with various concentrations using spotting techniques. (b) Multiplex system: iSPR system with microfluidic lab-on-a-chip. Microchannels are used for both immobilization and analyte transport using an external syringe pump or with capillary forces. (c) High-throughput multiplex system: iSPR with integrated microarray and microfluidics.

Microarrays have been constructed using various types of biomolecules for iSPR applications including proteins,[44-59] antibodies,[60-73] peptides,[74-83] DNA,[84-96] RNA,[97-100] carbohydrates,[101,102] antibiotics,[103] small molecules (drugs),[104] chemical species and glycoproteins[105]. There are hundreds of very interesting applications reported for such integrated systems as listed in table 2.1.

There are many commercial SPR systems capable of handling such integrated systems including IBIS iSPR,[68,74,78,103] GWC Imager II,[51,64,66,80,81,86,87,92,93,95,97-100] Flexchip,[54,55,70] Toyobo, [63,76,77,79,89,94,104] Autolab,[47] Genoptics[44,69] and Multiskop[60,67]. Apart from these commercially available integrated iSPR-microarray systems, there are many homemade systems with advanced functionality meant for increasing the sensitivity and throughput (e.g. 2D SPR,[45,46,50,57,61] SPR interferometry,[106] phase interrogation method,[85] etc.).

One of the most important points of consideration for microarray fabrication is the primary surface treatment for the biomolecules of interest. More detailed information about the surface chemistry adopted for SPR based measurements has also been discussed in Chapter 3. This step is very crucial and is the stepping stone for all surface based bioassays. The substrate material for SPR based assays is glass coated with a thin gold layer (a thin titanium or chromium layer improves the adhesion to the glass). Surface modification always starts with thiolation as a first step followed by modification according to the needs of the assay. Sometimes, an intermediate step such as coating the modified surface with streptavidin or a blocking layer to prevent protein adhesion or others for capturing biomolecular targets of interest. Most of the articles reported here use a gold surface modified with 11-mercaptoundecanoic acid (MUA) which forms a monolayer with a carboxylic functional group on the surface.[45-47,58,60-62,64,66,67,80,81,84,86,87,91,92,95,97-100] Some articles report a carboxymethyl dextran coated gold surface,[52,68,101,103] functionalized hydrogel coated gold surface,[74,78] glutathionylated gold surface,[50,59] amino modified gold chip,[75,76] poly (L-lysine) coated chip,[88] photo cross linker gold chip[104] or sometimes a bare gold surface[44,53,55,69,70,85,94,96] for the convenience of the assay. In some cases, instead of full gold surfaces, conventional gold arrays[47,57-59,61,67,87,92,96,99] have been fabricated to make use of manual spotting with pipettes. Another interesting approach uses a gold nanoparticle array for biomolecular interaction detection which in this case uses localized plasmons.[49]

In the case of microarray fabrication, the chemically modified surface is typically further treated with N-hydroxysuccinimide (NHS) for the conversion of carboxyl group to amine reactive NHS esters. This step also varies according to the

modified surfaces used for the array fabrication. At this point, biomolecules that are covalently immobilized are suitable for any further analysis. The important aspects and various ways of conjugating ligands to the sensing surface are reported in the literature.[107-109]

Various types of spotting devices are available for microarray fabrication. Spotting techniques can be classified into 3 types; 1. Contact printing (using pins or stamping), 2. non-contact printing and 3. microfluidic printing. Most of the articles listed here report pin-type contact spotting, which can easily destroy the surface. However, this is not discussed in most reports. Some describe dry spots (dried microarray of biomolecules) which can lead to protein denaturation. We have observed decreased signals for dried spots when compared to spots that are wet (results not shown here). The microarray spots fabricated should not merge with each other to avoid cross contamination. In order to avoid such problems, there is a need for continuous flow microfluidics for ligand immobilization.

Microarrays have been fabricated using different techniques such as inkjet printing,[110] diffraction gratings,[83, 111] as well as with poly(dimethylsiloxane) (PDMS) microchannel chips.[81] Corn et. al. reported a PDMS based microfluidic device for the immobilization of carbohydrates[112] and DNA.[113] The advantage of this spotting device includes the elimination of cross contamination between samples, no merging of ligand spots, the sensor surface not being destroyed by the channels, which is common for pin type contact printing, and well controlled spots' shapes (similar to the channel structures). One of the major advantages of using PDMS is that it is cheaper, and fabrication of microchannels is faster, when compared to glass based chips as it needs complicated microfabricated procedures. PDMS is often used for such purposes due to the fact that changing the mixing ratio of PDMS and its curing agents leads to "sticky" surfaces precluding the need for glue-based bonding. By plasma-oxygen treatment of the surface, the hydrophobic PDMS surface is converted to hydrophilic, which facilitates filling of the channels. The same kind of chip has been used for protein measurements,[114] lipid bilayer array fabrication,[115] as well as array fabrication for in-

vivo/in-vitro SPR measurements.[116] PDMS based chips have also been reported for stamping based microarray fabrication purposes.[117,118] Apart from the above mentioned array fabrication techniques, a nano-imprint lithography procedure was also reported for microarray integrated with SPR.[119]

Apart from ligand spotting problems, there are other issues to be addressed, for example, homogeneity of the fabricated spots and the inability to precisely quantify the immobilized biomolecules. Since most of the microarray fabrication is done offline, it is not easy to quantify such parameters. However, it can be approximately estimated with the SPR experiments to visualize immobilization problems. This problem has to be addressed in order to understand the assay thoroughly. Another critical point is spot reproducibility. This leads to giving importance to the error estimation. Very few published reports include statistical data, and measurement errors in their finding, which is problematic for accessing assay reliability.

In order to solve these issues, there is a need for continuous flow of biomolecules over the surface for immobilization at constant flow rate for a specified time in which diffusion of the molecules in the solution has no effect on the molecules at the surface. Natarajan et. al.[120] developed a continuous flow microfluidic printing device.[121-123] Recently, Eddings et. al. reported an improved version of such a device with internal referencing for the bulk refractive index corrections.[124] All the literature cited in this category use the conventional flowcell available with their respective SPR system, which is normally connected to syringe pumps or peristaltic pumps. Analytes are injected for the various studies conducted and the various types of analytes reported are listed in table 2.1.

The main applications of such an integrated platform include screening applications, biomarker discovery, concentration measurements, monitoring gene expression and gene related mutations, analysis of proteins, pathogen detections, crude cell analysis, drug discovery, food screening, protein kinases study, epitope mapping, virus interactions, bacterial interactions, etc. Apart from applications, research continues to demonstrate new integrated systems as well as increased sensitivity and throughput.[125-128] The study is not confined to experimental analysis and some reports

deal with theoretical aspects of such integrated systems for improved performance.[129]

The integrated systems discussed here are also integrated to other detection techniques, such as mass spectrometry, which is a popular method for the quantification of biomolecules.[66] Microarray patterns are also used as the extra cellular matrix environment for cells and this has been integrated to SPR.[130] Other special applications include fabrication of gold micro-wells in an array format integrated to SPR for monitoring the cell culture as well as nano hole array integrated to SPR for highly sensitive biosensing applications.[131] There were also reports about the fabrication of plasmonic nanohole arrays for multiplexed LSPR (excitation of plasmons on the nanostructures) detection.[132] However, there are many improvements which could be useful for this integrated system for improved performance. A high resolution camera is very important to image the biomolecular recognition. However increased resolution leads to the increased cost.

2.4 Combined Microfluidics and SPR

As mentioned earlier, irrespective of the biosensing method used, all systems require a fluid handling system. SPR in combination with microfluidics is ideal for bioassays as the integration of hardware is straightforward and microfluidics is capable of handling small sample volumes. This combination is now common on all commercially available SPR systems including Biacore,[133,134] Biorad,[20] GWC,[37] IBIS,[74] for example. Here the question is how well the fluid handling system has been developed in order to use the SPR based bioassays more efficiently. There have been reviews that describe the various flow techniques and development of lab-on-a-chip based devices for bioanalysis.[135,136] Some critical reviews with respect to this integration have been reported that use different microfluidic flowcells, such as parallel channels,[137] hydrodynamic flow focusing in a flow chamber,[138] as well as detection of small molecules in the application area of biomedical, food and environmental pathogens[139]. Some of the literature describes low cost microfluidic devices as well as the implementation of nanotechnology for improving the detection limits.[140]

In reality, all of the commercially available SPR systems reported in the previous section use flowcell for analyte injection, which is also called a fluid handling system,[133,134] and are completely different from microfluidic handling systems that we are describing. The fluid handling systems were initially started in the early 1990's for the commercial Biacore system. The microfluidic lab-on-a-chip systems use small sample quantities, as well as, scaling to large multiplex systems without contamination or cross reactivity problems.

Typical microfluidic lab-on-a-chip configurations are shown in Fig. 2.2b, which are comprised of microchannels used for sample flow. Every microchannel has individual sensing locations. The inlet and outlet reservoirs are either connected to tubing for pressure driven flow or to electrodes for electrokinetic based fluid transport. A very important point of consideration for such microfluidic devices is the mass transport limitation, due to the fact that small length scales lead to laminar flows and corresponding high surface to volume ratio implies that transport and reactions at surfaces requires special consideration. This problem was clearly addressed in the article by Gervais et. al. for surface biomolecular reactions.[141] When a conventional SPR system is considered, it was estimated that the protein captured at the surface is reduced and rest of the proteins in the bulk analyte flows over the capture region under diffusion limiting conditions in the entrance regions. However, the capture efficiency increases in the case of microchannels where the transport regime switches to fully a developed regime with bulk depletion of the samples.[142] High capture fractions are extremely important when analyzing expensive and small quantity samples. When such devices are not properly designed, the surface biomolecular interaction is affected by diffusion. However, it is not always the case that mass transport effects are due to the microfluidic design, but also due to the nature or concentration of the molecules. The latter phenomenon is described in Chapters 4 and 5.

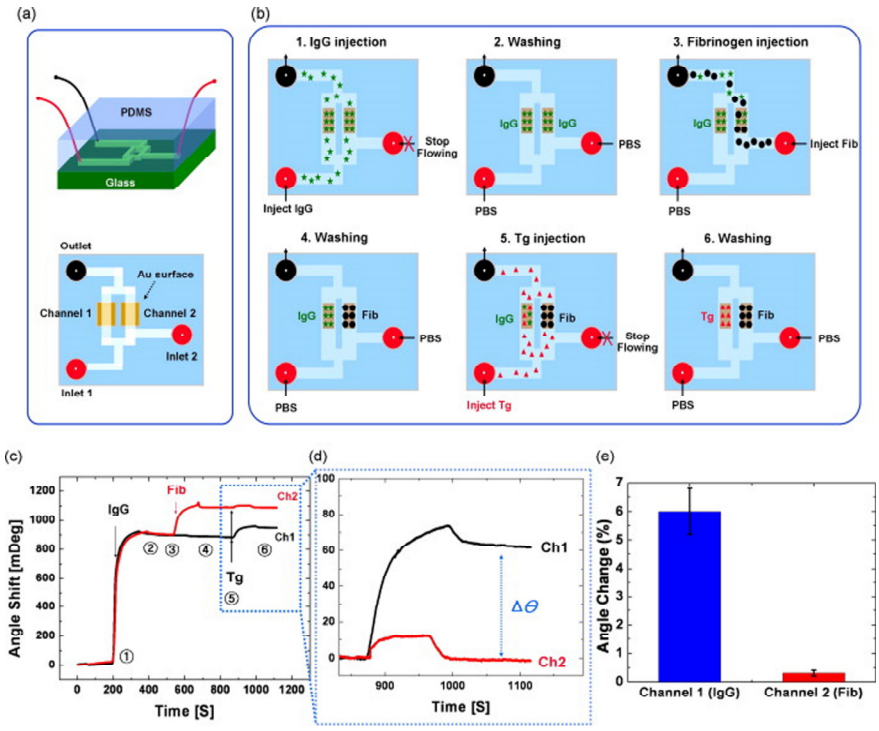

Figure 2.3 (a) A custom-made microfluidic device to demonstrate the Vroman effect-based protein biosensor. (b) A schematic of operating principle. 1. Immunoglobulin (IgG) is injected from the inlet 1 to cover both surfaces. 2. Washing process to remove unbound IgG. 3. fibrinogen flows from inlet 2 and displaces the pre-adsorbed IgG on one surface. 4. Washing process to remove any residue on the surface. 5. A target protein (Tg) flows from inlet 1. 6. Tg displaces IgG in channel 1 while it does not displace fibrinogen in channel 2. (c) SPR sensorgram of the displacement event; Tg detection of two engineered surfaces, pre-adsorbed by IgG and fibrinogen. (d) Normalized close-up SPR sensorgram after the Tg injection (e) final angle changes (%) on both surfaces (angle change/previous angle value × 100). Each has selectivity to a specific protein to be detected. (Reproduced from Biosens. Bioelec. 25 (2009) 118-123)[143]

The major advantage of integration is that multiplexing is easier when compared to conventional serial injection systems. For example, when there are four channels in a chip, each and every channel acts as a separate flow cell that leads to the measurement of four samples in parallel without cross contamination. In a

conventional system, when the microarray is kept in a single flow cell, there is an increased possibility for false determination due to the non-specific binding of unwanted molecules to the spots in the array.

Another critical issue is the selection of chip material that is suitable for easy fabrication. In many articles, PDMS is used mainly due to the simplicity of fabrication. But there are some basic problems that need to be discussed. One important problem is protein adsorption on the PDMS walls. This is especially important when electrokinetics based transport is used. Special coatings are required to prevent biomolecule adsorption on the PDMS walls. This issue is also discussed in Chapters 6 and 7. To the best of our knowledge, the first such microfluidic flowcell made of PDMS was reported by Wheeler et. al.,[144] which was integrated to a commercial SPR system. They showed that the sample volume could be reduced to 73 nL for bioassays. Flow rate is another point of consideration at this point where it is easier to use high pressure in conventional flow systems. However, in microfluidic systems, it is highly dependent on material types used for chip fabrication, as well as the way the chip layers are bonded together.

The microfluidics based approach also extends the opportunity to use one of the channels for reference measurements. For example, Choi et. al. used a 3 layer chip (glass-PDMS-glass) for biomarker discovery and to demonstrate the Vroman effect based protein biosensor.[143, 145] A diagram of the concept is shown in Figure 2.3. The chip has 2 inlets and 1 outlet with 2 sensing channels.[143] A detailed explanation of the assay procedure is contained in the figure caption. Since it has 2 channels in parallel and both are operated simultaneously, it is very easy to perform such an assay in parallel where the experimental conditions are very much similar. This approach is advantageous over the single flow cell experiments where such experiments are performed in serial manner. The list of literature reported microfluidics integration with SPR is given in table 2.2.

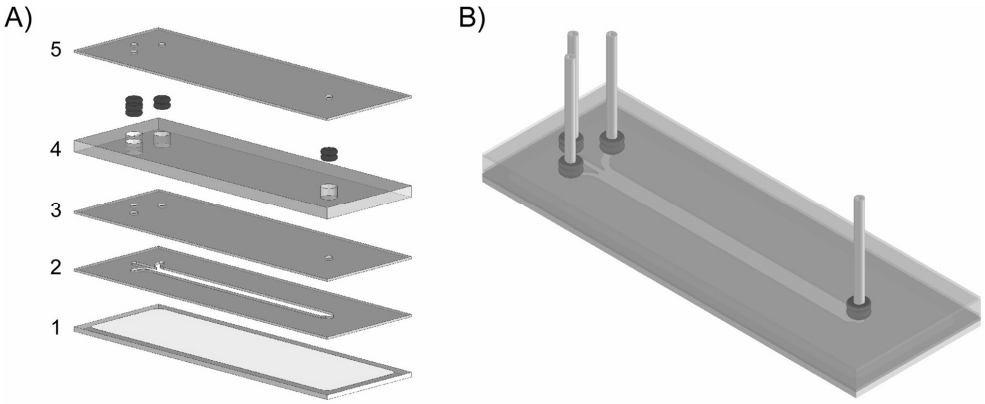

Figure 2.4 Microfluidic assay device and assembly. Exploded view (A) shows layers used (from bottom to top): (1) substrate, a soda lime glass 75 mm × 25 mm microscope slide coated with 4.5-nm gold on its upper surface; this gold surface is functionalized prior to device assembly (see text); (2) channel, a 12-µm Mylar sheet coated on both sides with 25-µm pressure-sensitive adhesive to produce a channel 62 µm in depth; it features a 3.6-mm channel laser-cut from center with three inlets and a single outlet; (3) device cap, a 25-µm Mylar layer (with adhesive on top only) with vias to permit fluid flow; (4) O-ring seat, a 2.5-mm PMMA layer with laser-cut holes for EPDM O-rings; (5) O-ring retainer, a 25-µm Mylar layer (adhesive on bottom) with laser-cut holes to pass tubing. (B) Rendering of assembled device and tubing (pumps, valves, and waste reservoir not shown). (Reproduced from Anal. Chem. 79 (2007) 3542-3548)[157]

PDMS based microfluidic lab-on-a-chip systems have also been reported for other applications such as DNA aptamer-protein interaction studies,[146] biomolecular interaction kinetics studies,[147] sensitivity enhancement studies using gold nanoparticles[148] as well as in the direction towards multi-analyte detection[137]. In the later stage, PDMS was replaced by polyurethane by Homola et.al. for their wavelength division multiplexed bioassays using SPR.[149] In this report, they claim to use four microchannels in parallel and these microchannels are operated with two peristaltic pumps. This approach was also reported for various application areas such as for the detection of oligo-neucleotides,[150] toxin detection in food[151] as well as in the development of Alzheimer disease biomarker.[152] The other reported lab-on-a-chip systems combined SPR applications such as low cost microfluidic chips for LSPR

based biosensing applications.[153] In this case, the chip was fabricated using cyclic olefin copolymer. Other applications describe the detection of carbaryl in natural water,[154] small molecules detection[155] as well as integration of digital microfluidics[156].

Another interesting lab-on-a-chip was developed by Yager et. al. for a concentration gradient immunoassay.[157] The reported device is shown in Fig. 2.4, which uses PMMA as a material for chip fabrication. The detailed description of the chip operation is shown in Fig. 2.4.

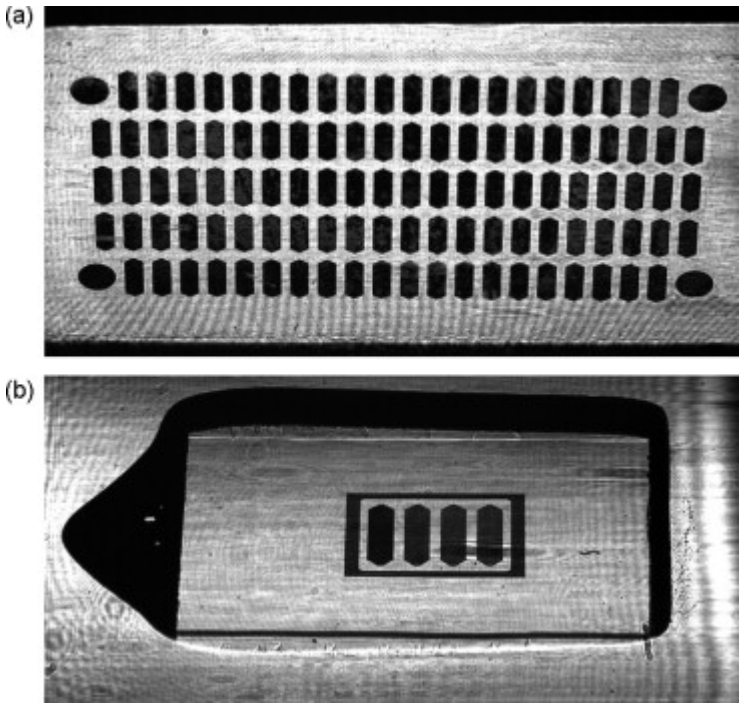

Figure 2.5 (a) SPR image of simulated 110 flow cell array. The camera-based multiplexing of the system affords flexibility in flow-cell shape and array format, as indicated by the circular elements in the corners. (b) SPR image of four flow cells obtained by the camera in our prototype system when a microfluidic module from a Biacore 3000 is coupled to the sensor. (Reproduced from Sens. Act. B 127 (2007) 341-349)[158]

Another very interesting high throughput microfluidic approach for biomolecular interaction analysis has been reported.[158] The authors claim to

accommodate as many as 110 flow cells in an array format that can operate in parallel. They show an example with an image of a Biacore system with four parallel flow cells (Fig. 2.5). It could have an impact of improved sensitivity which has nothing to do with the microfluidics configuration. But, implementing hundreds of flowcells in parallel is very critical with respect to number of valves and pumps necessary to make such a system practical. In a way, this also acts as an array formation where individual flowcells act as a single spot in the array. Recently, a commercial continuous flow spotting device has been introduced, which is capable of producing 64 spots in parallel primarily for SPR applications. More details about this spotter as well as its integration with iSPR are discussed in section 2.5.

2.5 Combined Microarray, Microfluidics and SPR

Knowing the advantages of two powerful methods, microfluidics and microarrays, and their usefulness when integrated with iSPR biosensing applications for multiplex bioassays, we now review the integration of all three components: microfluidics, microarrays and iSPR. To our surprise there are very few reports of the combined integration. The combined integration leads to many advantages, such as, 1. in-situ immobilization of biomolecules without using external spotters, 2. controlling and quantifying the immobilization according to the measured signal, 3. prevention of immobilized biomolecules from drying, 4. continuing with analyte injections for respective SPR study without any further delay or any other process in between. In order to make use of all these advantages, there are some critical points that have to be considered while designing such a system. These points include, material selection for chip, bonding procedures, size of the chip in order to accommodate all the necessary reservoirs and channels, proper and suitable fabrication procedures, proper pretreatment of chips prior to experiments, and over all ease in handling (user friendliness).

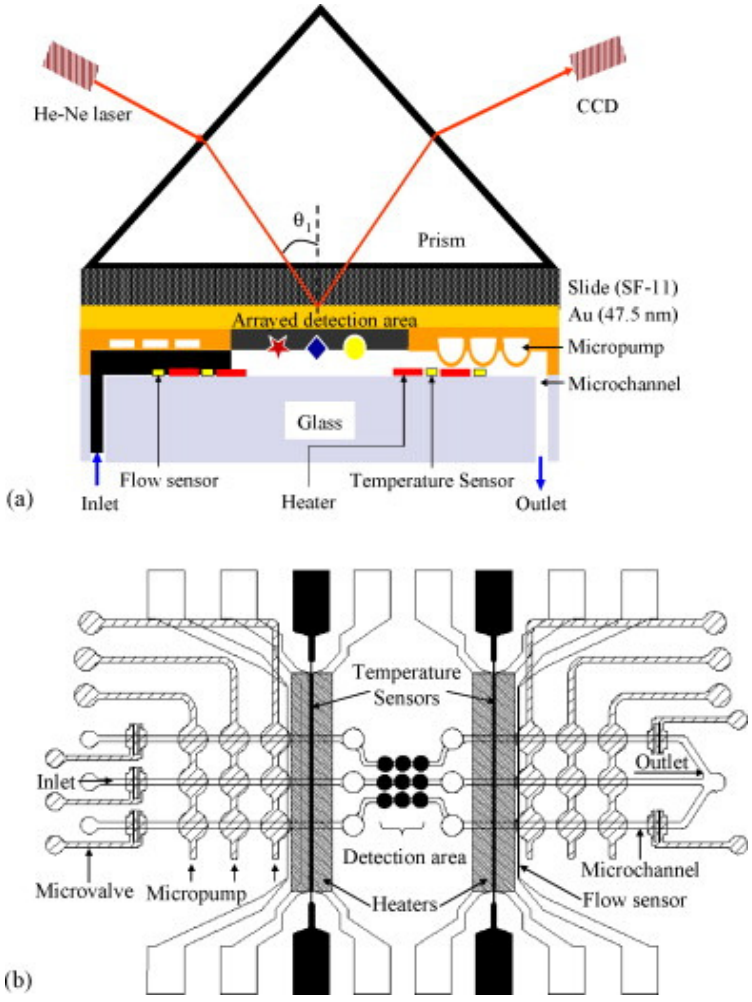

Figure 2.6 (a) Schematic illustration of a microfluidic system integrated with a 2D SPR phase imaging system for the detection of a microarray immunoassay. (b) Schematic illustration of a microfluidic chip comprising of a 3-to-1 converging microchannels, microvalves, micropumps, flow sensors, heaters and temperature sensors. (Reproduced from Biosens. Bioelec. 23 (2007) 466-472).[166]

Corn et al. used PDMS chips for DNA[159] and protein interaction studies[160]. McDermott et al. also used the same parallel channel PDMS chips to demonstrate antigen-antibody interactions[161] as well as toxin inhibition assays[162]. Homola et. al.

used a diffraction grating in combination with polyurethane based gaskets for multi-analyte biomolecular interaction measurements[163] including food screening for the food safety[164]. Apart from PDMS, Yager et. al. showed mylar flow cells to study electrochemical reactions using SPR.[165]

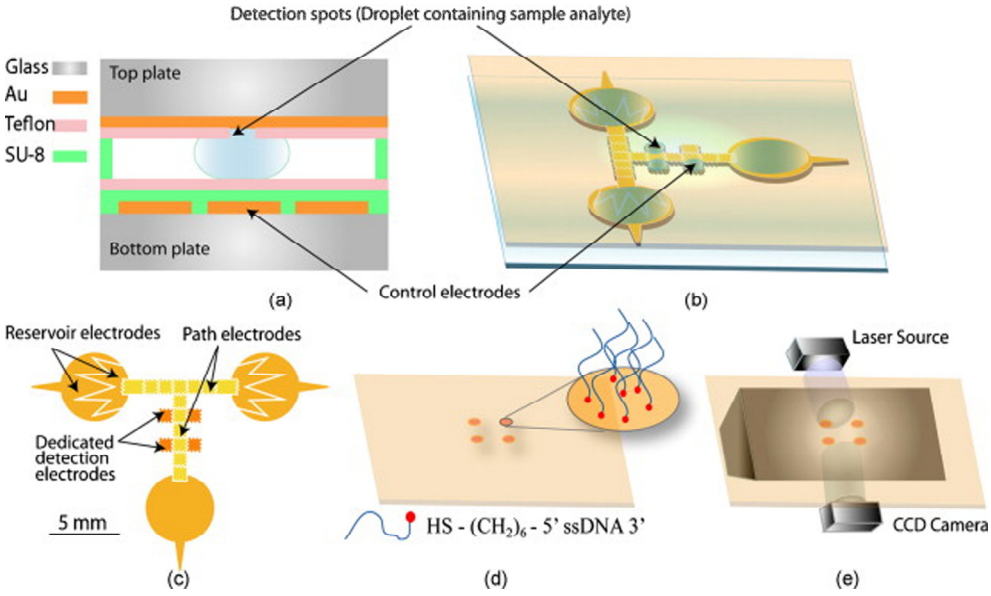

Figure 2.7 Schematic presentation of EWOD-based iSPR bio-chip design (a) vertical cross-section, (b) 3D view, (c) bottom plate layout showing reservoir, path and dedicated detection electrodes, (d) inverted top plate view showing the patterned detection spots with immobilized thiolated DNA probe, and (e) inverted top plate view showing SPRi assembly. (Reproduced from Biosens. Bioelec. 24 (2009) 2218-2224).[167]

Another interesting application of a combined system is in the development of a fully functional lab-on-a-chip for immunoassays.[166] The image of the chip is shown in Fig. 2.6. The reported chip was made from glass and PDMS, which includes microvalves, micropump, flow sensors, temperature sensors, heaters as well as a specific design of microchannels in order to visualize the sensing regions in an array format. This article has demonstrated a 3x3 array format for immunoassay applications.

The approach looks promising but the results are not well described. This kind of full integration is a welcome trend, and opens up a new direction in the SPR based biosensing.

While increasing the number of sensing sites (number of channels) for multiplex bioassays, it will be cumbersome to make use of so many (more than about 10) pumps and valves. If microvalves and micropumps are used as reported by Lee et. al.,[166] the process of making the chip is very complicated and will most likely make the chips more expensive. So there is a need for cheaper options for fabricating such chips with easy and practical handling procedures. To realize smoother integration of microarrays, microfluidics and SPR, there is a need for alternatives to pressure driven flow. It could be controlled electronically like described by Malic et. al. using digital microfluidics.[167] Digital microfluidics is used for both array fabrications and to perform SPR assays without the need of more samples. The system that they use is shown in Fig. 2.7.[167]

Since the combination uses microfluidics, it is also interesting to consider electrokinetics for fluid transport. Electrokinetics can avoid the complexity of having many valves and pumps. However, electrokinetic transport requires a thorough understanding of surface properties, which is of primary importance to control the flow using electrokinetics. We have recently demonstrated such an integrated system and it is described in chapters 6, 7, and 8.

2.6 Conclusion

We have reviewed the growing trend in the integration of microarrays and microfluidics with label-free iSPR for biosensing of high-throughput multiplex bioassays. We have seen a growing trend towards the integration of microarrays with SPR or microfluidics with SPR for simplified sample handling. The increased number of reports in literature towards high-throughput assays indicates the importance of developing such assays for extracting information faster than conventional assays. Mainly microfluidics is used for immobilization of ligands on the surface to avoid

possible practical problems with the conventional commercial spotters. Bioassays are performed mainly with their respective flowcells of the SPR system. Other reports describe a microfluidic chip based approach integrated with SPR and most of the reported articles use PDMS/glass materials. This is due to low cost as well as simple fabrication. However, the stable bonding of PDMS to most materials is problematic. For example, glass chips are ideal for any microfluidic based techniques. But glass-glass bonding needs a higher temperature which is not suitable for the gold sensing layer that leads to anonymous effects in SPR responses. The combination of microarrays, microfluidics and SPR is still in its infancy and not many reports are currently available. This is of great interest to develop such an integrated system for easy and faster handling of such a multiplex assay, which leads to faster diagnostics or discovery that can lead to saving lives of many more human beings. Multi-analyte detection is in its infancy for SPR based bioassays. The developed system for such high-throughput multiplex bioassays without complex plumbing networks e.g. electrokinetic transport could be ideal. However, it still needs more work to implement these alternative systems.

Table 2.1 Reported integrated microarray–SPR articles describing surface modification techniques, SPR system, ligands and analytes, and application.

S.No.	Ref. No.	Surface	Immobiliz -ation in Array	Analyte in Flow	Fabrication Technique	Application	SPR System
1	49	Gold nanoparticle spots and spots are grown in-situ	Protein (multiple)	Antibody	Inkjet printer (arrayjet)	Concentration measurement	LSPR
2	54	1D4 mAb surface	Protein (CCR5 - detergents coupled chemokine receptors)	2D7 Fab antibody	CFM	Detergent screening	Flexchip
3	50	Glutathionyl ated gold surface coated with GST:DEVD: EGFP protein	Protein (caspase-3)		Protein arrayer	caspase-3 activation monitoring	2D-SPR
4	53	Bare gold	Protein (Protein A/G)	Human IgG	Pin spotter	Array based kinetic analysis	Flexchip
5	59	Glutathionyl ated gold array	Protein (GST fusion proteins)	BSA		Demonstration of dual function SPR biosensors	Homemade
6	48	G4PAMAM dendrimer coated gold surface	Protein (substrate proteins)	anti-SUMO	Robotic arrayer with pin	On-chip analysis of SUMO	Biacore X
7	51	Gold surface with aldehyde terminated SAM	Protein (fibroblast growth factor)	baby hamster kidney cells	homebuilt robotic spotter	cell capture assay	GWC
8	45	Gold with MUA monolayers	Protein (multiple)	GdnHCl	homemade x-y microspottin g device	Monitoring denaturation of proteins	2D-SPR
9	57	Gold surface spots with dithiobis (succinimidy l propionate)	Protein (C-reactive proteins (CRP)	anti-CRP		Spectral analysis of protein spots	2D-SPR
10	47	Gold array with MUA monolayers	Protein (Biotin-avidin)	cell-free protein solution		monitoring on-line protein expression	Autolab

S.No.	Ref. No.	Surface	Immobiliz-ation in Array	Analyte in Flow	Fabrication Technique	Application	SPR System
11	56	Gold array with MUA monolayers	Protein (IgG)	anti-IgG		gene expression	Homemade
12	55	Gold surface	3D nanostruct-ured protein hydrogel	anti-IgG fab	Pin type spotter (Omni Grid Accent)	Sensitivity enhancement	Flexchip
13	58	Gold array with MUA monolayers	Protein (streptavid-in)	Biotinylated IgG		Spectral analysis of protein spots	Homemade
14	46	Gold with MUOH monolayers	Protein (Recombin ant fusion proteins)	Hexahistid-ine-ubiquitin-tagged human growth hormone	Microarrayer (Proteogen)	Fusion protein expression analysis	2D-SPR
15	52	Gold surface (CM5 sensor, Biacore)	Protein (affibody capture proteins)	Affibodies	Pin type contact arrayer	Affibody capture assays	Biacore
16	44	Gold coated prism	Protein (IgG)	anti-IgG	Microcontrol e (Newport)	Demonstration of highly specific and good sensitive assay with pyrole modified proteins	Genoptics
17	66	Gold with MUA monolayers	Antibody (multiple)	Protein specific to antibody immobilized	SpotBot Microarrayer (Telechem)	Demonstration of SPR - Mass spectrometry array platform	GWC
18	62	Gold with MUA monolayers	Antibody (IFN-g capture antibody)	IFN-g	Microarrayer (Proteogen)	Sensitivity enhancement	Biacore X
19	67	Gold patterns with MUA monolayers with Protein -G	Antibody (Pathogen specific antibodies)	Pathogens		Detection of pathogens	Multiskop
20	63	Gold surface with PEG-OH	Antibody (anti-mKIAA)	Cell lysates	Pin type automated spotter (Toyobo)	Measurement of proteins from crude cell lysates	Toyobo
21	64	Gold with MUA monolayers	Antibody (anti-cysC & anti-β2m)	β2m and cysC	SpotBot Microarrayer (Telechem)	Detection of low moelcular weight biomarker	GWC

S.No.	Ref. No.	Surface	Immobiliz -ation in Array	Analyte in Flow	Fabrication Technique	Application	SPR System
22	65	Streptavidin coated gold surface	Antibody (capture biotinylate d anti-HA & multiple avian scFv antibody)	C-Reactive proteins		High-throughput ranking assay	Biacore A100
23	60	Gold with MUA monolayers	Antibody (C1q antibody)	C1q complement	Robotic non-contact printing (nanoplotter)	Determination of site selective recognition of immune complex	Multiskop
24	68	Carboxymet hyl dextran coated gold surface	Antibody (anti IgG & antibodies for antibiotics)	IgG & Antibiotics	Microgrid contact printing (ApogenDisc overies)	Food screening applications	IBIS iSPR
25	69	Gold coated prism	Antibody (anti-CD3 & anti - CD19)	13G7 cells		Realtime lymphocytes detection	Genoptics
26	61	Gold with MUOH monolayers	Antibody (anti-Bax N-20 & anti-Bax 6A7)	Bax proteins from cell apoptosis		Detection of Bax protein conformational change	2D-SPR
27	70	Gold surface	Antibody (Fab fragment of antibody -96 different fabs)	hK1 antigen	Cartesian spotter (Genomic Solutions)	High throughput affinity ranking assay	Flexchip
28	73	Gold coated with Protein -A	Antibody	Proteins (GST & MBP proteins)	Microgrid II (Genomic Solutions)	Protein expression profiling	Toyobo
29	83	Bare gold	Antibody (anti-hlL-2)	Proteins (rhlL-2)	MicroCASTe r pin system (Schleicher & Schuell)	Demonstration of cell and protein array platforms	Home made Grating-coupled SPR

S.No.	Ref. No.	Surface	Immobiliz-ation in Array	Analyte in Flow	Fabrication Technique	Application	SPR System
30	82	Gold array with carboxymeth-yl dextran	Antibody (Fc specific IgG)	Proteins (IgG)	Hydrodynam-ic addressing	Antigen – Antibody screening	Biacore A100
31	78	Gold surface with functionalize-d hydrogel	Peptides (Citrullinat-ed peptides)	Patient sera	TopSpot (Biofluidics)	Monitoring autoantibodies	IBIS iSPR
32	74	Gold surface with functionalize-d hydrogel	Peptides (Biotinylat ed peptide)	anti-biotin	TopSpot (Biofluidics)	New system demonstration	IBIS iSPR
33	81	Gold with MUA monolayers	Peptides (cysteine modified peptides)	S-protein	PDMS based spotter	Surface enzymatic reaction adsorption/deso rption kinetics estimation	GWC
34	80	Gold with MUA monolayers	Peptides (FLAG peptides)	anti-FLAG peptides	PDMS based spotter	Epitope mapping	GWC
35	79	Gold with SH-EG_3-OH monolayers	Peptides (cysteine terminated peptides)	Cell lysates	Automated spotter	Evaluation of protein kinases in the cell lysates	Toyobo
36	77	Gold with 8-amino-1-octanethiol monolayer	Peptides (Biotinylat-ed peptide)	streptavidin conjugated Caspase-3 solution	Genex arrayer	Monitoring caspase reactions	Toyobo
37	76	Amino modified gold chip	Peptides (PKA & c-src)	anti-phosphoseri-ne and anti-phosphotyro sine	Automated spotter (Toyobo)	Onchip peptide phospohorylatio-n	Toyobo
38	75	Amino modified gold chip	Peptides (P1, P2 and P3 biotinylate-d)	Fab57p	Piezodispens-ation dispenser (Microdrop)	Extension of dynamic range of analyte quantification	Homemade
39	71	Gold surface coated with Streptavidin	Peptide	Antibody	Microsys spotter (Genomic Solutions)	Epitope mapping	Spotmatrix
40	72	Gold surface modified with Pyrole conjugates	Peptides	Antibody	Manual	Clinical applications	Genoptics

S.No.	Ref. No.	Surface	Immobiliz -ation in Array	Analyte in Flow	Fabrication Technique	Application	SPR System
41	88	Poly(L-Lysine) coated gold surface	DNA	(Yeast & bacteria transcription factors) & DNA	Not specified	Transcription factor binding profiling	Homemade
42	86	Gold spots with MUA monolayers	DNA (Locked Nucleic acid)	MicroRNA conjugated with nanoparticle		MicroRNA detection with nanoparticle amplification	GWC
43	89	Gold with PEG-thiol	DNA (double stranded DNA)	Transcriptio -n factor (MAfG)	Photo patterning	New method of affinity estimation between transcription factor and DNA interactions	Toyobo
44	87	Gold array with MUA monolayers	DNA	Viral RNA		Study viral RNA - Protein interactions	GWC
45	85	Gold surface	DNA (ssDNA)	DNA	Manual	Study the effect of secondary structures	SPR Phase interrogation method
46	92	Gold spots with MUA monolayers	DNA	RNA	Photo patterning	DNA - RNA hybridization	GWC
47	93	Gold surface with PEG groups	DNA	Ribosomal RNA	Photo patterning	Re-usuable DNA - Ribosomal RNA hybridization	GWC
48	91	Gold with MUA monolayers	DNA	DNA	Robotic deposition system (QArray)	Monitoring human genetic mutation	Homemade
49	84	Gold with MUA monolayers	DNA (DNA sequences)	Multiple biochemical -s	Robotic deposition system (QArray)	Detection of cyctic fibrosis mutations	Homemade
50	95	Gold with MUA monolayers	DNA	Bacterial response regulators (OmpR & VanR)	Photo patterning	DNA - Bacterial response regulators interactions	GWC
51	94	Gold surface	DNA	DNA conjugated with nanospheres	Manual Spotting	Point mutation detections	Toyobo
52	96	Patterned gold surface	DNA (DNA thio-oligoneucl eotides)	Oligoneucle -otides	Manual	DNA-DNA interactions	Homemade

S.No.	Ref. No.	Surface	Immobiliz-ation in Array	Analyte in Flow	Fabrication Technique	Application	SPR System
53	90	Gold coated prism with pyrole conjugates	DNA	Proteins (p53)	Manual (Chemical coupling)	Protein – DNA interactions	Home made
54	98	Gold with MUA monolayers	RNA	DNA	Photo patterning	Ultrasensitive detecton of Nucleic acids	GWC
55	99	Gold spots with MUA monolayers and DNA	RNA (RNA aptamer)	Thrombin Aptamer		Biomarker discovery	GWC
56	100	Gold with MUA monolayers and DNA	RNA (RNA aptamer)	Protein factor Ixa (flXa)	Photo patterning	Protein - Aptamer interactions	GWC
57	97	Gold with MUA monolayers and DNA	RNA	DNA	Photo patterning	DNA detection from RNA array	GWC
58	101	Gold surface with carboxy-methyl dextran	Carbohydr-ate (Heparin)	FGF-2	Automatic robot	Heparin - protein interaction	Biacore
59	102	Gold surface with fibronogen monolayer	Carbohydr-ate	Lectin		Carbohydrate - protein interactions	Biacore
60	103	Gold surface with carboxy-methyl dextran	Antibiotics	Milk & food samples	Microgrid contact printing (ApogenDiscoveries)	Detection of antibiotic residues in milk	IBIS iSPR
61	104	Photo cross linker coated gold surface	Small molecule ligands	Proteins	Automated spotter (Toyobo)	Fabrication of small molecule array and its interaction with proteins	Toyobo
62	105	Gold surface functionalize-d with dithiobis(succinimidyl propionate)	Glycoprote-ins	Lectin	Manual	Lectin recognition assay	Homemade

Table 2.2 Reported integrated microfluidics–SPR articles describing SPR system, materials used for chip fabrication, fabrication techniques, and applications.

S.No.	Ref. No.	Chip Materials	Fabrication Technique	Application	Number of Parallel Analytes	SPR System
1	144	PDMS	Novolak based positive photoresist replacing SU-8	Development of new microfluidic flowcell	1	Spreeta
2	145	Glass	Channel wet etching	Study Vroman effect	2	SPR (Biosensing instrument inc.)
3	143	Glass-PDMS-Glass	Soft lithography	Biomarker discovery	3	Bi SPR
4	146	PDMS	Aluminium master mold	DNA aptamer - protein interaction	3	Homemade
5	147	PDMS	Polyvinyl chloride master	Kinetics analysis	3	GWC
6	148	PDMS	Soft lithography	DNA modified gold nanoparticle detection	2	2D-SPR
7	137	PDMS		Review		Wavelength division multiplexing SPR (homemade)
8	149	Polyurethene	CO_2 laser beam cutting	New system demonstration	8	Wavelength division multiplexing SPR (homemade)
9	150	Multi-layer structures		Detection of Oligoneucleotides	3	Homemade

S.No.	Ref. No.	Chip Materials	Fabrication Technique	Application	Number of Parallel Analytes	SPR System
10	151			Detection of Botulinum neurotoxins	4	Homemade
11	152			Alzheimer disease biomarker discover	4	Homemade
12	153	Cyclic Olefin Polymer	Injection molding	Antigen-antibody interaction	2	Homemade
13	154			Natural water sample analysis	2	SENSIA
14	155	Plastic		Small molecules detection	8	Homemade
15	156			Demonstration of digital microfluidics coupled SPR		Homemade
16	157	PET or PMMA		Small molecules detection	3	Homemade
17	158			Demonstration of high-throughput highly sensitive SPR system	110	Homemade

Table 2.3 Reported integrated microarray-microfluidics-SPR articles describing SPR system, materials used for chip fabrication, fabrication techniques, and applications.

S. No.	Ref. No.	Chip Materials	Fabrication Technique	Application	Number of Parallel Analytes	SPR System
1	20			One shot kinetics extraction	6	Bio-rad
2	159	PDMS	2D chrome mask pattern created using e-beam lithography	1D - 2D DNA microarray fabrication	6 and 3	GWC
3	160	PDMS	3D Silicon master	Protein - protein and protein - DNA interactions	6 and 3	GWC
4	161	PDMS	Soft lithography	Development of microarray based immunoassay	4	GWC
5	162	PDMS	Soft lithography	Inhibition of Shiga-like toxin	4	GWC
6	163	PDMS	Holographic method	Array of diffraction gratings	4	Homemade
7	164			High-throughput food safety biosensor	6	Homemade
8	165	Mylar	CO_2 laser beam cutting	Investigation of heterogeneous electrochemical processes	3	Homemade
9	166	PDMS	SU-8	New microfluidic SPR demonstration for microarray immunoassay	3	Homemade
10	167	Glass		Digital microfluidics integration for DNA hybridization		Homemade

2.7 References

(1) Bond RPM., Boyce CBC., and French SJ.; Biochem J. 114 (1969) 477-488.
(2) Cheunga KY., Maka WC., and Trau D.; Anal. Chim. Acta 607 (2008) 204-210.
(3) Wang J., Guodong L., and Rasul JM.; J. Am. Chem. Soc. 126 (2004) 3010-3011.
(4) Silva MJ., and Wong JL.; Bioelectrochem. Bioener. 37 (1995) 141-148.
(5) Chung JW., Bernhardt R., and Pyun JC.; J. Immunol. Methods 311 (2006) 178-188.
(6) Han M., Gao X., Su JZ., and Nie S.; Nature Biotech. 19 (2001) 631-635.
(7) Grossman PD., Bloch W., Brinson E., Chang CC., Eggerding FA., Fung S., lovannisci DA., Woo S., and Winn-Deen ES.; Nucl. Acids Res. 22 (1994) 4527-4534.
(8) Hinman AR.; Vaccine 16 (1998) 1116–1121.
(9) Wulfkuhle JD., Liotta LA., and Petricoin EF.; Nat. Rev. Cancer 3 (2003) 267–275.
(10) Zheng G., Patolsky F., Cui Y., Wang WU., and Lieber CM.; Nat. Biotechnol. 23 (2005) 1294–1301.
(11) Southern EM.; J. Mol. Biol. 98 (1975) 503–517.
(12) Alsford S., Glover L., and Horn D.; Mol. Biochem. Parasitology 139 (2005) 129-132.
(13) Rowlands MG., Newbatt YM., Prodromou C., Pearl LH., Workman P., and Aherne W.; Anal. Biochem. 327 (2004) 176-183.
(14) Fultona RJ., McDade RL., Smith PL., Kienker LJ., and Kettman Jr. JR.; Clin. Chem. 43 (1997) 1749-1756.
(15) Zhao X., Hilliard LR., Mechery SJ., Wang Y., Bagwe RP., Jin S., and Tan W.; Proceedings of National Academy of Sciences, USA 101 (2004) 15027-15032.
(16) Wise DL., McCormick GJ., Willet GP., and Anderson LC.; Life Sciences 19 (1976) 867-873.
(17) Brunker SE., Cederquist KB., and Keating CD.; Nanomed. 2 (2007) 695-710.
(18) He B., Morrow TJ., and Keating CD.; Curr. Opin. Chem. Biol. 12 (2008) 522–528.
(19) King WH. Jr.; Anal. Chem. 36 (1964) 1735-1739.
(20) Bravman T., Bronner V., Lavie K., Notcovich A., Papalia GA., and Myszka DG.; Anal. Biochem. 358 (2006).
(21) Otto A.; Z. Physik 216 (1968) 398-410.
(22) Kretschmann E.; Z. Physik 241 (1971) 313-324.
(23) Rothenhaeusler B., and Knoll W.; Nature 332 (1988) 615-617.
(24) MacBeath G., and Schreiber SL.; Science 289 (2000) 1760-1763.
(25) Manz A., Harrison DJ., Verpoorte EMJ., Fettinger JC., Paulus A., Ludi H., and Widmer HM.; J. Chromatogr. 593 (1992) 253-258.
(26) Southern E., Mir K., and Shchepinov M.; Nature genetics 21 (1999) 5-9.
(27) Sreekumar A., Nyati MK., Varambally S., Barrette TR., Ghosh D., Lawrence TS., and Chinnaiyan AM.; Cancer Res. 61 (2001) 7585-7593.
(28) Wheeler DB., Carpenter AE., and Sabatini DM.; Nature genetics 37 (2005) S25-S30.
(29) Chiu CY., Alizadeh AA., Rouskin S., Merker JD., Yeh E., Yagi S., Schnurr D., Patterson BK., Ganem D., and DeRisi JL.; J. Clin. Microbiol. 45 (2007) 2340–2343.
(30) Hu H., Lan R., and Reeves PR.; J. Clin. Microbiol. 40 (2002) 3406-3415.
(31) Kononen J., Bubendorf L., Kallionimeni A., Bärlund M., Schraml P., Leighton S., Torhorst J., Mihatsch MJ., Sauter G., and Kallionimeni O.-P; Nature Medicine 4 (1998) 844-847.
(32) Funeriu DP., Eppinger J., Denizot L., and Miyake M.; Nature Biotechnol. 23 (2005) 622-627.
(33) MacBeath G., Koehler AN., and Schreiber SL.; J. Am. Chem. Soc. 121 (1999) 7967–7968.
(34) Whitesides GM.; Nature 442 (2006) 368-373.
(35) Melin J., and Quake SR.; Annu. Rev. Biophys. Biomol. Struct. 36 (2007) 213–231.
(36) Situma C., Hashimoto M., and Soper SA.; Biomol. Eng 23 (2006) 213-231.
(37) Wark. AW., Lee HJ., and Corn RM.; Angew. Chem. Int. Ed. 47 (2008) 644-652.
(38) Scarano S., Mascini M., Turner APF., and Minunni M.; Biosens. Bioelec. (2009).

(39) Gomez-Hens A., and Aguiliar-Caballos MP.; Trends in Anal. Chem. 26 (2007) 171-182.
(40) Boozer C., Kim G., Cong S., Guan H., and Londergan T.; Curr. Opi. Biotech. 17 (2006) 400-405.
(41) Myszka DG., and Rich RL.; Pharm. Sci. Tech. Today 3 (2000) 310-317.
(42) Campbell CT., and Kim G.; Biomaterials 28 (2007) 2380-2392.
(43) Kopf E., and Zharhary D.; Int. J. Biochem. Cell Biol. 39 (2007) 1305 – 1317.
(44) Grosjean L., Cherif B., Mercey E., Roget A., Levy Y., Marche PN., Villiers M-B., and Livache T.; Anal. Biochem. 347 (2005) 193-200.
(45) Huang H., and Chen Y.; Biosens. Bioelec. 22 (2006) 644-648.
(46) Jung J-M., Shin Y-B., Kim M-G., Ro H-S., Jung H-T., and Chung BH.; Anal. Biochem. 330 (2004) 251-256.
(47) Lee K-H., Joung H-A., Ahn J-H., Kim K-O., Oh I-S., Shin Y-B., Kim M-G., and Kim D-M.; Anal. Biochem. 366 (2007) 170-174.
(48) Oh Y-H., Hong M-Y., Jin Z., Lee T., Han M-K., Park S., and Kim H-S.; Biosens. Bioelec. 22 (2007) 1260-1267.
(49) Olkhov RV., and Shaw AM.; Anal. Biochem. (2009).
(50) Park K., Ahn J., Yi SY., Kim M., and Chung BH.; Biochem. Biophys. Res. Comm. 368 (2008) 684-689.
(51) Peelen D., Kodoyianni V., Lee J., Zheng T., Shortreed MR., and Smith LM.; J. of Prot. Res. 5 (2006) 1580-1585.
(52) Renberg B., Shiroyama I., Engfeldt T., Nygren P-A., and Karlström AE.; Anal. Biochem. 341 (2005) 334-343.
(53) Rich RL., Cannon MJ., Jenkins J., Pandian P., Sundaram S., Magyar R., Brockman J., Lambert J., and Myszka DG.; Anal. Biochem. 373 (2008) 112-120.
(54) Rich RL., Miles AR., Gale BK., and Myszka DG.; Anal. Biochem. 386 (2009) 98-104.
(55) Tanaka H., Hanasaki M., Isojima T., Takeuchi H., Shiroya T., and Kawaguchi H.; Coll. Surf. B: Bioint. 70 (2009) 259-265.
(56) Xinglong Y., Dongsheng W., Dingxin W., Hua OYJ., Zibo Y., Yonggui D., Wei L., and Sheng ZX.; Sens. Act. B 91 (2003) 133-137.
(57) Yuk JS., Hong D-G., Jung H-I., and Ha K-S.; Sens. Act. B 119 (2006) 673-675.
(58) Yuk JS., Jung J-W., Jung S-H., Han J-A., Kim Y-M, and Ha K-S.; Biosens. Bioelec. 20 (2005) 2189-2196.
(59) Yuk JS., Jung J-W., Kim Y-M., and Ha K-S.; Sens. Act. B 129 (2008) 113-119.
(60) Choi J-W., Lee W., Oh B-K., Lee H-J., and Lee D-B.; Biosens. Bioelec. 22 (2006) 764-767.
(61) Kim M., Jung SO., Park K., Jeong E-J., Joung H-A., Kim T-H., Seol D-W., and Chung B.H.; Biochem. Biophys. Res. Comm. 338 (2005) 1834-1838.
(62) Kim M-G., Shin Y-B., Jung J-M., Ro H-S., and Chung B.H.; Journal of Immunol. Methods 297 (2005) 125-132.
(63) Kyo M., Usui-Aoki K., and Koga H.; Anal. Chem. 77 (2005) 7115-7121.
(64) Lee HJ., Nedelkov D., and Corn RM.; Anal. Chem. 78 (2006) 6504-6510.
(65) Leonard P., Säfsten P., Hearty S., McDonnell B., Finlay W., and O'Kennedy R.; J. Immunol. Methods 323 (2007) 172-179.
(66) Nedelkov D.; Anal. Chem. 79 (2007) 5987-5990.
(67) Oh B-K., Lee W., Chun BS., Bae YM., Lee WH., and Choi J-W.; Biosens. Bioelec. 20 (2005) 1847-1850.
(68) Raz SR., Bremer MGEG., Giesbers M., and Norde W.; Biosens. Bioelect. 24 (2008) 552-557.
(69) Suraniti E., Sollier E., Calemczuk R., Livache T., Marche PN., Villiers M-B., and Roupioz Y.; Lab Chip 7 (2007) 1206-1208.
(70) Wassaf D., Kuang G., Kopacz K., Wu Q-L., Nguyen Q., Toews M., Cosic J., Jacques J., Wiltshire S., Lambert J., Pazmany CC., Hogan S., Ladner RC., Nixon AE., and Sexton DJ.; Anal. Biochem. 351 (2006) 241-253.
(71) Baggio R., Carven GJ., Chiulli A., Palmer M., Stern LJ., and Arenas JE.; J. Biol. Chem. 280

(2005) 4188–4194.
(72) Cherif B., Roget A., Villiers CL., Calemczuk R., Leroy V., Marche PN., Livache T., and Villiers M-B.; Clin. Chem. 52 (2006) 252–262.
(73) Usui-Aoki K., Shimada K., Nagano M., Kawai M., and Koga H.; Proteomics 5 (2005) 2396 – 2401.
(74) Beusink JB., Lokate AMC., Besselink GAJ., Pruijn GJM., and Schasfoort RBM.; Biosens. Bioelec. 23 (2008) 839-844.
(75) Andersson O., Nikkinen H., Kanmert D., and Enander K.; Biosens. Bioelec. 24 (2009) 2458-2464.
(76) Inamori K., Kyo M., Nishiya Y., Inoue Y., Sonoda T., Kinoshita E., Koike T., and Katayama Y.; Anal. Chem. 77 (2005) 3979-3985.
(77) Inoue Y., Mori T., Yamanouchi G., Han X., Sonoda T., Niidome T., and Katayama Y.; Anal. Biochem. 375 (2008) 147-149.
(78) Lokate AMC., Beusink JB., Besselink GAJ., Pruijn GJM., and Schasfoort RBM.; J. Am. Chem. Soc. 129 (2007) 14013–14018.
(79) Mori T., Inamori K., Inoue Y., Han X., Yamanouchi G., Niidome T., and Katayama Y.; Anal. Biochem. 375 (2008) 223-231.
(80) Wegner GJ., Lee HJ. and Corn RM.; Anal. Chem. 74 (2002) 5161-5168.
(81) Wegner GJ., Wark AW., Lee HJ., Codner E., Saeki T., Feng S., and Corn RM.; Anal. Chem. 76 (2004) 5677-5684.
(82) Saefsten P., Klakamp SL., Drake AW., Karlsson R., and Myszka DG.; Anal. Biochem. 353 (2006) 181–190.
(83) Unfricht DW., Colpitts SL., Fernandez SM., and Lynes MA.; Proteomics 5 (2005) 4432–4442.
(84) Bassil N., Maillart E., Canva M., Lévy Y., Millot M-C., Pissard S., Narwa R., and Goossens M.; Sens. Act. B 94 (2003) 313-323.
(85) Chen WY., Hu WP., Su YD., Taylor A., Jiang S., and Chang GL.; Sens. Act. B 125 (2007) 607-614.
(86) Fang S., Lee HJ., Wark AW., and Corn RM.; J. Am. Chem. Soc. 128 (2006) 14044-14046.
(87) Garcia II BH., and Goodman RM.; J. Vir. Methods 147 (2008) 18-25.
(88) Jeong E-J., Jeong YS., Park K., Yi SY., Ahn J., Chung SJ., Kim M., and Chung BH.; J. Biotech. 135 (2008) 16-21.
(89) Kyo M., Yamamoto T., Motohashi H., Kamiya T., Kuroita T., Tanaka T., Engel JD., Kawakami B., and Yamamoto M.; Genes Cells 2 (2003) 153-164.
(90) Maillart E., Brengel-Pesce K., Capela D., Roget A., Livache T., Canva M., Levy Y., and Soussi T.; Oncogene 23 (2004) 5543–5550.
(91) Mannelli I., Courtois V., Lecaruyer P., Roger G., Millot MC., Goossens M., and Canva M.; Sens. Act. B 119 (2006) 583-591.
(92) Nelson BP., Grimsrud TE., Liles MR., Goodman RM., and Corn RM.; Anal. Chem. 73 (2001) 1-7.
(93) Nelson BP., Liles MR., Frederick K., Corn RM., and Goodman RM.; Env. Microbiol. 4 (2002) 735-743.
(94) Okumura A., Sato Y., Kyo M., and Kawaguchi H.; Anal. Biochem. 339 (2005) 328-337.
(95) Smith EA., Erickson MG., Ulijasz AT., Weisblum B., and Corn RM.; Langmuir 19 (2003) 1486-1492.
(96) Spadavecchia J., Manera MG., Quaranta F., Siciliano P., and Rella R.; Biosens. Bioelec. 21 (2005) 894-900.
(97) Goodrich TT., Lee HJ., and Corn RM.; J. Am. Chem. Soc. 126 (2004) 4086-4087.
(98) Goodrich TT., Lee HJ., and Corn RM.; Anal. Chem. 76 (2004) 6173-6178.
(99) Li Y., Lee HJ., and Corn RM.; Anal. Chem. 79 (2007) 1082-1088.
(100) Li Y., Lee HJ., and Corn RM.; Nucleic Acids Res. 34 (2006) 6416-6424.
(101) de Paz JL., Noti C., Böhm F., Werner S., and Seeberger PH.; Chemistry & Biology 14 (2007)

879-887.
(102) Houseman BT., and Mrksich M.; Chemistry & Biology 9 (2002) 443-454.
(103) Raz SR., Bremer MGEG., Haasnoot W., and Norde W.; Anal. Chem. 81 (2009) 7743–7749.
(104) Kanoh N., Kyo M., Inamori K., Ando A., Asami A., Nakao A., and Osada H.; Anal. Chem. 78 (2006) 2226-2230.
(105) D'Agata R., Grasso G., Iacono G., Spoto G., and Vecchio G.; Org. Biomol. Chem. 4 (2006) 610-612.
(106) Yu X., Ding X., Liu F., and Deng Y.; Sens. Act. B 130 (2008) 52-58.
(107) Smith EA., Wanat MJ., Cheng Y., Barreira SVP., Frutos AG., and Corn RM.; Langmuir 17 (2001) 2502-2507.
(108) Mannelli I., Lecerf L., Guerrouache M., Goossens M., Millot M-C., and Canva M.; Biosens. Bioelec. 22 (2007) 803-809.
(109) Brockman JM., Frutos AG., and Corn RM.; J. Am. Chem. Soc. 121 (1999) 8044-8051.
(110) Hasenbank MS., Edwards T., Fu E., Garzon R., Kosar FT., Look M., Mashadi-Hossein A., and Yager P.; Anal. Chim. Acta 611 (2008) 80-88.
(111) Dostálek J., and Homola J.; Sens. Act. B 129 (2008) 303-310.
(112) Smith EA., Thomas WD., Kiessling LL., and Corn RM.; J. Am. Chem. Soc. 125 (2003) 6140–6148.
(113) Fang S., Lee HJ., Wark AW., Kim HM., and Corn RM.; Anal. Chem. 77 (2005) 6528-6534.
(114) Jeon SH., Kim US., Jeon WJ., Shin CB., Hong SR., Choi IH., Lee SS., and Yi JH.; Macromol. Res. 17 (2009) 192-196.
(115) Taylor JD., Phillips KS., and Cheng Q.; Lab chip 7 (2007) 927-930.
(116) Piehler J.; Curr. Opi. Stru. Biol. 15 (2005) 4-14.
(117) Chinowsky TM., Grow MS., Johnston KS., Nelson K., Edwards T., Fu E., and Yager P.; Biosens. Bioelec. 22 (2007) 2208-2215.
(118) Steiner G., Sablinskas V., Hübner A., Kuhne C., and Salzer R.; J. Mol. Stru. 509 (1999) 265-273.
(119) Hulme JP., An SSA., Goddard N., Miyahara Y., and Oki A.; Curr. Appl. Phys. 9 (2009) e185-e188.
(120) Natarajan S., Katsamba PS., Miles A., Eckman J., Papalia GA., Rich RL., Gale BK., and Myszka DG.; Anal. Biochem. 373 (2008) 141-146.
(121) Eddings MA., Miles AR., Eckman JW., Kim J., Rich RL., Gale BK., and Myszka DG.; Anal. Biochem. 382 (2008) 55-59.
(122) Natarajan S., Hatch A., Myszka DG., and Gale BK.; Anal. Chem. (2009).
(123) Liu J., Eddings MA., Miles AR., Bukasov R., Gale BK., and Shumaker-Parry JS.; Anal. Chem. 81 (2009) 4296-4301.
(124) Eddings MA., Eckman JW., Arana CA., Papalia GA., Connolly JE., Gale BK., and Myszka DG.; Anal. Biochem. 385 (2009) 309-313.
(125) Yuk JS., Jung J-W., Hyun J., Kim Y-M., and Ha K-S.; Sens. Act. B 131 (2008) 241-246.
(126) Thariani R., and Yager P.; Sens. Act. B 130 (2008) 765-770.
(127) Piliarik M., Vaisocherová H., and Homola J.; Biosens. Bioelec. 20 (2005) 2104-2110.
(128) Yuk JS., Kim H-S., Jung J-W., Jung S-H., Lee S-J., Kim WJ., Han J-A., Kim Y-M., and Ha K-S.; Biosens. Bioelec. 21 (2006) 1521-1528.
(129) Junfeng L., Xiang D., Xinglong Y., and Dongsheng W.; Sens. Act. B 108 (2005) 778-783.
(130) Jamil MMA., Youseffi M., Twigg PC., Britland ST., Liu S., See CW., Zhang J., Somekh MG., and Denyer MCT.; Sens. Act. B 129 (2008) 566-574.
(131) Kim M., Park K., Jeong E-J., Shin Y-B., and Chung BH.; Anal. Biochem. 351 (2006) 298-304.
(132) Yang J-C., Ji J., Hogle JM., and Larson DN.; Biosens. Bioelec. 24 (2009) 2334-2338.
(133) Sjoelander S., and Urbaniczky C.; Anal. Chem. 63 (1991) 2338-2345.
(134) Raghavan M., and Bjorkman PJ.; Structure 3 (1995) 331-333.
(135) Roman GT., Kennedy RT.; J. Chrom. A 1168 (2007) 170-188.

(136) Crevillen AG., Hervas M., Lopez MA., Gonzalez MC., and Escarpa A.; Talanta 74 (2007) 342-357.
(137) Homola J., Vaisocherová H., Dostálek J., and Piliarik M.; Methods 37 (2005) 26-36.
(138) Zimmermann B., Hahnfeld C., and Herberg FW.; Targets 1 (2002) 66-73.
(139) Ravishankaran D., Gobi KV., and Miura N.; Sens. Act. B 121 (2007) 158-177.
(140) Hoa XD., Kirk AG., and Tabrizian M.; Biosens. Bioelec. 23 (2007) 151-160.
(141) Gervais T., and Jensen KF.; Chem. Eng. Sci. 61 (2006) 1102-1121.
(142) Deen WM.; Oxford University Press, Newyork (1998).
(143) Choi S., and Chae J.; Biosens. Bioelec. 25 (2009) 118-123.
(144) Wheeler AR., Chah S., Whelan RJ., and Zare RN.; Sens. Act. B 98 (2004) 208-214.
(145) Choi S., Yang Y., and Chae J.; Biosens. Bioelec. 24 (2008) 893-899.
(146) Wang Z., Wilkop T., Xu D., Dong Y., Ma G.,and Cheng Q.; Anal. Bioanal. Chem. 389 (2007) 819-825.
(147) Grasso G., D'Agata R., Zanoli L., and Spoto G.; Microchem. J. 93 (2009) 82-86.
(148) Sato Y., Sato K., Hosokawa K., and Maeda M.; Anal. Biochem. 355 (2006) 125-131.
(149) Dostálek J., Vaisocherová H., and Homola J.; Sens. Act. B 108 (2005) 758-764.
(150) Piliarik M., Vaisocherová H., and Homola J.; Sens. Act. B 121 (2007) 187-193.
(151) Ladd J., Taylor AD., Homola J., and Jiang S.; Sens. Act. B 130 (2008) 129-134.
(152) Hegnerová K., Bocková M., Vaisocherová H., Krištofiková Z., Říčný J., Řípová D., and Homola J.; Sens. Act. B 139 (2009) 69-73.
(153) Huang C., Bonroy K., Reekman G., Verstreken K., Lagae L., and Borghs G.; Microelec. Eng. 86 (2009) 2437-2441.
(154) Mauriz E., Calle A., Abad A., Montoya A., Hildebrandt A., Barceló D., and Lechuga LM.; Biosens. Bioelec. 21 (2006) 2129-2136.
(155) Kim SJ., Gobi KV., Iwasaka H., Tanaka H., and Miura N.; Biosens. Bioelec. 23 (2007) 701-707.
(156) Galopin E., Beaugeois M., Pinchemel B., Camart J-C., Bouazaoui M., and Thomy V.; Biosens. Bioelec. 23 (2007) 746-750.
(157) Nelson KE., Foley JO., and Yager P.; Anal. Chem. 79 (2007) 3542–3548.
(158) VanWiggeren GD., Bynum MA., Ertel JP., Jefferson S., Robotti KM., Thrush EP., Baney DM., and Killeen K.P.; Sens. Act. B 127 (2007) 341-349.
(159) Lee HJ., Goodrich TT., and Corn RM.; Anal. chem. 73 (2001) 5525-5531.
(160) Wegner GJ., Lee HJ., Marriott G., and Corn RM.; Anal. Chem. 75 (2003) 4740–4746.
(161) Kanda V., Kariuki JK., Harrison DJ., and McDermott MT.; Anal Chem. 76 (2004) 7257-7262.
(162) Kanda V., Kitov P., Bundle DR., and McDermott MT.; Anal. Chem. 77 (2005) 7497-7504.
(163) Dostálek J., Homola J., and Miler M.; Sens. Act. B 107 (2005) 154-161.
(164) Piliarik M., Párová L., and Homola J.; Biosens. Bioelec. 24 (2009) 1399-1404.
(165) Hasenbank MS., Fu E., Nelson JB., Schwartz DT., and Yager P.; Lab Chip 7 (2007) 441-447.
(166) Lee K-H., Su Y-D., Chen S-J., Tseng F-G., and Lee G-B.; Biosens. Bioelec. 23 (2007) 466-472.
(167) Malic L., Veres T., and Tabrizian M.; Biosens. Bioelec. 24 (2009) 2218-2224.

3

Technical Background

This chapter summarizes the important technical aspects used throughout this thesis. Since we describe an integrated system for multiplex bioassays, there are several distinct technical disciplines that require background review of fundamental concepts and parameters that are important for biosensing applications. The technical disciplines important for this thesis include biomolecular interactions, microarrays, surface chemistry for ligand immobilization for high yield surface activity, electrokinetic transport in microfluidic systems, surface plasmon resonance (SPR), SPR imaging and kinetics parameter extraction from SPR sensorgrams.

3.1 Biomolecular Interactions

A biomolecular interaction is the process of coupling two or more biomolecules to each other forming a complex. Biomolecular interaction analysis can be used in a number of ways.

- To identify the binding of two or more interactants to each other
- To determine the affinity of the interactions
- To measure the actual association and dissociation rates

In addition, the binding of two interactants can be exploited to quantify the concentration of one of the interactants. Different types of biomolecular interactions performed using label-free detection techniques are DNA-DNA interactions, DNA-RNA (ribonucleic acid) interactions, DNA-PNA (peptide nucleic acid) interactions, DNA-protein interactions, protein-protein interactions, drugs-protein interactions, virus-antibody interactions, cells-antibody interactions and lipid-protein interactions. The main focus of the thesis will be on protein-antibody interactions.

3.1.1 Protein – Protein Interactions

Proteins are organic compounds made of amino acids arranged in a linear

chain and folded into a globular form. Normally these chains of amino acids are covalently linked peptide bonds between the carboxyl and amino groups of adjacent amino acid residues. When a chain contains more than 12 amino acid residues, it is called a polypeptide, and less than 12 amino acids is termed an oligopeptide. The structure of proteins is classified into four different categories, as shown in Fig. 3.1.[1] Figure 3.1a shows a representation of the primary structure of proteins, which are formed by an amino acid sequence of peptide chains. Figure 3.1b is a schematic representation of the secondary structure of proteins, which are mostly regular sub-structures and distinguished into two types, alpha helix and strands of beta sheet or pleated sheet. Secondary structures occur when the sequence of amino acids is linked by hydrogen bonds. There may be many different secondary motifs present in one single protein. Tertiary structures, shown in Figure 3.1c, are three dimensional structures, which are a spatial arrangement of secondary structures. This structure occurs when various bonding interactions occur between alpha helices and pleated sheets and also describe the completely folded and compacted polypeptide chains. The fourth structure is a quaternary structure (Fig. 3.1d) which is a complex of many proteins or polypeptide chains that function as part of the larger assembly.

In addition to these structural levels, a protein may shift between several reversible similar structures while performing its biological function. In the context of these functional rearrangements, these tertiary or quaternary structures are usually referred to as chemical conformation, and transitions between them are called conformational changes.

Protein-protein interactions involve not only the direct-contact association of protein molecules but also longer range interactions through the electrolyte, aqueous solution medium surrounding neighboring hydrated proteins over distances from less than one nanometer to distances of several tens of nanometers. Furthermore, such protein-protein interactions are thermodynamically linked functions[2] of dynamically bound ions and water that exchange rapidly with the surrounding solution in comparison to the molecular tumbling rate (or correlation times) of the interacting proteins. Protein associations are also studied from the perspective of biochemistry,

quantum chemistry, molecular dynamics, signal transduction and other metabolic or genetic/epigenetic networks. Indeed, protein-protein interactions are at the core of the entire interaction system of any living cell.

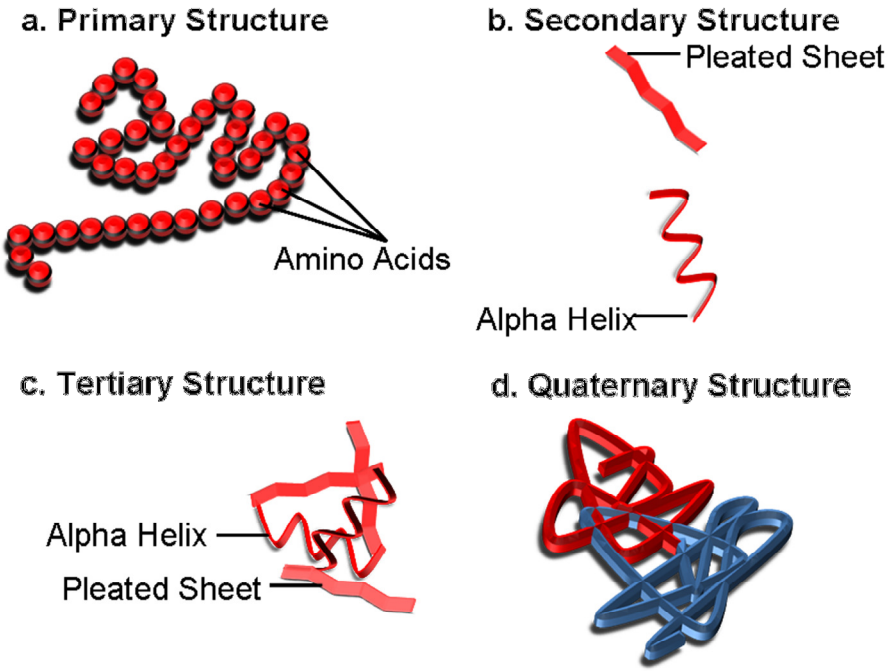

Figure 3.1 Protein structures: (a) Primary structure: sequence of amino acid chain; (b) Secondary structure: sequence of amino acids linked with hydrogen bond (alpha helix and pleated sheet); (c) Tertiary structures: combination of alpha helices and pleated sheets due to certain attractions between them; (d) Quaternary structures: a protein consists of more than one amino acid chain.

The interactions between proteins are important for numerous -if not all- biological functions. For example, signals from the exterior of a cell are mediated to the inside of that cell by protein-protein interactions of the signaling molecules. This process, called signal transduction, plays a fundamental role in many biological processes and in many diseases (e.g. cancers).[3] Proteins might interact for a long time to form part of a protein complex, a protein may be carrying another protein (for

example, from cytoplasm to nucleus or vice versa in the case of the nuclear pore importins), or a protein may interact briefly with another protein just to modify it (for example, a protein kinase will add a phosphate to a target protein).[4] This modification of proteins can itself change protein-protein interactions. For example, some proteins with SH_2 domains only bind to other proteins when they are phosphorylated on the amino acid tyrosine while the bromo-domains specifically recognize acetylated lysines. In conclusion, protein-protein interactions are of central importance for virtually every process in a living cell. Information about these interactions improves our understanding of diseases and can provide a basis for new therapeutic approaches.

Protein-protein/antibody interactions are normally measured by physical/biophysical techniques such as dual polarization interferometry,[5] quartz crystal microbalance,[6] static light scattering,[7] nuclear magnetic resonance,[8] surface plasmon resonance,[9] fluorescence correlation spectroscopy,[10] fluorescence resonance energy transfer,[11] and x-ray diffraction.[12,13] Out of these techniques, surface plasmon resonance is considered in this thesis (Section 3.2). While discussing protein-protein interactions, it is important to discuss the basics of antibodies (Section 3.1.2) and structures of most of the protein–protein interactions.

3.1.2 Antibodies

Antibodies (Fig. 3.2), also known as immunoglobulins,[14] abbreviated Ig are gamma globulin proteins that are found in blood or other bodily fluids of vertebrates, and are used by the immune system to identify and neutralize foreign objects, such as bacteria and viruses. They are typically made of basic structural units - each with two large heavy chains and two small light chains-to form, for example, monomers with one unit, dimers with two units or pentamers with five units.[15] Antibodies are produced by a kind of white blood cell called a plasma cell. There are several different types of antibody heavy chains, and several different kinds of antibodies, which are grouped into different isotypes based on which heavy chain they possess. Five different antibody isotypes are known in mammals (IgA, IgD, IgE, IgG and IgM), which

perform different functions, and help direct the appropriate immune response for each different type of foreign object they encounter.[16]

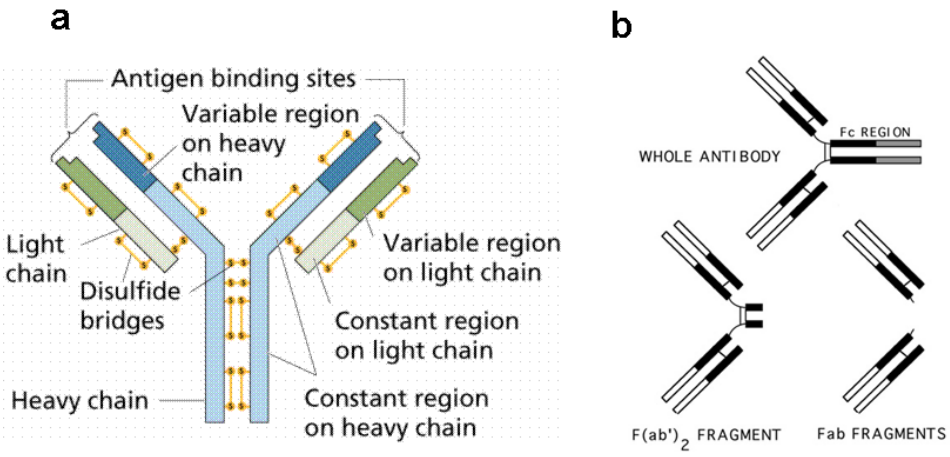

Figure 3.2 (a) Schematic representation of an antibody consisting of 2 heavy chains and 2 light chains having a constant region and highly variable regions. The disulfide bridges provide extra stability to the antibodies. (b) On enzymatic cleavage, antibody could be split into F(ab')$_2$ or Fab.

Although the general structure of all antibodies is very similar, the small region at the tip of the protein is variable, allowing millions of antibodies with slightly different tip structures, or antigen binding sites. This region is known as the hyper variable region. Each of these variants can bind to a different ligand, known as an antigen.[17] This huge diversity of antibodies allows the immune system to recognize an equally wide diversity of antigens. The unique part of the antigen recognized by an antibody is called an epitope. These epitopes bind with their antibody in a highly specific interaction, called induced fit that allows antibodies to identify and bind only their unique antigen in the midst of the millions of different molecules that make up an organism. Recognition of an antigen by an antibody tags it for attack by other parts of the immune system. Antibodies can also neutralize targets directly by, for example, binding to a part of a pathogen that it needs to cause an infection.[18]

3.2 Microarray

A microarray is a two-dimensional array of biomolecular ligand spots immobilized on a surface with predetermined spatial order in an assay used for gene expression and discovery,[19] disease diagnostics,[20] drug discovery,[21] biomarker discovery,[22] and toxicology.[23] The microarray was first described in literature in the late 1970's[24] and formally defined as a microarray in the late 1980's.[25] Since the initial application of high-throughput genomics, microarrays are being applied in different fields, including proteomics,[26] cellomics,[27] and small molecules,[28] as well as many different types of biomaterials, including antibodies,[29] chemicals,[30] tissues,[31] carbohydrates,[32] and peptides.[33] Each spot on the microarray acts as an individual sensing region, which is useful for increasing the throughput of the biosensing assays (detection of multiple biomolecules from single set of spots).

A protein microarray, sometimes referred to as a protein binding microarray,[34] provides a multiplex approach to protein-protein interactions identification, to identify the substrates of protein kinases, to identify transcription factor protein-activation, or to identify the targets of biologically active small molecules. The array substrate is a solid support typically made of glass on which different molecules of protein or specific DNA binding sequences (as ligands for the proteins) have been affixed at separate locations in an ordered manner thus forming a microscopic array. The most common protein microarray is the antibody microarray, where antibodies are spotted onto the protein chip and are used as capture molecules to detect proteins from cell lysate solutions. Although protein microarrays may use similar detection methods as DNA microarrays, a problem is that protein concentrations in a biological sample may be many orders of magnitude different from that for nucleic acids. Therefore, protein chip detection methods must have a much larger range of detection.

The preferred method of detection currently is fluorescence detection. The fluorescent detection method is compatible with standard microarray scanners, the spots on the resulting image can be quantified by commonly used microarray quantification software packages.[35] Other common detection methods include

colorimetric technqiues based on silver-precipitation,[36] chemiluminescent,[37] and label free surface plasmon resonance.[38]

3.3 Microfluidics

Microfluidics is defined as handling samples, typically in the mL to nL range, and is well suited for bio-analysis where limited sample volumes are available. This minimizes assay costs, reduces sample preparation and processing time, and facilitates sample preparation automation. Microfluidics was first demonstrated for capillary electrophoresis by Manz et. al.[39] and from that time, has become an important and prominent field of research. The development with respect to the integration of microfluidics with SPR was discussed in Chapter 2 (section 2.4).

Fluid transport in microfluidic devices is commonly done with either pressure or electrokinetic sources. More detailed theoretical background about electrokinetic fluid transport is discussed in this section as it has been used extensively in this work for the realization of integrated biochips for high-throughput multiplex bioassays.

3.3.1 Electrokinetics

Fluid flow induced by an electric field is termed as electrokinetics, which includes electro-phoretic and electro-osmotic transport. In this thesis, electro-osmotic flow (EOF) fluid transport has been used extensively and will be described in more detail. Additionally, a technique to control the position of sample transport in a reactor, called electrokinetic focusing (EKF), has been realized and will be discussed in more detail.

3.3.1.1 Electro Osmotic Flow

Most solid surfaces carry electrostatic charges, or an electrical surface potential, when it is in contact with aqueous solution. In equilibrium, the solution is electrically neutral (having an equal number of positive ions and negative ions). The counter-ions in the liquid are attracted by the electrostatic charges on the solid surface,

leading higher counter-ion concentration near the solid surface when compared to the bulk liquid which is far away from the solid surface. Due to electrical repulsion, the co-ion concentrations are near the solid surface, which leads to a net charge (excess counter-ions) close to the solid surface. The charged surface and the layer of liquid containing the balanced charges are known as the electrical double layer and are illustrated in Fig. 3.3a, for a flat surface, and Fig. 3.3b for microchannels.

The ions are immovable due to the very strong attraction close to the surface. This layer is called stern layer, or compact layer. The charge and potential distributions are mainly influenced by geometrical restrictions of ion and molecular size, short range interactions between ions, and the wall and adjoining dipoles. The net charge gradually reduces to zero from the stern layer to the electrically neutral bulk liquid. Ions in the bulk liquid are less influenced by electrostatic interaction and are mobile. This layer is called the diffuse layer of the electrical double layer and the ion and potential distributions can be described by the Poisson–Boltzmann equation.[40] The diffuse layer thickness is highly dependent on the bulk ionic concentration and electrical properties of the liquid. The boundary between the stern and diffuse layers is called the shear plane. The electrical potential at the solid–liquid interface (shear plane) is measured experimentally and called the zeta potential ζ and is considered an approximation of the surface potential in many electrokinetic models.[41, 42]

When an electric field is applied parallel to a charged wall with an electrical double layer, the mobile ions in the diffuse layer show a net migration into the opposite direction dragging the solvent with them, which causes flow and is referred to as EOF. According to the Helmholtz-Smoluchowski equation,[40] the contribution of EOF to the apparent mobility (electro osmotic mobility) of the ions μ_{EOF} is proportional to ζ_w, and permittivity of the solvent ε and inversely proportional to viscosity of the solution η. The induced bulk fluid velocity is

$$\upsilon_{EOF} = \mu_{EOF} E = \frac{\varepsilon \zeta E}{4\pi\eta} \tag{3.1}$$

Experiments performed with EOF are discussed in Chapters 7 and 8.

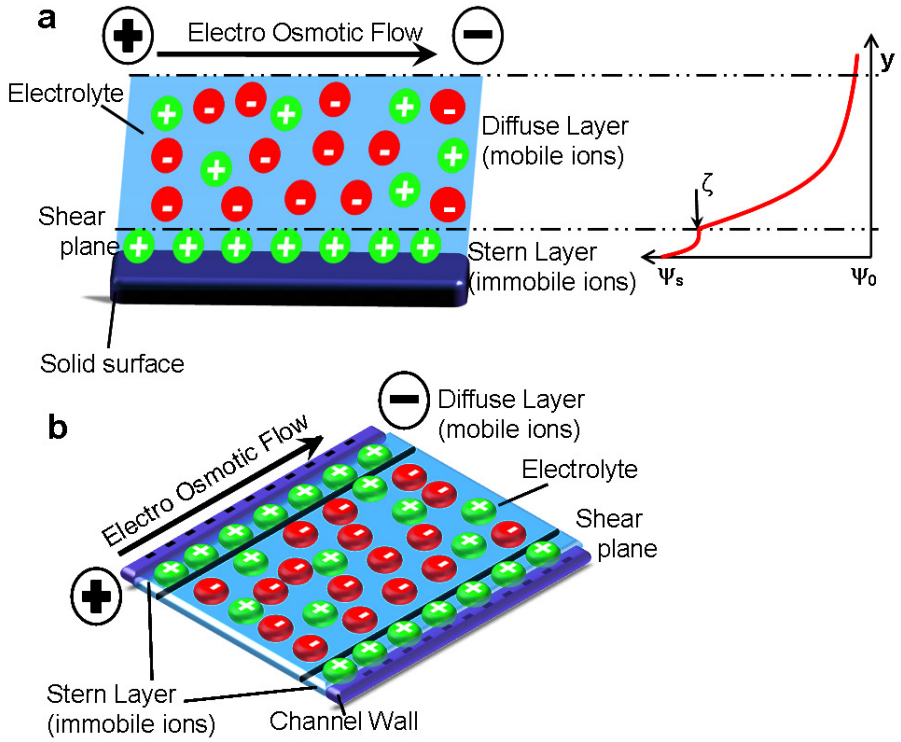

Figure 3.3 (a) Illustration of the electrical double layer for a flat surface that is negatively charged. The stern layer is a single ion layer in which the ions adhere to the surface; the diffuse layer is the adjacent charged layer with freely moving hydrated ions. The right side plot illustrates the potential distribution plot: ψ_0 is the surface potential, ζ is the zeta potential at the position of the first mobile ions in the diffuse layer.[40] (b) Schematic illustration of electrical double layer in microchannel.

3.3.1.2 Electrokinetic Focusing

EKF in a microfluidic chip was previously described in detail[43] and later reported for controlling the flow in a microreactor.[44] EKF is a valveless and pumpless method for controlling the sample stream profile in a laminar flow chamber. A schematic illustration of EKF is shown in Fig. 3.4a, where the sample from the center inlet is focused to the second row r_2 of the gold island imaging array. An equivalent electrical circuit is shown in Fig. 3.4b where resistances R_i are determined by sample

conductivity and channel dimensions. By altering the control voltages (V_u: upper channel voltage, V_l: lower channel voltage), the sample stream can be directed to each of the imaging array rows r_i. The sample flow is controlled by the center voltage (V_c: sample voltage), which also controls the flow velocity and sample stream width according to the distance X_1, shown in Fig. 3.4a. The upper and lower reservoirs were filled with guiding stream buffer and the center reservoir filled with the sample. The outlet reservoir voltage was set to ground and the voltages for the guiding streams, as well as sample streams, were individually controlled.

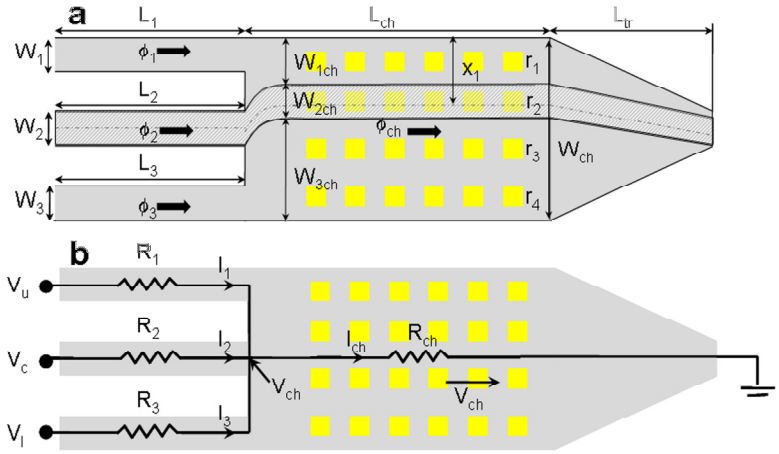

Figure 3.4 (a) Schematic illustration of the EKF chip and corresponding parameters. Example shows EKF to row 2. Here, r_1, r_2, r_3 and r_4 represent row 1 through row 4. The microchannel widths are W_1, W_2 and W_3, and the reaction chamber width is W_{ch}. W_{1ch}, W_{2ch} and W_{3ch} are the width of the top guiding stream, sample stream and bottom guiding stream, respectively. ϕ_1, ϕ_2, ϕ_3 and ϕ_{ch} represent the flux in channel 1, channel 2, channel 3 and reaction chamber, respectively. L_1, L_2, L_3, L_{ch}, and L_{tr} are the length of channel 1, channel 2, channel 3, rectangular chamber and trapezoid, respectively. X_1 is the distance from the top of chip to the center of the sample stream. (b) Electrical circuit representation of the electrokinetic focusing chip. R_1, R_2, R_3 and R_{ch} represent the resistors in the corresponding channel and reaction chamber. I_1, I_2, I_3 and I_{ch} are the current in the corresponding channels and chamber. V_u, V_c, V_l and V_{ch} represent voltage in upper channel (channel 1), sample channel (channel 2), lower channel (channel 3) and chamber, respectively. (Reproduced from chapter 6 to discuss the model used to describe electrokinetic focusing).

The required voltage settings were estimated from the previously developed analytical model for any position, velocity and width of the sample stream.[43-47] The model assumes that the fluid velocity is constant throughout the reaction chamber from the exit of the microchannels. This assumption leads to the conclusion that all the electric potentials at the entrance of the reaction chamber from the microchannel should be the same. Once this potential is known, fluid flux through each of the three channels can be calculated using

$$\phi_i = v_i A_i = \mu_{EOF} A_i E_i = \mu_{EOF} A_i \frac{V_i - V_{ch}}{L_i} \tag{3.2}$$

where v is the fluid velocity, A is the *cross* sectional area, μ_{EOF} is the electroosmotic mobility, E is the electrical field, l is the length of the channel, V is the applied voltage at the inlet and V_{ch} is the electric potential at the entrance of the reaction chamber which is given by

$$V_{ch} = \frac{\frac{V_u}{R_1} + \frac{V_c}{R_2} + \frac{V_l}{R_3}}{\frac{1}{R_{ch}} + \frac{1}{R_1} + \frac{1}{R_2} + \frac{1}{R_3}} \tag{3.3}$$

With the known channel and reaction chamber geometries and buffer conductivity, the equivalent electrical resistance can be calculated. The liquid volume flux through each channel directly corresponds to the width of the corresponding stream inside the flow chamber due to mass conservation. Therefore, the position of the sample stream X_1 and width of the sample stream W_{2ch} are given by

$$X_1 = \frac{\phi_1 + \frac{1}{2}\phi_2}{\phi_1 + \phi_2 + \phi_3} W_{ch} \tag{3.4}$$

and

$$W_{2ch} = \frac{\phi_2}{\phi_1 + \phi_2 + \phi_3} W_{ch} \tag{3.5}$$

In general, the guiding stream and sample transport voltages are calculated using

$$V_i = \frac{\phi_i L_i}{A_i \mu_{EOFi}} + \frac{R_{ch}}{\mu_{EOFi}} \sum \frac{\phi_j L_j}{R_j A_j} \tag{3.6}$$

where A_i and A_j (m^2) are the cross-sectional areas of the channels and chamber, Φ_i and Φ_j are the flow fluxes (m^3/min), and R_{ch} and R_j are the electrical resistances (Ω) of the channels and chamber, respectively. Thus, the calculated voltages could be directly applied to focus the sample stream in specific velocity and width to specific locations of the chips (experiments using EKF are discussed in Chapter 6).

3.4 Surface Modification

3.4.1 Surfaces for biomolecular interaction analysis: Basics

Molecular recognition plays a vital role in the understanding of almost all processes involving living organisms. To characterize such a molecular recognition, direct label-free optical biosensors are interesting tools as they allow for fast and quantitative analysis without molecular labeling. Early descriptions of applying SPR technology for bioanalytical applications were based on simple physical adsorption of proteins to an active metal surface.[48] There is a long history for the immobilization of molecules on the solid surfaces or matrices. However, SPR biosensors pose unique requirements. The heart of proper SPR technology operation relies on how well the sensor surface is immobilized with ligands such that biological function and SPR sensing performance are optimal. The gold layer used for generating the surface plasmon polaritons tends to adsorb biomolecules instantaneously, which results in loss of bioactivity. This tendency (2–10% reduced signal) was reported in enzyme-linked immunosorbent assays when the molecules were directly adsorbed on the plastic surface.[49] These effects can be explained by a reorganization of the immobilized molecule to attain the most favorable thermodynamic state. For example, adsorption to hydrophobic surfaces is driven by rearrangements that optimize contact of hydrophobic segments with the substrate. Passive binding to a surface substrate also opens possibilities for uncontrolled exchange of the immobilized molecule during an analysis cycle. If the unmodified surface is used for repeated analysis cycles, the probability of

exchange will be further enhanced and can lead to unreliable assays. Another disadvantage of the direct adsorption approach is non-specific binding of other matrix components. The ratio of specific to non-specific binding responses should be large for the extraction of reliable binding kinetics. The surface can be treated to prevent non-specific binding of molecules with surface modification procedures that are discussed in the following section.

Electrostatic (charged and manipulated through ionic strength) and hydrophobic (not controllable) interactions account for approximately 85% of the overall energy and are therefore very important in biomolecular interactions.[50] An increasing salt concentration screens charged groups and usually has a practically pH-independent repulsion effect on hydrophilic and charged immobilization matrices because ion pairs are formed which can neutralize the charged domains. At low ionic strengths, the pH of the buffer becomes more important as the electrostatic interactions dominating this regime are governed by the ligands overall charge, which is positive at pH values below the isoelectric point and negative in a more alkaline pH range. Strong attractive or repulsive forces between the dissolved species and surface are greatly dependent on the charge on the sensor surface.

The hydrophobic interaction cannot be controlled as it is not an attractive force but the exclusion of hydrophobic domains of low surface energy in highly energetic solvents such as water. An entropy effect (reduced organization of water molecules) tends to induce hydrophobic effects.[85] Choosing a buffer pH close to pI of the molecule usually minimizes the extent of electrostatic forces and thus increases the relative influence of hydrophobic interactions. As a consequence, precipitation of protein molecules often occurs at the pI caused by the decreased electrostatic repulsion between molecules. As hydrophobic interactions can lead to partial unfolding and as a consequence to significant activity loss of the immobilized proteins, the fraction of hydrophobic domains on the sensor chip surface should – with the exception of surfaces for immobilization of membrane proteins – be kept as low as possible.

Careful control of surface charge and surface energy is very important in case of biosensors for high immobilization yields, to minimize non-specific interactions,

and to retain the biological activity of the immobilized ligands. This is commonly done by coating the metal surface with self assembled monolayers of thiol- or disulfide molecules followed by modification with carboxy methyl dextran or functionalized hydrogel, which are further modified with functional groups suitable for a particular application.

3.4.2 Self-Assembled Monolayers

Extensive efforts have been made to develop approaches for coating metal surfaces before immobilization. This serves to minimize non-specific adsorption, as well as to introduce reactive groups for specific immobilization. The most successful methods are based on the concept of molecular self-assembly of thiol- or disulfide molecules, commonly called self-assembled monolayers (SAM), on the metal surface as shown in the first two steps of Fig. 3.5. The spontaneous formation of organic disulfide monolayers on gold was initially shown by Allara and Nuzzo in 1983[51] in the context of models for interface studies. Monolayer formation is driven by a strong coordination of sulfur with the metal, accompanied by van der Waals interaction forces between the alkyl chains. With a sufficient chain length, the resulting monolayer forms a densely packed and very stable structure that is oriented approximately 30º, with respect to the normal, for a smooth surface. These nanometer-thick layers are easily fabricated using commercially available substances, or can at least be synthesized with relative ease.[52] The first applications of SAMs for biosensors were described in the late 1980s and developed for Biacore SPR instruments.[53,54] Hydroxyl-terminated long chain thiol alkanes have been designed that can be activated for direct linkage of various functional groups or further derivatized with different moieties for more advanced surface modifications.

A different functional end group of the alkyl thiols creates a high degree of flexibility in terms of the types of surface properties that can be obtained. Extensive studies involving various types of coatings have been reviewed elsewhere.[52,55,56] For example, in early applications,[53,54] a terminal hydroxyl functionality was introduced to

give the surface a highly hydrophilic character, while acting as a means for immobilization of various molecules, either directly or via suitable linkers. Direct covalent immobilization of proteins to various ω-terminated groups has also been described, although there are limitations to such approaches.

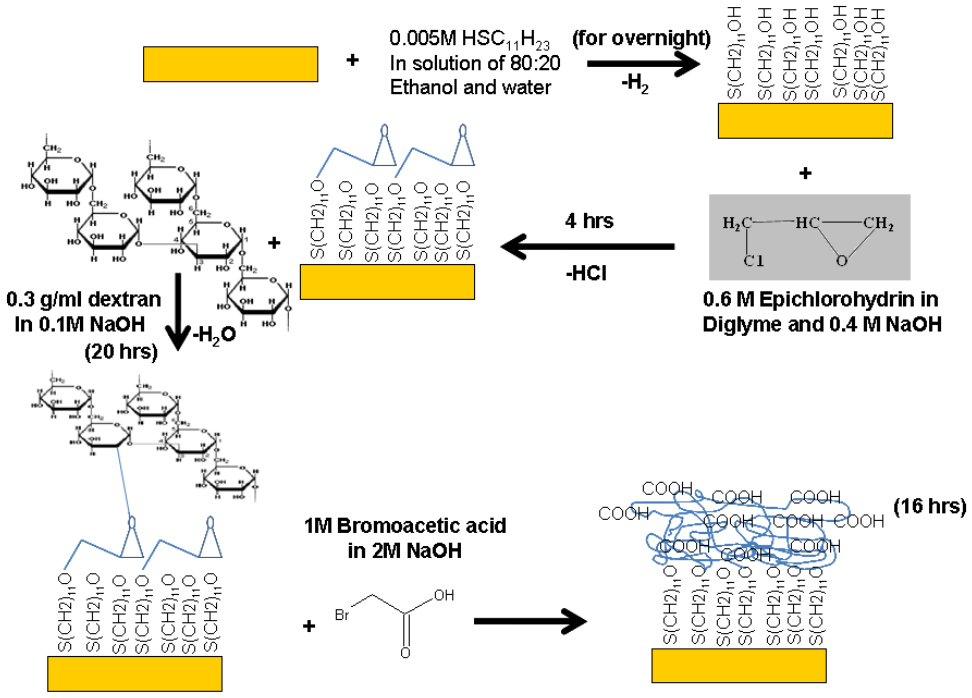

Figure 3.5 Schematic illustration of reaction scheme involved in gold surface modification for the coupling of functionalized hydrogel/dextran for covalent immobilization of ligands.

3.4.3 Dextran/Hydrogel Surfaces

The rigidness of the flat surface may induce denaturation or impaired activity of the protein even when the surface is hydrophilic.[57] It is also known that mass-dependent refractive index changes are sensitive until a few hundred nanometers from the metal surface during the SPR measurements. In other words, the evanescent field of the SPP extends several hundred nm into the region above the gold surface. The first surface modification technique for SPR was developed by Biacore AB, which was a thin hydrogel-like polymer based on dextran as shown in Fig. 3.5. The dextran polymer

is composed mainly of unbranched glucose units, and is highly flexible and water soluble. Immobilization is facilitated via epoxy modification of the terminal hydroxyl SAM and subsequent nucleophilic reaction of the dextran under alkaline conditions.[53,54,58] The surface can be further activated with suitable linkers for subsequent immobilization, and here the introduction of carboxymethyl groups has proven a versatile alternative. By choosing different sizes of dextran, ranging from 10^3 Da to over 10^6 Da, surfaces tailored for specific applications can be created. This kind of surface modification makes not only the surface hydrophilic, but also is well suited for covalent immobilization of proteins. Furthermore, the extended matrix structure has been shown to increase the binding capacity several-fold compared to flat surfaces.[58] In addition, the thin dextran layer matches well with respect to the penetration depth of the evanescent wave.[59,60] The linkage of dextran polymer chains to the sensor surface provides an open, non-cross-linked structure on which immobilized molecules can attain a solution-like state with a certain level of freedom within the derivatized layer.[61] These types of negatively charged layers may exhibit electrostatic background binding of basic compounds, which needs to be considered in the design of the immobilization procedure and the assay. However, working under physiological buffer conditions normally suppresses such effects by electrostatic shielding. Alternatively, lowering the degree of carboxymethylation can also be used to reduce this effect.

3.4.4 Covalent Immobilization

Limitations in simple adsorption processes have led to the development of advanced surface coatings designed for controlled immobilization. Different functional groups have been introduced on the surface, enabling the formation of a stable linkage to an appropriate functional group (Fig. 3.6). This may include an activation step of one or both of the functional groups, which results in the transformation into a more reactive form. For proteins in particular, the chemistries utilized also need to be performed under relatively mild conditions and in aqueous solutions, placing certain limitations on the available repertoire.

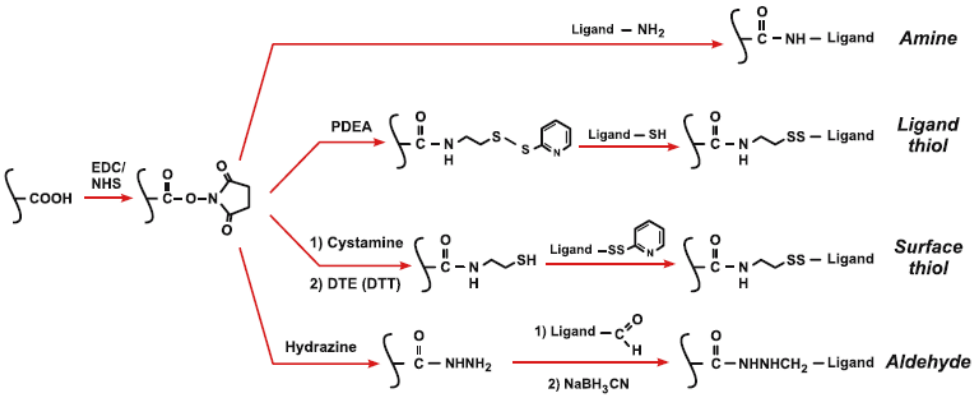

Figure 3.6 Schematic illustration of reaction schemes involved in activating the functionalized hydrogel/dextran surface for the immobilization of ligands.

The possibility of having a transformable functional group on the sensor surface is an attractive concept as a general starting surface for use with a wide range of coupling chemistries. The carboxymethylated dextran coating described in the previous section was designed to include the carboxylic acid residue as a functional group that can be used either for direct coupling, or switched to other functionalities. Figure 3.6 shows how carboxylic groups can either be directly reacted with amine groups or converted for use in coupling chemistries based on thiol reactions, aldehyde and carboxylic acid condensations, and biotin capture techniques. Notably, a literature review indicated that the carboxymethyl dextran surface used in Biacore instruments in combination with the amine coupling method is by far the most widely used immobilization strategy.[62] The proteins, small molecules and other molecules used in this thesis have been conjugated to the sensing surface using the methods presented in this section. With the aspects of surface modification for optimal biosensing, another important advantage of performing such a SPR based interaction analysis is to extract the kinetics and affinity of the biomolecular interactant pairs straightaway from the measured response. More details about the kinetic models are given in the next section of this chapter.

3.5 Surface Plasmon Resonance

3.5.1 Surface plasmon polaritons

A surface plasmon polariton (SPP) is a transverse-magnetic mode (magnetic vector is perpendicular to the direction of propagation of the wave and parallel to the plane of interface) and is characterized by its propagation constant and field distribution. The frequency ω of the longitudinal oscillations of surface plasmons is related to its wave vector β, by a dispersion relation $\omega(\beta)$.The dispersion relation shown in Fig. 3.7a never crosses the light line $\frac{\omega}{c}\sqrt{\varepsilon_M}$, so surface plasmons cannot couple with the excitation photons and are said to be non-radiative surface plasmons. The propagation constant, β can be expressed as follows:[63]

$$\beta = \frac{\omega}{c}\sqrt{\frac{\varepsilon_M \varepsilon_D}{\varepsilon_M + \varepsilon_D}} \tag{3.7}$$

Here ω is the angular frequency of the excitation light; c is the speed of light in vacuum; ε_M is the dielectric function of the metal and ε_D is the dielectric constant of the material (electrolyte) above the metal surface.[9] This equation demonstrates the propagation of surface plasmons along the interface. This is true only when the real part of ε_M is negative and its absolute value is smaller than ε_D. This condition is satisfied for many metals at its optical wavelengths. At large β, $\varepsilon_D \rightarrow -\varepsilon_M$ and the value of ω approaches the following form for free electrons.

$$\omega_{sp} = \left(\frac{\omega_p}{1+\varepsilon_M}\right)^{1/2} \tag{3.8}$$

where ω_p is the plasma frequency and is given by $(4\pi n e^2 m^{-1})^{1/2}$ with n, the bulk electron density, e is the electric charge and m is the effective mass of the electron.

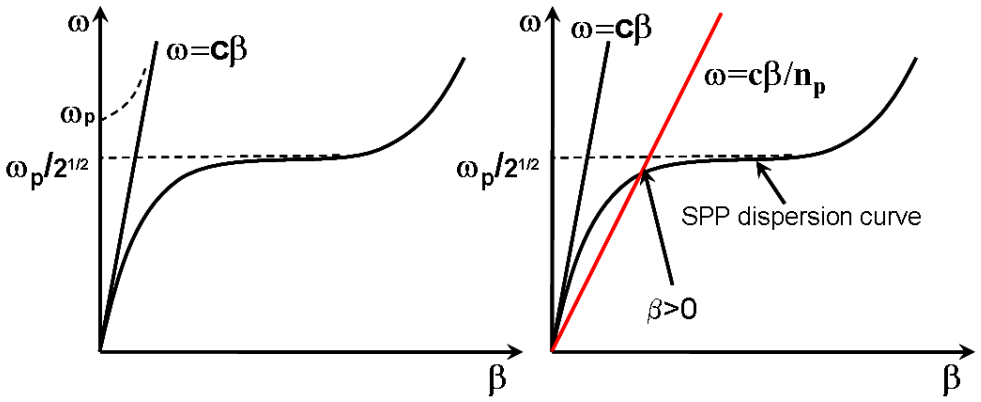

Figure 3.7 (a) No SPP generation: Illustration of dispersion relation of non-radiative surface plasmons, right of the light line $\omega=c\beta$. The dashed line, right of $\omega=c\beta$, represents surface plasmons on a metal surface coated with a dielectric film. ω_p is the starting point of the radiative surface plasmons. The dotted line represents the dispersion of light in a metal: $\omega/\beta=c/\varepsilon_D{}^{1/2}$ or in the case of free electrons $\omega^2=\omega_p{}^2+c^2\beta^2$. (b) SPP generation: Dispersion curves for surface plasmons, air ($\omega=c\beta$) and glass prism ($\omega=c\beta/n_p$, n_p is refractive index of the prism, assuming, it is independent of wavelength). Note that the curves do not intersect for air and plasmons, indicating that surface plasmon polaritons cannot be generated by direct exposure at the metal surface with the light excitation.

The metal must have conduction band electrons capable of resonating with the incoming light at a suitable wavelength. Metals that satisfy this condition in the visible spectrum are silver, gold, copper, aluminium, sodium and indium. In addition, the metal on the sensor surface must be free of oxides, sulphides and not react to other molecules on exposure to the atmosphere or liquid. Of the metals, indium is too expensive, sodium too reactive, copper and aluminium have broad SPR responses and silver is susceptible to oxidation. In most cases, gold is used because it gives a SPR signal at convenient combinations of reflectance angle and wavelength. Gold is very resistant to oxidation and other atmospheric contaminants and is compatible with many chemical modification systems. In addition, gold is chemically inert to solutions and solutes typically used in biochemical contexts.[9] The optimum thickness of the gold

should be ~50 nm. The thickness of the metal layer is of great importance. When the thickness of the metal layer increases or decreases, it has a direct impact on the penetration depth of the photons of the light on the gold layer which affects the sensitivity of the SPR measurements. Above an optimum thickness of the metal layer, the SPR dip in reflective light becomes shallow, below the optimum thickness, the dip becomes broader which is directly related to reflectivity of the light that is measured .[64]

The wavelength of light used in the SPR biosensor is very important as the optimum light wavelength tends to increase the sensitivity of the SPR instruments. Apparently, the field of the surface plasmon is concentrated at the metal-dielectric interface and decreases exponentially into both media with an increasing distance from the interface.[65] For a surface plasmon at the gold – aqueous interface, the penetration depth (the distance from the interface at which the amplitude of the field falls to *1/e* of its value at the surface) is typically 20-30 nm and 100-500 nm in metal and dielectric, respectively, in visible and near infrared regions. The surface plasmon penetration depth in the dielectric is particularly important for SPR sensing, as it determines the region probed by the SPR sensor.

3.5.2 Surface Plasmon Resonance Instrumentation

Surface plasmon resonance is a physical process that can occur when plane-polarized light hits a metal film under total internal reflection conditions.[9] The basic information about the surface plasmon polaritons has been discussed in the previous section. However, the coupling of prism leads to the SPR measurement which is discussed below. This is also of interest to understand the theoretical background behind the SPR instrumentation to study the biomolecular interactions. While one of the interactants is immobilized to the sensor surface termed as ligands, the others are free in solution and are known as analytes and passed over the surface. A typical illustration of SPR instrumentation is described in the book[66] and is shown in figure 3.8a.

According to the Kretschmann configuration (Fig. 3.8a),[67] when a light beam

hits a half circular prism, the light is bent towards the plane of interface, when it is passing from a denser medium to a less dense one. Changing the incidence angle (Θ) changes the outcoming light until a critical angle is reached. At this point, all the incoming light is reflected within the circular prism. This is called total internal reflection (TIR). Although no light is coming out of the prism in TIR, the electrical field of the photons extends about a quarter of a wavelength beyond the reflecting surface. The evanescent wave propagates along the interface with the propagation constant which can be adjusted to match that of the surface plasmon by controlling the angle of incidence light. This matching condition can be fulfilled and allows light to couple with surface plasmons. This matching method is known as attenuated total reflection (ATR) method (Fig. 3.7b). Assuming that the prism has only a minor influence on the propagation constant of the surface plasmon at the interface of the metal and a low refractive index dielectric, the coupling condition can be approximately expressed as:

$$\sqrt{\varepsilon_p}\,\sin(\theta) = \mathrm{Re}\left\{\sqrt{\frac{\varepsilon_M \varepsilon_D}{\varepsilon_M + \varepsilon_D}}\right\} \tag{3.9}$$

where θ represents the angle of incidence light, and ε_p is the dielectric constant of the prism; $\varepsilon_p > \varepsilon_D$. When the momentum of the excitation photons is equal to momentum of the surface plasmons on the gold surface, then coupling is possible and the SPP is created. When the photons get coupled to electrons on the metal surface, the reflection of light on the other side goes to minimum and is called the SPR dip (Fig. 3.8b). The SPR dip profile is converted to the respective angle shift, which is a measure of response in real time domain and is known as the sensorgram (Fig. 3.8c).

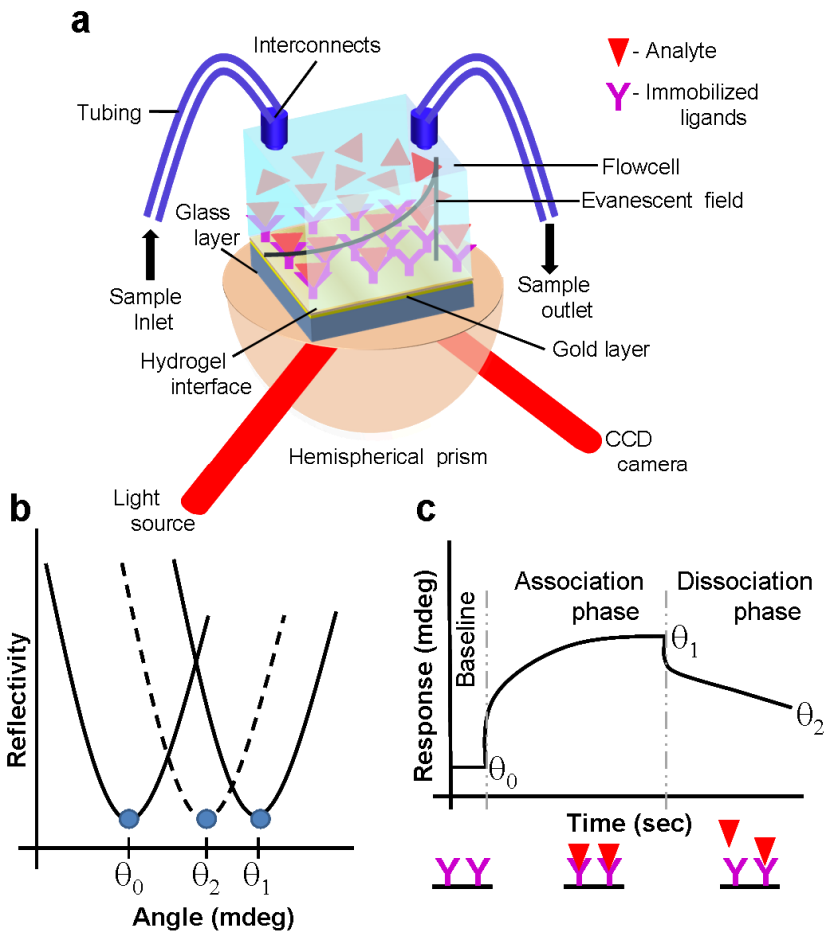

Figure 3.8 (a) Schematic illustration of SPR instrumentation; b) SPR dips from the reflectivity measured using CCD camera; c) Sensorgram showing various phases of SPR measurements.

There are three main measurement phases in the sensorgram; 1) baseline phase: a running buffer in contact with the sensor surface to establish the baseline responses, 2) association phase: sample containing the target analyte [A] is injected into the interaction chamber and the ligands [B] immobilized on the surface; the capturing element on the sensor surface binds to the target resulting in complex formation [AB], and 3) dissociation phase: injection of a running buffer again which

leads to dissociation of bound molecules from the surface.

The surface plasmon resonance angle mainly depends on the properties of the metal film, the wavelength of the incident light and the refractive index of the media on either side of the metal film.[9] Because the refractive index is sensitive to temperature, it is important to perform the measurements at defined temperatures. In some cases, this dependency can be exploited.[68] The refractive index is not dependent on the density of the media.[69] Since in experiments the metal film, the incident light and temperature are kept constant, the SPR signal is directly dependent on the change of the refractive index of the medium on the sensor side of the SPR surface.

3.6 SPR Kinetics and Data Fitting

A model is a formal representation of a chemical or physical process.[70] The model parameters represent the behavior of a particular process, and in this case include rate constants, affinities, maximum response and mass transport rate. The details of the models, parameters and data fitting will be discussed in this section.

3.6.1 First Order Model

The simplest biomolecular interaction between two proteins is modeled using the law of mass action.[70,71] The interaction between an immobilized ligand [B] and analyte [A] can be assumed to follow a pseudo first order kinetics.[72-74]

$$A + B \underset{\leftarrow\ k_d}{\overset{k_a\ \rightarrow}{}} AB \tag{3.10}$$

The interaction rate at time t may be written as

$$\frac{d[\,AB\,]}{dt} = k_a[\,A\,][\,B\,] - k_d[\,AB\,] \tag{3.11}$$

where the complex formation [AB] is called the association phase and its rate is called the association rate constant k_a (a measure of how fast the interactions are). The units of k_a are $M^{-1}s^{-1}$ and typically in the range between 10^3 and 10^7 $M^{-1}s^{-1}$ in biological systems. Dissolution of the complex is termed as the dissociation phase and its rate is

typically called the dissociation rate constant k_d (measure of how fast the interactions breaks) and its unit is s^{-1} and is typically between 10^{-1} and 10^{-6} s^{-1} in biological systems. A k_d = 0.01 s^{-1} means that 1 % of the complexes dissociate per second. The ratio of k_d and k_a is termed as dissociation constant K_D which describes the stability of the formed complex.

3.6.2 Data Analysis

An important data analysis method is "fitting" the data to a mathematical model where model parameters that represent physical phenomenon are extracted. For a linear model the model parameters can be extracted using linear regression. For non linear mathematical models more advanced techniques are employed to extract model parameters and will be described in more detail in the following sections.

3.6.2.1 Linear Regression Analysis

The process of fitting a straight line to data points with minimal global fitting error is called linear regression. Examples include Lineweaver-Burke plots of enzyme kinetics, Scatchard plots of binding data and logarithmic plots of kinetic data.[70,75] In the case of SPR, the recorded data, which is known as sensorgram, is shown in Fig. 3.8c. For a simple interaction scheme (eq. 3.5), the response at a given time R_t is given as:

$$R_t = \frac{k_a [A] R_{max}}{k_a [A] + k_d} (1 - e^{-(k_a [A] + k_d) t}) \quad (3.12)$$

$$k_{obs} = k_a . C + k_d \quad (3.13)$$

The parameter R_t is proportional to the amount of complex formed on the surface.[76,77] The change in response with respect to the change in time dR_t/dt is estimated from the obtained data and plotted against the dR_t. All the converted data should be linear and the slope obtained from this plot is k_{obs}. k_{obs} is defined as shown in equation 3.7. A plot of k_{obs} vs. analyte concentrations C (Fig. 3.9) is linearly fitted and the extracted slope dk_{obs}/dC is termed as "association rate" k_a and the intercept (when C = 0) is termed as "dissociation rate" k_d. However, due to the very small value of k_d, this method does not

give an accurate value and hence the same linearization method is followed for the dissociation phase data.[72] The reliability of kinetic data is questionable in linear analysis as the outcome of such analysis is very sensitive to mass transport limitations.[66]

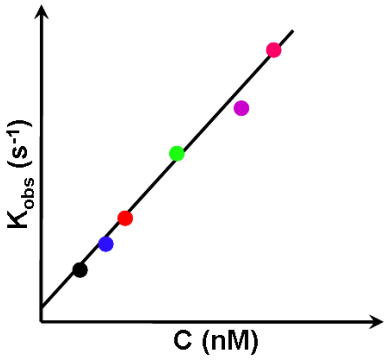

Figure 3.9 Illustration of k_{obs} analysis plot for the extraction of rate constants of the biomolecular interactions.

3.6.2.2 Non-linear Analysis

An alternative method for analyzing the SPR sensorgram data directly is using non-linear regression with the integrated rate equations,[76] which describe the entire non linear model. The classical Langmuir surface adsorption relationship[78] can be described with the following integrated rate equation[76]

$$R = R_{eq}\,(1 - e^{-(k_a C + k_d)(t - t_0)}) \qquad (3.14)$$

where R_{eq} is the response at equilibrium. R_{eq} could be measured as a function of ligand concentration and the binding data could be analyzed using Scatchard plots using the equation 3.15.

$$\frac{R_{eq}}{C_f} = K_a R_{\max} - K_a R_{eq} \qquad (3.15)$$

Here C_f is the concentration of free proteins in solution. The plot of R_{eq}/C_f vs. C_f has a slope equivalent to K_a (association constant). From this, equilibrium dissociation

constant is calculated, which is an inverse of K_a ($1/K_a$).[79]

3.6.2.3 Non linear regression

Simple rate equations can be easily integrated, however, more complex rate equations need a special approach using numerical methods. One such example is the equations with mass transport parameters. The advantage of using numerical integration, which is a non linear regression based analysis, is that one can perform global analysis of the SPR data, which means, several curves are fitted simultaneously leading to a singe robust estimation of rate constants.[80] A more detailed discussion about the non-linear regression and goodness-of-fit with respect to global fit analysis of the SPR data is presented in Chapter 4 (section 4.2).

3.6.3 Kinetic models

Choosing the right model is the most critical part of the kinetic analysis of the SPR based biomolecular interactions. It is based on several scientific facts particular to the biomolecules used, as well as underlying chemistry and physiology. Some of the details of the interactant pairs such as stoichiometry of the interaction (monovalent or multivalent), influence of transport rate, homogeneity of ligands on the surface as well as analytes, stability of the ligands, and some properties of the interactant pairs such as conformation change of molecules due to the interaction process, should be studied before choosing the model However, most of the SPR literature use a 1:1 interaction model. For all analyses in subsequent chapters, we use a 1:1 interaction model to describe the measured sensorgrams.

3.6.3.1 1:1 interaction model

The reaction between immobilized ligand [B] and analyte [A] is assumed to follow a pseudo first order kinetics[72,73,81,82] and is discussed above (section 3.6.1). It is also assumed that the binding is equivalent and independent for all binding sites.[75] The rate and differential equations (eq. 3.5) are described above. It is assumed that the

flow in the cell is sufficiently high so that there is no depletion or accumulation of analyte in solution and that the analyte concentration remains constant.

3.6.3.2 1:1 interaction model with mass transport limitation

When the biomolecular interaction is mass transport limited, binding of analyte to the ligand on the sensor chip is in principle a two step event (eq. 3.10). First, the analyte is transferred out of the bulk solution towards the sensor chip surface. Second, the binding of the analyte to the ligand takes place. The first step is also known as mass transfer and is carried out by convection and diffusion.[83] Both events have their own rate constants. The coefficient for mass transfer k_t is the same in both directions.[81] The coefficient for mass transfer can be calculated in two different ways. The one without the molecular size of the analyte is k_t. The one with the molecular size of the analyte is k_m. The reaction equation is represented as

$$A_{bulk} \underset{\leftarrow k_t}{\overset{k_t \rightarrow}{}} A_{surface} + B \underset{\leftarrow k_d}{\overset{k_a \rightarrow}{}} AB \tag{3.16}$$

Here A_{bulk} is the concentration of analyte in bulk (M); $A_{surface}$ is the concentration of analyte in surface (M); A is the concentration of free analytes (M); B, the concentration of ligands (M); k_t, coefficient of mass transfer (response units $M^{-1}s^{-1}$); k_a, association rate constant ($M^{-1}s^{-1}$); k_d, dissociation rate constant (s^{-1}). The differential equations for the inclusion of mass transport are

$$\frac{d[A_{surface}]}{dt} = k_t([A_{bulk}] - [A_{surface}]) - k_a[B].[A_{surface}] - k_d[AB] \tag{3.17}$$

$$\frac{d[B]}{dt} = k_a[A_{surface}][B] - k_d[AB] \tag{3.18}$$

$$\frac{d[AB]}{dt} = k_a[A][B] - k_d[AB] \tag{3.19}$$

3.6.4 Extracted kinetics parameters: consistency check

Model fitting is used to extract the rate parameters. An important question is:

how reliable are the extracted parameters? In the case of biomolecular interactions, simple consistency checks were discussed in the literature.[84] These are:

1. The extracted K_D from the equilibrium reaction must be the same as the K_D calculated from the individual k_a and k_d values from the association phase.

$$R_{eq} = R_{\max} \frac{C}{K_D + C} + R_0 \tag{3.20}$$

$$K_D = \frac{k_d}{k_a} \tag{3.21}$$

2. The fitted k_d in the association phase must be the same as in the dissociation phase.

$$R = R_{eq} [1 - e^{-(k_a C + k_d)}] + R_0 \tag{3.22}$$

3. The fitted observed rate constant k_{obs} in the association phase must comply with the condition:

$$R = R_t . e^{-k_a t} + R_0 \tag{3.23}$$

4. Must be aware of the fact that the evaluation software (CLAMP) calculates the k_{obs} from k_a, C and k_d.

$$k_{obs} = k_a C + k_d \tag{3.24}$$

$$k_{obs} \rangle k_d \;\&\; k_d \rangle 0 \tag{3.25}$$

3.7 References

(1) Brander C., and Tooze J.; Introduction to protein structure, Garland Publishing, New York, 1999.
(2) Bollenbach TJ., and Nowak T.; Biochemistry, 40 (2001) 13097–13106.
(3) Rensing, L.; Int. J. Biometeorol. 16 (1972) 113–125.
(4) Hunter T.;Meth. Enzymol. 200 (1991) 3–37.
(5) Cross GH., Reeves A., Brand S., Popplewell JF., Peel LL., Swann MJ., and Freeman NJ.; Biosens. Bioelectron., 19 (2003) 383-390.
(6) Höök F., Rodahl M., Brzezinski P., and Kasemo B.; J. Colloid Inter. Sci., 208 (1998) 63-67 .
(7) Attri AK., and Minton AP.; Anal. Biochem., 346 (2005) 132–138.
(8) Baianu IC., and Kumosinski T., Ch.9 in Physical Chemistry of Food Processes: Advanced Techniques and Applications. (New York: Van Nostrand-Reinhold) 2 (1993) 338–420.
(9) Raether H.; Surface Plasmons on Smooth and Rough Surfaces and on Gratings. Springer-Verlag, Berlin, Germany, 1986.
(10) Baudendistel N., Müller G., Waldeck W., Angel P., and Langowski J.; E. J. Chem. phys.

chem., 6 (2005) 984-990.
(11) Gadella TW. Jr.; FRET and FLIM techniques, 33. (2008) 560 pages.
(12) Bonvin AM.; Cur. Opin. Struct. Biol., 16 (2006) 194–200.
(13) Gray JJ.; Cur. Opin. Struct. Biol., 16 (2006) 183–193.
(14) Litman GW., Rast JP., Shamblott MJ., Haire RN., Hulst M., Roess W., Litman RT., Hinds-Frey KR., Zilch A., and Amemiya CT.; Mol. Biol. Evol. 10 (1993) 60–72.
(15) Unkeless JC., Scigliano E., and Freedman VH.; Ann. Rev. Immun., 6 (1988) 251-281.
(16) Market E., and Papavasiliou FN.; PLoS Biol., 1 (2003) 24-27.
(17) Janeway CA. Jr., Travers P., Walport M., and Shlomchik MJ.; Immunobiology. (5th ed.). Garland Publishing. 2001.
(18) Rhoades RA, and Pflanzer RG.; Human Physiology (4th ed.). Thomson Learning. 2002.
(19) DeRisi J., Penland L., Brown PO., Bittner ML., Meltzer PS., Ray M., Chen Y., Su YA., and Trent JM.; Nature Genetics, 18 (1996) 457-460.
(20) Steel LF., Haab BB., and Hanash SM.; J. Chrom. B, 815 (2005) 275-284.
(21) Debouck C., and Goodfellow PN.; Nature Genetics, 21 (1999) 48-50.
(22) Ilyin SE., Belkowski SM., and Plata-Salamán CR.; Trends in Biotech., 22 (2004) 411-416.
(23) Afshari CA., Nuwaysir EF., and Barrett JC.; Cancer Res., 59 (1999) 4759-4760.
(24) Southern EM.; J. Mol. Biol., 98 (1975) 503-517.
(25) Kulesh DA., Clive DR., Zarlenga DS., and Greene JJ.; PNAS, 84 (1987) 8453-8457.
(26) Macbeath G., and Schreiber SL.; Science, 289 (2000) 1760-1763.
(27) Yamauchi F., Kato K., and Iwata H.; Biochim. Biophy. Acta, 1672 (2004) 138-147.
(28) Ekins RP.; Clin. Chem.; 44 (1998) 2015-2030.
(29) Gosalia DN., and Diamond SL.; PNAS, 100 (2003) 8721-8726.
(30) Hoever M., and Zbinden P.; DDT, 9 (2004) 358-365.
(31) Kononen J., Bubendorf L., Kallionimeni A., Baerlund M., Schrami P., Leighton S., Torhorst J., Mihatsch MJ., Sauter G., and Kallionimeni O-P.; Nature Med., 4 (1998) 844-847.
(32) Houseman BT., and Mrksich M.; Chem. Biol., 9 (2002) 443-454.
(33) Inoue Y., Mori T., Yomanouchi G., Han X., Sonoda T., Niidome T., and Katayama Y.; Anal. Biochem., 375 (2008) 147-149.
(34) Bulyk ML.; Adv Biochem Eng Biotechnol., 104 (2007) 65-85.
(35) Brazma A., Hingamp P., Quackenbush J., Sherlock G., Spellman P., Stoeckert C., Ansorge W., Ball CA., Causton H., Glenison P., Holstege F., Kim IF., Markowitz V., Matese JC., Robinson A., Steward J., Taylor R., and Vingron M.; Nature Genetics, 29 (2001) 365 - 371.
(36) Lundquist JJ., and Toone EJ.; Chem. Rev., 102 (2002) 555-578.
(37) Corgier BP., Li F., Blum LJ., and Marquette CA.; Langmuir, 23 (2007) 8619-8623.
(38) Lokate AMC., Beusink JB., Besselink GAJ., Pruijn GJM., and Schasfoort RBM.; J. Am. Chem. Soc., 129 (2007) 14013-14018.
(39) Manz A., Harrison DJ., Verpoorte EMJ., Fettinger JC., Paulus A., Ludi H., and Widmer HM.; J. Chromatogr. 593 (1992) 253-258.
(40) Li D.; " Electrokinetics in microfluidics", Academic Press, London, 2004.
(41) Hunter RJ.; "Zeta potential in colloid science: principles and applications", Academic Press, London, 1988.
(42) Lyklema J.; "Fundamentals of interface and colloid science", Vol I and II, Academic press, London, 1995.
(43) Besselink GAJ., Vulto P., Lammertink RGH., Schlautmann S., van den Berg A., Olthuis W., Engbers GHM., and Schasfoort RBM.; Electrophoresis 25 (2004) 3705-3711.
(44) Kohlheyer D., Besselink GAJ., Lammertink RGH., Schlautmann S., Unnikrishnan S., and Schasfoort RBM.; Microfluid. Nanofluid. 1 (2005) 242-248.
(45) Ajdari A.; C. R. Physique 5 (2003) 539-546.
(46) Qiao R., and Aluru NR.; J. Micromech. Microeng. 12 (2002) 625-635.
(47) Kohlheyer D.;Microfluidic Free-Flow Electrophoresis for Proteomics-on-a-Chip, PhD

Dissertation, University of Twente (2008) ISBN: 978-90-365-2666-1.
(48) Liedberg B., Nylander C., and Lundström I.; Sens. Act. 4 (1983) 299-304.
(49) Lin JN., Chang IN., Andrade JD., Herron JN., and Christensen DA.; J. Chromatogr., (1991) 542-548.
(50) Hassan SA.; J. Phys. Chem. B, 111 (2007) 227-241.
(51) Nuzzo RG., and Allara J.; J. Am. Chem. Soc., 105 (1983) 4481-4483.
(52) Ulman A.; Thin films: self-assembled monolayers of thiols. Academic, San Diego, 1998.
(53) Löfås S., and Johnsson B.; J. Chem. Soc. Chem. Commun. 21 (1990) 1526-1528.
(54) Bergström J., Johnsson B., and Löfås S.; Sensing surfaces capable of selective biomolecular interactions, to be used in biosensor systems. Patent appl. WO90/05303, 1990.
(55) Bishop AR., and Nuzzo RG.; Curr. Opin. Colloid. Interface Sci. 1 (1996) 127.
(56) Ostuni E., Chapman RG., Holmlin RE., Takayama S., and Whitesides GM.; Langmuir 17 (2001) 5605-5620.
(57) Sigal GB., Mrksich M., and Whitesides GM.; J. Am. Chem. Soc. 120 (1998) 3464-3473.
(58) Löfås S.; Pure Appl Chem 67 (1995) 829-834.
(59) Löfås S., Malmqvist M., Rönnberg I., Stenberg E., Liedberg B., and Lundström I.; Sens. Act. B, 5 (1991) 79-84.
(60) Lundström I.; Biosens. Bioelectron. 9 (1994) 725-736.
(61) Day YSN., Baird CL., Rich RL., and Myszka DG.; Protein Sci. 11 (2002) 1017-1025.
(62) Myszka DG.; J. Mol. Recognit. 12 (1999) 390-408.
(63) Homola J., Yee SS., and Gauglitz G.; Sens. Act. B., 54 (1999) 3-15.
(64) Nagata K., and Handa H.; Real-Time Analysis of Biomolecular Interactions. Springer, Newyork, (2000).
(65) Homola, J.; Surface Plasmon resonance (SPR) biosensors and their applications in food safety and security. In Frontiers in Planar Lightwave Circuit Technology; (Ed: Janz S., Ctyroki J., Tanov S.); Springer: Cambridge, USA, (2006) 101-118.
(66) Schasfoort RBM., and Tudos AJ.; Handbook of surface plasmon resonance, RSC Publishing, UK, 2008.
(67) Bulyk ML.; Adv. Biochem. Eng. Biotechnol., 104 (2007) 65-85
(68) Roos H., Karlsson R., Nilshans H., and Persson A.; J.Mol.Recognit. 11 (1998) 204-210.
(69) Barr ES.; Am. J. Phys. 23 (1955) 623-624.
(70) Graphpad Software Graphpad Prism. (1998).
(71) Elwing H.; Biomaterials 19 (1998) 397-406.
(72) Bjorquist P., and Bostrom, S.; Throm. Res. 85 (1997) 225-236.
(73) Chaiken IM.; Anal. Biochem., 212 (1993) 457-468.
(74) Johnsson B., Löfås S., and Lindquist G.; Anal. Biochem., 198 (1991) 268-277.
(75) O'Shannessy DJ., Brigham-Burke M., Soneson KK., Hensley P., and Brooks I.; Anal. Biochem., 212 (1993) 457-468.
(76) BIACORE AB BIACORE Technology Handbook. (1998).
(77) BIACORE AB Application note 301. Bia note (1998).
(78) BIACORE AB Bia Journal Article. Bia Journal 2: 18 (1998).
(79) MacKenzie CR., Hirama T., Deng S-j, Bundlei DR., Narang SA., and Young NM.; J. Biol. Chem., 271 (1996) 1527–1533.
(80) Karlsson R., and Falt A.; J. Immunol. Methods 200 (1997) 121-133.
(81) BIACORE AB; BiaEvaluation 3.0; 1997.
(82) Jonsson U., Fagerstam L., Ivarsson B., Johnsson B., Karlsson R., Lundh K., Lofas S., Persson B., Roos H., Ronnberg I., Sjolander S., Stenberg E., Stahlberg R., Urbaniczky C., Ostlin H., and Malmqvist M.; Biotechniques; 11 (1991) 620-627.
(83) Glaser RW.; Anal. Biochem., 213 (1993) 152-161.
(84) Schuck P., and Minton AP.; Trends Biochem. Sci., 21 (1996) 458-460.
(85) Doig AJ., and Williams DH.; J. Mol. Biol., 217 (1991) 389-398.

4

Single Injection Microarray-based Biosensor Kinetics

Binding affinity of biomolecular interactions can be directly extracted from measured surface plasmon resonance biosensor sensorgrams by fitting the data to the appropriate model equations. The conventional method for affinity estimation uses a series of analytes and buffers that are injected serially to a single immobilized ligand on the sensing surface, including a regeneration step between each injection, to generate information about the binding behavior. We present an alternative method to estimate the affinity using a single analyte concentration injected to multiple ligand densities in a microarray format. This parameter estimation method eliminates the need for multiple analyte injections and surface regeneration steps, which can be important for applications where there is limited analyte serum, fragile ligand-surface attachment, or the detection of multiple biomolecule interactions. The single analyte injection approach for binding affinity estimation has been demonstrated for two different interactant pairs, β2 microglobulin/anti-β2 microglobulin (β2M) and human IgG/Fab fragments of anti-human IgG (hIgG), where the ligands are printed in a microarray format. Quantitative comparisons between the estimated binding affinities measured with the conventional method are β2M: K_D=1.48±0.28 nM and hIgG: K_D=12.6±0.2 nM and for the single injection method are β2M: K_D=1.52±0.22 nM and hIgG: K_D=12.5±0.6 nM, which are in good agreement in both cases. This chapter was modified from Anal. Methods 3 (2009) 162-169.

4.1 Introduction

A microarray is a two-dimensional array of biomolecular capture probe spots immobilized on a surface with predetermined spatial order that is an assay used for gene expression and discovery, disease diagnostics, drug discovery, biomarker discovery and toxicology. The microarray was first described in literature in the late 1970's,[1] and formally defined as a microarray in the late 1980's.[2] Since the initial application of high-throughput genomics, microarrays are being applied in different

fields, including proteomics,[3] cellomics,[4] and drug discovery,[7] as well as many different types of biomaterials, including antibodies,[5] chemicals,[6] tissues,[8] carbohydrates,[9] and peptides.[10]

Since the first report of the surface plasmon resonance imaging (iSPR) biosensor system in the late 1980's,[11] the iSPR technique is now commonly accepted as suitable for the label-free measurement of multiple simultaneous biomolecular interactions, compared to other established methods, such as the quartz crystal microbalance,[12] Suprex MALDI mass spectroscopy,[13] and kinetic capillary electrophoresis,[14] due to its compatibility with microarray substrates. Currently, there are many commercially available iSPR systems, including the Biacore flexchip,[15] GWC SPRimagerII,[16] IBIS-iSPR,[17,53] Genoptics SPRi-Lab+,[18] and also many custom-made iSPR systems.[19,20]

Biomolecular interactions measured with iSPR,[21-23] can provide binding information, such as binding quantitation and specificity, and rate and affinity constants[24] of two or more interactants, which can lead to further understanding of interactant binding. For example, in the development process of new drugs, kinetic experiments provide insights into potential drug candidates as well as the definition of lead targets.[25] Kinetic parameter estimation of biomolecular interactions from integrated microarray-iSPR is increasingly being utilized for multi-analyte or multi-ligand studies.[24-36] Table 4.1 shows a compilation of SPR-microarray studies from literature for various application areas, including protein-DNA interactions,[26,27] epitope mapping,[28,32] antibody screening,[29,31] demonstration of new imaging systems,[30,34,36] protein-carbohydrate interactions,[33] allergen-antibody interactions,[35] affinity ranking,[37] and small molecules analysis.[38]

Conventional kinetic parameter estimation is done by measuring sensor responses in a serial way by introducing a range of analyte concentrations to a fixed ligand density on the sensing surface where between each analyte injection steps, dissociation and surface regeneration steps are performed each requiring a different buffer solution. Although the conventional procedure is important for general ligand-

ligate binding parameter estimation, there are certain applications that can benefit from alternative parameter estimation methods. We present an alternative binding affinity estimation method that uses a single analyte injection and multiple ligand densities in a microarray format; different than the conventional estimation method used to extract the binding affinity. This parameter estimation method eliminates the need for multiple analyte injections and surface regeneration steps, which can be important for applications where there is limited analyte serum, fragile ligand-surface attachment, or the detection of multiple biomolecule interactions. In this article we demonstrate the effectiveness of the new method by comparing the estimated binding affinity of two well-known interactant pairs along with the conventional method. Differences between various measurement scenarios in this combination (microarray-iSPR) are discussed, as well as advantages and disadvantages of the single-injection method.

4.2 Measurement Scenarios

Three general iSPR-microarray measurement scenarios, shown in Fig. 4.1, can be defined as: i) single ligand type and density with multiple analyte concentrations (Figs. 4.1a and 4.1b) referred to as the conventional measurement, ii) multiple ligand densities with multiple analyte concentrations (Figs. 4.1c and 4.1d), and iii) multiple ligand densities and types with multiple analyte concentrations and types (Figs. 4.1e – 4.1h).

The most commonly reported SPR binding kinetics measurement, or conventional measurement, uses p analytes $[A]_p$ serially injected to a single ligand density $[B]$, where each of the p injections is separated by a surface regeneration step (Fig. 4.1a) and measurement responses are recorded over the entire experimental time. The responses are recorded as $\underline{R}_t = \left[\overline{R}_{1_t}, \overline{R}_{2_t}, \ldots, \overline{R}_{p_t}\right]$, where $\underline{R}_t$ is a matrix of p response vectors $\overline{R}_{i_t}$ for each analyte concentration i sampled over the experimental time t_e.

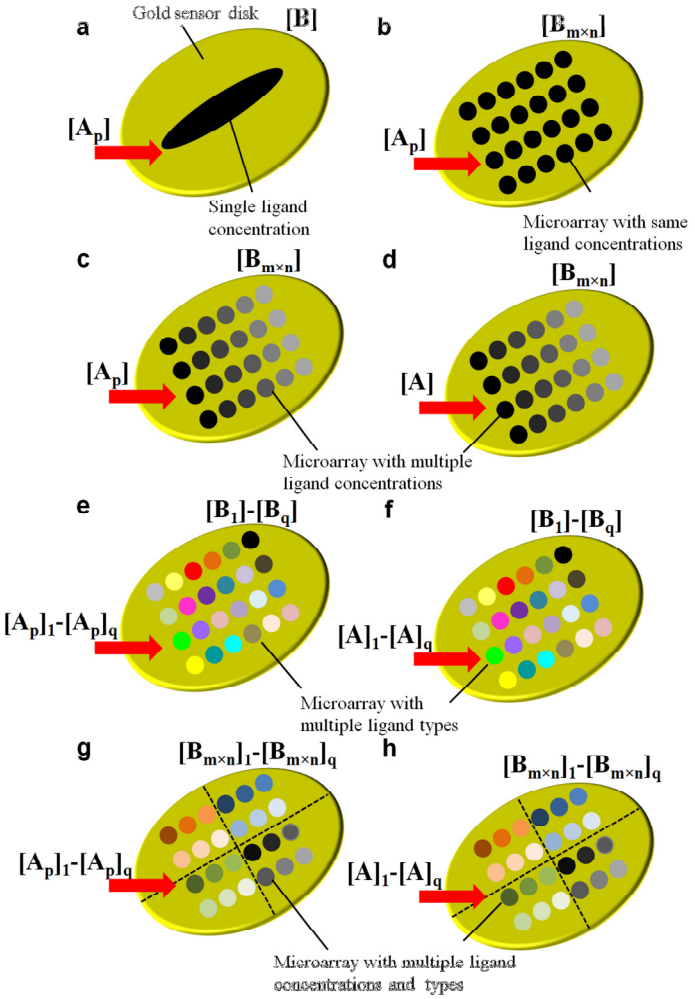

Figure 4.1 Measurement scenarios (a) Conventional method with single ligand [B] and multiple analyte concentrations [A_p] (b) Single ligand density microarray [$B_{m\cdot n}$] and multiple analyte concentrations [A_p] (c) Multiple ligand densities and multiple analyte concentrations (d) Multiple ligand density and single analyte concentration (e) Multiple ligand types [B_1]-[B_q] and multiple analyte concentrations [A_p]$_1$-[A_p]$_q$ (f) multiple ligand types [B_1]-[B_q] and multiple analyte concentrations of [A]$_1$-[A]$_q$ (g) Multiple ligand densities and types [$B_{m\cdot n}$]$_1$-[$B_{m\cdot n}$]$_q$ and multiple analyte concentrations [A_p]$_1$-[A_p]$_q$ (h) Multiple ligand densities and types [$B_{m\cdot n}$]$_1$-[$B_{m\cdot n}$]$_q$ and multiple analyte concentrations [A]$_1$-[A]$_q$. ($m\cdot n$ is multiplication of the number of row m and the number of columns n of the microarray).

Table 4.1 Reported integrated microarray-SPR measurements for various application areas using multiple analyte and ligand densities as well as multiple ligand types (Spots: regions of immobilized ligands; Ligands: target molecules immobilized on the sensor surface). The microarray arrangement of ligand spots is represented as a·b where a is the number of ligands and b is the number of times the ligand is repeated.

Ref.	No. Spots	Spot Conc.	No. Ligands	No. Analytes	Analyte Conc.	Application
26	20	Same	5·4	1	Same	Protein-DNA interaction
27	36	Same	6·6	1	Same	Protein-DNA interaction
28	54	Same	18·3	18 (1/ligand type)	Different	Epitope mapping
29	96	Same	2·36; 1·4; 1·20	4	Multiple	Antibody screening
30	900	Same	30·30	30 (1/ligand type)	Different	New iSPR system demonstration
31	8	-	1·8	386 (1/ligand type)	Different	Antibody screening
31	16	-	16·1	80 (5/ligand type)	Different and multiple	Antibody screening
32	12	-	12·1	1	Same	Epitope mapping
32	9	-	9·1	1	Same	Epitope mapping
33	8	Multi-ple	2·4	2 (1/ligand type)	Different	Protein-carbohydrate interaction
34	156	Same	12·13 Matrix+15 6 (ref.)	5	Multiple	New iSPR system demonstration
35	24	-	24·1	24 × (8/10/12)	Multiple	Allergen-antibody interactions
36	110	Same	1 sample shown	6	Multiple	New iSPR system demonstration
37	302	Same	2·151	191	Different	Affinity ranking
37	288	Same	3·96	191	Different	Affinity ranking
38	36	Same	1·6	6	Multiple	Small molecules analysis
38	36	Same	1·6 (8 comp.)	40 (5/ligand type)	Different and multiple	Small molecules analysis

Kinetic model parameters are extracted from the measured responses by finding the global-minimum of an error function, such as the “chi-square”

function $\chi^2 = \sum_{i=1}^{p}\sum_{t=0}^{t_e}\left[(R_{i_t} - f_t(a_j))/\sigma_{i_t}\right]^2$, where σ_{i_t} is the standard deviation of each data point, such that the chosen model function $f_t(a_j)$, best matches the measured responses $\underline{R}_t$ with an optimal set of model parameters a_j. This type of parameter extraction is referred to as a "global" fitting procedure since the model parameters a_j are estimated over all measured responses, which is considered a more accurate method for parameter estimation.[39] The scenario where a constant ligand density is printed in a microarray (Fig. 4.1b) is similar to the single spot ligand density (Fig. 4.1a).

The second experimental scenario consists of multiple ligand densities of the same type printed in a microarray format (Figs. 4.1c and 4.1d). For the case where both the analyte and ligand densities are varied (Fig. 4.1c), the measured responses form a three-dimensional matrix consisting of p response vectors for all $m \cdot n$ ligands $\underline{R}_t = \left[\overline{R}_{1_t}, \overline{R}_{2_t}, \ldots, \overline{R}_{m \cdot n_t}\right]_p$. The model parameters are extracted with a global fitting procedure as previously described. An interesting alternative, and the topic of this article, is the injection of a single analyte concentration, referred to as "single-injection", and using multiple ligand densities (Fig. 4.1d) to extract the model parameters. In this case, the measured response matrix contains $m \cdot n$ response vectors $\overline{R}_t = \left[R_{1_t}, R_{2_t}, \ldots, R_{m \cdot n_t}\right]$. Compared to the conventional method (Figs. 4.1a and 4.1b), this method offers some clear advantages such as a reduction in analyte sample and the elimination of regeneration steps. For example, five different analyte concentrations used in a conventional kinetics experiment, each 100 µL, requires about 500 µL of sample; a five-fold reduction in sample volume. We expect a reduction in ligand consumption using a microarray-based approach. The main disadvantage with the single analyte injection approach is that ligand surface density cannot be well controlled with conventional spotting techniques, which can be problematic if each spot requires calibration, which is usually the case when screening for binding interaction parameters, however, this limitation will diminish with improvements in

spotting techniques. From a model parameter extraction perspective, the accuracy of the fitting procedure favors the former method (Fig. 4.1c) where $m \cdot n$ response vectors is typically larger than p response vectors from multiple analyte concentrations, however, requires the greatest experimental effort and requires surface regeneration.

The third experimental scenario consists of four possibilities, shown in Figs. 4.1e-h, consisting of multi-analyte and multi-ligand measurement scenarios. In this case, multiple ligand types (Figs. 4.1e and 4.1f) with duplicates as well as multiple ligand densities (Figs. 4.1g and 4.1h) are immobilized on the surface. This approach is mainly useful in the screening of drug targets where hundreds to thousands of molecules are to be screened. These scenarios are not described in detail in this article and have been included for sake of completeness.

In this article we evaluate the single-injection kinetics method (Fig. 4.1d) and compare results from two different ligand-analyte systems with measurements from the conventional method (Fig. 4.1a/4.1b) and assess its use for actual experimental applications described in Figs. 4.1c and 4.1d.

4.3 Biomolecular Interaction Model Functions

Different biomolecular interaction models have been reported for describing SPR data including 1:1 interaction models,[39-41] 1:1 interaction model with mass transport effects,[42-44] heterogeneous ligand model,[45] decaying surface model,[46] heterogeneous analyte model,[47] avidity effects,[48] and conformation change model.[47]

The most commonly used model is the 1:1 interaction model represented by

$$A_i + B_j \underset{k_d}{\overset{k_a}{\rightleftarrows}} A_iB_j \tag{4.1}$$

where i is the number of analytes and j is the number of ligands and k_a and k_d are the association and dissociation rates, respectively. The affinity constant is defined as $K_D = k_d / k_a$ [39]. The observed SPR response signal R_t is proportional to the formation of 'AB' complexes at the surface with respect to the ligand density. Accordingly, the

maximum signal R_m represents the maximum ligand capacity that can bind with analytes without any dissociation of the *AB* complex and is proportional to the active ligand density at the surface.

From the rate equation, assuming [*A*] >> [*B*] and initial conditions $f(t=0)=0$, the model response function is $f = \alpha\left(1-e^{-\beta t}\right) = f(k_a, k_d, R_m)$, where $\alpha = k_a[A]R_m / k_a[A] + k_d$ and $\beta = -k_a[A] + k_d$ [39]. The dissociation rate constant can be evaluated using the initial condition $f_d(t=t_d) = R_0$ resulting in $f_d(t) = R_0 e^{-k_d t}$, where R_0 is the response at time t_d, the onset of the dissociation phase[39]. The simple 1:1 interaction model is used for parameter extraction in this article.

4.4 Experiments

Experiments have been performed to quantitatively compare extracted kinetic parameters K_D and R_m between the scenarios described in Figs. 4.1a/4.1b, 4.1c and 4.1d. A single ligand density, which is obtained when a ligand concentration of 250 µg/mL is exposed to the surface, was used for the conventional measurement. Additionally, the measurement scenario in Fig. 4.1c provides information about the reproducibility of the extracted affinity constants with respect to the varying ligand densities for the ligand-analyte pairs.

4.4.1 β2 Microglobulin-Monoclonal Antiβ2 Microglobulin

Experiments are performed with the interactant pair β2 Microglobulin (β2M) (Sigma, the Netherlands)/Monoclonal Antiβ2M (a-β2M) (Abcam, Cambridge, United Kingdom), which follows the 1:1 interaction model function[49]. Twenty-four β2M ligand spots were spotted (TopSpot, Biofluidics, Germany) on a sensor disk with varying ligand densities: $[B_1]$=0, $[B_2]$=250, $[B_3]$=125, $[B_4]$=62.5, $[B_5]$=31.2, and $[B_6]$=15.6 µg/mL.[17,50,53] The immobilization buffer consisted of 10 mM sodium acetate

buffer (pH 5.4) and the binding/running buffer was HBS-EP buffer (GE Healthcare/Biacore, Sweden) with pH 7.2. Prior to ligand spotting, the functionalized hydroxy gel sensor disk (HC-80m, XanTec, Germany) was activated with 400 mM EDC (Sigma, the Netherlands) and 100 mM NHS (Sigma, the Netherlands) for 20 minutes followed by rinsing with 0.25% acetic acid. The activated disk was dried for 30 minutes under continuous dry nitrogen flow. The β2M ligand was spotted on the sensor disk and incubated in a humidity chamber for one hour. Following protein immobilization, the sensor surface was blocked with 1M ethanolamine (Sigma, The Netherlands). The sensor containing the protein microarray was mounted in the IBIS-iSPR (IBIS Technologies BV, Hengelo, The Netherlands) with a drop of refractive index matching oil (n_{oil}=1.518 from Cargille Lab, USA). The system was equilibrated using 1 mL binding buffer in the flow-cell at a flow-speed of 2 µL/sec at 25^{o}C. After defining the ROIs of 30 x 30 pixels each, corresponding to 225×225 µm^2, the SPR-dip was measured automatically by the IBIS-iSPR software (IBIS Technologies BV, Hengelo, The Netherlands). A baseline measurement was made by injecting the binding buffer.

4.4.1.1 Different analyte concentrations

$[A_1]$=72, $[A_2]$=36, $[A_3]$=18, $[A_4]$=9, $[A_5]$=4.5, $[A_6]$=2.25, $[A_7]$=1.1 and $[A_8]$=0.5 nM, were prepared in the binding buffer. An iSPR image of the fabricated microarray is shown in Fig. 4.2a. The SPR dips were measured for all the 24 spots (Fig. 4.2b). Regeneration was done with 10 mM Glycine-HCl (pH 1.6) between each analyte injections in the case of multiple analyte injections. In this case, the association and dissociation profiles were measured for 900 and 600 seconds respectively.

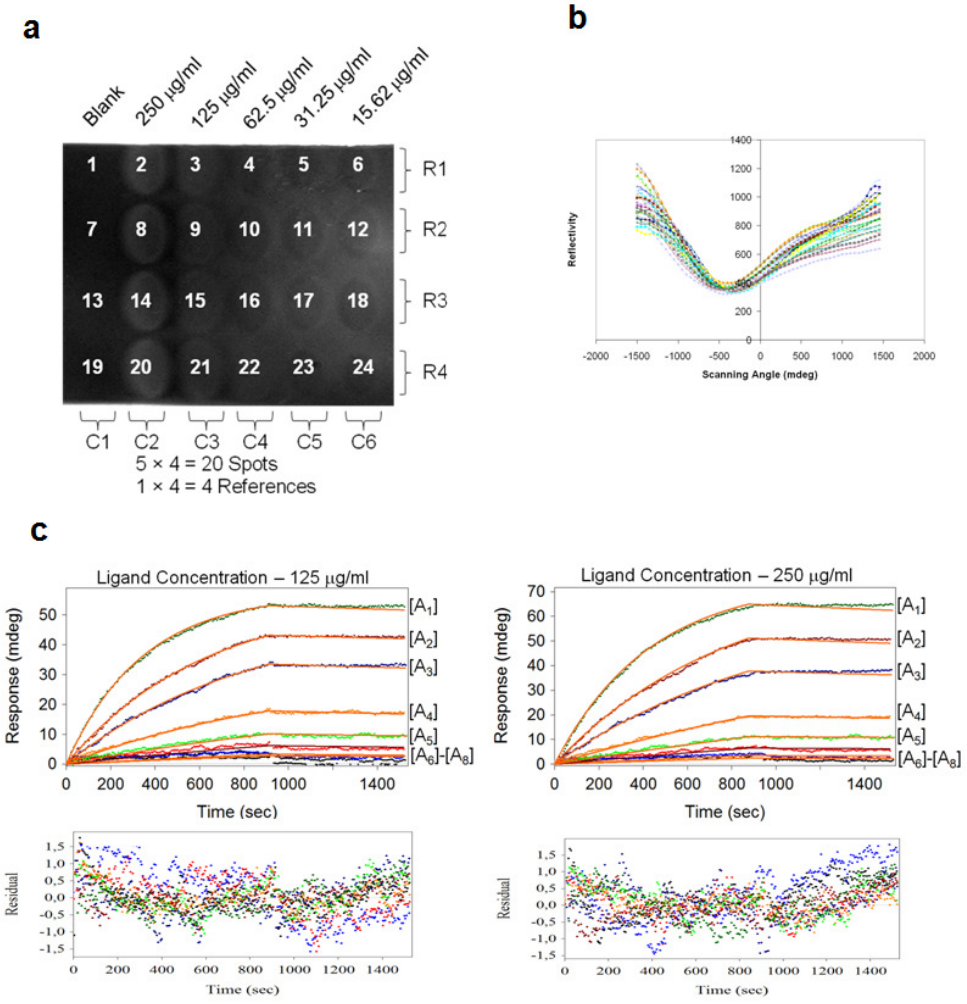

Figure 4.2 (a) Real-time image of the microarray with multiple ligand densities of β2M (b) SPR measurement dips for twenty-four ligand spots (c) Conventional kinetics estimation for ligand concentration 125 µg/mL and 250 µg/mL and different analyte concentrations [A_1]-[A_8]. The point plots represents the residual plots obtained from the results of 1:1 model fit function to the recorded iSPR data.

4.4.2 Human IgG-Fab fragments of monoclonal antihuman IgG

Experiments were also performed with Human IgG (Sigma, the Netherlands)-Fab fragments of Antihuman IgG (a-IgG) (Jacksons, UK), which follows 1:1 interaction model function[51]. Human IgG was spotted as previously described, ($[B_1]$=500, $[B_2]$=250, $[B_3]$=125, $[B_4]$=62.5, $[B_5]$=31.2 and $[B_6]$=0 μg/mL). An iSPR image is shown in Fig. 4.4a. Fig. 4.4b shows the measured SPR dips for all the 24 spots. The analyte (a-IgG) concentrations were $[A_1]$=200, $[A_2]$=100, $[A_3]$=50, $[A_4]$=25, $[A_5]$=12.5, $[A_6]$=6.25, $[A_7]$=3.1 and $[A_8]$=1.5 nM. Both association and dissociation profiles were measured for 1800 seconds in this case

4.5 Data Analysis

Data analysis was performed with the SPRint software (IBIS Technologies BV, Hengelo, The Netherlands) and kinetic parameter extraction was performed using Scrubber 2 (Biologic software, Australia).[45] All model functions are plotted in orange. The 1:1 interaction model was considered here for both the interactant pairs used in this paper. Global fit analyses was carried out for the conventional experiments whereas global fit analyses were carried out with the exception that R_m is estimated as a local fit for the single injection experiments is because of the varying ligand densities.

4.6 Results and Discussions

Experiments of scenarios in Figs. 4.1b, 4.1c and 4.1d have been performed and model parameters representing binding affinity K_D and maximum response R_m were extracted using the 1:1 interaction model.

4.6.1 β2Microglobulin-Monoclonal Antiβ2 Microglobulin

The conventional measurement profiles were observed for the ligand spot with concentration 250 μg/mL. The affinity K_D and R_m were extracted and listed in the first

column of Table 4.2. The results of various β2M concentration spots were recorded simultaneously for the whole array. Representative sensorgrams from ligand spots 14 and 15 are shown in Fig. 4.3c. Since the ligand density varies from spot to spot, the measured responses can also vary with different analyte concentration.

The single-injection measurement (Fig. 4.1d) was performed and example images and sensorgrams are shown in Figs. 4.3a and 4.3b, respectively. The affinity for each analyte concentration is listed in the third column of Table 4.2 (see appendix for more details). The R_m values are not listed in tables for the single injection kinetics approaches as different analyte concentration used has 5 different R_m values and is due the 5 different ligand densities. It is also due to the well known fact that R_m is directly proportional to ligand densities and is the indirect way to quantify the ligand spots. The varying spacing between measured responses from ligand densities $[B_2]$ and $[B_3]$ in figure 4.3 is due to the lack of precise control of the spot concentration as recently described.[52] A certain ligand density is achieved by a timed exposure of the ligand with the surface; we use the term density rather than concentration to describe the final amount of ligand. The ligand densities are directly proportional to the extracted R_m values (see appendix for more details). In figure 4.2 the values of the ligand concentration for creating the spots are given. The extracted affinities K_D are in good agreement among all three measurements shown here, as well as another recent report.[49]

For the single-injection measurement, it is important that the analyte concentration is large enough to ensure that the response signal-to-noise ratio is large enough to avoid measurement errors. Another important consideration for the single-injection approach is that at least one injection of a known analyte concentration has to be done to calibrate the analyte/ligand behavior. If the affinity constant is known, then one can easily prepare the analyte close to the affinity constant. The obtained rate constants are shown in table 4.4.

Table 4.2 Extracted K_D and R_m for different scenarios for β2M / Anti β2M interactions. The K_D unit nM in all cases.

Multi-analyte / Single-ligand (Fig. 4.1a/4.1b)	Multi-analyte / Multi-ligand (Fig. 4.1c)	Single-analyte / Multi-ligand (Fig. 4.1d)
	$[B_2]$: K_D=1.48±0.28	
	R_m=66.4±5.4mº	$[A_1]$: K_D=1.50±0.60
	$[B_3]$: K_D=1.21±0.18	$[A_2]$: K_D=1.57±0.67
	R_m=52.6±3.7mº	$[A_3]$: K_D=1.50±0.66
K_D=1.48±0.28	$[B_4]$: K_D=1.37±0.29	$[A_4]$: K_D=1.61±0.58
R_m=66.4 mº	R_m=12.8±3.6mº	$[A_5]$: K_D=1.57±0.53
	$[B_5]$: K_D=1.43±0.28	$[A_6]$: K_D=1.29±0.55
	R_m=5.9±1.0mº	$[A_7]$: K_D=1.60±0.64
	$[B_6]$: K_D=1.49±0.27	$[A_8]$: K_D=1.57±0.82
	R_m=1.6±0.9mº	
Weighted average	K_D=1.36±0.11	K_D=1.52±0.22

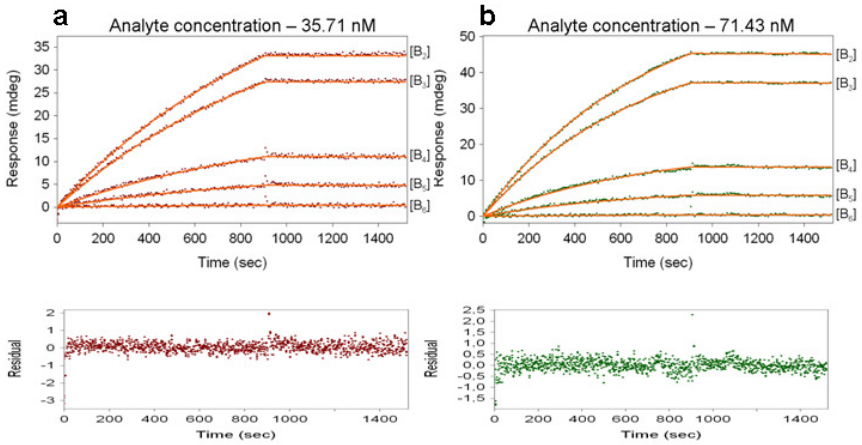

Figure 4.3 Single-injection kinetics estimation of β2M/a-β2M: Sensorgram obtained for the injection of single analyte concentration over five different ligand concentration for creating the spots (1:1 (a) a-β2M: [A]=35.71 nM (b) a-β2M: [A]=71.43 nM. Residual plots are shown for the respective analyte concentrations.

4.6.2 Human IgG-Fab fragments of monoclonal antihuman IgG

The experiment with the second interactant pair (human IgG/a-IgG) was

performed for the three measurement scenerios. Fig. 4.4c shows the recorded sensorgrams with ligand concentrations 250 and 500 µg/mL. The affinity K_D and R_m extracted with the conventional measurement are listed in the first column of Table 4.3.

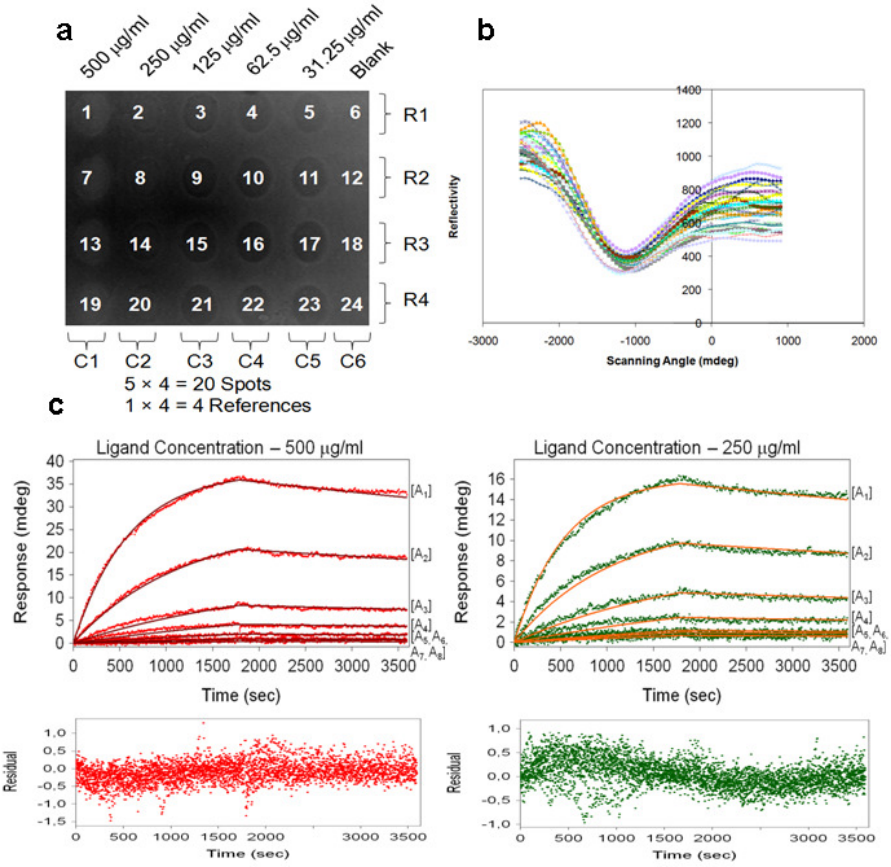

Figure 4.4. (a) Real-time SPR image of multiple concentration human IgG ligand spots (b) SPR measurement dips for twenty-four ligand spots (c) Conventional kinetics estimation (1:1 model) of 500 µg/mL and 250 µg/mL ligand spots and multiple analyte concentrations. Residual plots shown for the respective ligand concentrations.

Since the affinity is approximately 12 nM, the lower analyte concentrations can be neglected. Also mass transport affected the high concentration ligand spots when the analyte concentration is very low, as well as the low concentration spots with a high analyte concentration (results not shown). The single-injection measurement

was performed and example images and sensorgrams are shown in Figs. 4.5a and 4.5b, respectively.

The affinity for each analyte concentration is listed in the third column of Table 4.3. The extracted affinities K_D are in good agreement among all three measurements. The estimated maximum response R_m shows a systematic decrease that is proportional to the reduced ligand densities (see appendix for more details). The advantage of experimental time reduction and elimination of regeneration steps must be balanced with larger measurement errors when using the single injection approach as shown in Tables 4.2 and 4.3 for the second scenario (Fig 4.1d). This is due to the fact that ligand immobilization is not well controllable with our present spotting technique, which is done offline and the immobilization is completely due to the diffusion of molecules from liquid droplets to the sensor surface over an incubation time. The obtained rate constants are shown in table 4.4.

For the conventional measurement, the analyte concentrations are highly controllable as demonstrated by the near equidistant sensor response curves (Fig. 4.2c). The number of sample points for each scenario is also different. In general, larger sample sizes (number of samples) result in higher accuracy parameter extraction compared to smaller sample sizes. Single-injection kinetic estimations of multiple interactant pairs can reduce the time for kinetic experiments, as well as measurement costs as only a single sensor chip and single analyte injection are required.

The single-injection approach can be extended to any number of target biological systems. As long as the ligand density is small and the analyte concentration is close to the real affinity of the biomolecules, this approach can be used. Considerations to mass transport limitations, rebinding effects, steric hindrance in hydrogels and other factors that may complicate the 1:1 binding model should be taken into account and low ligand densities are always the best to determine kinetic rate constants. The application of single injection kinetics over a microarray with multiple ligand densities can lead to fast kinetic parameter estimation of many samples from the same sensor surface. Certain aspects should be considered when designing such

experiments, one of which is sample cross reactivity that can lead to inaccurate kinetic estimation.

The experiment with the second interactant pair (human IgG/a-IgG) was performed for the three measurement scenerios. Fig. 4.4c shows the recorded sensorgrams with ligand concentrations 250 and 500 µg/mL. The affinity K_D and R_m extracted with the conventional measurement are listed in the first column of Table 4.3.

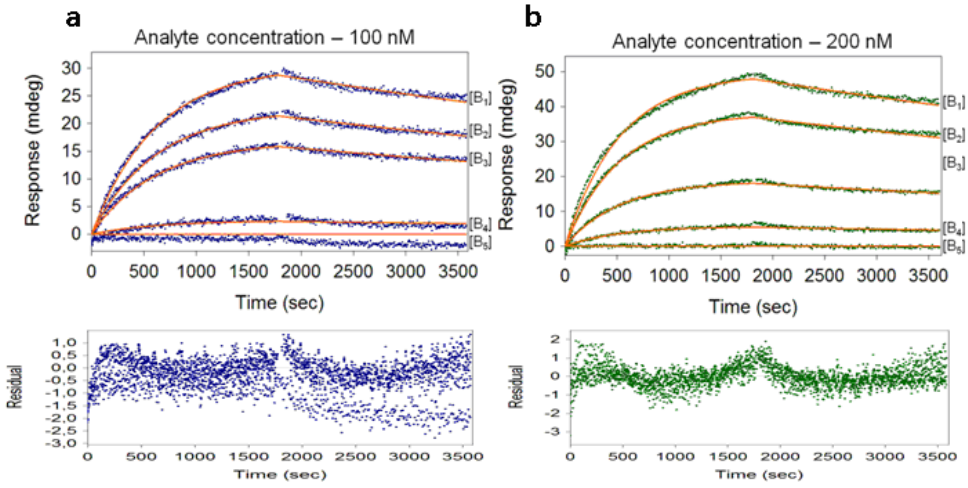

Figure 4.5 Single-injection kinetics estimation of Human IgG/a-IgG interaction: Sensorgram obtained for the injection single analyte concentration over five different ligand concentrations (1:1 (a) a-IgG: [A]=100 nM (b) a-IgG: [A]=200 nM. Residual plots shown for the respective analyte concentrations.

4.7 Conclusion

The single injection kinetics estimation method was successfully demonstrated for two well known interactant pairs with the major advantage that a reduced amount of sample is used and that the binding affinities were extracted in a couple of minutes rather than in a couple of hours compared to the conventional method. Quantitative comparisons between the estimated binding affinities measured with the conventional method are β2M: K_D=1.48±0.28 nM and HIgG: K_D=12.6±0.2 nM and for the single

injection method are β2M: K_D=1.52±0.22 nM and HIgG: K_D=12.5±0.6 nM, which are in good agreement in both cases. The extracted affinity constants in both cases were in good agreement with parameters described in literature as well as with the conventional measurement method.

Table 4.3 Extracted K_D and R_m for different scenarios for Human IgG/a-IgG interactions. The K_D unit is nM in all cases.

Multi-analyte / Single-ligand (Fig. 4.1a/4.1b)	**Multi-analyte / Multi-ligand (Fig. 4.1c)**	**Single-analyte / Multi-ligand (Fig. 4.1d)**
	[B_1]: K_D= 12.6±0.2 R_m= 43.8 mº	[A_1]: - [A_2]: -
	[B_2]: K_D=12.0±1.3 R_m= 41.0 mº	[A_3]: K_D= 11.1±3.2 [A_4]: K_D= 10.0±3.0
K_D=12.0±1.3 R_m=41.0 mº	[B_3]: K_D= 13.0±1.7 R_m= 2.6 mº	[A_5]: K_D= 12.6±4.7 [A_6]: K_D= 12.1±1.7
	[B_4]: K_D= 12.8±3.8 R_m= 1.9 mº	[A_7]: K_D= 12.9±0.8 [A_8]: K_D= 12.3±1.6
	[B_5]: K_D= 12.3±3.96 R_m= 0.8 mº	
Weighted average	K_D=12.6±0.2	K_D=12.5±0.6

Table 4.4 Estimated kinetic parameters for both the model systems (β2M / Anti β2M and hIgG/a-IgG) using conventional kinetics and single injection kinetics approaches. The number of sample points for the estimation of standard deviation is five (n = 8) for conventional approach and eight (n =5) for single injection approach.

Interactant Pairs	**Conventional Kinetics**		**Single Injection Kinetics**	
	k_a ($M^{-1} s^{-1}$)	k_d (s^{-1})	k_a ($M^{-1} s^{-1}$)	k_d (s^{-1})
β2M / Anti β2M	$(1.31 \pm 2.77) \times 10^6$	$(2.47 \pm 5.32) \times 10^{-3}$	$(2.77 \pm 4.36) \times 10^6$	$(3.52 \pm 5.64) \times 10^{-3}$
HIgG/a-IgG	$(1.42 \pm 0.69) \times 10^4$	$(1.78 \pm 0.88) \times 10^{-5}$	$(1.88 \pm 0.89) \times 10^4$	$(1.72 \pm 1.31) \times 10^{-4}$

4.8 References

(1) Southern EM.; J. Mol. Biol., 98 (1975) 503-517.
(2) Kulesh DA., Clive DR., Zarlenga DS., and Greene JJ., P. Nat. Acad. Sci., 84 (1987) 8453-8457.
(3) Macbeath G., and Schreiber SL.; Science, 289 (2000) 1760-1763.
(4) Yamauchi F., Kato K., and Iwata H.; Biochim. et Biophy. Acta, 1672 (2004) 138-147.
(5) Ekins RP.; Clin. Chem.; 44 (1998) 2015-2030.
(6) Gosalia DN., and Diamond SL.; P. Nat. Acad. Sci., 100 (2003) 8721-8726.
(7) Hoever M., and Zbinden P.; Drug Discov. Today, 9 (2004) 358-365.
(8) Kononen J., Bubendorf L., Kallionimeni A., Baerlund M., Schrami P., Leighton S., Torhorst J., Mihatsch MJ., Sauter G., and Kallionimeni O-P.; Nature Med., 4 (1998) 844-847.
(9) Houseman BT., and Mrksich M.; Chem. Biol., 9 (2002) 443-454.
(10) Inoue Y., Mori T., Yomanouchi G., Han X., Sonoda T., Niidome T., and Katayama Y.; Anal. Biochem., 375 (2008) 147-149.
(11) Rothenhaeusler B., and Knoll W.; Nature 332 (1988) 615-617.
(12) Marx KA.; Biomacromolecules, 4 (2003) 1099-1120.
(13) Ghaemmaghami S., Fitzgerald MC., and Oas TG.; P. Nat. Acad. Sci., 97 (2000) 8296-8301.
(14) Petrov A., Okhonin V., Berezovski M., and Krylov SN.; J. Am. Chem. Soc., 127 (2005) 17104-17110.
(15) Myszka DG., and Rich RL., Pharm. Sci. Technol. To., 3 (2000) 310-317.
(16) Nelson BP., Grimsrud TE., Liles MR., Goodman RM., and Corn RM.; Anal. Chem., 73 (2001) 1-7.
(17) Lokate AMC., Beusink JB., Besselink GAJ., Pruijn GJM., and Schasfoort RBM.; J. Am. Chem. Soc., 129 (2007) 14013-14018.
(18) Cherif B., Roget A., Villiers CL., Calemczuk R., Leroy V., Marche PN., Livache T., and Villiers MB.; Clin. Chem., 52 (2006) 255-262.
(19) Bassil N., Maillart E., Canva M., Levy Y., Millot MC., Pissard S., Narwa R., and Goossens M.; Sensor. Actuat. B-Chem., 94 (2003) 313-323.
(20) Mannelli I., Courtois V., Lecaruyer P., Roger G., Millot MC., Goossens M., and Canva M.; Sensor. Actuat. B-Chem., 119 (2006) 583-591.
(21) O'Shannessy DJ., Burke MB., Soneson KK., and Hensley P.; Anal. Biochem., 212 (1993) 457-468.
(22) Karlsson R., and Stahlberg R.; Anal. Biochem., 228 (1995) 274-280.
(23) Schuck P.; Annu. Rev. Bioph. Biom., 26 (1997) 541-566.
(24) Karlson R., Michaelsson A., and Mattsson L.; J. Immunol. Methods, 145 (1991) 229-240.
(25) George AJT, Gallop JL., and Rashid M.; Expert Opin. Ther. Pat., 7 (1997) 947-963.
(26) Maillart E., Brengel-Pesce K., Capela D., Roget A., Livache T., Canva M., Levy Y., and Soussi T.; Oncogene, 23 (2004) 5543-5550.
(27) Kyo M., Yamamoto T., Motohashi H., Kamiya T., Kuroita T., Tanaka T., Engel JD., Kawakami B., and Yamamoto M.; Genes cells, 9 (2004) 153-164.
(28) Baggio R., Carven GJ., Chiulli A., Palmer M., Stern LJ., and Arenas JE.; J. Biol. Chem., 280 (2005) 4188-4194.
(29) Olkhov RV., Fowke JD., and Shaw AM.; Anal. Biochem., 385 (2009) 234-241.
(30) Boozer C., Kim G., Conh S., Guan HW., and Londergan T.; Curr. Opin. Biotech., 17 (2006) 400-405.
(31) Saefsten P., Klakamp SL., Drake AW., Karlsson R., and Myszka DG.; Anal. Biochem., 353 (2006) 181-190.
(32) Wegner GJ., Lee HJ., and Corn RM.; Anal. Chem., 74 (2002) 5161-5168.

(33) Smith EA., Thomas WD., Kiessling LL., and Corn RM.; J. Am. Chem. Soc., 125 (2003) 6140-6148.
(34) Rich RL., Cannon MJ., Jenkins J., Pandian P., Sundaram S., Magyar R., Brockman J., Lambert J., and Myszka DG.; Anal. Biochem., 373 (2008) 112-120.
(35) Hantusch B., Schoell I., Harwanegg C., Krieger S., Becker WM., Spitzauer S., Boltz-Nitulescu G., and Jensen-Jarolim E.; Immunol. Lett., 97 (2005) 81-89.
(36) Van Wiggeren GD., Bynum MA., Ertel JP., Jefferson S., Robotti KM., Thrush EP., Baney DM., and Killeen KP.; Sensor. Actuat. B-Chem., 127 (2007) 341-349.
(37) Wassaf D., Kuang G., Kopacz K., Wu QL., Nguyen Q., Toews M., Cosic J., Jacques J., Wiltshire S., Lambert J., Pazmany CC., Hogan S., Ladner RC., and Nixon AE., and Sexton DJ.; Anal. Biochem., 351 (2006), 241-253.
(38) Bravman T, Bronner V., Lavie K., Notcovich A., Papalia GA., and Myszka DG.; Anal. Biochem., 358 (2006) 281-288.
(39) Chaiken IM., Rose S., and Karlsson R.; Anal. Biochem., 201 (1992) 197-210.
(40) Myszka D.G.; Curr. Opin. Biotech., 8 (1997) 50-57.
(41) Khalifa M.B., Choulier L., Jacob H.L., Altschuh D., and Vernet T.; Anal. Biochem., 293 (2001) 194-203.
(42) Schuck P.; Biophys. J., 70 (1996) 1230-1249.
(43) Myszka DG., Morton TA., Doyle M., and Chaiken IM.; Biophys. Chem., 64 (1997) 127-137.
(44) Glaser RW.; Anal. Biochem., 213 (1993),152-161.
(45) Morton TA., Myszka DG., and Chaiken IM.; Anal. Biochem., 227 (1995), 176-185.
(46) Joss L., Morton TA., Doyle ML., and Myszka DG.; Anal. Biochem., 261 (1998) 203-210.
(47) Karlsson R., and Faelt A.; J. Immunol. Methods, 200 (1997) 121-133.
(48) Baumann S., Grob P., Stuart F., Pertlik D., Ackermann M., and Suter M.; J. Immunol. Methods, 221 (1998) 95-106.
(49) Svitel J., Boukari H., Van Ryk D., Willson RC., and Schuck P.; Biophys. J., 92 (2007) 1742-1758.
(50) de Heij B., Daub M., Gutmann O., Niekrawietz R., Sandmaier H., and Zengerle R.; Anal. Bioanal. Chem., 378 (2004) 119-122.
(51) Papalia GA., Baer M., Luehrsen K., Nordin H., Flynn P., and Myszka DG.; Anal. Biochem., 359 (2006)112-119.
(52) Beusink JB.; Label-free biomolecular interaction sensing on microarrays using surface plasmon resonance imaging; PhD dissertation, University of Twente (2009).
(53) Beusink JB., Lokate AMC., Besselink GAJ., Pruijn GJM., and Schasfoort RBM.; Biosens. & Bioelec., 23 (2008) 839 – 844.

4.9 Appendix

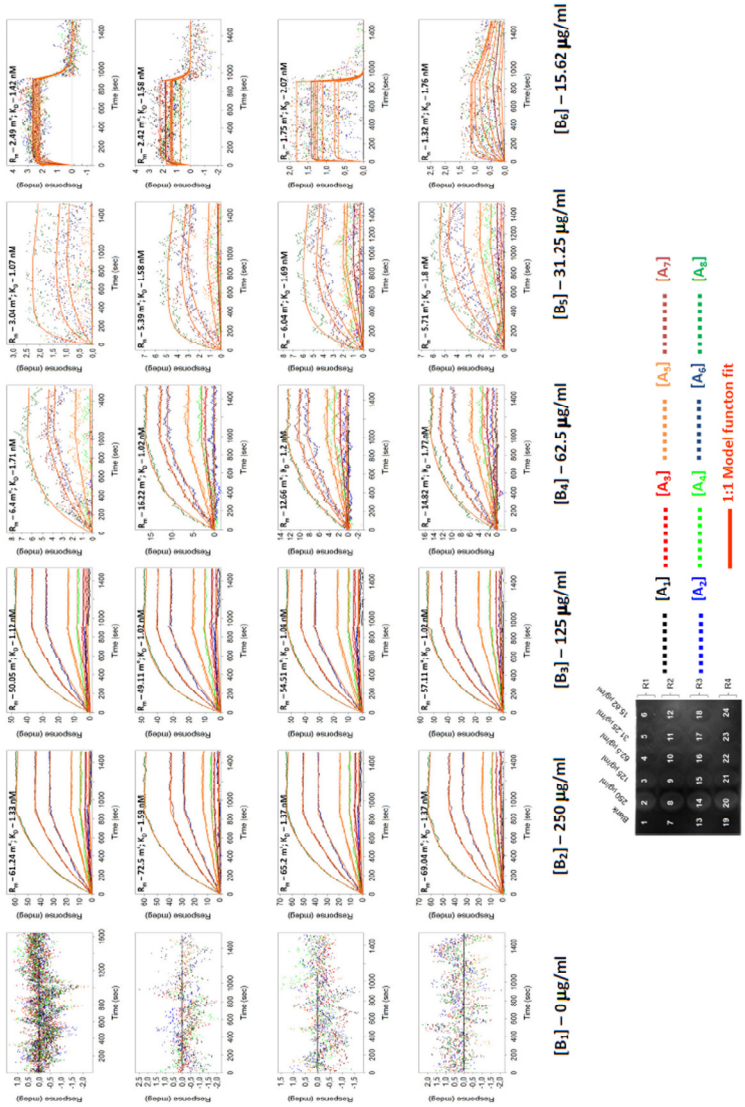

Figure 4A.1 β2M – a-β2M interaction conventional kinetics measurements using iSPR. The overlayed sensorgrams for the measured responses for the whole array is represented in array format. Various colours in each sensorgram represent various analytes injections. The real time iSPR image of the array is shown.

β2M – a-β2M interaction is explained in detail to provide extra information with respect to the article. Since the first column of figure 4A.1 represents buffer spots (spots 1, 7, 13, 19), there is hardly any reaction of analyte which also gives us information about the non-specific binding. The sensorgrams are of various shapes when the spot ligand concentrations are varied and that could be observed here (Fig. 4A.1). Here the sensorgrams with various analyte concentrations are overlayed and were fitted to the 1:1 interaction model. The respective ligand and analyte concentrations are listed in the main article. At very low spot ligand concentrations (spots 6, 12, 18, 24), the on-rates are much faster as well as faster dissociation. These sensorgrams are typical, which can be observed in the literature for this interactant pair as this might be because of the lower immobilized density (approximately 100 RU). This value corresponds with approximately 10 mdeg which is low and close to the lowest applied spot concentrations. As a rule of thumb 1000 RU SPR units corresponds to 1 ng/mm^2 protein while 1 mdeg <> 10.8 pg/mm^2 protein on the surface (according to calibration supplied by the manufacturer). So if a response is measured of 2.5 mdeg SPR angle shift then in refractive units introduced by Biacore is 25 RU. Since the ligand concentration for creating the spot is not equal to the effective immobilized ligand density because the ligand coupling is not followed in real time, proper quantification of the signal could not be performed in our case. In the article[50], the authors do not use any regeneration step as the signal goes to zero in the dissociation steps. A regeneration step for the low concentration spots is not necessary as we can see that the dissociation curves reach zero (column 6 – Fig 4A.1). But the higher ligand concentration spots need a regeneration step or a longer time for dissociation as could be seen in the sensorgrams of the higher spot concentrations (column 2, 3 and 4 of the array – Fig 4A.1). The estimated affinity for the respective spots is shown in Fig 4A.1 together with its extracted R_m values. The average K_D calculated for the whole array is 1.40 ± 0.26 nM. The obtained affinity is similar to that of the affinity listed in the literature [50]. The basic difference between GE Healthcare's Biacore instruments and IBIS systems are that the Biacore use a flow-through approach for injection of the sample whereas in the latter case in IBIS system a back and forth mixing of a small amount of sample is used. This is advantageous with respect to less sample volume consumption and high and constant mass transport rates but there is also a major disadvantage at the dissociation phase when molecules are dissociating from the surface and intrinsically increasing the concentration from zero to a certain value. Then molecules may rebind to the surface again and the off-rate will be decreased. This might be a reason that we observe some deviation in the fits of dissociation phase at higher ligand concentration spots (ligand spot numbers 2, 3, 8, 9, 14, 15, 20, 21). In the IBIS-iSPR system this problem has been solved by applying both back and forth mixing while at the same time fresh buffer is flown through the flow cell.

The single injection kinetics results are shown in Fig 4A.2. When the concentration of analyte is increased for example Fig 4A.2d for the analyte [A_4], 2 different sensorgram profiles can be observed in which for higher concentration ligand spots, the dissociation seems to be slower. This could be due to the fact that the ligand spot has reached saturation and therefore the applied ligand concentrations to create the

spots are not linearly correlated always to the effective density. The effective ligand density can be better correlated to the Rm value. The affinity constant estimated using this new approach is shown in Fig 4A.2. The overall calculated affinity is 1.53 ± 0.63 nM. This is an average value with standard deviation calculated for 4 series of data with 8 different analytes. This affinity value correlates with the value that was estimated with conventional measurements. The R_m values extrapolated in this method are not a global parameter and therefore linked with each other as the ligand density is different at each spot of the microarray. The extracted R_m values are listed in table 4A.1 with respect to various analyte concentrations for the varying ligand concentrations. Higher noise values affect the kinetic parameter extraction for low ligand density spots. K_D and R_m extracted using conventional analysis are plotted against various ligand concentrations with standard deviation (Fig 4A.3a).

The same profile was already reported for other interactant pairs.[51] K_D extracted using the single injection approach is plotted against various analyte concentrations and standard deviations (Fig 4A.3b).

The best is to restrict injection to a single analyte concentration which is close to the affinity constant value to obtain the kinetics and affinity of the interactant pairs. Normally if the affinity is unknown, then this is the first step to calibrate the interactant pairs with various analyte concentrations and single injection could be useful for a series of measurements. Also this approach is really useful for screening multiple ligands in a microarray and injection of multi-analytes leads to multiple kinetics in the same time which drastically reduces the time and costs of experiments that are in progress in our lab at present.

Table 4A.1 β2M – a-β2M interactions; R_m extrapolated from global fitting of the data for various ligand concentrations with respect to various analyte concentrations

Ligand conc. (µg/mL)	**Analyte conc. (nM)**							
	0.5	1.1	2.2	4.5	9	18	36	72
	Maximum response R_m (mdeg)							
250	1.1	4.4	6.0	29	48	52	61	77
125	1.0	1.1	1.9	9.8	22	42	46	59
62.5	3.6	1.0	3.0	4.7	4.0	6.4	7.6	10.9
31.2	0.6	0.9	3.2	1.3	2.1	3.0	3.3	3.9
15.6	2.0	0.4	0.5	0.9	0.5	0.6	1.3	1.8

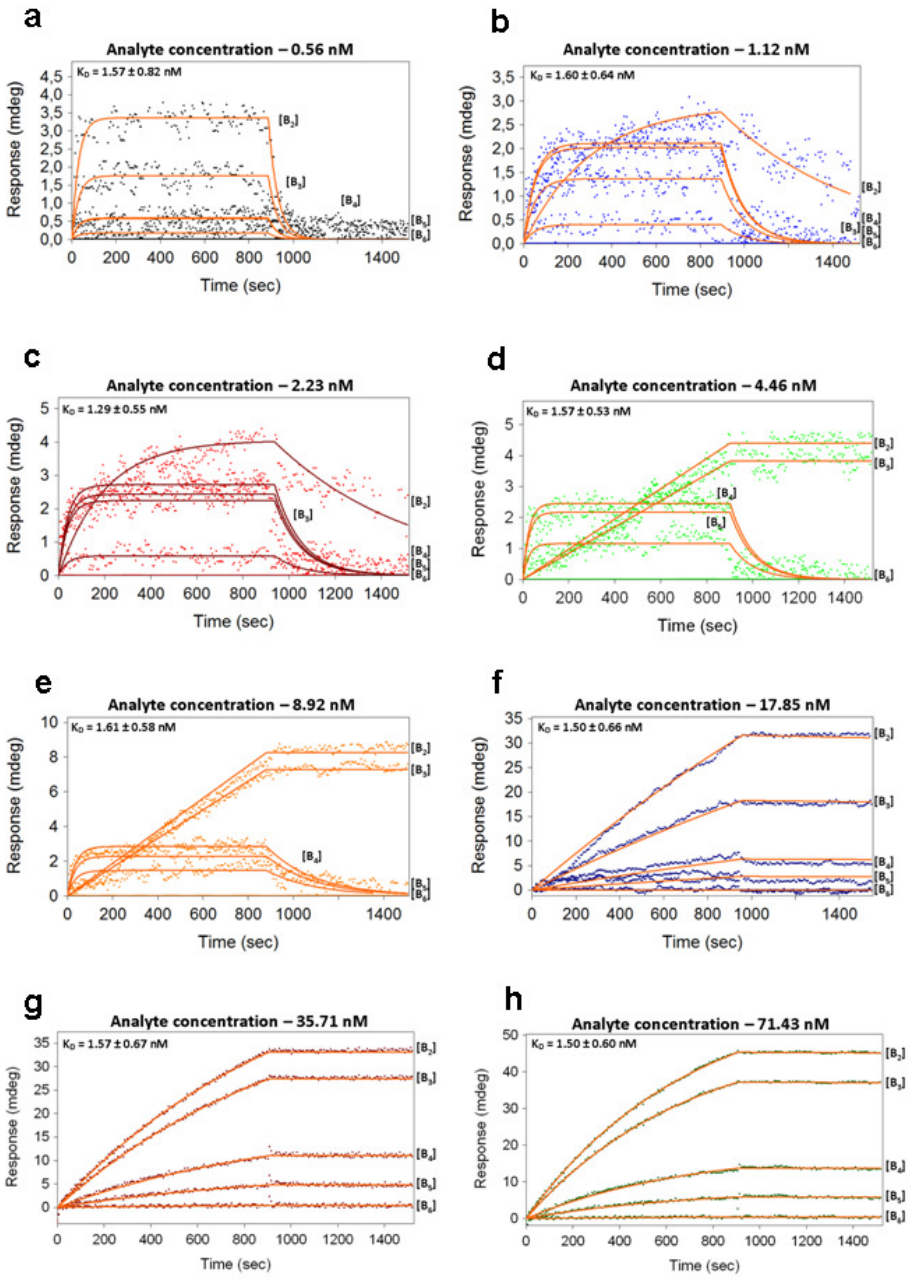

Figure 4A.2 β2M – a-β2M interaction single injection kinetics measurements using iSPR. Each plot is the representation of single injection of analyte interacted with the 5 different spots with various ligand concentrations.

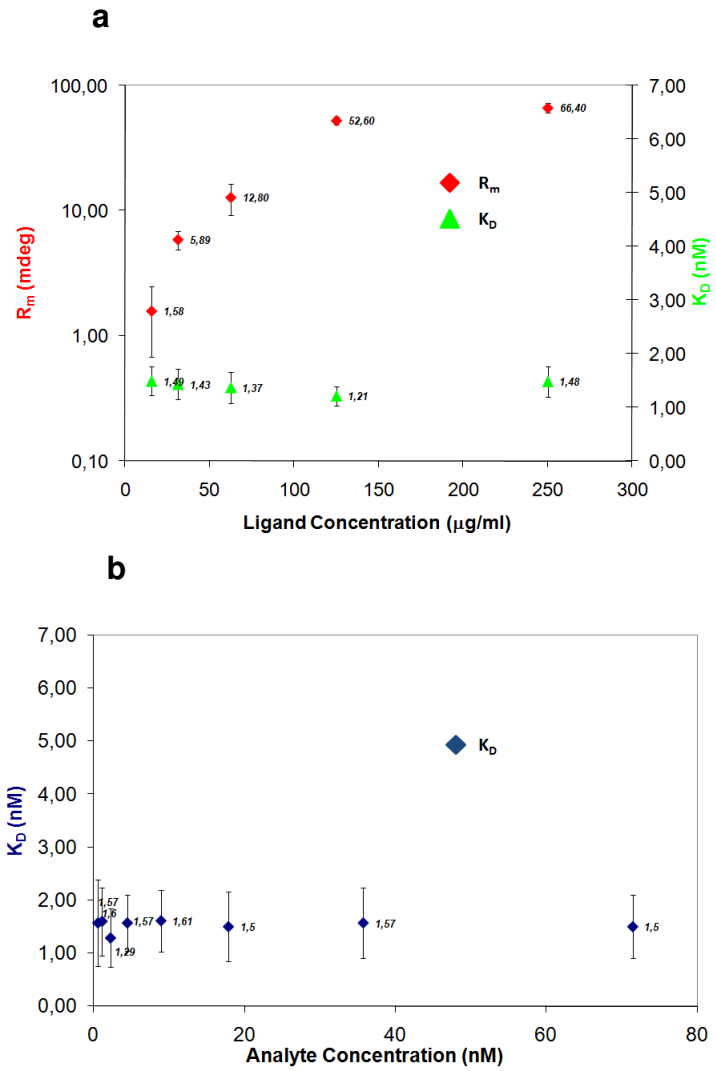

Figure 4A.3 (a) Plot of ligand concentration vs. R_m (which represents the ligand density) and K_D for the conventional kinetics measurements. (b) Plot of analyte concentration vs. K_D for the single injection kinetics measurements.

5

Multiplexed Biosensor: Parallel Kinetics Screening Assay for Multiple Biomolecular Interactions

In this chapter, we have demonstrated a method to simultaneously screen components of interest in a multiple target analyte, as well as to extract the binding affinities of all interactant pairs on a single sensor surface, using a commercially available surface plasmon resonance imaging system. For demonstration, we have prepared our sensor disk with five different ligands, varying from low molecular weight antibiotics to high molecular weight human IgG, all immobilized in a microarray format. The analyte was prepared by mixing five antibodies, where each one is highly specific for one of the immobilized ligands. A range of concentrations were prepared for the typical kinetics experiments. The major advantages of such a multiplexed assay include gradual reductions in experimental and analysis time, low cost, and flexibility since the same microarray can be used for assays with a single target analyte specific for the single ligand. A part of this chapter has been submitted as Research paper (2010).

5.1 Introduction

Biomolecular screening is normally performed using flow cytometry,[1] enzyme linked immunosorbant assay (ELISA),[2] quantum dots,[3] mass spectrometry[4] and optical biosensors such as wavelength interrogated optical biosensors[5] and surface plasmon resonance imaging (iSPR).[6-18] iSPR systems that are currently commercially available, such as, IBIS,[19] GWC,[20] Biacore,[21] and Agilent[22] appear to be useful for making such multiplexed assays with the help of microarrays.[23] This interesting combination is reported for various screening applications in biomarker discovery[19] and fragment based drug discovery[24] as well as in disease diagnostics, where small sample sizes are

required.[25] The main advantage in combining iSPR and microarrays is that each spot in the array is an individual sensing area, which can be specific for a variety of different analytes.[26] Other advantages include that is a label-free technique where real time binding kinetics information, such as the association rate (k_a) and dissociation rate constant (k_d),[27] can be directly extracted from the measured sensorgrams for each ligand spot simultaneously.

A number of application areas have been reported for the equilibrium kinetics extraction for various application areas such as DNA-RNA hybridization,[28] DNA-DNA interaction,[29] peptide-protein interactions,[30] epitope mapping,[31] protein-carbohydrate interactions,[32] polymer-enzyme studies,[33] polymer-protein interactions,[34] biomarker discovery[35] and chemical patterns through microfluidic channels for protein immobilization.[36] All of these articles deal with the injection of various concentrations of a single target analyte in serial dilutions with regeneration steps. In order to increase the throughput and reduce assay time, we propose a new approach by injecting multiple target analytes in various concentrations with regeneration steps. In this way, the kinetics and affinity can be extracted not only for single interactant pairs, but also for all the interactant pairs that are present in the analytes in parallel. This method offers several advantages compared to conventional systems including reduced sample and reagent volumes, reduced time for experimental procedures and real-time binding kinetics information for all the interactant pairs.

Multiple target analytes have been previously reported for bio-detection purposes.[37-38] We have recently reported on the advantages of a microarray integrated iSPR system for kinetic analysis.[39] Combining these two things leads to our newly proposed parallel kinetics screening approach where we use microarray with multiple types of ligands and kinetics screening experiment was performed with multi-target analytes where each target molecule in the sample are specific for every single immobilized ligand.

For demonstration of our approach, we have prepared our sensor disk with five different ligands varying from low molecular weight antibiotics to high molecular

weight human IgG. The multiple target analytes were prepared by mixing five antibodies in a single sample, where each one is highly specific for one of the immobilized ligands. Ranges of concentrations of single target analytes and also multiple target analytes were prepared for the typical kinetics experiments. The binding kinetics and affinity of interactant pairs obtained from the single target analytes acts as a reference value for the assay developed with multiple target analytes.

5.2 Material and Methods

Experiments have been performed to screen multiple biomolecular interactions and extract binding affinities from multiple biomolecular interactant pairs from an analyte solution containing multiple different targets using a single sensor surface. Various ligand types with replicates were immobilized in a microarray format. The experiments were conducted by injecting various mixtures of monoclonal antibodies and quantitatively comparing the extracted kinetic parameters k_a, k_d, R_m and $K_D = k_d/k_a$[27] with results from single target antibody samples. All experiments were conducted with serial analyte injections of varying concentrations separated by surface regeneration steps.

5.2.1 Multi-Ligand Immobilization

Prior to ligand spotting, the functionalized hydrogel sensor disk (HC-80m, XanTec, Germany) was activated with 400 mM EDC (Sigma, the Netherlands) and 100 mM NHS (Sigma, the Netherlands) for 20 minutes followed by rinsing with 0.25% (v/v) acetic acid. The activated disk was dried for 30 minutes under continuous dry nitrogen flow. Five ligand spots of 0.7 mg/mL β2-microglobulin (β2M) in sodium acetate buffer (pH 5.4), four spots of 0.5 mg/mL human IgG in MES Buffer (pH 5.4), six spots of 10 mg/mL neomycin in MES buffer (pH 4.5) and five spots of 2.5 mg/mL gentamycin in MES buffer (pH 4.5) and four spots of 1 mg/mL human IgG Fab fragments (Jacksons Immuno research, USA) in MES buffer (pH 5.4) were printed

(TopSpot, Biofluidics, Germany) on the sensor surface.[40]

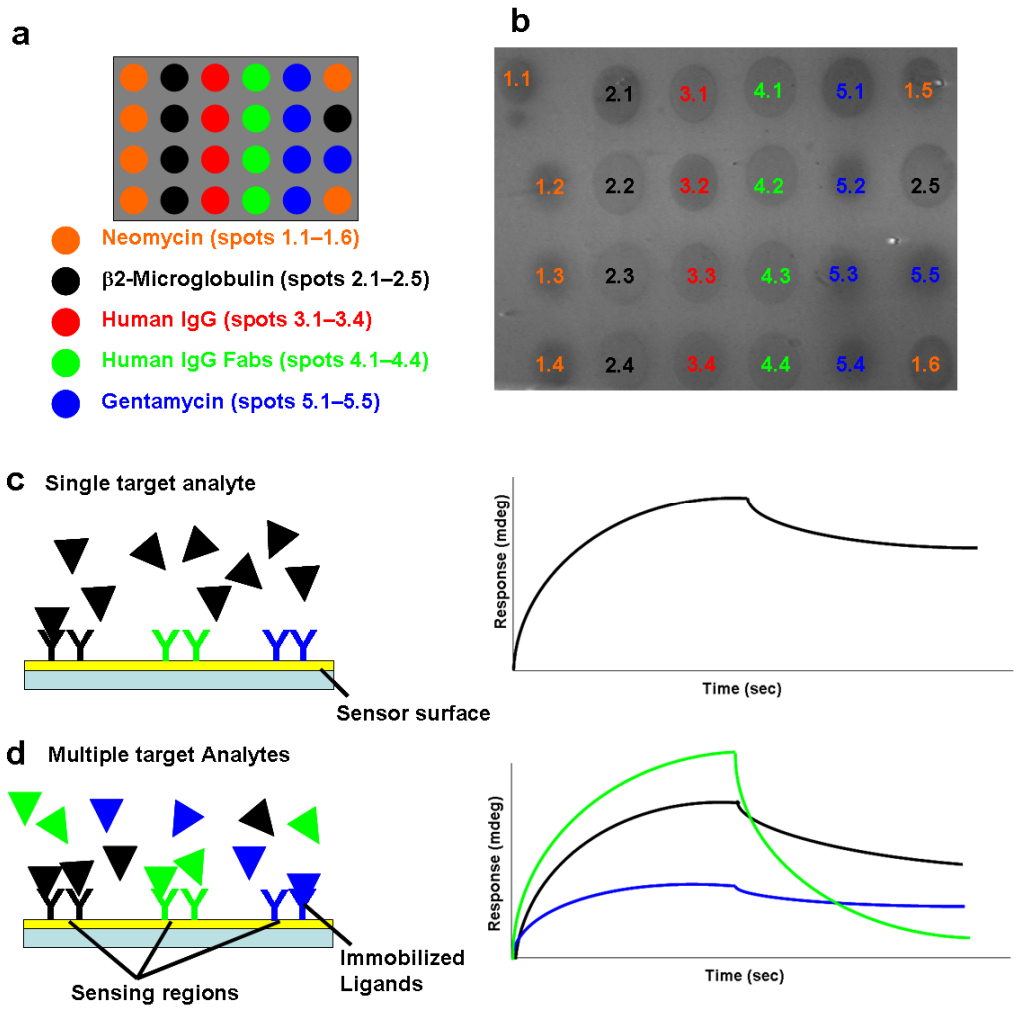

Figure 5.1 (a) Schematic illustration of the immobilized spot locations. b) Real-time iSPR image of the array of 24 immobilized spots. c) Schematic illustration of the classical experiment where single target analyte is injected over the array and its measured response for the specific spot. d) Schematic illustration of newly developed approach while injecting a multiple target analyte (each specific for different ligands immobilized) and its measured responses for all the different spots.

All the chemicals mentioned above except the human IgG Fab fragments were

purchased from Sigma, the Netherlands. The respective spot arrangements are shown in Fig. 5.1a. The fabricated microarray was incubated in a humidity chamber for one hour. Following protein immobilization, the sensor surface was blocked with 1M ethanolamine (Sigma, The Netherlands). The sensor containing the protein microarray was mounted in the IBIS-iSPR[12,14,36] (IBIS Technologies BV, Hengelo, The Netherlands) with a drop of refractive index matching oil (n_{oil}=1.518 from Cargille Lab, USA). The system was equilibrated using 1 mL binding buffer in a flow-cell at a flow-speed of 2 µL/sec at 25ºC. A representative real time iSPR image of the fabricated microarray spots is shown in Fig. 5.1b. In order to reduce the sample, buffer and regeneration solution volume to 100 µL, a back- and forth mixing technique was used. After defining the ROIs of 30 x 30 pixels each, corresponding to 225×225 μm^2, the SPR-dip was measured. A baseline measurement was made by injecting the binding buffer for 120 seconds. In addition to 24 ligand spots, 8 separate ROIs were placed on blank spaces for referencing.

5.2.2 Multi-Analyte Kinetic Screening

The various monoclonal antibodies (mAb) used in these experiments were mAb for β2-microglobulin (Abcam, UK), mAb for neomycin and mAb for gentamycin (Meridian life sciences. USA), and Fab specific antihuman IgG (Jacksons Immuno Research, USA). Polyclonal goat antihuman IgG (H+L) (Zymed, USA) was used to study the difference between the interaction of polyclonal antibody and Fab of antihuman IgG to the Fab of human IgG and human IgG respectively. Multiple target analytes as well as single target analyte were prepared in HBS-EP buffer (GE Healthcare/Biacore, Sweden). The different analyte concentrations used in these experiments are shown in Table 5.1. The first sets of experiments were performed with varying concentrations of single target analytes for the kinetic parameter estimation (Fig. 5.1c) in a serial order. The approach described in this article uses multiple target analytes (each target molecule in the mixture is specific to single immobilized ligands) from which responses of all the interactant pairs are measured simultaneously (Fig.

5.1d). Multiple target analytes used in these experiments also have the same concentrations and were prepared accordingly. Mixture 1 is a combination of mAb for neomycin, mAb for β2M, and Fab of antihuman IgG, mixture 2 is a combination of mAb for neomycin, mAb for β2M and mAb for gentamycin, and mixture 3 is a combination of all the 4 antibodies. In each case, regeneration was done with 10 mM glycine-HCl (pH 1.6) between each analyte injection. In this case, the association and dissociation profiles were measured for 1200 and 600 seconds, respectively.

Table 5.1 Analyte concentrations used in multi-ligand/multi-analyte kinetics experiment.

Sample	Antibodies	Concentrations (nM)
1	mAb β2-microglobulin	22, 44, 88, 176 and 352
2	mAb neomycin	7, 14, 28, 56 and 112
3	mAb gentamycin	5, 10, 20, 40 and 80
4	Fab antihuman IgG	33, 65, 130, 260 and 520
5	Goat antihuman IgG (H+L)	166, 332, 664, 1328 and 2656

5.2.3 Binding Kinetics Model

The 1:1 interaction model represented by $A_i + B_j \underset{k_d}{\overset{k_a}{\rightleftharpoons}} A_i B_j$, where *i* is the number of analytes and *j* is the number of ligands and k_a and k_d are the association and dissociation rates, respectively has been used for all parameter extraction. The affinity constant is defined as $K_D = k_d / k_a$.[27] The observed SPR response R_t is proportional to the formation of '*AB*' complexes at the surface with respect to the ligand density. Accordingly, the maximum signal R_m represents the maximum ligand capacity that can bind with analytes without any dissociation of the *AB* complex and is proportional to the active ligand density at the surface.

5.2.4 Data Analysis

Data analysis was performed with the SPRint software (IBIS Technologies BV., Hengelo, The Netherlands) and kinetic parameter extraction was performed using Scrubber 2 (Biologic software, Australia).[27] All model functions are plotted in orange color in the respective sensorgrams. Microsoft Excel was used to calculate the average and standard deviations.

5.3 Results and discussion

The experiments were conducted with multiple target analytes as well as single target analytes. All experiments described in this article were conducted using a single sensor disk. The details of the interaction scheme for the various analytes and ligands are shown in Table 5.2. The miniaturization of assays offers several advantages compared to conventional systems including reduced sample and reagent volumes, reduced time for experimental procedures and real-time binding information from the interactant pairs. Some disadvantages include cross-reactivity of multiple targets to the other immobilized ligands on the surface, as well as, the possibility of aggregation of biomolecules in the solution when mixed together especially for large differences in molecular weights.[38, 41]

All experiments were performed using conventional biomolecular interaction kinetics experimental approach, where a series of serially diluted analyte samples are injected over the immobilized ligands on the sensor surface. In this article, we describe the measurement of kinetics and affinity of five different interactant pairs in parallel for each injection of multiple target analytes, which can reduce the total experimental time. In conventional SPR systems, one ligand is immobilized prior to binding measurements. However in our case, the immobilization procedure is done offline, which requires sometime for the biomolecules from the 1nL solution to the surface.

Immobilization of biomolecules requires longer time in our case when compared to conventional approaches reported in the literatures. At the same time, we could use multiple ligands (approx. up to 400 spots) and all immobilized in parallel that can lead to a high throughput assay. There is no need for extra time for multi-ligand

immobilization in our case. Since all the ligands are immobilized in parallel, this reduces the amount of reagent consumed and number of sensor chips.[42] The results from the various combinations of multiple target analytes and single target analytes have been compared.

Table 5.2 Reaction scheme lists the analytes that are reactive to the specific ligand types in the array.

Experi-ments	Analytes	Immobilized Ligands				
		neo-mycin	β2M	human IgG	Fab human IgG	gentamycin
1	mAb neomycin	+	-	-	-	-
2	mAb gentamycin	-	-	-	-	+
3	mAb β2M	-	+	-	-	-
4	Fab antihuman IgG	-	-	+	+	-
5	Goat antihuman IgG (H+L)	-	-	+	+	-
6	Mixture 1	+	+	+	+	-
7	Mixture 2	+	+	-	-	+
8	Mixture 3	+	+	+	+	+

Table 5.3 Interactant pairs that follow 1:1 interaction model functions.

Experi-ments	Analytes	Immobilized Ligands				
		neo-mycin	β2M	human IgG	Fab human IgG	genta-mycin
1	mAb neomycin[43]	Yes	-	-	-	-
2	mAb gentamycin[43]	-	-	-	-	No
3	mAb β2-microglobulin[44]	-	Yes	-	-	-
4	Fab antihuman IgG[45]	-	-	No	Yes	-
5	Goat antihuman IgG (H+L) [45]	-	-	No	No	-
6	Mixture 1	Yes	Yes	No	Yes	-
7	Mixture 2	Yes	Yes	-	-	No
8	Mixture 3	Yes	Yes	No	Yes	No

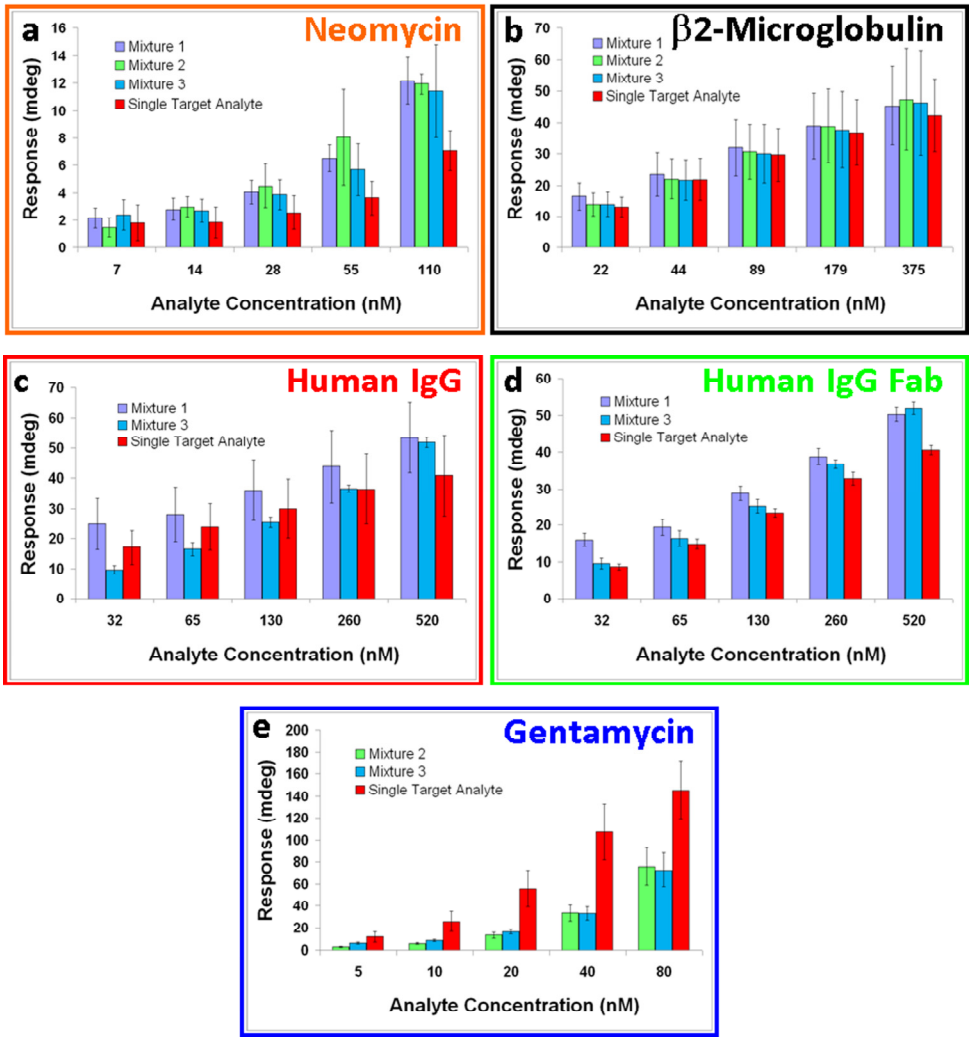

Figure 5.2 Response analysis of all the ligand-ligate pairs for varying analyte concentrations. Mixture 1 is the mixture of mAb for neomycin, mAb for β2 microglobulin and fab specific antihuman IgG. Mixture 2 is the mixture of mAb for neomycin, mAb for β2 microglobulin and mAb for gentamycin. The mixture is the combination of all the five antibodies. a) neomycin – mAb for neomycin b) β2-microglobulin – antiβ2-microglobulin pair c) human IgG – Fab of antihuman IgG d) Fab of human IgG – Fab of antihuman IgG e) gentamycin – mAb for gentamycin. The number of analytes injected is 5. The number of sample points considered for standard deviation estimation is 4.

Each of the ligands used in this experiment is spotted multiple times in order to check the reproducibility of the measurement, but another approach could be to use a serial dilution of the ligands spotted to the sensor chip. With the present spotting method for ligand immobilization, exact quantification of the spots is not possible; however, quantification is done indirectly with the extracted R_m values when the data is fitted to the model function. If the response deviations are high between spots of the same component, there is evidence that the immobilization is not uniform.

Although the 1:1 interaction model has been used to extract kinetics parameters from all interactant pairs presented in this article, some poor fits have been shown due to the fact that the biomolecule is bivalent or multivalent that can lead to various effects including avidity,[46] heterogeneity of analytes,[47] other ligand heterogeneity factors affecting the binding process includes, conformational change[47] and mass transport effects.[48] However, to demonstrate the multi-ligand/multi-analyte kinetics approach, we have considered the 1:1 interaction model in this article. Table 5.3 describes the model fit scheme for the various interactant pairs used in this article. The deviation from this model is clearly observable in some cases and explained in the respective section of this paper.

From Fig. 5.1b, spots 2.1 (β2M) and 5.1 (gentamycin) show a ligand immobilization problem, where the intensity of the SPR image is different compared to the duplicate spots of the same ligand. The heterogeneity of ligand spots is typically caused by a leakage in the microchannel in the TopSpot print head. This type of problem was also observed in the SPR dip measurement plot (not shown) for β2M and gentamycin. The initial SPR dips for the neomycin showed small variations, which can have direct influence on the responses measured during the interaction processes (results not shown).

The measured responses are plotted as bar plots (Fig. 5.2) for all individual ligand types and the standard deviation was calculated from the various ligand spots with the same concentration. These are, neomycin (Fig. 5.2a), β2-microglobulin (Fig. 5.2b), human IgG (Fig. 5.2c), Fab of human IgG (Fig. 5.2d) and gentamycin (Fig.

5.2e). The response values shown here are extracted from the various SPR sensorgrams at the transition from the association and dissociation phases (t = 1200 s). When multiple target analytes were used, the response was enhanced as previously reported.[38, 41] There is no direct co-relation between varying composition of antibodies in the mixture and the variation in enhanced response levels. However, there is not much deviation between the responses observed for the single target analyte and multiple target analytes used in the case of β2-microglobulin. Higher analyte concentrations, show larger deviations. But these deviations are lower compared to the other components used. Since the experiment was done with serial injections, the reduced signal could also be due to the regeneration steps. In reality, the numbers of regeneration steps are minimal because of the multiple target analytes used. High molecular weight components cause steric hindrances when they started to accumulate on the sensor surface, which might create pockets for other molecules to sit resulting in non-specific binding. This could be the reason for the slightly enhanced response measured in the case of multiple target analytes compared to single target analyte measurements. It does not appear to have a significant impact as there is little variation in the extracted kinetics and affinity of the interactant pairs. However, in the case of gentamycin, single target response is higher compared to the multiple target analyte samples. The exact reason for this specific difference is not known.

Sensorgrams obtained for the large analyte concentrations have been neglected in this paper as they typically deviate from the 1:1 interaction model irrespective of the valency of the biomolecules. Large analyte concentrations lead to saturation effects that can result in slightly different degrees of heterogeneity on the surface.[49] In addition, if the surface is loaded with large amounts of biomolecules then mass transport limitations can also introduce deviations from the 1:1 model behavior.[50]

Conventional kinetics experiments were performed with the fabricated microarray with varying concentrations of single target analytes. The sensorgrams and model fits are shown in Fig. 5.3 with duplicate injections of the same analyte to check the reproducibility of the fabricated spots. Neomycin results (Fig. 5.3a) indicate

antibody re-binding where response increases in the dissociation phase are evident. The re-binding effects are reproducible independent of the analyte concentration for neomycin. However, the model fit is in good agreement with the measured data in the association phase. Another reason for the increased signal in the dissociation phase may be due to the back-and-forth dissociation phase buffer flow. With a flow through approach, we have not observed such re-binding behavior (results not shown).

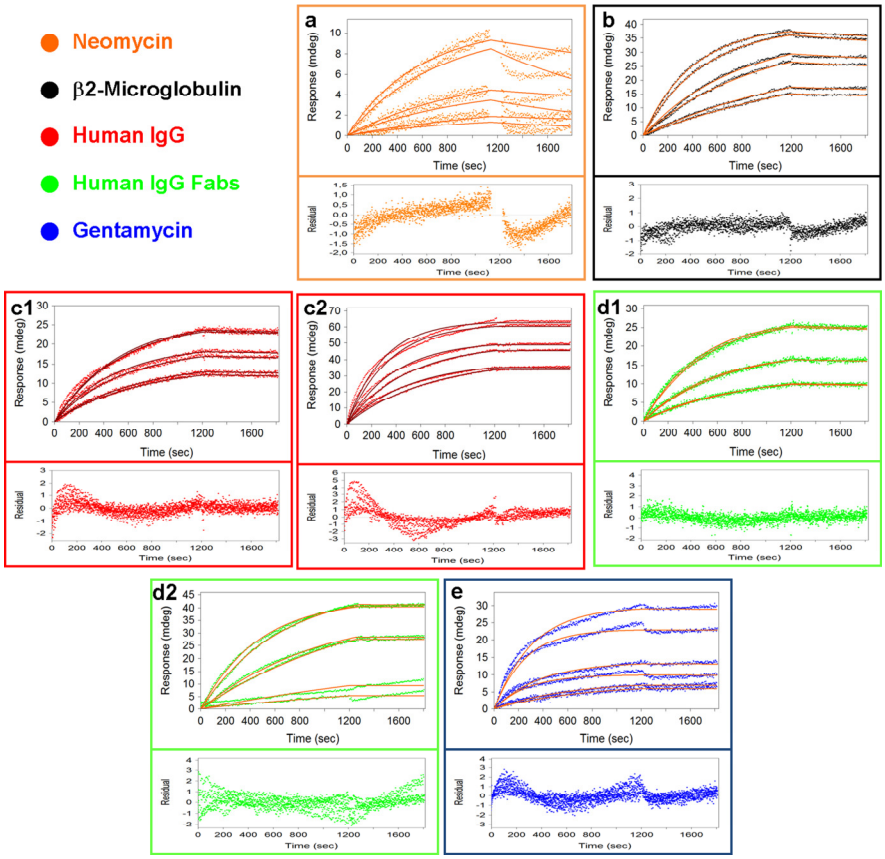

Figure 5.3 iSPR sensorgrams recorded for various analyte concentrations with duplicate injections. a) neomycin – mAb for neomycin b) β2-microglobulin – antiβ2-microglobulin pair c1) human IgG – antihuman IgG Fabs c2) human IgG – antihuman IgG d1) Fab of human IgG – Fab of antihuman IgG d2) human IgG Fab – Fab of antihuman IgG e) gentamycin – mAb for gentamycin. Orange curves show the 1:1 model fit functions.

In the cases where the measured interaction correlates well to the 1:1 model, such as β2-microglobulin (Fig. 5.3b) and human IgG Fabs (Fig. 5.3c1 and Fig. 5.3d1 & 5.3d2), the deviation between duplicate injections had a negligible effect. When both the ligand and analytes are Fab fragments, the sensorgrams are very reproducible (Fig 5.3d1) and the model fit is in good agreement with the measured responses. Therefore, it is reasonable to consider Fab fragments rather than the entire molecule when designing an assay.[45] Knowing that human IgG – antihuman IgG interactions (Fig. 5.3c2) do not follow a 1:1 interaction,[45] we have clearly observed poor fits and the sensorgrams of duplicate injections were not reproducible. Gentamycin (Fig. 5.3e) sensorgrams show a biphasic behavior and hence the fitting to 1:1 model function does not work either, as shown in the sensorgram (Fig. 5.3e). This small difference in the responses of the duplicate injections does not affect the extracted kinetics and affinity constants. The missing points in the sensorgrams (e.g. Fig. 5.3a) were removed due to spikes that were observed during the buffer change for dissociation phase measurements.

Another type of screening involves the same analyte that could be reactive to many immobilized ligands,[51] for example in drug discovery.[52] To demonstrate this, we have considered human IgG and fragments of human IgG both immobilized on the sensor surface and the experiments were conducted with Fab specific antihuman IgG and antihuman IgG. The kinetics and affinity extracted clearly show deviations in the measurements. Fab of human IgG reacts with Fab specific antihuman IgG as well as when one of the components (either ligand or analyte) is Fab (Fig. 5.3c1 & 5.3d2); thus negligible deviations in the model fit. The small deviation in the model fits observed for the high analyte concentration sensorgrams (Fig. 5.3c1) is most likely caused by higher analyte concentrations. The extraction of accurate kinetic and affinity parameter values from a polyclonal antibody with 1:1 interaction model is not possible, further experiments were performed only with monoclonal antibodies.

Mixtures of mAb for neomycin, mAb for β2M and Fab of antihuman IgG are represented as mixture 1. This mixture is reactive with 4 ligand types and is not

reactive to gentamycin spots. Fig. 5.4a shows the sensorgrams and fit obtained for neomycin spots when the spots are exposed to mixture 1 samples. This shows clearly the same behavior observed for the single analyte specific for neomycin spots. The fits to the 1:1 model in all cases are in good agreement with the resultant measured data. The slight deviation in the fits at higher concentrations of mixture 2 specific for human IgG spots (Fig. 5.4c) is due to the multi-valency of the human IgG which has 2 (H+L) sites for Fab specific antihuman IgG. As in the single analyte responses described above, β2M (Fig. 5.4b) and human IgG Fabs (Fig. 5.4d) show good agreement with measured data.

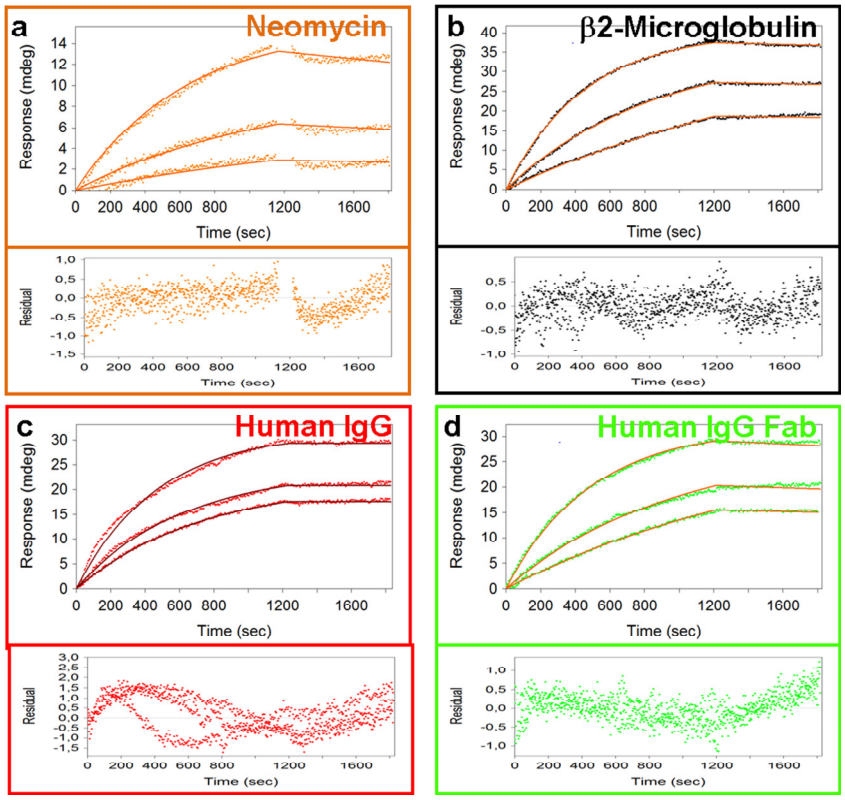

Figure 5.4 Sensorgram recorded for the injection of sample mixture 1 (mAb for neomycin, mAb for β2M and Fab of antihuman IgG). Orange curves show the 1:1 model function. a) neomycin b) β2-Microglobulin c) human IgG d) human IgG Fab.

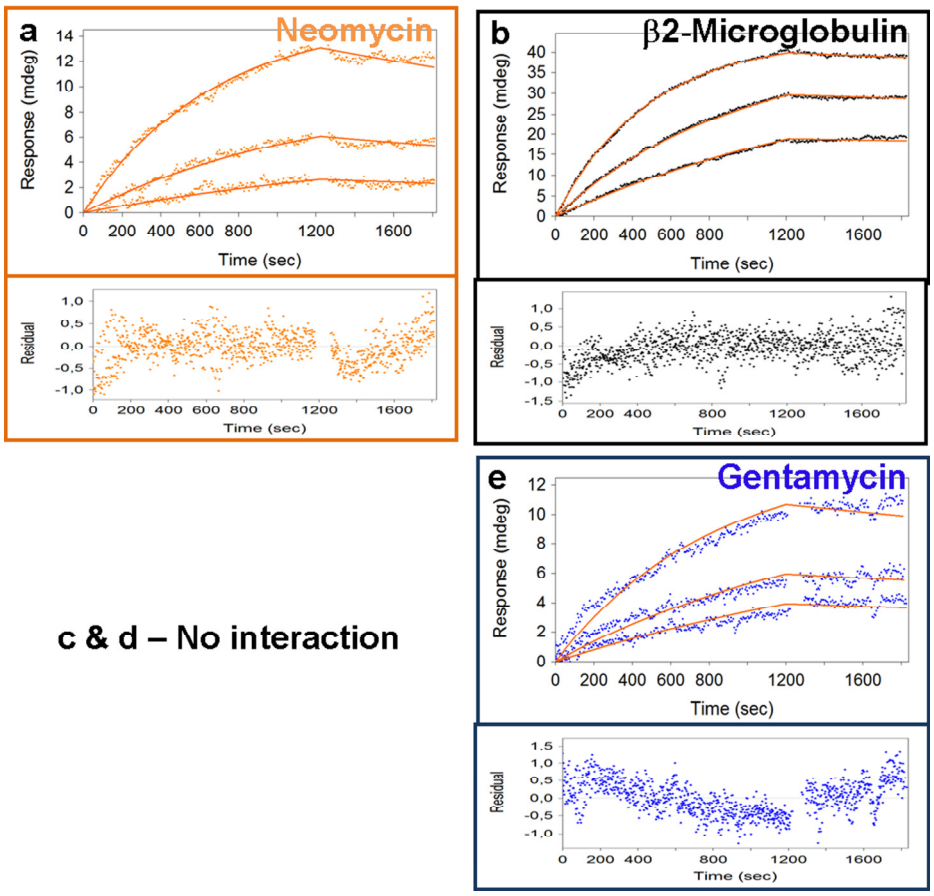

Figure 5.5 Sensorgram recorded for the injection of sample mixture 2 (mAb for neomycin, mAb for β2M and mAb for gentamycin). Orange curves show the 1:1 model function. a) neomycin b) β2-microglobulin c) & d) human IgG and human IgG Fabs - No interactions e) gentamycin.

The sample mixture 2 consists of mAb for neomycin, mAb for β2M and mAb for gentamycin. Since mixture 2 is without antihuman IgG, we don't expect any reaction with immobilized human IgG or its Fab fragments. For neomycin spots (Fig. 5.5a) and β2M spots (Fig. 5.5b), the trend with respect to the measured responses and model fit function is similar to the other sample mixtures or single target analytes. However, gentamycin responses (Fig. 5.5e) show comparatively lower measured intensity and hence the 1:1 model fit is in fair agreement with the measured data.

Additionally, biphasic behavior was not observed with the concentrations used for kinetics estimation.

The mixture of all five antibodies is represented as sample mixture 3. The resultant sensorgrams and fits are shown in Fig. 5.6. The results are quite comparable with those of the other sample mixtures (Fig. 5.6a – 5.6d), except gentamycin (Fig. 5.6e). Gentamycin spot responses are quite similar to that of the sensorgrams obtained with the other sample mixtures, however, deviates from the single target analyte specific for gentamycin. The reason for this variation is not exactly known and it could be due to the multivalent behavior of the antibody or the gentamycin molecules.

All the extracted kinetic parameters for all the sample mixtures as well as single target analytes are listed in Table 5.4. Since the re-binding effect is not considered in this parameter estimation, the extracted parameters show large variations in the case of neomycin. Since we have not considered the biphasic behavior of the gentamycin interactions, we have observed large deviations in the kinetics and affinity parameters extracted using the 1:1 interaction model. In other cases, such as, human IgG, human IgG Fabs and β2M, the extracted kinetics and affinity parameters are in very good agreement. Fab of human IgG interactions with polyclonal antihuman IgG shows higher affinity because of the multivalent behavior of the molecules and hence the dissociation becomes slower when compared to the Fab specific antihuman IgG. However, when the immobilized ligand is multivalent, as in human IgG, it does not show a large variation in the affinity constant extracted using the 1:1 interaction model when it interacts with antihuman IgG or Fab specific antihuman IgG. At present, the reason for this is not exactly known. One of the major disadvantages of a multiplexed assay is that an initial calibration is required to quantify all the interactant pairs involved in the experiments. However, this could indirectly be used as an initial screening to identify cross contamination. Optimizing regeneration conditions that should be same for all the interactant pairs is problematic in some cases and should be considered carefully.

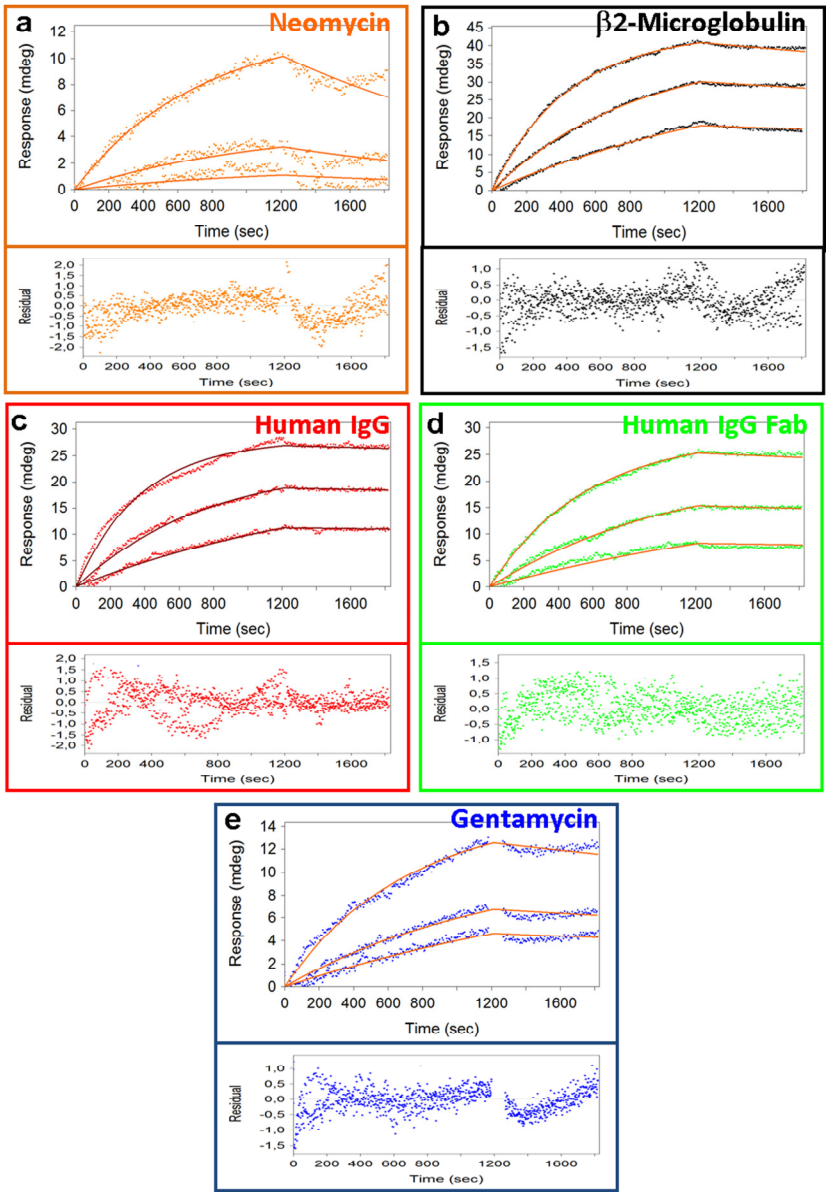

Figure 5.6 Sensorgram recorded for the injection of sample mixture 3 (mAb for neomycin, mAb for β2M, mAb for gentamycin and Fab of antihuman IgG). a) neomycin b) β2-microglobulin c) human IgG d) human IgG Fab e) gentamycin. Orange curves show the 1:1 model function.

Table 5.4 Extracted kinetic parameters with various mixtures of analytes and pure antibody samples. The number of analytes considered for kinetics estimation is 3. The number of sample points considered for standard deviation estimation is 4.

a. Mixture 1 Results

Ligand-ligate pairs	k_a x 10^4 $M^{-1}s^{-1}$	k_d s^{-1}	R_m m°	K_D nM
Neomycin	1.3 ± 0.3	(4.2 ± 2.4) x 10^{-4}	29.9 ± 4.4	30.0 ± 15.2
Microglobulin	2.8 ± 0.3	(6.7 ± 12.1) x 10^{-3}	34.2 ± 10.5	1.0 ± 0.2
HIgG	2.1 ± 0.3	(5.7 ± 2.3) x 10^{-5}	38.1 ± 10.1	2.8 ± 1.5
HIgG Fab	1.6 ± 0.2	(7.1 ± 1.5) x 10^{-5}	32.1 ± 1.1	4.3 ± 1.0

b. Mixture 2 Results

Ligand-ligate pairs	k_a x 10^4 $M^{-1}s^{-1}$	k_d s^{-1}	R_m m°	K_D nM
Neomycin	1.3 ± 0.1	(4.3 ± 2.4) x 10^{-4}	34.0 ± 8.7	31.6 ± 15.1
Microglobulin	2.3 ± 0.2	(4.4 ± 8.0) x 10^{-3}	34.5 ± 10.7	1.1 ± 0.6
Gentamycin	5.7 ± 1.5	(3.2 ± 1.5) x 10^{-4}	50.6 ± 8.4	6.1 ± 3.2

c. Mixture 3 Results

Ligand-ligate pairs	k_a x 10^4 $M^{-1}s^{-1}$	k_d s^{-1}	R_m m°	K_D nM
Neomycin	1.2 ± 0.2	(2.2 ± 0.4) x 10^{-4}	36.4 ± 9.6	18.7 ± 6.7
Microglobulin	2.3 ± 0.3	(1.1 ± 0.1) x 10^{-4}	36.7 ± 11.5	4.7 ± 0.7
HIgG	2.3 ± 0.2	(3.2 ± 0.3) x 10^{-5}	35.8 ± 9.1	1.4 ± 0.2
HIgG Fab	1.5 ± 0.3	(7.1 ± 1.6) x 10^{-5}	40.6 ± 6.6	4.5 ± 0.7
Gentamycin	6.4 ± 1.2	(1.7 ± 0.9) x 10^{-4}	41.4 ± 12.3	2.5 ± 1.1

d. Pure Component Results

Ligand-ligate pairs	k_a x 10^4 $M^{-1}s^{-1}$	k_d s^{-1}	R_m m°	K_D nM
Neomycin	1.3 ± 0.7	(3.9 ± 2.0) x 10^{-4}	38.8 ± 9.5	41.3 ± 28.4
Microglobulin	2.5 ± 8.8	(1.2 ± 3.3) x 10^{-4}	36.3 ± 9.6	5.0 ± 2.8
HIgG/AHIgGf	2.3 ± 0.3	(2.9 ± 0.2) x 10^{-5}	29.1 ± 10.7	1.3 ± 0.2
HIgG/AHIgG	0.6 ± 0.1	(5.8 ± 1.8) x 10^{-6}	66.5 ± 15.9	0.9 ± 0.3
HIgG Fab/AHIgGf	0.6 ± 0.03	(3.0 ± 0.1) x 10^{-5}	29.4 ± 2.8	5.2 ± 0.2
HIgG Fab/AHIgG	0.2 ± 0.03	(4.5 ± 0.1) x 10^{-3}	73.7 ± 8.4	1.7 ± 0.2
Gentamycin	19.0 ± 1.0	(7.7 ± 14.3) x 10^{-4}	109.9 ± 43.4	0.2 ± 0.1

The distribution of the extracted affinity was low between various ligand spots fabricated when the interactant pairs follow the 1:1 interaction model. The affinity distributions are presented by the plot of k_d versus k_a (Fig. 5.7). The deviations in the affinity constants for neomycin (Fig. 5.7a), β2M (Fig. 5.7b), human IgG (Fig. 5.7c), human IgG Fab fragments (Fig. 5.7d) and gentamycin (Fig. 5.7e) are between 10 – 100 nM, less than 1 - 10 nM, 1 – 10 nM, 4 – 6 nM and 0.1 – 15 nM, respectively. The large deviation in the neomycin and gentamycin is due to a poor fit to the 1:1 model. The distribution of affinity constants in duplicate spots might also be due to our spotting technique, which requires the diffusion of molecule from a 1nL volume to the surface over a fixed time. Other properly controlled microfluidic immobilization might avoid this problem. An important point to consider while designing such an assay is that there may be cross interaction of the analyte sample to other immobilized ligands, which can lead to inaccurate kinetics estimation. There might also be heterogeneity in the analyte sample that could lead to experimental error due to the varying molecular weights of the multiple components used in the mixture of analytes. Vigorous mixing of bio-samples typically leads to the agglomeration that can lead to steric hindrance on the sensor surface, which could block the immediate available site for the other molecules to reach. This is due to the improper orientation of immobilized ligands which cannot

be controlled precisely with the existing spotting techniques.

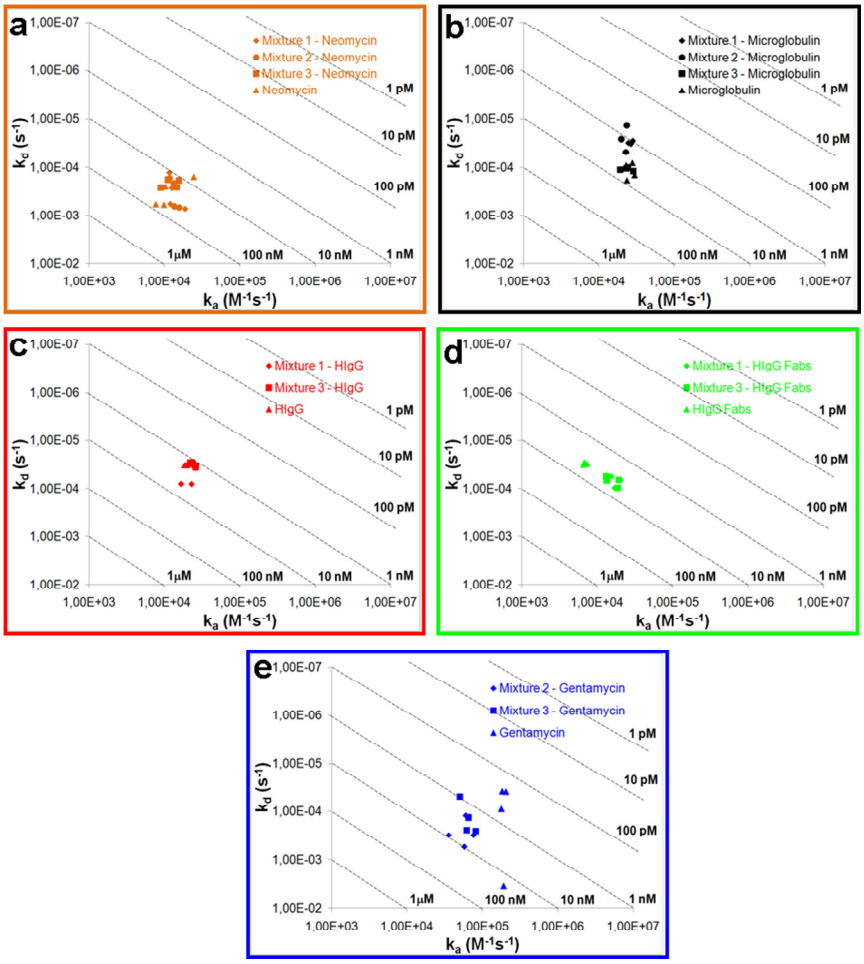

Figure 5.7 Kinetic distribution plot for various ligand-ligate pairs. The result shown here is plotted from the parameters extracted from various ligand spots and also various sample mixtures used, as well as the pure ligate components. a) neomycin – mAb for neomycin b) β2M – antiβ2M c) human IgG – antihuman IgG Fabs d) human IgG Fabs – antihuman IgG Fabs e) gentamycin – mAb for gentamycin.

5.4 Conclusion

The design of a miniaturized multi-ligand/multi-analyte kinetics screening assay was successfully demonstrated with five different interactant pairs using a single sensor surface. The kinetics and affinity parameters were extracted for all the interactant pairs, by injecting the mixture of various antibodies, which are in very good agreement with results from conventional measurements using a single analyte. The experimental time was reduced for such experiments when compared to typical kinetics experiments and this approach could be extended further to more interactant pairs. This new approach facilitates the simultaneous screening and kinetics estimation of various multi-parameter samples e.g. drug targets in the drug discovery arena and also in many other interesting fields like biomarker discovery or antibody production.

5.5 References

(1) Kellar KL., and Lannone MA.; Exp. Hematol., 30 (2002) 1227-1237.
(2) Buckler DR., Park A., Viswanathan M., Hoet RM., and Ladner RC.; Drug Discov. Today, 13 (2008) 318-324.
(3) Soman C., and Giorgio T.; Nanomed. Nanotechnol. 2009 (In press).
(4) Andrea KQ., William AL., Jayhyuk M., Can CO., James AL., and Kevin JL.; J. Biomol. Screen., 12 (2007) 473-480.
(5) Adrian J., Pasche S., Pinacho DG., Font H., Diserens J-M., Sanchez-Baeza F., Granier B., Voirin G., and Marco M-P.; Trends in Anal. Chem., 28 (2009) 769-777.
(6) Abdiche YN., Malashock DS., Pinkerton A., and Pons J.; Anal. Biochem., 386 (2009) 172-180.
(7) Boer AR-de., Hokke CH., Deelder AM., and Wuhrer M.; Glycoconjugate J., 25 (2008) 75-84.
(8) Boozer C., Ladd J., Chen S., and Jiang S.; Anal. Chem., 78 (2006) 1515-1519.
(9) Campbell CT., and Kim G.; Biomaterials, 28 (2007) 2380-2392.
(10) Dostalek J., and Homola J.; Sensor. Actuat. B-Chem., 129 (2008) 303-310.
(11) Im H., Lesuffleur A., Lindquist NC., and Oh S-H.; Anal. Chem., 81 (2009) 2854-2859.
(12) Liu J., Eddings MA., Miles AR., Bukasov R., Gale BK., and Shumaker-Parry JS.; Anal. Chem., 81 (2009) 4296-4301.
(13) Beusink JB., Lokate AMC., Besselink GAJ., Pruijn GJM., and Schasfoort RBM.; Biosens. and Bioelec., 23 (2008) 839-844.
(14) Moriarty L.; Genet. Eng. Biotechn. N., 29 (2009) Issue 2.
(15) Raz SR., Bremer MGEG., Giesbers M., and Norde W.; Biosens. and Bioelec., 24 (2008) 552-557.
(16) Stubenrauch K., Wessels U., Vogel R., and Schleypen J.; Anal. Biochem., 390 (2009) 189-196.
(17) Taylor JD., Linman MJ., Wilkop T., and Cheng Q.; Anal. Chem., 81 (2009) 1146-1153.

(18) Rothenhaeusler B., and Knoll W.; Nature, 332 (1988) 615-617.
(19) Lokate AMC., Beusink JB., Besselink GAJ., Pruijn GJM., and Schasfoort RBM.; J. Am. Chem. Soc., 129 (2007) 14013-14018.
(20) Nelson BP., Grimsrud TE., Liles MR., Goodman RM., and Corn RM.; Anal. Chem., 73 (2001) 1-7.
(21) Zimmerman B., Hahnefeld C., and Herberg FW.; Targets, 1 (2002) 66-73.
(22) VanWiggeren GD., Bynum MA., Ertel JP., Jeffereson S., Robotti KM., Thrush EP., Baney DM., and Killen KP.; Sensor. Actuat. B-Chem., 127 (2007) 341-349.
(23) Macbeath G., and Schreiber SL.; Science, 289 (2000) 1760-1763.
(24) Samantha P., David B., Jörg B., Francis M., Daniel S., and Walter H.; J. Biomol. Screen. 14 (2009) 337-349.
(25) Yager P., Domingo GJ., and Gerdes J.; Ann. Rev. Biomed. Eng., 10 (2008) 107-144.
(26) Andersson O., Nikkinen H., Kanmert D., and Enander K.; Biosens and Bioelec., 24 (2009) 2458-2464.
(27) Morton TA., Myszka DG., and Chaiken IM.; Anal. Biochem., 227 (1995) 176-185.
(28) Nelson BP., Grimsrud TE., Liles MR., Goodman RM., and Corn RM.; Anal. Chem., 73 (2001) 1-7.
(29) Wark AW., Lee HJ., and Corn RM.; Anal. Chem., 77 (2005) 3904-3907.
(30) Wegner GJ., Wark AW., Lee HJ., Codner E., Saeki T., Fang S., and Corn RM.; Anal. Chem., 76 (2004) 5677-5684.
(31) Wegner GJ., Lee HJ., and Corn RM.; Anal. Chem., 74 (2002) 5161-5168.
(32) Smith EA., Thomas WD., Kiessling LL., and Corn RM.; J. Am. Chem. Soc., 125 (2003) 6140-6148.
(33) Lee HJ., Wark AW., Goodrich TT., Fang S., and Corn RM.; Langmuir, 21 (2005) 4050-4057.
(34) Hook AL., Thissen H., and Voelcker NH.; Langmuir, 25 (2009) 9173–9181.
(35) Lee HJ., Nedelkov D., and Corn RM.; Anal. Chem. 78 (2006) 6504-6510.
(36) Shi J., Yang T., and Cremer PS.; Anal. Chem., 80 (2008) 6078-6084.
(37) Klenkar G., and Liedberg B.; Anal. Bioanal. Chem. 391 (2008) 1679-1688.
(38) Homola J., Vaisocherova H., Dostalek J., and Piliarik M.; Methods, 37 (2005) 26–36.
(39) Krishnamoorthy G., Carlen ET., Beusink JB., Schasfoort RBM., and van den Berg A.; Anal. Methods, 1 (2009) 162-169.
(40) de Heij B., Daub M., Gutmann O., Niekrawietz R., Sandmaier H., and Zengerle R.; Anal. Bioanal. Chem., 378 (2004) 119-122.
(41) Ehrlich PH., Moyle WR., Moustafa ZA., and Canfield RE.; J. Immunol., 128 (1982) 2709-2713.
(42) Haasnoot W., Cazemier G., Koets M., and van Amerongen A.; Anal. Chim. Acta., 488 (2003) 53-60.
(43) Svitel J., Boukari H., van Ryk D., Willson RC., and Schuck P.; Biophys. J., 92 (2007) 1742-1758.
(44) Papalia GA., Baer M., Luehrsen K., Nordin H., Flynn P., and Myszka DG.; Anal. Biochem., 359 (2006) 112-119.
(45) Baumann S., Grob P., Stuart F., Pertlik D., Ackermann M., and Suter M.; J. Immunol. Methods, 221 (1998) 95-106.
(46) Karlsson R., and Faelt A.; J. Immunol. Methods, 200 (1997) 121-133.
(47) Glaser RW.; Anal. Biochem., 213 (1993) 152-161.
(48) Sadana A., and Ramakrishnan A.; Sensor. Actuat. B-Chem., 85 (2002) 61-72.
(49) Mol NJ-de., Plomp E., Fischer MJ., and Ruijtenbeek R.; Anal. Biochem., 279 (2000) 61-70.
(50) Pless DD., Torres ER., Reinke EK., and Bavari S.; Infect. Immun., 69 (2001) 570-574.
(51) Rich LR., and Myszka DG; Drug Discov. Today: Technol., 1 (2004) 301-308.

6

Integrated Electrokinetic Sample Focusing and Surface Plasmon Resonance Imaging System for Measuring Biomolecular Interactions

In this chapter, we present an integrated microfluidics and iSPR platform that uses only electrokinetic transport and guiding of ligands and analytes, and therefore, requires only electrical inputs for sample transport. An important advantage of this new approach, compared to conventional systems, is the ability to direct a single analyte to a specific ligand location in the microarray, which can facilitate analysis parallelization. Additionally, this simple approach does not require complicated microfluidic channel arrangements, external pumps, or valves. As a demonstration, kinetics and affinity have been extracted from measured binding responses of human IgG and goat antihuman IgG using a simple 1:1 model and compared to responses measured with conventional pressure driven analyte transport. The measured results indicate similar binding kinetics and affinity between the electrokinetic and pressure-driven sample manipulation methods and no observable cross contamination to adjacent measurement locations has been observed. This chapter was modified from Anal. Chem., 85 (2009) 1957-1963.

6.1 Introduction

Surface plasmon resonance (SPR) and surface plasmon resonance imaging (iSPR)[1] are rapidly developing instruments for monitoring biomolecular interactions in the fields of genomics,[2,3] proteomics,[4,5] and cellomics,[6,7] where affinity and binding kinetics can be estimated directly from their measured responses.[8] The combination of SPR with microfluidics, or lab-on-a-chip (LOC) technology, is particularly compelling for bioanlytical systems[9,10] because the two techniques can be integrated relatively

easily and has the potential for fast and automated biomolecular analysis systems with ultra-small sample volumes.[11]

Integrated SPR-LOC systems are not new.[12] Commercially available SPR systems, such as the Biacore (GE Healthcare, USA)[13] and ProteOn (Bio-Rad Laboratories, USA)[14] instruments use LOC flow cells for fluid transport to their SPR systems. Additionally, there are many recent reports describing new trends and designs for integrated SPR-LOC based measurement systems[15-19] and many reports of applications for integrated LOC-SPR systems, such as, immunoassays,[20] protein-aptamer interactions[21] and cellular detection.[22] Although significant progress has been made over the last several years, more development is needed to further automate and simplify SPR-LOC systems. Additionally, the amount of sample required for diagnostic purposes can be further reduced by adopting ligand microarray formats on the SPR imaging surface, which will facilitate multi-analyte iSPR assays.[23] Integrating LOC technology to microarray based detection techniques has been previously described[24,25] and is currently an active area of research.[26-29] Commercial systems, such as Biacore's Flexchip[30] and the IBIS-iSPR (IBIS Technologies, b.v. Hengelo, Netherlands)[31,32] use a microarray approach together with an iSPR-LOC system. One of the major advantages of these new systems is that they are completely automated. However, the conventional systems use syringe pumps for sample transport, which requires a complex matrix of valves and connectors for multiple analyte analysis and it is not currently possible to guide a single analyte to a single ligand location. One way to achieve this is to use a combination of electro-osmotic flow (EOF)[33-35] for sample transport and electrokinetic focusing (EKF)[36-42] for sample guiding to specific array locations, which may be important for instrument miniaturization and scaling to larger numbers of the samples where conventional techniques will no longer be possible

A simple technique is reported here which combine EOF, for in-situ ligand immobilization and sample transport, and EKF, for sample guiding, in a LOC simultaneously with iSPR for biomolecular interaction measurements in a microarray format with multiple sites and all electrical control. For demonstration purposes, we use a single ligand type immobilized on various locations of an array with 24 gold

imaging sites (6x4 array) and a single sample is focused to each row and the subsequent real-time biomolecular interactions have been measured. We first demonstrate EKF with a sample (3% glycerol in 5 mM HEPES buffer and Rhodamine-B) focused to various location of the chip using predetermined guiding voltages. Fluorescence microscopy images of the focused flow at each location were captured in order to clearly identify the flow profile. Subsequently, the SPR signal changes were measured during sample focusing. Finally, combined EKF and iSPR is demonstrated by measuring biomolecular interactions of human IgG and goat antihuman IgG during sample focusing and results are presented and compared to iSPR measurement results with conventional pressure driven sample transport.

6.2 Materials and Methods

6.2.1 Microfabrication

The microfluidic biochip (size: 15x15 mm^2) presented here has two layers. The top PDMS layer includes channel structures, interaction chamber and reservoir holes for sample introduction and electrode interfacing. The PDMS mold was prepared in a cleanroom using a standard procedure.[43] More detailed information about the chip fabrication is described in appendix (section 6.6). The reservoir holes were manually punched with a sharp hollow tube. The bottom glass layer, refractive index matched (n=1.52) to the hemispherical prism of the iSPR instrument (IBIS Technologies b.v., Hengelo, Netherlands), has patterned gold islands for SPR imaging. The gold iSPR islands were electron beam evaporated externally (sSens b.v. Hengelo, Netherlands) and patterned on the glass layer. Following, gold island patterning, the glass chips were coated with derivatized hydrogel pre-activated for covalent immobilization (XanTec GmbH, Muenster, Germany). The PDMS chips were ultrasonically cleaned in isopropanol for 15 minutes prior to any further processing and subsequently dried with dry nitrogen and cleaned with oxygen plasma for 5 min. A thin glue (Norland Optical Adhesive 81, Norland, USA) was spin coated on a blank wafer at 8000 rpm for 60 s, which is used as the blotter for the stamp-and-stick bonding technique.[44]

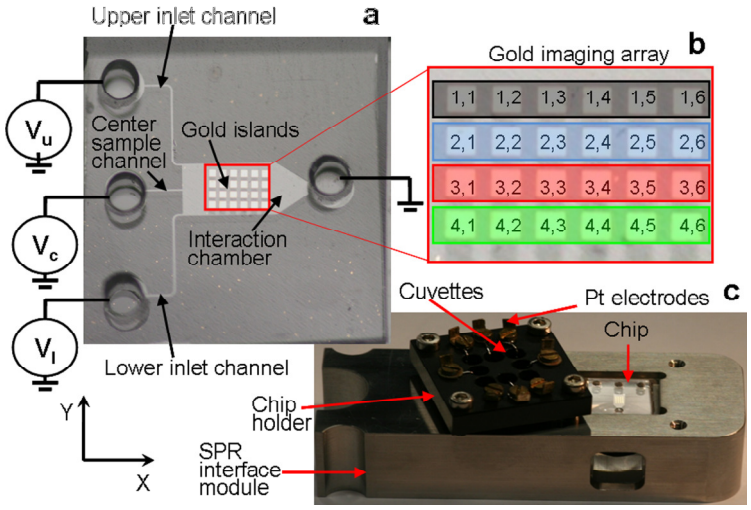

Figure 6.1 (a) Microfabricated chip with electric circuit representation (b) iSPR gold imaging array with location (row, column) (c) iSPR chip interface module comprises of SPR slider for hemispherical prism and chip with chip holder inserted with platinum electrodes for high voltage electric power supply.

The molded PDMS layers were carefully pressed into the glue blotter layer, removed and subsequently bonded to the glass chip. The bonded stack was then cured in UV light (λ=359 nm) for 45 min. The final chip is shown in Fig. 6.1a. The patterned square gold islands are 200 µm on a side and the pitch (center to center distance) is 500 µm. The thickness of the gold imaging layer is 47 nm. The thickness of the bottom glass layer is 1.1 mm and the PDMS layer is 2 mm. Each reservoir hole is 2 mm in diameter and the depth of the microchannel and interaction chamber is 35 µm. The interaction chamber has width W_{ch}= 2.5 mm and length L_{ch}=4.5 mm (Fig. 6.2).

6.2.2 Electrokinetic Focusing

The main goal of using EKF is to focus the sample stream over various rows of gold islands immobilized with ligands and to simultaneously measure the biomolecular interaction using an iSPR system. EKF in a microfluidic chip was described in detail elsewhere[38] and later reported for controlling the flow in a

microreactor.[39] In brief, EKF is a valveless and pumpless method for controlling the sample stream profile in a laminar flow chamber. A schematic illustration of EKF is shown in Fig. 6.2a, where the sample from the center inlet is focused to the second row r_2 of the gold island imaging array. An equivalent electrical circuit is shown in Fig. 6.2b where resistances R_i are determined by sample conductivity and channel dimensions.

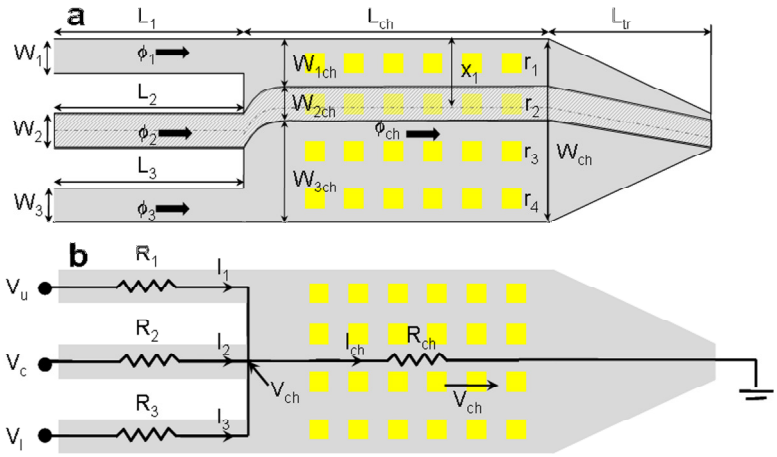

Figure 6.2 (a) Schematic illustration of the EKF chip and corresponding parameters. Example shows EKF to row 2. Here, r_1, r_2, r_3 and r_4 represent row 1 through row 4. The microchannel widths are W_1, W_2 and W_3, and the reaction chamber width is W_{ch}. W_{1ch}, W_{2ch} and W_{3ch} are the width of the top guiding stream, sample stream and bottom guiding stream, respectively. ϕ_1, ϕ_2, ϕ_3 and ϕ_{ch} represent the flux in channel 1, channel 2, channel 3 and reaction chamber, respectively. L_1, L_2, L_3, L_{ch}, and L_{tr} are the length of channel 1, channel 2, channel 3, rectangular chamber and trapezoid, respectively. X_1 is the distance from the top of chip to the center of the sample stream. (b) Electrical circuit representation of the electrokinetic focusing chip. R_1, R_2, R_3 and R_{ch} represent the resistors in the corresponding channel and reaction chamber. I_1, I_2, I_3 and I_{ch} are the current in the corresponding channels and chamber. V_u, V_c, V_l and V_{ch} represent voltage in upper channel (channel 1), sample channel (channel 2), lower channel (channel 3) and chamber, respectively.

Table 6.1 Calculated voltages required to focus to various rows of gold islands by keeping the flow speed of 300 μm/s and sample stream width of 300 μm.

Rows	V_u (V)	V_c (V)	V_l (V)
1	189	84	668
2	360	84	497
3	531	84	326
4	702	84	155

By altering the control voltages (V_u: upper channel voltage, V_l: lower channel voltage), the sample stream can be directed to each of the imaging array rows r_i. The sample flow is controlled by the center voltage (V_c: sample voltage), which also controls the flow velocity and sample stream width according to the distance x_1, shown in Fig. 6.2b. The chip was placed in a SPR slider (Fig. 6.1c) and clamped with the custom chip holder, which includes platinum electrodes that are connected to computer controlled power supply (IBIS 411, IBIS Technologies b.v., Hengelo, Netherlands). The upper and lower reservoirs were filled with 5 mM HEPES buffer and the center reservoir filled with the sample. The outlet reservoir voltage was set to ground and the voltages for the guiding streams, as well as sample streams, were individually controlled. Electro-osmotic mobility is assumed to be constant $\mu_{EOF} \approx 5\times10^{-8}$ m^2/Vs.[39] The guiding stream and sample transport voltages are calculated using $V_i = (\Phi_i L_i/A_i\mu_{EOFi}) + (R_{ch}/\mu_{EOFi})\ \Sigma(\Phi_j L_j/R_j A_j)$, where A_i and A_j (m^2) are the cross-sectional areas of the channels and chamber, Φ_i and Φ_j are the flow fluxes (m^3/min), and R_{ch} and R_j are the electrical resistances (Ω) of the channels and chamber, respectively. A detailed derivation and explanation of the equation was previously discussed.[39] The calculated guiding voltages are summarized in table 1. Some parts of the experiment use electro-osmotic flow (EOF) to transport the buffer to the various location of the chip, which is done with constant voltages (V_a and V_b) applied to the upper and lower reservoirs. Rhodamine B was added to the sample solution (3% glycerol in 5mM HEPES) for flow profile visualization and images were recorded with an inverted fluorescence microscope (Olympus IX51) color CCD imaging camera.

6.2.3 Surface Plasmon Resonance

The angle scanning iSPR system (IBIS-iSPR, IBIS Technologies b.v., Hengelo, Netherlands) used for experiments has been described previously.[31,32] In brief, the gold islands of the microarray are exposed to polarized light at a certain controlled incident angle. The refractive index change is proportional to the amount of adsorption or binding at the surface, which results in a measurable shift of the surface plasmon resonance condition, called the resonant angle. The measured response is converted to the time domain, which is referred to as a sensorgram. There are three main measurement phases of the sensorgram; baseline phase: a running buffer in contact with the sensor surface to establish the baseline responses, association phase: sample containing the target analyte [A] is injected to the interaction chamber and the ligands [B] immobilized on the surface, the capturing element on the sensor surface binds to the target resulting in complex formation [AB], and dissociation phase: injection of running buffer again which leads to dissociation of bound molecules from the surface. The EKF chip was placed on the hemispherical prism, separated by a droplet of refractive index matching oil, which is integrated in the SPR slider (Fig. 6.1c).

The SPR responses as well as real time images were recorded during EKF to each row using a solution of 3% glycerol in 5 mM HEPES buffer. Biomolecular interaction experiments of human IgG – goat anti-human IgG were also performed using the EKF technique. A solution of 1 mg/mL human IgG (Sigma, Netherlands) was immobilized on the gold islands using an EOF (V_a = V_u = V_l = 200 V DC) transport. The remaining active sites were blocked with 1M ethanolamine (Sigma, Netherlands) for 1 hr and subsequently washed. A baseline measurement was done using a 5 mM HEPES buffer. An analyte solution of 133 nM goat anti-human IgG (Molecular Probes, USA) was focused to the first row for 300 s followed by a dissociation phase with a running buffer over the gold islands for 300 s (V_b=V_u=V_l=200 V). This procedure was repeated for the various rows of the array. The measured sensorgrams were fitted to a 1:1 interaction model[13] using the commercially available software (Scrubber, Biologics

Inc., Australia). The results are discussed in detail in the next section.

6.3 Results and Discussion

6.3.1 Electrokinetic Flow Profiling

Fluorescence microscopy images of 3% glycerol/Rhodamine B focused to each row of the array is shown in Fig. 6.3a – 6.3d, clearly showing the flow profile. The measured fluorescence intensity profiles are shown in the insets of Figs. 6.3a–6.3d, which show uniform sample concentrations along each row of imaging islands. The dark regions are caused by the gold islands blocking light from the inverted microscope. Low flow rates can be affected by sample diffusion, and therefore, proper flow velocity (~300 μm/s) has to be considered for measurements. Following sample focusing to different rows, we have observed a small amount of fluorescence remaining in the previous row. We assume this is due to Rhodamine adsorption to the PDMS surface, but further investigation is required to verify the cause. However, the SPR images do not indicate any sample crossover to adjacent rows. The chip alignment of the reaction chamber to the gold-island imaging array is very important and unsymmetrical alignment results in unsymmetric focusing voltages. Additionally, the distance from the sample inlet to rows r_1 and r_4 is larger than the distance to rows r_2 and r_3, and therefore, requires higher focusing voltages. Finally, the voltage drop across the gold imaging array may lead to electrochemical reactions, as previously reported,[45-47] when the gold layer is exposed to high voltages for long times. A low conductivity (5 mM HEPES, $\sigma \approx 127$ μS/cm) buffer is used to minimize current across the gold islands in the interaction chamber, which significantly reduces degradation of gold imaging islands.

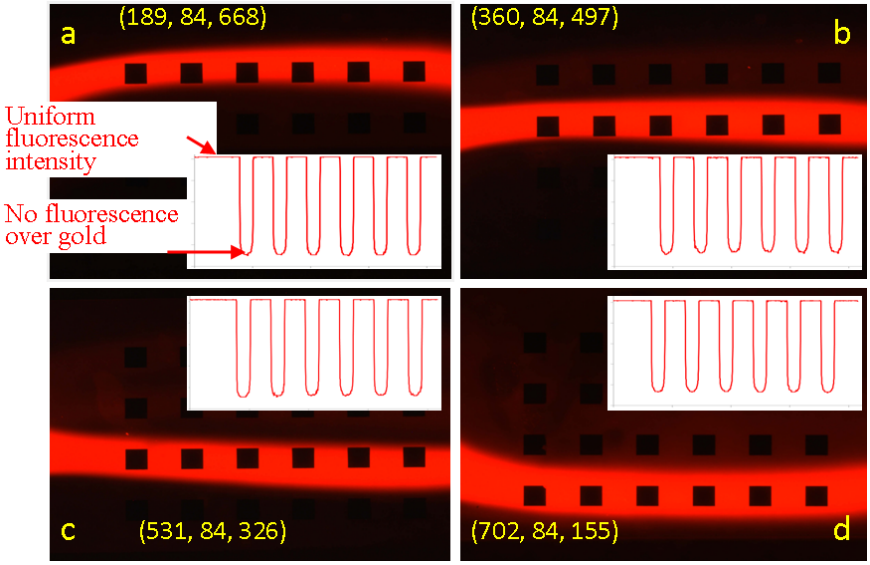

Figure 6.3 Fluorescence microscopy images demonstrating sample stream focusing (3% glycerol in 5 mM HEPES + Rhodamine B over the 6 gold islands in each row (a) – (d). Inset plot shows the uniform intensity profile of the focused sample stream. No fluorescence over gold islands was visible due to the observation from bottom of the chip.

6.3.2 Integrated EKF – SPR: Glycerol

The combination of EKF and SPR imaging has been demonstrated by EKF of a 3% glycerol sample to each array row and simultaneous SPR measurement at each gold island in the row, as shown in Figs. 6.4a – 6.4d. The gold islands with EK focused glycerol sample shows the shifted resonant angle with respect the buffer clearly showing the combination of EKF with SPR imaging.

The left inset of Figs. 6.4a – 6.4d shows a captured SPR image of the surface using a CCD camera integrated with iSPR system while focusing to the respective rows. The gold islands of the focused row clearly become a darker color. The right insets in Fig. 6.4 show grayscale pixel maps of the measured SPR response in each row. There are 24 pixels in the image map, separated by dotted lines, corresponding to the 24 imaging islands and the grayscale color of each pixel represents the measured

response of each imaging island at time t=200 sec. The lower scale bar in each case shows how the gray scale varies from R_l=0 to R_l=340 mº. As can be seen from each pixel map, the measured response of the focused row is ~300x higher than the neighboring rows indicating minimal sample cross-over and very uniform measured response across the row.

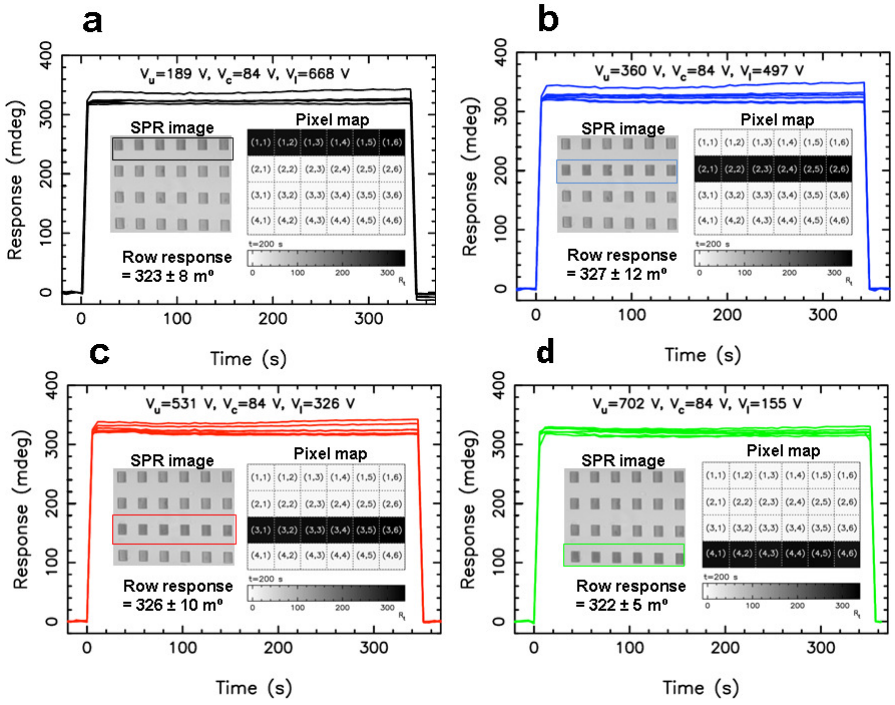

Figure 6.4 iSPR measurements of 3% Glycerol in 5 mM HEPES focused at each rows (columns shown with different colours) (a) Row 1 (b) Row 2 (c) Row 3 (d) Row 4. Inset image obtained from SPR CCD camera while focusing was done to those rows. Clear colour distinction was observed between focused and non-focused rows. A grey scale pixel map of each row is also shown. Electrical focusing voltages are shown as (V_u, V_c, V_l).

6.3.3 Integrated EKF – SPR: Biomolecular interaction

Biomolecular interaction measurements in combination with sample focusing were conducted. First, 500 µg/mL of human IgG ligand was introduced to the interaction chamber with EOF (V_c = 200 V), which is covalently immobilized on the

hydrogel coated gold islands. The analyte sample was introduced to the interaction chamber through the center inlet only, and therefore, a long time was required to uniformly adsorb the ligand on the gold islands. A low voltage is required to prevent damaging the gold islands.[48,49]

Unbound ligands were removed from the surface by electrically washing with 5 mM HEPES buffer and applying 200V to both of the buffer inlets V_u and V_l. During the surface washing step, the gold islands were SPR imaged and the sample focusing was conducted after a steady baseline signal was achieved. The results of the focusing experiments are shown in Figs. 6.5a – 6.5d. The measured responses are proportional to immobilized ligand density (not shown). Before the sample stream is focused to the next row, the flow is stopped and buffer was injected through the chip with an applied voltage of 200 V to the buffer reservoirs. The dissociation profile was measured in each case. For example, when the sample was focused to row 2, the dissociation profile of row 1 was measured continuously since the guiding stream consists of a buffer suitable for dissociation (not shown). We have not observed any cross-reaction with other rows while performing the focusing experiment. A problem encountered while performing the biomolecular measurements was a reduction in flowrate with increased time, which is attributed to protein adsorption to the PDMS channel walls. By careful control of the protein concentration and experiment time, the effects of protein adsorption to PDMS can be significantly reduced. This problem can be addressed by using a surface treatment to reduced protein adsorption to PDMS[50] or by using a different channel material. Presently, regeneration steps have not been developed for this system.

The raw sensorgram data were fitted to a 1:1 simple interaction model and the results are shown as orange overlay plots in Figs. 6.5a-6.5d. The 1:1 interaction model is used in this case for comparing the different sample transport methods only and not a rigorous kinetics evaluation, which is beyond the scope of this article. Since it is well known that the analyte goat anti-human IgG used in this work is bivalent in nature, a 1:1 interaction model is not appropriate for a meaningful kinetics evaluation. The maximum measurement response R_{max} extrapolated from the sensorgram data was fixed at a constant value for parameter extraction and fitting.[14] The data analysis results in

single association and dissociation rates, and therefore, a single affinity constant representing the interactant pair binding. Since the concentration of the analyte and ligands are approximately uniform, the extracted kinetics and affinity should be in the same order of magnitude for various rows. The extracted parameters are shown in Table 6.2. The affinity constant K_D extracted for all the four rows is of same order of magnitude even though the values are different due to differences in ligand densities, which can be solved by optimizing the immobilization procedure.

The possible sources of error include the iSPR system, heterogeneity in analytes, gold surface homogeneity and rebinding effects. In practice, the analyte concentration should be considered in the same range as the affinity constants in order to predict accurate kinetic parameters. The analyte concentration used in these experiments is larger than the extracted affinity constant, however, this does not affect the demonstration of combined EKF sample focusing and iSPR. The SPR dips shown in the insets of Figs. 6.5a – 6.5d show that the SPR minimum varies between the gold islands. Since the data measured during the baseline is zeroed, it is assumed that the effect of EKF is negligible as does not show any significant difference during the EKF. The average and standard deviation of the response and extracted parameters were obtained from six measurement sites called “region of interests” (ROI) from a single array row. The standard deviations of the estimated affinity constants from the six ROIs are shown in Table 2. The fitting residuals are shown in Figs. 6.5a–6.5d. Table 4 shows the mean and standard deviation for each gold island during the association and dissociation phases, which was calculated from the residuals obtained from the fitting of the raw data to a 1:1 model assuming a Gaussian distribution (histograms not shown). The assocation and dissociation phases are each 300 s in duration.

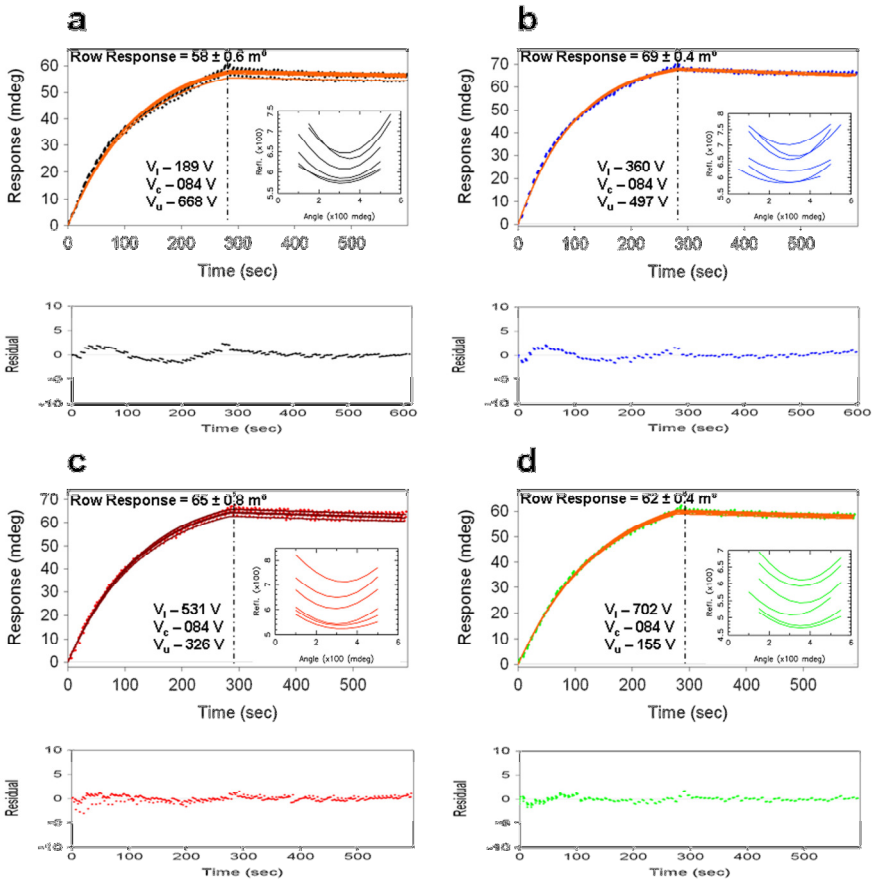

Figure 6.5 Raw sensorgrams (a) – (d) of each row of human IgG (500 µg/mL) – antihuman IgG (10 µg/mL) interaction using electrokinetic focusing. Human IgG immobilized on gold surface by direct physical adsorption using 200 V EOF. It also shows the uniformity of the response observed with very little standard deviation. Insets: SPR dips of each gold islands (ROIs). Kinetics and affinity calculated from 1:1 interaction model (global analysis) fit using Scrubber software. Fit results are represented by orange curve and the resultant values are shown in table 2. Fitting residual plots for each row are shown with their respective colours.

Additional experiments have been performed and compared to the EKF – SPR results. First, the human IgG – antihuman IgG interactant pair was investigated with the same analyte concentration on a commercially available hydrogel coated gold sensor disc (HCX 80m from XanTec GmbH, Muenster, Germany) with conventional

pressure driven flow. The sensorgrams fits and residual plots are shown in Fig. 6.6a. There is a small response variation (~1.5%) between different ROIs in a single row, however, these variations are not caused by EKF as similar results were obtained from experiments done using conventional pressure driven flow as shown in Fig. 6.6a. The extracted pressure driven flow kinetic parameters are compared to the average results of EKF results in rows 1 and 2 of table 6.3.

Table 6.2 Extracted 1:1 model parameters - association rate (k_a), dissociation rate (k_d) and affinity constant (K_D) from experimental data for each row using electrokinetic focusing. Total number of measurement sites in each row is 6.

Rows	Response	Stdev	k_a x 10^4	k_d x 10^{-5}	K_D	R_{max}
	m°	m°	$M^{-1}s^{-1}$	s^{-1}	nM	
1	58	0.60	6.18 ± 0.01	9.27 ± 1.54	1.50 ± 0.25	64 ± 0.88
2	69	0.38	7.39 ± 0.05	8.61 ± 0.32	1.16 ± 0.04	72 ± 0.43
3	65	0.83	5.84 ± 0.25	11.3 ± 1.46	1.99 ± 0.23	73 ± 1.96
4	62	0.39	5.24 ± 0.09	10.4 ± 0.87	1.97 ± 0.19	71 ± 0.40

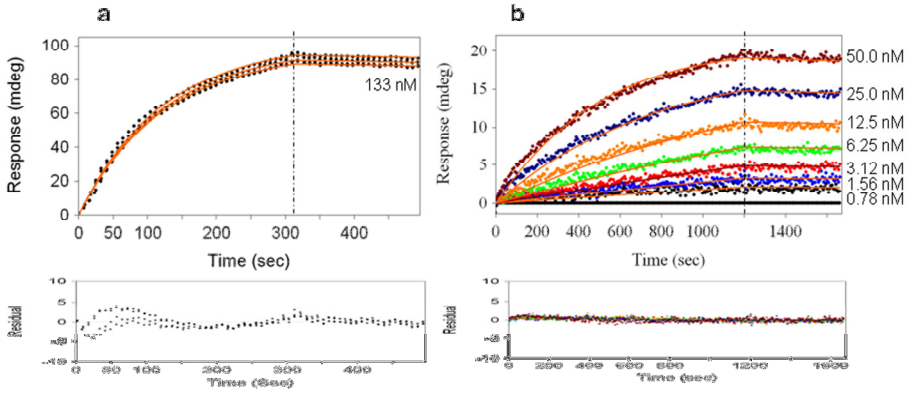

Figure 6.6 (a) Sensorgrams of the four spots having the same concentrations of analyte solution (133 nM) from a hydrogel/gold surface (b) Sensorgram of human IgG immobilization on hydrogel/gold surface (500 µg/mL) and various goat antihuman IgG concentrations (50, 25, 12.5, 6.25, 3.125, 1.5625 and 0.78 nM). Fit results are represented by orange curve and the resultant values are shown in table 3.

Table 6.3 Comparison of extracted 1:1 interaction model parameters from a three different measurement approaches: conventional (7 different analyte concentrations), pressure driven (4 different measurement sites) and electrokinetic focusing experiments (24 measurement sites that is 6 from each rows).

No	Approach	k_a x 10^4 $M^{-1}s^{-1}$	k_d x 10^{-5} s^{-1}	K_D nM
1	Electrokinetic focusing	6.17 ± 0.10	9.88 ± 0.56	1.66 ± 0.35
2	Pressure driven flow	5.95	6.64	1.11
3	Conventional kinetics	4.91	4.96	1.01

A classical kinetics experiment with varying analyte concentrations of 50, 25, 12.5, 6.25, 3.125, 1.5625, and 0.78 nM has been performed as an additional comparison to the EKF results. The sensorgrams and fits are shown in Fig. 6.6b. The measured response in this case is ~3x less than the EKF responses because the maximum concentration of antihuman IgG ~ 2.7x less than the EKF experiments. The conventional kinetics results are shown in third row of table 3. The kinetic parameters and affinity are generally in the same order of magnitude, despite the varying experimental conditions of these experiments, such as pressure driven flow, higher flow rate (120 μL/s) and sample mixing (back and forth motion with 2 μL/sec speed using 100 μL volume) in the flow-cell.

Since high conductivity buffers such as phosphate buffered saline (PBS), are typically used for hybridization of complex interactant pairs more investigation is required to minimize the degradation effects of the metal layer. This problem can be solved by coating the gold with a thin silicon-dioxide layer deposited by chemical vapor deposition[51,52] (results not shown). Research is ongoing in our lab to implement these improvements, and extend the designs from single interactant pairs to multiple interaction measurements. Multiplexing will lead to multiple simultaneous interactions, which do not require any regeneration steps. The large interaction chamber can also be

changed to individual microchannels in which the biomolecular interactions are performed, which also not require any regeneration steps and should be useful for one-shot kinetic analysis.[14]

Table 6.4 Analysis of the fitting residuals from Scrubber for all 24 imaging islands. For each island the mean and standard deviation are calculated over the time duration of the measurement phase. The association and dissociation phases are each 300 s in duration. The statistical distribution was graphically estimated with histograms and fit to a Gaussian distribution model (data not shown). Approximately 50 data points was considered in each association phase and dissociation residual values obtained from the fit.

Association Phase (m^o)

	Spot 1	Spot 2	Spot 3	Spot 4	Spot 5	Spot 6
R_1	0.03 ± 1.14	0.02 ± 1.14	0.07 ± 1.14	-0.01 ± 1.15	0.01 ± 1.14	0.12 ± 1.18
R_2	-0.04 ± 0.97	-0.02 ± 0.95	0.05 ± 0.98	0.08 ± 0.98	0.10 ± 0.99	0.07 ± 0.98
R_3	0.15 ± 0.55	0.20 ± 0.55	0.11 ± 0.51	-0.77 ± 0.80	0.22 ± 0.55	0.01 ± 0.55
R_4	0.08 ± 0.60	-0.05 ± 0.62	-0.17 ± 0.66	-0.10 ± 0.63	0.02 ± 0.61	-0.03 ± 0.61

Dissociation Phase (m^o)

	Spot 1	Spot 2	Spot 3	Spot 4	Spot 5	Spot 6
R_1	0.03 ± 0.37	0.04 ± 0.36	0.01 ± 0.37	0.06 ± 0.36	0.04 ± 0.36	-0.05 ± 0.38
R_2	0.09 ± 0.38	0.07 ± 0.37	0.04 ± 0.38	0.02 ± 0.36	0.01 ± 0.36	0.03 ± 0.37
R_3	0.01 ± 0.37	-0.01 ± 0.38	-0.01 ± 0.40	0.39 ± 0.38	-0.02 ± 0.37	0.07 ± 0.36
R_4	0.01 ± 0.40	0.06 ± 0.40	0.10 ± 0.40	0.10 ± 0.40	0.04 ± 0.40	0.07 ± 0.40

6.4 Conclusion

An all electrical electrokinetic sample transport chip has been successfully coupled to an SPR imaging system. Coupled EKF and SPR imaging was successfully demonstrated with 3% glycerol sample as well as biomolecular interaction of the well known interactant pairs: human IgG and goat anti-human IgG. The kinetics and affinity parameters extracted from the sensorgrams have been compared to experiments using conventional pressure driven flow and are in good agreement. The distribution of the responses from individual ROIs in the same row was similar for EKF – SPR and conventional pressure driven flow SPR indicating that this approach is viable and does

not affect SPR measurements. This successful demonstration of an electrically controlled sample transport system directly coupled to SPR imaging may be important for SPR miniaturization and for scaling systems to accept larger numbers of different samples.

6.5 References

(1) Piscevic D., Knoll W., and Tarlov MJ.; Supramolecular Science, 2 (1995) 99-106.
(2) Baldrich E., Restrepo A., and O'Sullivan CK.; Anal. Chem., 76 (2004) 7053-7063.
(3) Ehlers I., Horke S., Reumann K., Rang A., Grosse F., Will H., and Heise T.; J. Biol. Chem., 279 (2004) 43437-43447.
(4) Ikeda Y., Imai Y., Kumagai H., Nosaka T., Morikawa Y., Hisaoka T., Manabe I., Maemura K., Nakaoka T., Imamura T., Miyazono K., Komuro I., Nagai R., and Kitamura T.; Proc. Natl. Acad. Sci. USA, 101 (2004) 10732-10737.
(5) Yamaguchi S., Mannen T., and Nagamune T.; Biotechnol. Lett., 26(2004) 1081-1086.
(6) Sadamoto R., Niikura K., Ueda T., Monde K., Fukuhara N., and Nishimura S-I.; J. Am. Chem. Soc., 126 (2004) 3755-3761.
(7) Verdonck F., Cox E., Vancaeneghem S., and Goddeeris BM.; FEMS Immunol. Med. Microbiol., 41 (2004) 243-248.
(8) Doyle ML., Myszka DG., and Chaiken IM.; J. Mol. Recognit., 9 (1996) 65-74.
(9) Brockman JM., Frutos AG., and Corn RM.; J. Am. Chem. Soc., 121 (1999) 8044-8051.
(10) Lee HJ., Goodrich TT., and Corn RM.; Anal. Chem., 73 (2001) 5525-5531.
(11) Lew HS., and Fung YC.; J. Biomech., 2 (1969) 105-119.
(12) Sjoelander S., and Urbaniczky C.; Anal. Chem., 63 (1991) 2338-2345.
(13) Morton TA., Myszka DG., and Chaiken IM.; Anal. Biochem., 227 (1995) 176-185.
(14) Bravman T., Bronner V., Lavie K., Notcovich A., Papalia GA., and Myszka DG.; Anal. Biochem., 358 (2006) 281-288.
(15) Figeys D., and Pinto D.; Electrophoresis, 22 (2001) 208-216.
(16) Schasfoort RBM.; Expert Rev. Proteomics, 1 (2004) 123-132.
(17) Gervais T., and Jensen KF.; Chem. Eng. Sci., 61 (2006) 1102-1121.
(18) Galopin E., Beaugeois M., Pinchemel B., Camart JC., Bouazaoui M., and Thomy V.; Biosens. Bioelec., 23 (2007) 746-750.
(19) Skottrup PD., Nicolaisen M., and Justesen AF.; Biosens. Bioelec., 24 (2008) 339-348
(20) Luo Y., Yu F., and Zare RN.; Lab Chip, 8 (2008) 694-700.
(21) Wang Z., Wilkop T., Xu D., Dong Y., Ma G., and Cheng Q.; Anal. Bioanal. Chem., 389 (2007) 819-825.
(22) Lei KF., Law WC., Suen YK., Li WJ., Ho HP., Lin C., and Kong SK.; Proc. 5th IEEE Conf. Nanotechnol., 1 (2005) 515-518.
(23) MacBeath G., and Schreiber SL.; Science, 289 (2000) 1760-1763.
(24) Figeys D.; Proteomics, 2 (2002) 373-382.
(25) Situma C., and Hashimoto M., Soper SA.; Biomol. Eng., 23 (2006) 213-231.
(26) Lee KH., Su YD., Chen SJ., Tseng FG., and Lee GB.; Biosens. Bioelec., 23 (2007) 466-472.
(27) Mauriz E., Calle A., Manclus JJ., Montoya A., Escuela AM., Sendra JR., and Lechunga LM.; Sensor. Actuat. B-Chem., 118 (2006) 399-407.
(28) Yuk JS., Kim HS., Jung JW., Jung SH., Lee SJ, Kim WJ., Han JA., Kim YM., and Ha KS.; Biosens. Bioelec., 21 (2006) 1521-1528.
(29) Homola J., Vaisocherová H., Dostálek J., and Piliarik M.; Methods, 37 (2005) 26-36.

(30) Rich RL., Cannon MJ., Jenkins J., Pandian P., Sundaram S., Magyar R., Brockman J., Lambert J., and Myszka DG.; Anal. Biochem., 373 (2008) 112-120.
(31) Lokate AMC., Beusink JB., Besselink GAJ., Pruijn GJM., and Schasfoort RBM.; J. Am. Chem. Soc., 129 (2007) 14013-14018.
(32) Beusink JB., Lokate AMC., Besselink GAJ., Pruijn GJM., and Schasfoort RBM.; Biosens Bioelectron., 23 (2008) 839-844.
(33) Ellender RD., Morton F., Whelan J., and Sweet BH.; Prep. Biochem., 2 (1972) 215-228.
(34) Gao Y., Lin FYH., Sherman PM., and Li D.; Anal. Chim. Acta, 543 (2005) 109-116.
(35) Hu G., Gao Y., Sherman PM., and Li D.; Microfluid. Nanofluid., 1 (2005) 346-355.
(36) Fu LM., Yang RJ., Lee GB., and Liu HH.; Anal. Chem., 74 (2002) 5084-5091.
(37) Fu LM., Yang RJ., and Lee GB.; Anal. Chem., 75 (2003) 1905-1910.
(38) Besselink GAJ., Vulto P., Lammertink RGH., Schlautmann S., van den Berg A., Olthuis W., Engbers GHM., and Schasfoort RBM.; Electrophoresis, 25 (2004) 3705-3711.
(39) Kohlheyer D., Besselink GAJ., Lammertink RGH., Schlautmann S., Unnikrishnan S., and Schasfoort RBM.; Microfluid. Nanofluid., 1 (2005) 242-248.
(40) Wu CH., and Yang RJ.; Electrophoresis, 27 (2006) 4970-4981.
(41) Kohlheyer D., Unnikrishnan S., Besselink GAJ., Schlautmann S., and Schasfoort RBM.; Microfluid. Nanofluid., 4 (2007) 557-564.
(42) Pan YJ., Ren CM., and Yang RJ.; J. Micromech. Microeng., 17 (2007) 820-827.
(43) Linder V., Verpoorte E., Thormann W., and de Rooij NF., Sigrist H.; Anal. Chem., 73 (2001) 4181-4189.
(44) Schlautmann S., Besselink GAJ., Radhakrishna PG., and Schasfoort RBM.; J. Micromech. Microeng., 13 (2003) S81-S84.
(45) Abelès F., and Lopez-Rios T.; Solid State Comm., 16 (1975) 843-847.
(46) Gordon II JG., and Ernst S.; Surf. Sci., 101 (1980) 499-506.
(47) Kolb DM.; Prog. In Surf. Sci., 51 (1996) 109-173.
(48) Genshaw MA., Damjanovic A., and Bockris JO'M.; J. Electroanal. Chem., 15 (1967) 163-172.
(49) Damjanovic A., Genshaw MA., and Bockris JO'M.; J. Electroanal. Chem., 15 (1967) 173-180.
(50) Huang B., Wu H., Kim S., and Zare RN.; Lab Chip, 5 (2005) 1005-1007.
(51) Szunerits S., and Boukherroub R.; Electrochem. Comm. 8 (2006) 439-444.
(52) Manesse M., Stambouli V., Boukherroub R., and Szunerits S.; The Analyst, 133 (2008) 1097-1103.
(53) Moser I., Schalkhammer T., and Urban G.; Biosens. Bioelec., 12 (1997) 729-737.
(54) Mooney JF., Hunt AJ., McIntosh JR., Liberko CA., Walba DM., and Rogers CT.; Proc. Natl. Acad. Sci., 93 (1996) 12287-12291.
(55) Elender G., Kuehner M., and Sackmann E.; Biosens. Bioelec. 11 (1996) 565-577.
(56) Ajdari A.; C. R. Physique, 5 (2003) 539-546.
(57) Qiao R. and Aluru NR.; J. Micromech. Microeng., 12 (2002) 625-635.
(58) Kohlheyer D.; Microfluidic Free-Flow Electrophoresis for Proteomics-on-a-Chip, PhD Dissertation, University of Twente (2008) ISBN: 978-90-365-2666-1.

6.6 Appendix

6.6.1 Microfabrication Procedure

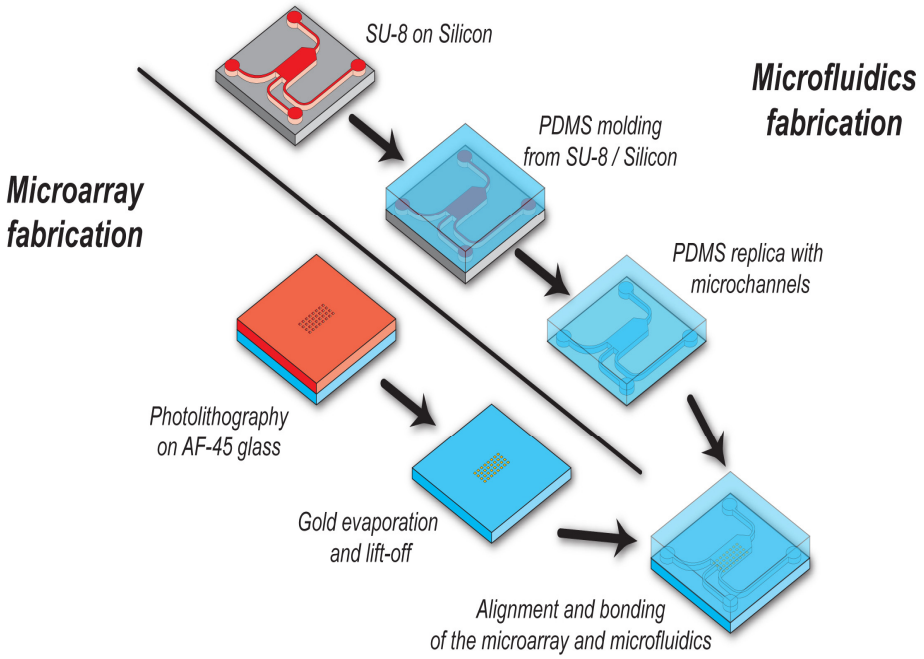

Figure 6A.1 Schematic representation of EKF-iSPR chip fabrication.

The Microfabrication for EKF-iSPR chip involves 2 different processing steps (Fig. 6A.1). The first step involves microarray fabrication and the second involves the microfluidics fabrication. The microarray fabrication was done in cleanroom which involves several steps. A special AF-45/D263 glass was considered in our case as the refractive index of the glass should be 1.51 is necessary for our chips. Initial photolithography was carried out followed by gold evaporation step. In our case gold evaporation was done externally (sSens BV, Hengelo, the Netherlands). After this step, lift-off was carried out using a standard protocol with acetone. After this step, the chips were coated with pre-activated functionalized hydrogel for covalent immobilization of proteins which was also done externally (XanTec, Dusseldorf, Germany).

The microfluidic chip was fabricated with PDMS which again involves two stages of fabrication steps. The first one is the production of mold in the clean room which involves the spin coating of SU-8 (SU-8 is an epoxy based, chemically amplified resist system with excellent sensitivity and high aspect ratios) on the P-type silicon wafer with <1 0 0> orientation followed by soft bake and stepwise hard bake steps according to the standard protocol43. The second step involves the PDMS chip fabrication in the laboratory. PDMS monomer was taken in the ratio of 10:1 with

curing agent for PDMS and mixed thoroughly. The PDMS mixture was degassed and it was poured over the SU-8 mold. The proper thickness of the chip was obtained using the special homemade molding kit with special tracers. The mold was cured 80 deg C for 1 hour. The PDMS chip was properly diced and reservoir holes were punched manually. The final PDMS chip was cleaned in isopropanol and then in plasma treatment system for 15 minutes prior to bonding. The bonding procedure is described in the main chapter (section 6.2.1).

7

Electrokinetic Lab-on-a-BioChip for Multi-Ligand/Multi-Analyte Biosensing

In this chapter, we present a very simple electrokinetic lab-on-a-biochip (EKLB) with four microchannels that is operated using a single electrical voltage for the simultaneous transport of reagents in all microchannels without any conventional fluidic plumbing. We have demonstrated various types of experiments that can be performed with the biochip, including single injection kinetics (various ligand densities and single analyte concentration), one shot kinetics (single ligand densities and various analyte concentrations) and multi-ligand/multi-analyte detections. In all cases, the binding kinetics and affinity were extracted using a conventional 1:1 interaction model. Since the reagent transport is done with only a single electrical voltage source, scaling up the number of channels such that the biosensing chip is capable of running 100s to 1000s of simultaneous measurements is straight forward. A part of this chapter has been submitted as Research paper (2010).

7.1 Introduction

Label-free biosensors are becoming commonly used to detect biological moieties in solution using a variety of detection techniques, such as, electrochemical, mechanical or optical.[1] The simultaneous detection of multiple biomolecular targets, also known as a multiplexed assay, such as nucleic acids, antibodies and proteins, is important for medical diagnostics. For example, multiplexed assays for the detection of respiratory pathogens because many different pathogens present similar symptoms; accurate pathogen identification and fingerprinting are important for patient recovery and public health monitoring.[2] Multiplexed assays are also important for diagnosing cancers.[3,4] Multiplexed label-free bioassays have been previously reported.[1, 5-6] The

main advantages of bioassay multiplexing are related to experimental time reduction and reduced cost since assays are performed simultaneously.

Optical biosensors based on surface plasmon resonance (SPR) are currently the most commonly used systems for quantitative bioassays. The extension of the single spot SPR to imaging surface plasmon resonance (iSPR) biosensors and the integration with lab-on-chip (LOC) and microarrays is an ideal platform for multiplexed assays,[7, 8] where each ligand spot in the microarray is used as an individual sensing area with a unique functionality. Multiplexed iSPR assays have been reported for various application areas such as serum antibody screening,[9] lipid-protein interactions,[10] blocking assays,[11] DNA-protein interactions,[12] food screening,[13] and monitoring auto-antibodies.[14] Lab-on-a-Chip technology is a very important tool for multiplexed iSPR assays and can lead to multi-analyte detection. Most of the commercially available SPR systems, such as Biacore[15] and Bio-rad,[16] are integrated with automatic computer controlled microfluidic systems where they use multiple syringe pumps for sample and reagent delivery. The number of flow cells is limited due to size limitations of the imaging area and instrument size. Therefore, an alternative transport method that can reduce the complexity of the fluidic interconnects will aid in scaling the instruments to larger numbers of simultaneous measurements that can take advantage of conventional microarray ligand spot densities.

We recently demonstrated the integration of surface plasmon resonance imaging (iSPR) with electrokinetic focusing and microarrays for multiplexed bioassays.[17] However, that system had the possibility of sample cross contamination on the gold sensing islands when we try to move the sample stream to various locations of the chip. In addition, changing between samples was complicated. In order to solve some of the previous problems encountered while employing electrokinetic transport, the chip was modified where a single reaction chamber is converted into individual microchannels for various ligands and/or analytes, which leads to highly multiplexed multi-ligand/multi-analyte detection. The schematic illustration of the set-up is shown in Fig. 7.1.The advantages of the new configuration include pumpless and valve-less fluid transport and all transport can be accomplished with a single power supply. A

condition for using a single power supply is that the electrical resistance of the reactions microchannel is approximately the same throughout the entire array.

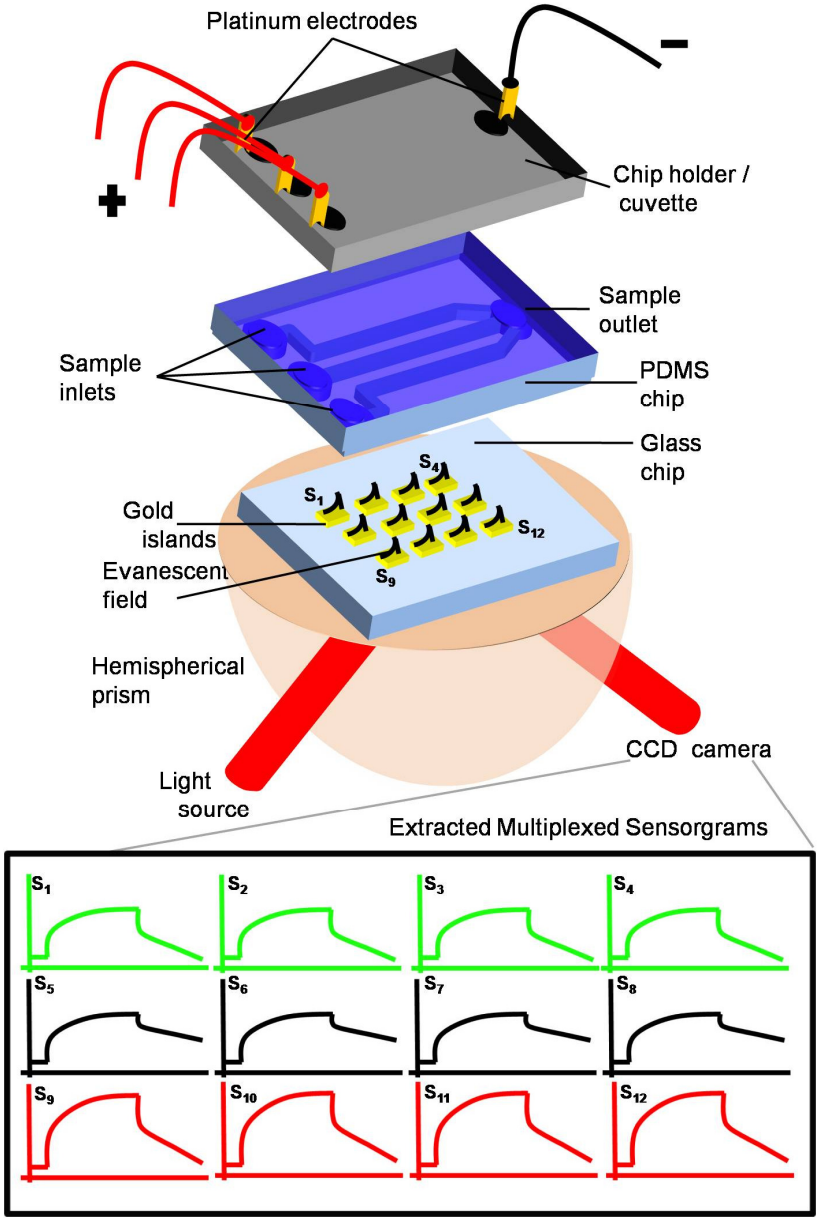

Figure 7.1 Illustration of integrated surface plasmon resonance imaging system with our newly developed electrokinetic lab-on-a-biochip.

Multiple channels with pressure driven fluidic transport integrated to SPR have been previously reported for several applications including high throughput screening[18-28] as well as small molecule detection[29]. The new device could be used for multiple purposes, such as, the estimation of biomolecular interactions with a single injection of analytes[30] over various densities of immobilized ligand, one-shot injection[16] of multiple concentrations of analytes, and for the multi-ligand/multi-analyte detection.[31] For the experiments presented here, we have considered three well-known interactant pairs such as Fab fragments of Human IgG–Fab specific antihuman IgG, β2 microglobulin–antiβ2 microglobulin and neomycin–antineomycin. The kinetics and affinity of all the interactant pairs were extracted from the measured iSPR sensorgrams. A detailed explanation of each different approach is described in the following sections. To the best of our knowledge, this is the first imaging system integrated directly with parallel flow channels using electrokinetic transport for biosensing applications. Success of this work enables increased throughput by increasing the number of flow channels.

7.2 Materials and Methods

7.2.1 Microfabrication

The EKLB chip (size: 15x15 mm^2) is made of two layers. The top PDMS layer has four channel structures as well as reservoir holes (punched manually with a sharp hollow needle) for sample and electrode interfacing. The bottom glass layer, refractive index matched (n=1.52) to the hemispherical prism of the iSPR instrument (IBIS Technologies b.v., Hengelo, Netherlands), has patterned gold islands for SPR imaging. The gold iSPR islands were electron beam evaporated on the glass layer (SSens b.v. Hengelo, Netherlands) and subsequently photo-lithographically patterned. The patterned square gold islands are 200 µm on a side and the pitch (center to center distance) is 500 µm (Fig. 7.2a). The thickness of the gold imaging layer is 47 nm. The thickness of the bottom glass layer is 1.1 mm. Following, gold island patterning, the glass chips were coated with carboxymethyl dextran (CMD) of 100 nm thickness for

covalent ligand immobilization (XanTec GmbH, Muenster, Germany). The PDMS chips (2 mm thick) were ultrasonically cleaned in isopropanol for 15 minutes prior to any further processing and subsequently dried with dry nitrogen and cleaned with oxygen plasma for 5 min. Each reservoir hole is 2 mm in diameter and the depth of the microchannel is 40 µm. The various interaction channels are listed as C_1, C_2, C_3 and C_4 for channel 1, channel 2, channel 3 and channel 4, respectively. All interaction channels have width W_c= 220 µm and length L_c= 22 mm. The stamp and stick technique[32] was used to bond the PDMS chips to the glass chips. A thin layer of glue (Norland Optical Adhesive 81, Norland, USA) was applied to one side of a microscope slide which is continuously purged with dry nitrogen in order to avoid the contacts with oxygen as well as to have a more uniform layer of glue on the surface.[33] The molded PDMS layers were carefully pressed onto the glue blotter layer, removed and subsequently bonded to the glass chip. The bonded stack was then cured in UV light (λ=359 nm) for 2 min. The final chip is shown in Fig. 7.2b.

7.2.2 Surface Plasmon Resonance Imaging

The angle scanning iSPR system (IBIS-iSPR, IBIS Technologies b.v., Hengelo, Netherlands) used for experiments has been described previously.[14,17,34] A Kretschmann-Raether attenuated total reflection (ATR) configuration is used where a p-polarized light source incident on a hemispherical prism couples to the interface as a surface plasmon at a certain angle of incidence and source wavelength. At this angle of incidence, the reflected intensity of the ATR signal decreases, which results in an intensity dip or SPR-dip.[45] A refractive index change at the solution/gold interface, is related to the amount of adsorption or binding of (bio)molecules at the surface, which results in a measurable shift of the SPR-dip. The measured SPR-dip position is converted to the time domain, which is referred to as a sensorgram. There are three main measurement phases of the sensorgram; 1) baseline phase: a running buffer in contact with the sensor surface to establish the baseline responses, 2) association phase: sample containing the target analyte [A] is injected to the interaction chamber and the

ligands [B] immobilized on the surface, the capturing element on the sensor surface binds to the target resulting in complex formation [AB], and 3) dissociation phase: injection of a running buffer again which leads to dissociation of bound molecules from the surface. The microfabricated chip was placed on the hemispherical prism that is integrated in the SPR interface module and separated by a droplet of refractive index matching oil (Fig. 7.2c).

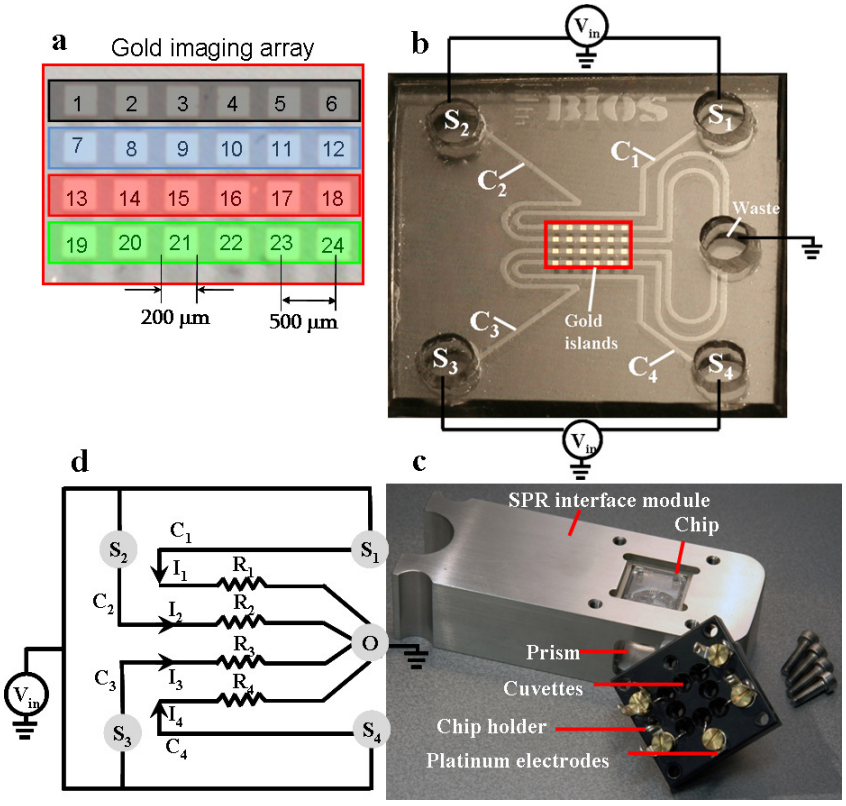

Figure 7.2 (a) 6×4 microarray of gold iSPR sensing islands (b) 15×15 mm² glass-PDMS microfluidic chip showing channels C_1 - C_4. S_1 - S_4 are sample fluidic inlets. (c) iSPR interface module with chip fixture with integrated platinum electrodes. (d) Electrical circuit representation of the EKLB chip. R_1 - R_4 represents electrical resistances in the respective channels. I_1 - I_4 represents electrical current in the respective channels. O represents the common fluidic outlet and electrical ground.

7.3 Results and Discussions

Various experiments were conducted with the new EKLB chip. Prior to experiments, two-dimensional finite element simulations were performed to estimate the electrokinetic sample flow rate with respect to applied voltage and buffer. Electrokinetic flow profiles were measured using fluorescence microscopy followed by iSPR measurements with a standard calibrating sample (Glycerol). Finally biomolecular interaction experiments were performed. Details about the performed experiments are discussed in the respective discussion sections below.

7.3.1 Electrokinetics Simulation

The electrokinetic flow behavior, such as flow rate and potential distribution across the gold islands, was calculated using a numerical solution of the 2D Navier-Stokes equation with a commercial finite element software (Conductive media model, COMSOL, USA).[35,36] The electrical circuit representation is shown in Fig. 7.2d. R_1 – R_4 are electrical resistances across each channels and I_1 – I_4 are electrical currents flowing from the inlet to the outlet in each channels, respectively. In this case, the channel inlets are connected to single voltage source, and therefore, the total electrical current is the sum of all currents, (i.e. $I_t = I_1+I_2+I_3+I_4$). This is only true when all the R's are the same. The resistances are estimated with $R = L_c/\sigma A$, where σ is conductivity of the buffer and A is the cross sectional area of the microchannel. The channels are designed in such a way that $R_1=R_2=R_3=R_4$, such that the flow rate is approximately the same in each channel. Controlling and minimizing the current in each channel is important in order to avoid any electrochemical reaction with the gold islands, which can adversely affect the thin gold layer and SPR measurements.[37–39] Channel dimensions are chosen in such a way that the current in the microchannel should be ≤ 20 mA as well as the electric field across gold sensing islands should be ≤ 10 V/mm to avoid electrochemical reaction with the gold sensing regions. The maximum electric field of 10 V/mm over the gold islands is the upper limit for such systems as the increase the V_{in} voltage leads to removal of gold from the sensing surface (results not

shown here). These parameter selections are important to eliminate any electrochemical reactions with the gold sensing regions.[17] The initial boundary conditions were set according to the conditions mentioned above. The electroosmotic mobility was assumed to be 5×10^{-8} m^2/Vs.[40] Fig. 7.3a shows the typical electric potential profiles in the channels and Fig. 7.3b shows the flow speed (v_f) profile. The estimated flow speed v_f ~50 μm/s in all cases. The electric field across each channel is ~9 V/mm. Our experimental results show that the electric fields in this range do not damage the thin gold layer. We have found that a dextran coating over the gold islands can help to protect the gold layer. Experiments were performed in the new chip and are discussed in the following section.

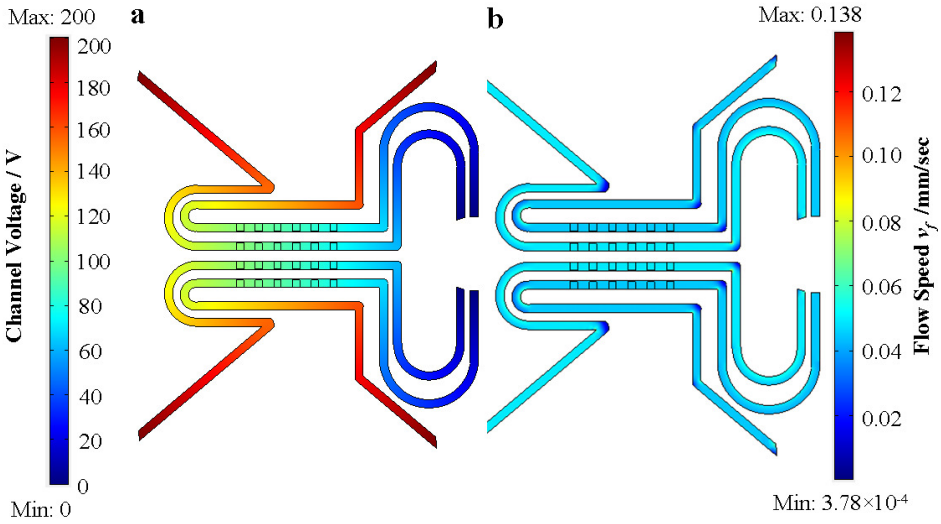

Figure 7.3 Simulation of 2D Navier-Stokes equation with Conductive media model (COMSOL, USA). (a) Voltage profile across each microchannels. (b) Flow speed profile with V_{in}=200V resulting in v_f ~50 μm/s

7.3.2 EKLB – Microscopy Flow Profiling

The electrokinetic flow profile was observed with fluorescence microscopy in which four different concentrations (0, 0.5, 1.0 and 2.0 μg/mL) of alexafluor488 (Molecular probes, USA) were injected into the different microchannels

simultaneously. The flow profile is shown in the Fig. 7.4a. The measured fluorescence intensity profiles at location A-A' is shown in Fig. 7.4b. The dark regions are caused by the gold islands blocking light from the inverted microscope.

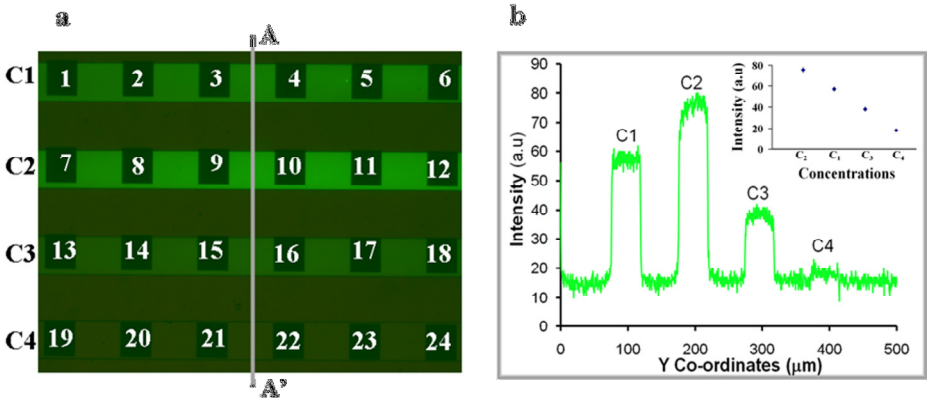

Figure 7.4 (a) Fluorescence microscopy images of various concentrations of alexafluor488 in 10mM HEPES in all channels. C_1 – 1:10 dilution; C_2 – 1:5 dilution; C_3 – 1:20 dilution (b) Fluorescence intensity measurements at A-A' (gray line) showing the highest intensity for the highest concentration (C_2) and lowest intensity for the lowest concentration (C_4). The inset plot shows the fluorescence intensity – concentration relationships.

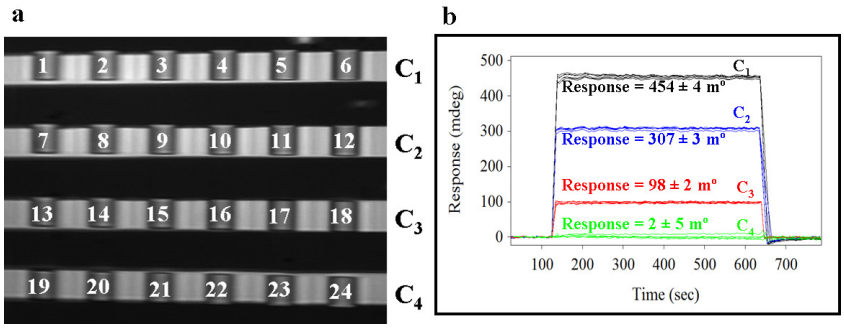

Figure 7.5 (a) iSPR image of the chip with gold sensing islands. (b) Measured iSPR response for different glycerol concentrations showing the largest response for the highest concentration (C_1) and lowest response for the lowest concentration (C_4).

The intensities observed in C_2 and C_3 are not uniform and show a slight decrease of intensity near the channel walls. This is very important when choosing

region of interests (ROIs) for the iSPR measurements, where it is best to have a uniform flow speed in the region where the iSPR measurement occurs. The inset of Fig. 7.4b is the relationship observed for fluorescence intensity versus concentration of alexafluor488.

The chip alignment of the microchannels to the gold-island imaging array is very important and misalignment can result in wasted sensing area and possible channel leakage. The difference between the channel dimensions and sensing array dimensions are very small in this case, the chip alignment problem was minor. This could be avoided by considering larger flow channel dimensions. Finally, the voltage drop across the gold imaging array may lead to electrochemical reactions, as previously reported,[37-39] when the gold layer is exposed to high voltages for long times. A low conductivity (10 mM HEPES, $\sigma \approx 238$ μS/cm) buffer is used to minimize current across the gold islands.

7.3.3 Integrated EKLB – iSPR: Multi-analyte measurements (various concentrations of glycerol)

The SPR responses, as well as real time images, were recorded with injections of various concentrations (0, 1, 2 and 3%) of glycerol in 10 mM HEPES buffer. The real time iSPR image of the EKLB chip is shown in Fig. 7.5a. The resulting iSPR sensorgrams are shown in Fig. 7.5b. The total measurement time is 800 s in which 120 s of baseline measurement with 10 mM HEPES buffer followed by 500 s of glycerol injection (V_{in} = 200 V DC) and 180 s of 10 mM HEPES buffer again. In channel 1, a 3% glycerol solution resulted in measured response of 454 ± 4 mº. In channel 2, a 2% glycerol solution resulted in measured response of 307 ± 3 mº. In channel 3, a 1% glycerol solution resulted in measured response of 98 ± 4 mº. In channel 4, the signal observed was 2 ± 5 mº.

7.3.4 Integrated EKLB – iSPR: Biomolecular interaction measurements

Various types of biomolecules (the immobilized biomolecules are ligands and

the biomolecules in flow are analytes) have been used in the experiments: Ligand 1 – Fab of human IgG (Sigma, Netherlands); Ligand 2 – neomycin (Sigma, Netherlands); Ligand 3 – β2 microglobulin (sigma, Netherlands); Analyte 1 – Fab specific goat antihuman IgG (Jacksons Immuno Research, USA); Analyte 2 – antineomycin (Biodesign, USA); Analyte 3 – mAb for β2 – microglobulin (Abcam, USA). All the samples were injected with the constant voltage V_{in} = 200 V DC (IBIS Technologies b.v., Hengelo, Netherlands). Prior to the biomolecular interaction experiments, the chip with gold sensing array coated with CMD was activated with 0.4 M EDC and 0.1 M NHS for 20 minutes followed by rinsing with acetic acid to maintain the pH suitable for immobilization. The chip was completely dried with dry nitrogen. After the immobilization of biomolecules, the active sites were blocked with 1M ethanolamine followed by washing with 10 mM HEPES buffer. Various experiments performed include: Scenario 1 "Single injection kinetics"[30]; four different concentrations of ligand 1 (C_1=2 mg/mL; C_2=1 mg/mL; C_3=0.5 mg/mL and C_4=0 mg/mL) in 50 mM MES buffer (pH 5.4) were immobilized and single concentration of analyte 1 (C_1=C_2=C_3=C_4=50 nM) was injected into the chip using EOF (V_{in}=200 Volts DC). This also gives information about reproducibility of the extracted kinetics with respect to various densities of ligand immobilized on the surface, which might provide information about re-binding effects, steric hindrance and mass transport limitations. Scenario 2: "One shot kinetics"[16]; Single concentration of ligand 1 (C_1=C_2=C_3=C_4=2 mg/mL) was immobilized and different concentration of analyte 1 (C_1=12.5 nM; C_2=25 nM; C_3=50 nM and C_4=0 nM) was injected into the chip. As described in literature[16], this approach reduces the duration of kinetics experiments where various concentrations of analytes used for kinetics and affinity parameter extraction could be done with a single injection of various concentrations of analytes in different channels simultaneously. Scenario 3: "Multi-ligand/multi-analyte detection"[31]; Three different ligands (C_1=85 mg/mL ligand 3, C_2=20 mg/mL ligand 2 and C_3=2 mg/mL ligand 1) were immobilized each in one channel and three different analytes (C_1=35 nM analyte 1, C_2=110 nM analyte 2 and C_3=50 nM analyte 3), which is specific to these ligands,

are injected in to the respective channels. In all the cases, after immobilization, the remaining active sites were blocked with 1M ethanolamine (Sigma, Netherlands) for 10 minutes and subsequently washed prior to biomolecular interaction experiments. A baseline measurement was done using a 10 mM HEPES buffer for 100 s. In all experiments, the association phase was measured for 500 s followed by a dissociation phase with a running buffer for 500 s. The measured sensorgrams were fitted to a 1:1 interaction model[41] using the commercially available software (Scrubber, Biologics Inc., Australia). The results are discussed below in detail.

7.3.4.1 Scenario 1 – Single injection kinetics

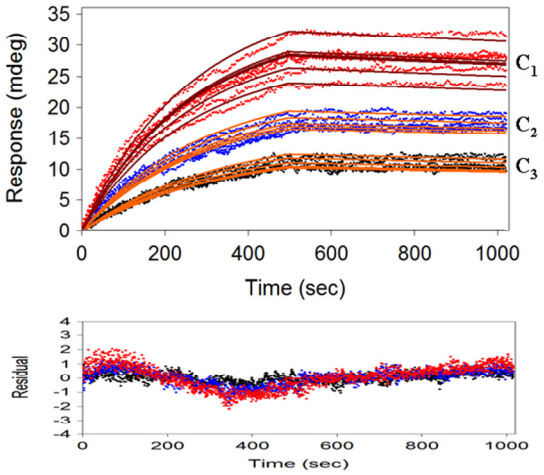

Figure 7.6 Experiment and model fit (orange curves) results of scenario 1. (a) The concentrations of Human IgG Fabs immobilized are C_1=2 mg/mL; C_2=1 mg/mL; C_3=0.5 mg/mL and C_4=0 mg/mL. The analyte concentrations in all the channels are 50 nM. The residuals of the model fit are shown in the lower plot.

The first biomolecular interaction experiment performed with the EKLB chip was a single injection kinetics measurement. The immobilization of different concentrations of ligand 1 were performed using the electrokinetic voltage V_{in}=100 V DC for 30 minutes. The biomolecular interaction was carried out with analyte 1. The resultant sensorgram is shown in Fig. 7.6 together with its 1:1 model function. The residuals of the fit are shown in the bottom plot. Results are shown in different colors.

The extracted parameters are shown in table 7.1. The affinity constant calculated in three channels varies between 1.3 and 2.2 nM. Channel 1, which has the highest concentration of immobilized ligand shows larger response variations.

Table 7.1 Summary of results for scenario 1. Various concentrations of human IgG Fabs immobilized and single concentration of Fab specific antihuman IgG as analyte. The number of points considered for estimating the standard error is 6.

Channels	**Interactant pairs**	**Response (t=500 s)**	k_a	k_d	R_{max}	K_D
		m°	**$M^{-1}s^{-1}$**	**s^{-1}**	**m°**	**nM**
C_1	HIgG Fab – Fab specific AHIgG	28 ± 3	$(5.8 \pm 2.1) \times 10^4$	$(1.3 \pm 2.1) \times 10^{-4}$	34 ± 3.0	2.2 ± 1.1
C_2		17 ± 1	$(6.7 \pm 3.6) \times 10^4$	$(9.0 \pm 4.3) \times 10^{-5}$	22 ± 1.5	1.3 ± 0.8
C_3		11 ± 1	$(7.6 \pm 1.8) \times 10^4$	$(7.6 \pm 3.2) \times 10^{-5}$	15 ± 1.2	1.3 ± 1.0
C_4	Buffer	-	-	-	-	-

The standard errors shown in the table are calculated from the 6 ROIs that are in a single channel. The large variations could be due to the fact that the ligand was not uniformly immobilized in the channel. The model fit is in very good agreement for the lower concentration ligands. The deviation from model fit was observed for the higher ligand concentration measurements and is due to the fact that molecules are completely saturated or active sites are not accessible by the analyte molecules. High analyte concentrations can also lead to mass transport limited interactions.[42–44] Analyte concentrations for the kinetics experiment have to be in the range of the affinity constants to estimate the accurate results. In this experiment, we have included high

analyte concentrations and used the conventional 1:1 interaction model fit for the demonstration purpose only. In channel 1, the top most sensorgram is far away from the rest of the sensorgrams. This could be due to fabrication problem that might have existed in the specific gold sensing array. The standard error is comparatively less in the scenario 2 experiments.

7.3.4.2 Scenario 2 – One shot kinetics

The second demonstration that we have performed with the EKLB chip is one shot kinetics as previously reported.[16] The immobilization of ligand 1 followed by blocking and washing steps were done prior to the bonding of the top layer of chip. In this way, the electrical contact time with the surface gets reduced because of the offline immobilization. The interaction was performed with various concentrations of analyte 1. The resultant sensorgram and its 1:1 model fit are shown in Fig. 7.7. The residual plots are shown in the lower plot in Fig. 7.7. This is an ideal experiment that also works in the classical kinetics approach where various concentrations of analytes were used for the extraction of kinetics and affinity parameters of the interactant pairs. The experimental data and fit are in very good agreement in this case. Higher analyte concentrations used in channel 3 slightly deviates from the 1:1 interaction model, which is reproducible when we compare the results of the experiment in scenario 1. The response level observed was in the same range and the standard error is slightly lower in this case.

The association rate (k_a), as well as, dissociation rate (k_d) extracted using a global fit analysis are quite similar to the values extracted in scenario 1 and are shown in Table 7.2. The large distribution observed in k_a and k_d is due to the deviations observed in responses. Proper immobilization or well quantified immobilization would be very helpful in order to reduce the response variations.

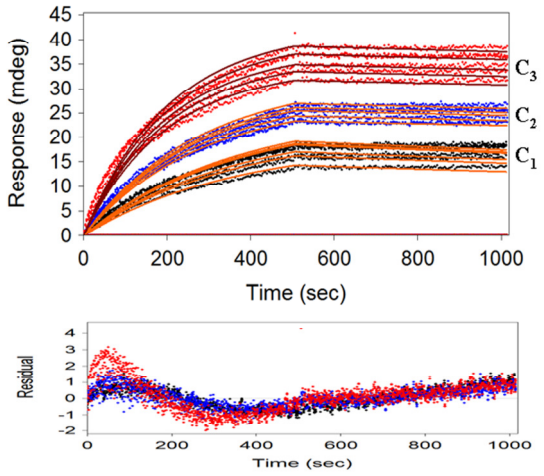

Figure 7.7 Experiment and model fit (orange curves) results of scenario 2. (a) The concentrations of Human IgG fabs immobilized in all the channels are 2 mg/mL. The analyte concentrations used are C_1=12.5 nM; C_2=25nM; C_3=50 nM and C_4=0 nM as reference. The residuals of the model fit are shown in the lower plot.

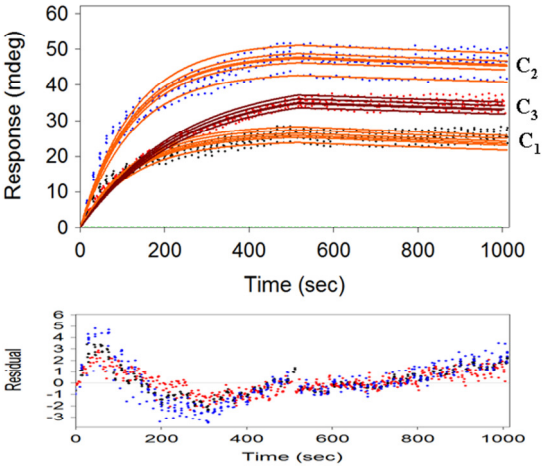

Figure 7.8 Experiment and model fit (orange curves) results of scenario 3. (a) C_1=85 mg/mL β2 microglobulin immobilized and 35 nM anti-β2 microglobulin as analyte; C_2=20 mg/mL neomycin immobilized and 110 nM anti-neomycin as analyte; C_3=2 mg/mL human IgG fabs immobilized and 50 nM anti-human IgG specific to fab as analyte; C_4=10 mM HEPES as reference. The residuals of the model fit are shown in the lower plot.

7.3.4.3 Scenario 3 – Multi-Ligand/Multi-Analyte detection

When kinetics information of a biomolecular interaction is not important, especially in the case of bio-detections or diagnostics, a single analyte (normally serum) is injected to detect and identify the presence of specific proteins or antibodies in the samples. If multiple components have to be detected in parallel, the assay time could be reduced which can make diagnostics faster. To demonstrate this scenario, we used each of the single channels for single interactant pairs and hence detected 3 different interactant pairs at the same time. The fourth channel is used for referencing with the 10 mM HEPES buffer.

Table 7.2 Summary of results for scenario 2. Single concentration of human IgG Fabs immobilized and various concentrations of Fab specific antihuman IgG as analyte (1 concentration in each channel). The number of points considered for estimating the standard error is 6.

Channels	**Interactant pairs**	**Response (t=500 s)**	k_a	k_d	R_{max}	K_D
		m°	**$M^{-1}s^{-1}$**	**s^{-1}**	**m°**	**nM**
C_1		35 ± 2				
C_2	HIgG Fabs - Fab Specific AHIgG	24 ± 1	(5.2 ± 2.2) × 10^4	(9.7 ± 4.9) × 10^{-5}	37 ± 3.2	1.9 ± 0.7
C_3		16 ± 2				
C_4	Buffer	-	-	-	-	-

In this experiment we see three different resultant sensorgram profiles, as well as, 1:1 model fits in Fig. 7.8. The extracted parameters for all 3 interactant pairs are listed in Table 7.3. In this case, similar results were observed in case of human IgG Fabs that were used in the previous experiments. The responses and extracted parameters are in the same range. This is a better indication that there is no cross contamination in the microchannels due to effects, such as, sample back flow from the

outlet reservoir. To avoid this effect, we have designed our chips with additional length in the microchannels from the sensing area to the outlet.

We have chosen three well known interactant pairs for this experiment to demonstrate the concept the new chip. All three interactant pairs follow the conventional 1:1 interaction model when the proper analyte and ligand concentration is used for the experiments. Kinetics information is not very important in this case as we try to detect multiple components at the same time. In general, the dissociation part of the sensorgram in all cases shows higher deviation which directly leads to higher error in dissociation rates. As of now, the exact reason for this deviation is unknown. However, the possible source of error could be due to the rebinding of desorbed analyte molecules to the surface which might arise from low flow rate.

Table 7.3 Summary of results for scenario 3. Various components immobilized in each channel and various antibodies specific to the immobilized ligands as analyte. The number of points considered for estimating the standard error is 6.

Channels	**Interactant pairs**	**Response (t=500 s)**	k_a	k_d	R_{max}	K_D
		m°	**$M^{-1}s^{-1}$**	**s^{-1}**	**m°**	**nM**
C_1	Neo - mAb Neo	47 ± 3	$(7.4 \pm 3.6) \times 10^4$	$(1.7 \pm 1.1) \times 10^{-4}$	50 ± 3.0	2.3 ± 0.9
C_2	HIgG Fab – Fab Specific AHIgG	35 ± 1	$(8.5 \pm 2.8) \times 10^4$	$(1.1 \pm 0.8) \times 10^{-4}$	41 ± 1.4	1.3 ± 0.8
C_3	β2M - mAb β2M	26 ± 2	$(2.2 \pm 1.2) \times 10^5$	$(1.9 \pm 1.0) \times 10^{-4}$	27 ± 1.7	0.9 ± 0.5
C_4	Buffer	-	-	-	-	-

There are some areas for future development in order to take full advantage of this method. The chips have been used for prototype development and this general

technique can be transferred to other materials such as glass. Another area for future development is overcoming the problem of gold degradation. We have observed that low conductivity buffers resulted in reduced damage to the gold sensing regions following a series of experiments. Hydrolysis leads to bubble formation in such circumstances on the corner of the gold sensing array and leads to detachment of the gold from the surface. This might be due to oxidation and subsequent removal of the titanium adhesion layer. Other adhesion layers, such as, tantalum can avoid this problem (results not shown). Coating of gold layers with functionalized hydrogel can protect the metal layer to a certain extent.[30]

7.4 Conclusion

We have successfully demonstrated various possibilities of biosensing including multi-ligand/multi-analyte detection with the new device using electrokinetic fluid transport. The demonstration of the multi-ligand/multi-analyte concept using electrokinetics shows a new direction for biosensing chips when large numbers of reagents are simultaneously measured. At present, the possibility of extending this chip to greater than 10 channels where each channel has 12 sensing locations leading to the measurement of more than 100 sensing areas simultaneously, which are within the dimensions of CCD camera of iSPR system.

7.5 References

(1) He B., Morrow TJ., and Keating CD.; Curr. Opin. Chem. Biol., 12 (2008) 522-528.
(2) Hinman AR.; Vaccine., 16 (1998) 1116–1121.
(3) Wulfkuhle JD., Liotta LA., and Petricoin EF.; Nat. Rev. Cancer, 3 (2003) 267-275.
(4) Zheng G., Patolsky F., Cui Y., Wang WU., and Lieber CM.; Nat Biotechnol., 23 (2005) 1294-1301.
(5) Yue M., Majumdar A., and Thundat T.; BioMEMS and Biomedical Nanotechnology, 2007, Springer US (pp.21 - pp.33).
(6) Brunker SE., Cederquist KB, and Keating CD.; Nanomed., 2 (2007) 695-710.
(7) Rothenhaeusler B., and Knoll W.; Nature, 332 (1988) 615-617.
(8) Macbeath G., and Schreiber SL.; Science, 289 (2000) 1760-1763.
(9) Boer AR-de, Hokke CH., Deelder AM., and Wuhrer M.; Glycoconjugate J., 25 (2008) 75-84.
(10) Taylor JD., Linman MJ., Wilkop T., and Cheng Q.; Anal. Chem., 81 (2009) 1146-1153.

(11) Abdiche YN., Malashock DS., Pinkerton A., and Pons J.; Anal. Biochem., 386 (2009) 172-180.
(12) Boozer C., Ladd J., Chen S., and Jiang S.; Anal. Chem., 78 (2006) 1515-1519.
(13) Raz SR., Bremer MGEG, Giesbers M., and Norde W.; Biosens. Bioelect., 24 (2008), 552-557.
(14) Lokate AMC., Beusink JB., Besselink GAJ., Pruijn GJM., and Schasfoort RBM.; J. Am. Chem. Soc., 129 (2007) 14013-14018.
(15) Karlsson R., Kullman-Magnusson M., Hamalainen MD., Remaeus A., Andersson K., Borg P., Gyzander E., and Deinum J.; Anal Biochem., 278 (2000) 1-13.
(16) Bravman T., Bronner V., Lavie K., Notcovich A., Papalia GA., and Myszka DG.; Anal Biochem., 358 (2006) 281-288.
(17) Krishnamoorthy G., Carlen ET., Kohlheyer D., Schasfoort RBM., and van den Berg A.; Anal. Chem., 81 (2009) 1957-1963.
(18) Piliarik M., Vaisocherová H., and Homola J.; Biosens. Bioelec., 20 (2005) 2104-2110.
(19) Homola J., Lu HB., Nenninger GG., Dostálek J., and Yee SS.; Sens. Act. B, 76 (2001) 403-410.
(20) Berger CEH., Beumer TAM., Kooyman RPH., and Greve J., Anal. Chem., 70 (1998) 703–706.
(21) Dong Y., Wilkop T., Xu D., Wang Z., and Cheng Q.; Anal, Bioanal. Chem., 390 (2008) 1575-1583.
(22) Kuo-Hoong L., Yuan-Deng S., Shean-Jen C., Fan-Gang T., and Gwo-Bin L.; Biosens. Bioelec., 23 (2007) 466-472.
(23) Situ C., Crooks SRH., Baxter GA., Ferguson J., and Elliott CT.; Anal. Chim. Acta., 473 (2002) 143–149.
(24) Naimushin AN., Soelberg SD., Nguyen DK., Dunlap L., Bartholomew D., Elkind J., Melendez J., and Furlong CE.; Biosens. Bioelect., 17 (2002) 573-584.
(25) Taylor AD., Ladd J., Yu Q., Chen S., Homola J., and Jiang S.; Biosens. Bioelect., 22 (2006) 752-758.
(26) Wang Z., Wilkop T., Xu D., Dong Y., Ma G., and Cheng Q.; Anal. Bioanal. Chem., 389 (2007) 819-825.
(27) Homola J., Dostálek J., Chen S., Rasooly A., Jiang S., and Yee SS.; Int. J. Food Microbiol. 75 (2002) 61-69.
(28) Palumbo M., Pearson C., Nagel J., and Petty MC.; Sensor. Actuat. B-Chem., 90 (2003) 264-270.
(29) Kawazumi H., Vengatajalabathy KG., Ogino K., Maeda H., and Miura N.; Sensor. Actuat. B-Chem., 108 (2005) 791-796.
(30) Krishnamoorthy G., Carlen ET., Beusink JB., Schasfoort RBM., and van den Berg A.; Anal. Methods, 1 (2009) 162-169.
(31) Andersson O., Nikkinen H., Kanmert D., and Enander K.; Biosens. Bioelect., 24 (2009) 2458-2464.
(32) Schlautmann S., Besselink GAJ., Radhakrishna Prabhu G., and Schasfoort RBM.; J. Micromech. Microeng., 13 (2003) S81–S84.
(33) Jeong HE., and Suh KY.; Lab Chip, 8 (2008) 1787–1792.
(34) Beusink JB., Lokate AMC., Besselink GAJ., Pruijn GJM., and Schasfoort RBM.; Biosens. & Bioelec., 23 (2008) 839-844.
(35) Krishnamoorthy S., Feng J., Henry AC., Locascio LE., Hickman JJ., and Sundaram S.; Microfluid. Nanofluid., 2 (2006) 345-355.
(36) Gao Y., Wong TN., Chai JC., Yang C., and Ooi KT.; Intl. J. Heat and Mass Trans., 48 (2005) 5103-5111.
(37) Abelès F., and Lopez-Rios T.; Solid State Comm., 16 (1975) 843-847.
(38) Gordon II JG., and Ernst S.; Surf. Sci., 101 (1980) 499-506.
(39) Kolb DM.; Prog. In Surf. Sci., 51 (1996) 109-173.

(40) Kohlheyer D., Besselink GAJ., Lammertink RGH., Schlautmann S., Unnikrishnan S., and Schasfoort RBM.; Microfluid. Nanofluid 1 (2005) 242-248.
(41) Morton TA., Myszka DG., and Chaiken IM.; Anal. Biochem., 227 (1995) 176-185.
(42) Schuck P.; Biophy. J., 70 (1996) 1230-1249.
(43) Myszka DG., Morton TA., Doyle M., and Chaiken IM.; Biophys. Chem., 64 (1997) 127-137.
(44) Glaser RW.; Anal. Biochem., 213 (1993) 152-161.
(45) Raether H.; Surface Plasmons on Smooth and Rough Surfaces and on Gratings, Springer-Verlag, Berlin, Germany (1986).

8

Electrokinetic Drug Screening Chip

In this chapter, we present an extended version of the electrokinetic multi-ligand multi-analyte chip described in Chapter 7, where upto 10 samples can be simultaneously processed on chip. This approach reduces the time of experiment when compared to the conventional experimental methods. This new device offers a high degree of parallelization for not only analytes, but also for ligands where upto 90 ligands are present on the sensing surface. This proof of concept has been demonstrated with well known interactant pairs. A discussion of drug screening applications concludes the chapter. A part of this chapter was modified from Lab Chip DOI:10.1039/C000705F (2010).

8.1 Introduction

We have already discussed the importance of surface plasmon resonance in the field of biomolecular interaction studies in previous chapters of this thesis. Hence, the focus of this chapter is the development of a new integrated device for drug screening applications. But the question is "are the SPR based diagnostic approaches useful for drug discovery?" We try to answer this question. The drug discovery companies are shifting their focus from high throughput screening towards more focused screening of drugs[1] and drug fragments[2]. This type of analysis is where SPR biosensors are most effective and are quite commonly accepted as an important method. SPR is regularly used in the drug discovery process where some important parameters, such as kinetics[3] and affinity[3] of drugs to the proteins, can be extracted in real-time in a label-free manner. Previously, drug screening was performed with fluorescent labels[4] or radioactive labels[5], where extra time and cost are required for the labeling process. There are many ways in which drug screening can be performed, but this is not the scope of this chapter. Previously reported reviews of various types of drug screening

approaches, as well as, the application of optical biosensors in drug discovery are available.[6,7]

Microfluidic lab-on-a-chip (LOC) systems play a very important role in drug discovery as previously reported.[8,9] However, there are no reports, to the best of our knowledge, that address integrated SPR – LOC devices in the field of drug discovery. In general, the combination of SPR with LOC technology, was previously reported for bioanalytical systems[10,11] because the two techniques can be integrated relatively easily and have the potential for fast, automated biomolecular analysis with ultra-small sample volumes.[12] Integrated LOC systems were also demonstrated previously by others[13] as well as by us in previous chapters (Chapter 6 and 7).[14,15] There are many recent reports describing new trends and designs for integrated SPR-LOC based measurement systems[16-20] and many reports of applications for integrated LOC-SPR systems, such as, immunoassays,[21] protein-aptamer interactions[22] and cellular detection.[23] A detailed review of integrated SPR-LOC systems has been discussed in Chapter 2. While the SPR and integration of microfluidics leads to a highly multiplex system, the integration of microarray to this integrated system leads to high-throughput multiplex system. This is currently an active area of research.[24-27] As we mentioned previously, there is still plenty of room for improvement of such integrated systems to make efficient handling of samples as well as the more stable and robust operation of such integrated chips. We demonstrated an integrated iSPR-microarray-microfluidics system with electro osmotic flow (EOF)[28-30] (also see chapter 7) for sample transport and electrokinetic focusing (EKF)[31-37] (also see chapter 6) for sample guiding to specific array locations, which may be important for instrument miniaturization and scaling to larger numbers of the samples where conventional techniques will no longer be possible as the fluid handling would be tedious and cumbersome when more number of microchannels has to be handled simultaneously.

We report here a simple integrated system with 12 microchannels in parallel and each microchannel has 12 gold sensing islands with electrokinetic transport of samples. For demonstration purpose, we use well-known interactant pairs in each

channel that results in the demonstration of nine different biomolecular interaction measurements simultaneously. One channel has been used for blank measurements for an experimental control.[38] By observing the technical problems involved in such an integrated systems for highly parallel measurements, we propose the solution for solving those problems and also proposed a new hyphenated approach in the application area of drug screening.

8.2 Materials and Methods

8.2.1 Chip Descriptions

A two layer (Glass-PDMS) chips was used in this work. The chip fabrication was similar to that of the procedures described in Chapters 6 (section 6.6.1) and 7. The chip size is 15x15 mm^2. The top PDMS layer includes the channel structures (12 parallel channels), and reservoir holes for samples and buffer introduction. The bottom glass chip layer, which is refractive index matched (n=1.52) to the hemispherical prism of the iSPR instrument (IBIS Technologies b.v., Hengelo, Netherlands),[14,15] has patterned gold islands (12x12 array) of 150 μm in diameter and 500 μm in pitch (center to center distance between two gold islands), as well as thickness of 47 nm (with 2 nm thick of titanium adhesion layer to enhance the gold adhesion) for iSPR. These sensing islands were coated with carboxymethyl dextran hydrogel (XanTec GmbH, Muenster, Germany) for covalent immobilization of biomolecules. The bonding of two layers of chips was done with UV-curable glue[39] and the protocol described in chapter 7.

Each reservoir hole is 1 mm in diameter and the depth of the microchannel and interaction chamber is 48 μm. The illustration of the two layer chip together with chip holder integrated with platinum electrodes, as well as electrical connection representation is shown in Fig. 8.1. The length of each microchannel is different and the voltages that are required to calculate the same flow-rate has been listed in table 8.1.

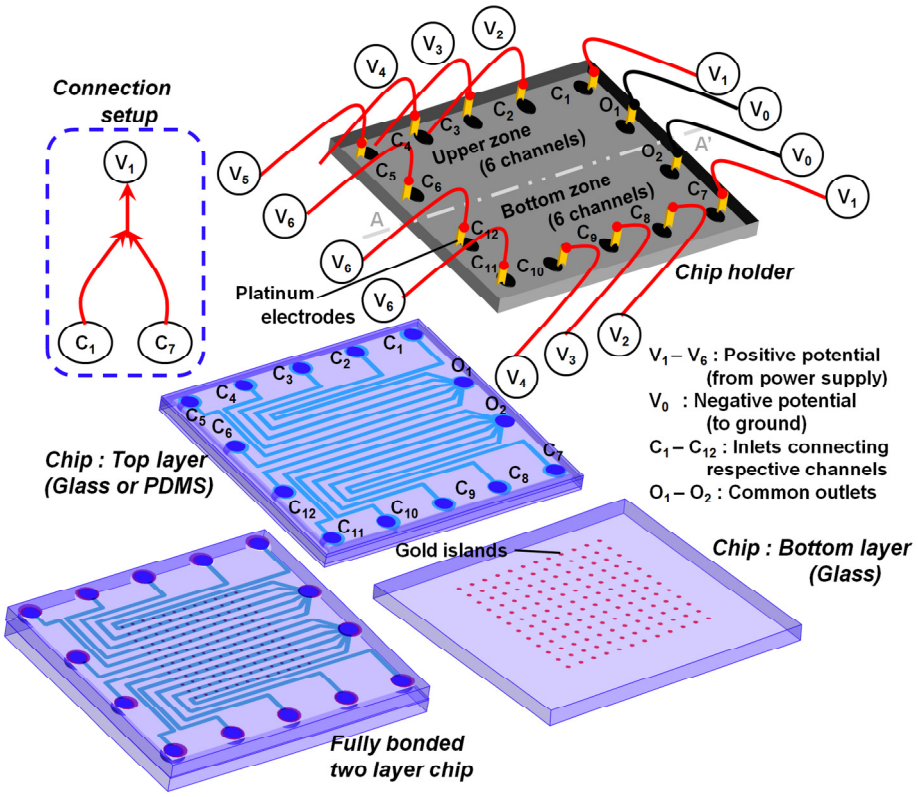

Figure 8.1 Illustration of the biochip (top layer – PDMS and bottom layer – glass with gold islands) with chip holder (integrated with platinum electrodes as well as reservoir holes for extra sample volume). The UV curable glue bonded chip is also shown here. Top left side image represents the electrical connections (For example: Channel 1 and channel 7 are connected to the same voltage source). A-A' (Grey) line represents the splitting of two groups of channels structures and is also shown in chip images.

8.2.2 Materials

The immobilization buffer used in this study was 10 mM sodium acetate (Sigma, the Netherlands), pH 5.2 and the running buffer was 10 mM HEPES buffer (Sigma, the Netherlands), pH 7.2 and conductivity of 29.6 µS/mm. The ligands used in this study are bovine serum albumin (BSA), human serum albumin (HSA), human immunoglobulin G (HIgG), β2-microglobulin (β2M) and antibiotics such as neomycin,

gentamycin, all bought from Sigma, the Netherlands. Other ligands such as Fab fragment of HIgG, $F(ab')_2$ fragment of HIgG and Fc fragments of HIgG, all bought from Jacksons Immunoresearch, USA. Various analytes used in the study are antibodies specific for HSA and BSA (Sigma, the Netherlands); antibodies of Fab specific, $F(ab')_2$ specific, and Fc fragment specific HIgG (Jacksons Immunoresearch, USA); antibody specific to β2M (Abcam, USA); antibodies specific to HIgG (Zymax, USA); antibodies specific to antibiotics (Neomycin and Gentamycin) (Biodesign, USA).

Table 8.1 Summary of various channel dimensions as well as the respective voltages used for fluid transport.

Channels	Channel Length (mm)	Voltage (V)
C_2	18.88	185 (V_2)
C_3	17.40	171 (V_3)
C_4	16.20	159 (V_4)
C_5	16.18	159 (V_5)
C_6	13.26	130 (V_6)
C_8	18.88	185 (V_2)
C_9	17.40	171 (V_3)
C_{10}	16.20	159 (V_4)
C_{11}	16.18	159 (V_5)
C_{12}	13.26	130 (V_6)

8.3 Results and Discussions

8.3.1 Electrokinetic flow simulations

Electrokinetic flow has been used in this study for the transport of all samples and buffers. The electrokinetic behavior in the microchannel has been modeled with a two-dimensional finite element code (conductive media model[40] integrated with Navier-stokes equation[41]) using a commercial finite element software "COMSOL Multiphysics (COMSOL, USA)" (section 7.3.1)., and the same has been implemented

here to extract the parameters such as voltages necessary for the uniform velocity in all the channels according to the channel dimensions. The representation (C_n, V_n) in Fig. 8.2 represents the respective channel numbers and voltages used in the simulation and experiments. The gold sensing islands have been set as floating during the simulation process. Since the area of gold is small compared to the total area of the channel, it does not show any macroscopic effects. However, the detailed evaluation of the simulated results shows the non-linear electrokinetic phenomenon.[42] The electric field lines intersects the gold islands at a certain angle to the gold islands. In reality, this might not be true as the gold islands are coated with polymers such as dextran. The boundry condition has been changed to "surface insulation" from "floating potential". In this situation, the later phenomenon has not been observed. Under steady state conditions, even without a dextran layer, the electrical double layer over the floating potential insulates the surface completely when the current drives positive ions towards one half side and negative ions to the other half side of the gold islands. In this situation, no electric field penetrates through the gold islands and electric field lines are tangential to the gold islands. When the electroosmotic slip was assumed, then the situation is different. However, simulations were carried out with no-slip boundry conditions.

The required flow velocity in each channel was set as 50 μm/sec and the voltage required to achieve such a flow velocity was estimated and applied in all experiments. The channel dimensions were chosen in such a way that there won't be electrochemical reactions near the gold islands due to current flowing over the gold.[14] The electroosmotic mobility was assumed to be 5×10^{-8} m^2/Vs.[43] The electric field across each channel is ~9 V/mm. As previously mentioned, our experimental result does not show any gold damage in this range. Also the dextran coating over the gold island prevents the electrochemical reaction up to a certain extent. iSPR experiments were performed with the known interactant pairs with the newly developed chip and are discussed in the following section.

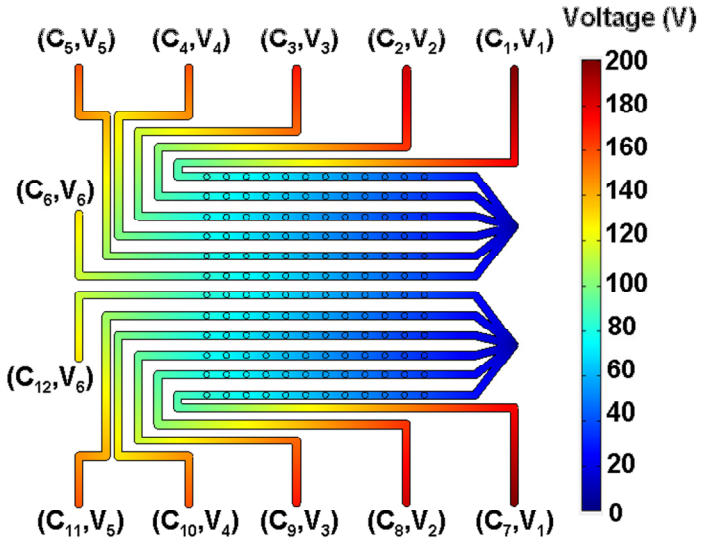

Figure 8.2 Voltage profile across each channels using simulation of 2D Navier-Stokes equation with Conductive media model (COMSOL, USA). To have uniform velocity in all the channels, the input voltages were calculated accordingly and are listed in table 8.1

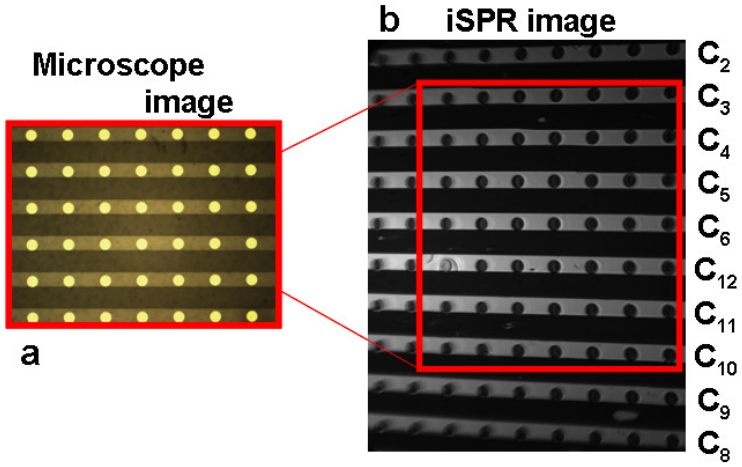

Figure 8.3 (a) Microscope image of the chip (2x magnification) (b) iSPR image of 10 channels and 10x9 (90) gold islands for the iSPR measurement. Channels 1 and 7 as well as some gold islands (10x3 + 2x12 = 54) were not included in the study as this is out of the image area and iSPR signal could not be measured in those channels.

8.3.2 iSPR Experiment: Biomolecular Interactions

The integration of electrokinetics and iSPR was previously reported by our group,[15] Hence, the new device has been used directly for the iSPR experiments. To demonstrate the proof of principle, a well known model biomolecular interaction pairs (table 8.2) has been considered. The chip was inspected in the microscope for any fabrication artifacts (Fig. 8.3 left side). The initial iSPR image is shown in Fig. 8.3 b.

The reproducibility of the iSPR measurement could be checked directly without repeating the experiment as each channel has 12 gold sensing islands for the measurement of same interactant pairs 12 times. However, the full sensing area did not completely fit in the iSPR camera (the range where the biomolecular interactions are measured) and hence could not measure all the channels, and hence reducing the number of samples measured simultaneously to 10. There were also a reduction in number of gold sensing islands in each channels (12 → 9). In the end, we could measure 90 simultaneous interactions instead of 144 for which, the chip has been initially designed. This is due to the restriction in the size of sensing area on the iSPR system only. Changing the chip design to accommodate the required number of channels and gold sensing islands required in the specific dimensions of the iSPR CCD camera resolution, then it would be possible to measure all the ligands and analyte samples in the same time. We have considered the chip as it is, to demonstrate the proof of principle of our new device.

All ligands used in this study were diluted 1:2 times from stock solutions using 10 mM sodium acetate buffer of pH 5.2 and its respective final concentrations used are listed in Table 8.3. Prior to the PDMS chip bonding to the glass chip, the chip surface has been activated with mixture of 0.4 M EDC and 0.1 M NHS for 20 minutes.[44] After the activation step, the chip surface was washed with 0.25% acetic acid to maintain the acidic property for the covalent immobilization of ligands. The processed chip is then dried with dry nitrogen. After chip bonding, 4μL of sample ligands have been immobilized in each channel. The chip has been kept in a humidity chamber (1 hour).

Table 8.2 Ligands and analytes used in this study in the respective channels.

Channels	Ligands	Analytes
C_2	Bovine Serum Albumin (BSA)	Anti-BSA
C_3	Human Serum Albumin (HSA)	Anti-HSA
C_4	Human Immunoglobilin G (HIgG)	Anti-HIgG
C_5	Neomycin	Anti-Neomycin
C_6	Gentamycin	Anti-Gentamycin
C_8	Fab HIgG	Fab Specific AHIgG
C_9	$(Fab)_2$ HIgG	$(Fab)_2$ Specific AHIgG
C_{10}	Fc HIgG	Fc Specific AHIgG
C_{11}	β2-Microglobulin	Anti-β2M
C_{12}	Buffer	Buffer

The microchannels were washed and filled with a running buffer, and the chip has been placed over the iSPR interface module with a drop of refractive index matching oil. The iSPR interface module together with the chip is docked into the iSPR system followed by fixing of chip holder on the top of the chip. Various analyte samples were filled in their respective cuvettes of the chip holder. The electrodes are connected to the voltage power supply (IBIS Technologies B.V., Hengelo, the Netherlands). The voltages were controlled using an in-home developed C++ interface module, which is different than previously used (Chapter 6 and 7). The analyte sample concentrations used in this study are listed in Table 8.3. The results are shown in Fig. 8.4 for all the channels and gold sensing islands. The response observed in the association phase (t = 500 sec) with its standard error over the entire channel (n=9) are also listed in last column of Table 8.3.

Deviations in the response intensity were observed in the iSPR responses of the channels C_2 and C_4 (Fig. 8.4). This could be due to the uncontrolled immobilization where there is no control or quantitative measurement of the same. This could also be due to the fact that the molecules are multivalent.[56] The responses observed in the

channels: C_2, C_3, C_6, C_8 and C_9 could be influenced by steric hindrance due to the fact that the analyte sample used is bigger (150 KDa) than the immobilized molecules[45] (For example, the immobilized ligands, such as BSA or HSA (66 KDa), neomycin (615 Da), gentamycin (576 Da) and Fab fragments of HIgG (50 KDa) and F(ab')$_2$ fragments of HIgG (100 KDa)). Highly oriented or high ordered spaced immobilization could be helpful in these cases or immobilizing very small amount of samples (low ligand density) could avoid this problem and should not affect the binding kinetics.

Table 8.3 Concentration of sample ligands and analytes used in this study. The last column shows the response observed in the interface of association and dissociation phase (t = 500 sec) with its standard error (n=9).

Channels	Ligand Conc. (mg/mL)	Analyte Conc. (μg/mL)	Response (mdeg)
C_2	5.0	80	54±7
C_3	5.0	80	142±5
C_4	0.5	20	51±4
C_5	17.0	66	20±1
C_6	7.5	12	124±3
C_8	2.2	26	16±1
C_9	2.2	46	49±2
C_{10}	1.2	26	63±2
C_{11}	0.13	20	42±1
C_{12}	0	0	0±0.3

Another factor that could be instantly observed is slow dissociation rates, indicating the strong complex formation (C_3, C_4, C_6 and C_{10}). In the following cases, Fab HIgG (C_8), β2M (C_{11}) and neomycin (C_5), the dissociation phase starts slightly after 500 seconds, and could be the indication of effect of flow rate change during the experiment which might be due to the adsorption of molecules on the PDMS walls.[46] For the demonstration, there is no need for any model functions and fitting routines, as well as kinetics parameter extractions. It could be of beneficial only in a later stage.

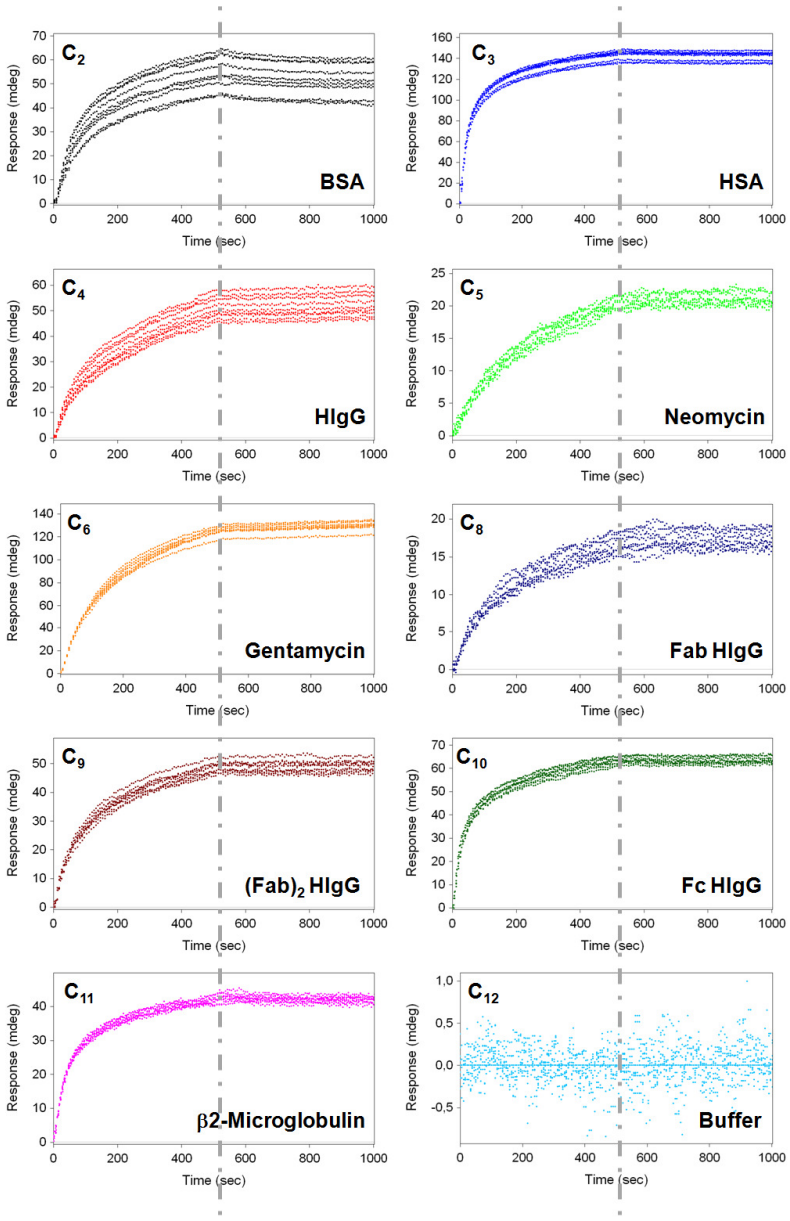

Figure 8.4 Processed iSPR sensorgrams from the various well known interactant pairs used in this study as a proof of concept. The sensorgrams are split into two parts with grey lines (Left side: association phase for 500 sec; Right side: dissociation phase for 500 sec). The channel numbers are displayed in the top left hand corner with its identities respectively.

8.3.3 Technical Problems

There are some issues that have to be addressed immediately to perform the experiments more efficiently. In our preliminary experiments demonstrated here, we have observed some practical and technical difficulties. Overcoming these following practical difficulties could be beneficial for the drug discovery community for easy drug screening in reduced time.

The first major issue was the problem of measuring all the region of interests "ROIs" (gold islands where the iSPR signals are measured) due to CCD camera restrictions of the iSPR system used. As we mentioned above, this problem could be handled carefully by designing the chips more carefully. However another major technical problem being the sensitivity of the interactions are affected when the ROIs are away from the center of the measurement zone (see Fig. 8.3). Corners are bit faded and no sharp images have been observed and hence the data obtained in the corners are not reliable as well as leads to higher standard deviations. It is also necessary to have good and reliable results from the SPR based assays. Better SPR dips (deep and narrow dip) leads to reliable data.[47] The chip design for multi-ligand/multi-analyte detection becomes crucial in the space available (when corners are excluded) for the powerful and reliable measurement in the iSPR system. In order to validate this critical point, more experimental work has to be performed in the same configuration.

We have used PDMS as the top chip layer, which has to be diced perfectly in order to avoid the alignment problems with the gold sensing islands (150 μm diameter) and the channel width (200 μm). To avoid this problem, as well as the surface treatment step (to prevent protein adsorption to the PDMS wall), we propose to make the device in glass/glass. However the low temperature bonding that is required for the bonding of glass/glass chips is problematic. In the preliminary bonding procedures, we have observed bubble formation between the two glass layers when UV curable glue (NOA 81) is used. The reason is not yet known. High temperature glass/glass bonding[48] which is normally used cannot be used in our case as the high temperature leads to diffusion of the titanium layer (adhesion layer for gold) through the gold layer and we

have observed anamalous iSPR signals (results not shown).[49]

8.4 Proposed New Drug Screening Approach

This new device can, in principle, directly implemented for drug screening applications with certain improvements mentioned in the previous section. Normally, a drug screening is done with immobilizing HSA on the sensing surface followed by the injection of various concentrations of sample drugs, one after the other, with regeneration steps. With the collected iSPR data, the affinity was calculated and ranked in order to choose the right hits in the drugs that were screened. This process of performing an experiment can take days to weeks. Our idea is to reverse the drug screening assay by immobilizing various drugs on the sensing surface and inject various concentration of HSA to extract the required parameters. This is also due to the fact that small molecule measurements in the IBIS iSPR system are not possible. Reversing the assay leads to the injection of proteins or antibodies over the immobilized small molecules surface, in which case, the molecular weight is higher, there won't be any problem in measuring the SPR signal during the drug-protein interaction measurements. However, there is a need for more amount of ligands that has to be immobilized on the sensing surface. The list of drugs that would be considered in this study is listed in Fig. 8.6.

There are many ways to perform drug screening assay in this newly developed device. These are:

1. Various drug molecules can be immobilized in various channels followed by the injection of HSA in order to measure the drug-protein interactions in real-time. The data is then fitted to the model functions to extract the affinity constants of drug-protein complex. Since a single channel is completely used and measures a single set of drug-protein sets, which has multiple gold sensing islands, there is no need for multiple experiments to check the consistency and reproducibility of the measured responses.[15]
2. The method mentioned in "1" can also be extended to perform experiments to record kinetic titration data for which, regeneration steps can be completely neglected. In this

approach, the affinity parameter can be extracted in the same way as the conventional approach where multiple concentrations of analytes were used.[50]

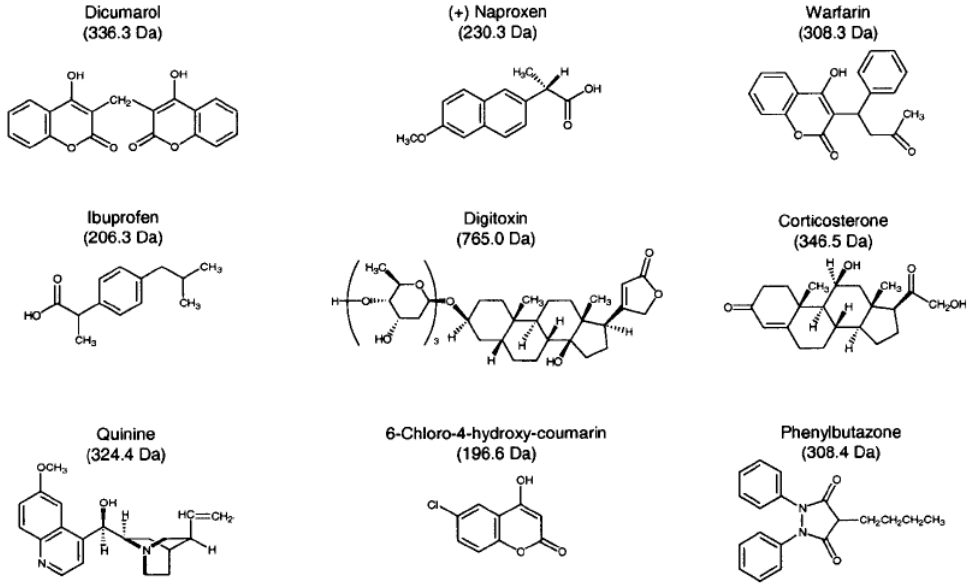

Figure 8.6 Panel of useful drugs for assay development.

3. Another possible approach could be to immobilize the same drug in various channels and inject various concentrations of HSA of each concentration in the single channels and to extract the kinetics and affinity constant of the interactant sets similar to that of conventional approach and is also termed as "one shot kinetics".[51] A major disadvantage to this approach is that, only a limited number of drugs can be screened simultaneously as many channels are used for a single drug component.

4. Various drug molecules can be immobilized on each gold sensing island (could also be different molecules in single channel) using a commercially available spotter.[52] Injecting the HSA in all the channels leads to data recording of all the drug-protein interactant sets. The affinity constant is extracted for all the sets in a single experiment. In this case, with the present chip design and technical aspects, it is possible to screen

80-90 drugs in a single experiment.

In all the above mentioned cases, one critical point of consideration is the immobilization of drugs on the sensing surface.[53] This is different when compared to immobilizing proteins or antibodies that have discussed throughout this thesis booklet. In this case, the covalent immobilization of drug molecules to the sensing surface should happen with the –OH groups that are on the molecules.[54] In this case, different surface chemistry protocol have to be followed in order to achieve good immobilization. The immobilization procedure is as follows: The hydrogel surface could be considered and immobilized dry with heating (mild SO_4 catalysis). However, carboxymethyl dextran is less suitable as there could be a cross reactivity of the abundant hydroxyl groups of the dextran matrix. The formed esters are also subject to slow hydrolysis. For a very stable immobilization, it might make more sense to partially amino-functionalize the hydrogel (activation of sensor chip with EDC/NHS, but for very short time and functionalize it with 1M ethanolamine), followed by the introduction of epichlorohydrine (generation of epoxy functionalities) and again immobilize dry. In this way, the linkage is through amide and ether bond which gives more stable and robust immobilization.

It is also not necessary to wait for more than 10 hours to have a stable baseline measurement as is the case in immobilizing HSA on the surface.[55] In general, for unknown reasons, the stable baseline could be achieved after 10 hours of continuous injection of buffer and regeneration solution over the HSA surface. This saves a huge amount of time in performing such an assay using the proposed approach.

8.5 Summary

The successful implementation of a newly designed chip was demonstrated for the multiple ligand - multiple analyte (upto 10) interactions. However there are many technical problems that have to be addressed before it is suitable for drug screening applications. The problems include, the corrected chip design as per the CCD camera dimensions, sensitivity issues in the corners, replace the PDMS with glass chips for

which, the low temperature bonding problem must be addressed. The electrochemical reaction problem arises due to high electric current flow could be avoided by choosing proper design of the microchannels as well as with changing the titanium adhesion layer to tantalum layer for which the preliminary experiments already shows the promising results. But it needs optimization with respect to the optical settings of the iSPR system used. With all the improvements, the newly developed chip would be promising for performing the drug screening assay. This small scientific and technical contribution would be beneficial for high throughput – multiplex drug screening, where faster techniques are still in demand.

8.6 References

(1) Skehan P, Storeng R., Scudiero D., Monks A., McMahon J., Vistica D., Warren JT., Bokesch H., Kenney S., and Boyd MR.; J. Natl. Cancer Inst., 82 (1990) 1107-1112.
(2) Hajduk PJ., and Greer J.; - Nature Reviews Drug Discovery, 6 (2007) 211-219.
(3) Doyle ML., Myszka DG., Chaiken IM.; J. Mol. Recognit. 9 (1996) 65-74.
(4) Smilkstein M., Sriwilaijaroen N., Kelly JX., Wilairat P., and Riscoe M.; Antimicrobial Agents and Chemotherapy, 48 (2004) 1803-1806.
(5) Wise DL., McCormick GJ., Willet GP., and Anderson LC.; Life Sciences, 19 (1976) 867-873.
(6) Cooper MA.; Nature Reviews Drug Discovery, 1 (2002) 515-528.
(7) Bleicher KH., Böhm H-J., Müller K., and Alanine AI.; Nature Reviews Drug Discovery, 2 (2003) 369-378.
(8) Dittrich PS., and Manz A.; Nature Reviews Drug Discovery, 5 (2006) 210-218.
(9) Weigl BH., Bardell RL., and Cabrera CR.; Advanced Drug Delivery Reviews, 55 (2003) 349-377.
(10) Brockman JM., Frutos AG., and Corn RM.; J. Am. Chem. Soc., 121 (1999) 8044-8051.
(11) Lee HJ., Goodrich TT., and Corn RM.; Anal. chem., 73 (2001) 5525-5531.
(12) Lew HS., and Fung YC.; J. Biomech. 2 (1969) 105-119.
(13) Sjoelander S., and Urbaniczky C.; Anal. Chem. 63 (1991) 2338-2345.
(14) Krishnamoorthy G., Carlen ET., Kohlheyer D., Schasfoort RBM., and van den Berg A.; Anal. Chem., 81 (2009) 1957-1963.
(15) Krishnamoorthy G., Carlen ET., deBoer HL., van den Berg A., and Schasfoort RBM.; (2010) Manuscript submitted. (Chapter 7)
(16) Figeys D., and Pinto D.; Electrophoresis 22 (2001) 208-216.
(17) Schasfoort RBM.; Expert Rev. Proteomics 1 (2004) 123-132.
(18) Gervais T., and Jensen KF.; Chem. Eng. Sci., 61 (2006) 1102-1121.
(19) Galopin E., Beaugeois M., Pinchemel B., Camart JC., Bouazaoui M., and Thomy V.; Biosens. Bioelec. 23 (2007) 746-750.
(20) Skottrup PD., Nicolaisen M., and Justesen AF.; Biosens. Bioelec. 24 (2008) 339-348.
(21) Luo Y., Yu F., and Zare RN.; Lab Chip 8 (2008) 694-700.
(22) Wang Z., Wilkop T., Xu D., Dong Y., Ma G., and Cheng Q.; Anal. Bioanal. Chem. 389 (2007) 819-825.

(23) Lei KF., Law WC., Suen YK., Li WJ., Ho HP., Lin C., and Kong SK.; Proc. 5th IEEE Conf. Nanotechnol. 1 (2005) 515-518.
(24) Lee KH., Su YD., Chen SJ., Tseng FG., and Lee GB.; Biosens. Bioelec. 23 (2007) 466-472.
(25) Mauriz E., Calle A., Manclus JJ., Montoya A., Escuela AM., Sendra JR., and Lechunga LM.; Sens. Act. B, 118 (2006) 399-407.
(26) Yuk JS., Kim HS., Jung JW., Jung SH., Lee SJ, Kim WJ, Han JA., Kim YM., and Ha KS.; Biosens. Bioelec., 21 (2006) 1521-1528.
(27) Homola J., Vaisocherová H., Dostálek J., and Piliarik M.; Methods, 37 (2005) 26-36.
(28) Ellender RD., Morton F., Whelan J., and Sweet BH.; Prep. Biochem., 2 (1972) 215-228.
(29) Gao Y., Lin FYH., Hu G., Sherman PM., and Li D.; Anal. Chim. Acta, 543 (2005) 109-116.
(30) Hu G., Gao Y., Sherman PM., and Li D.; Microfluid. Nanofluid., 1 (2005) 346-355.
(31) Fu LM., Yang RJ., Lee GB., and Liu HH.; Anal. Chem., 74 (2002) 5084-5091.
(32) Fu LM., Yang RJ., and Lee GB.; Anal. Chem., 75 (2003) 1905-1910.
(33) Besselink GAJ., Vulto P., Lammertink RGH., Schlautmann S., van den Berg A., Olthuis W., Engbers GHM., and Schasfoort RBM.; Electrophoresis, 25 (2004) 3705-3711.
(34) Kohlheyer D., Besselink GAJ., Lammertink RGH., Schlautmann S., Unnikrishnan S., and Schasfoort RBM.; Microfluid. Nanofluid., 1 (2005) 242-248 .
(35) Wu CH., and Yang RJ.; Electrophoresis, 27 (2006) 4970-4981.
(36) Kohlheyer D., Unnikrishnan S., Besselink GAJ., Schlautmann S., and Schasfoort RBM.; Microfluid. Nanofluid., 4 (2007) 557-564.
(37) Pan YJ., Ren CM., and Yang RJ.; J. Micromech. Microeng., 17 (2007) 820-827
(38) Morton TA., Myszka DG., and Chaiken IM.; Anal. Biochem., 227 (1995) 176-185.
(39) Schlautmann S., Besselink GAJ., Radhakrishna PG., and Schasfoort RBM.; J. Micromech. Microeng. 13 (2003) S81-S84.
(40) Gawad S., Schild L., and Renaud Ph.; Lab Chip, 1 (2001) 76-82.
(41) Ghia U., Ghia KN., and Shin CT.; J. Comp. Phys., 48 (1982) 387-411
(42) Soni G., Squires TM., and Meinhart CD.; Proc. of Comsol Users Conf., 2007.
(43) Kohlheyer D., Besselink GAJ., Lammertink RGH., Schlautmann S., Unnikrishnan S., and Schasfoort RBM.; Microfluid. Nanofluid., 1 (2005) 242-248.
(44) Lokate AMC, Beusink JB, Besselink GAJ., Pruijn GJM., and Schasfoort RBM.; J. Am. Chem. Soc., 129 (2007) 14013-14018.
(45) D. Hall, and D.J. Winzor; Int. J. Biochromatogr. 4 (1999) 175-186.
(46) Huang B., Wu H., Kim S., and Zare RN.; Lab Chip, 5 (2005) 1005-1007.
(47) Tobiška P., and Homola J.; Sens. Act. B, 107 (2005) 162-169.
(48) S.C. Jacobson SC., Hergenro der R., Koutny LB., Warmack RJ., and Ramsey JM.; Anal. Chem., 66 (1994) 1107-1113.
(49) Kohlheyer D.;Microfluidic Free-Flow Electrophoresis for Proteomics-on-a-Chip, PhD Dissertation, University of Twente (2008) ISBN: 978-90-365-2666-1
(50) Karlsson R., Katsamba PS., Nordin H., Pol E., and Myszka DG.; Anal. Biochem., 349 (2006) 136-147.
(51) Bravman T., Bronner V., Lavie K., Notcovich A., Papalia GA., and Myszka DG.; Anal. Biochem. 358 (2006) 281-288.
(52) Raz SR., Bremer MG., Haasnoot W., and Norde W.; Anal Chem., 81 (2009) 7743-7749.
(53) Köhn M., Wacker R., Peters C., Schröder H., Soulère L., Breinbauer R., Niemeyer CM., and Waldmann H.; Angew Chem Int Ed Engl., 42 (2003) 5830-5834.
(54) MacBeath G., Koehler AN., and Schreiber SL.; J. Am. Chem. Soc., 121 (1999) 7967-7968.
(55) Day YSN., and Myszka DG.; J. Pharm. Sci., 92 (2003) 333-343.
(56) Gomes P. and Andreu D.; J. Immunol. Method., 259 (2002) 217-230.

9

Concluding Remarks and Recommendations for Future Work

This chapter summarizes the overall results obtained in this four year research work on the development of an electrokinetic lab-on-a-chip for screening applications based on iSPR. We conclude this chapter with some important recommendations to improve the newly developed integrated device for drug screening applications.

9.1 Conclusion

The major goal of the project is to design and develop an electrokinetic lab-on-a-chip for high-throughput (multi-ligand) and multiplex (multi-analyte) detection focusing on biological screening applications (for eg. food, drugs, etc.). The major effort in this project includes the development of microarray-based bioassays on an iSPR platform in a conventional manner, transformation to a chip-based approach and improvement of the chip design to achieve the project goal. The major conclusion of the chapters of the thesis is summarized here. In chapter 1, chapter 2 and chapter 3 respectively the aim of the project, state of the art and theoretical background has been described.

Chapter 4: While trying to develop a microarray based bioassay with well known biomolecular interaction pairs, we developed an interesting and simplified biomolecular interaction kinetics approach (single injection kinetics) which could successfully extract kinetics and affinity parameters in a couple of minutes rather than hours using the conventional method. Quantitative comparisons between the estimated binding affinities measured with the conventional method are β2M: K_D=1.5±0.3 nM

and HIgG: K_D=12.6±0.2 nM and for the single injection method are β2M: K_D=1.5±0.2 nM and HIgG: K_D=12.5±0.6 nM, which are in good agreement in both cases, as well as, with parameters described in literature.

Chapter 5: We demonstrated another miniaturized multi-ligand/multi-analyte kinetics screening assay using iSPR with five different interactant pairs on a single sensor surface. The kinetics and affinity parameters which were extracted for all the interactant pairs by injecting the mixture of various antibodies are in very good agreement with results from conventional measurements using a single analyte. The experimental time was less for such experiments when compared to typical kinetics experiments. This approach could be extended further to more interactant pairs. The new approach facilitates the simultaneous screening and kinetics estimation of various multi-parameter samples e.g. drug targets in the drug discovery arena and also in many other interesting fields like biomarker discovery or antibody production. However, there are some limiting factors to implement such an assay to many real-time applications, as there might be cross-reactivity of various species in analyte mixture to the various immobilized ligands, which leads to false estimation of the kinetics.

Chapter 6: Knowing the kinetic behavior of the biomolecular interactant pairs of interest, we proceeded with the design and development of a biochip. Finally, an all-electrical electrokinetic sample transport chip has been successfully coupled to an SPR imaging system. The integrated system was successfully demonstrated with 3% glycerol sample, as well as biomolecular interaction of the well known interactant pairs: human IgG and goat anti-human IgG. The kinetics and affinity parameters extracted from the sensorgrams have been compared with results obtained from experiments using conventional pressure-driven flow and have been found to be in good agreement. The distribution of the responses from individual ROIs in the same row was similar for EKF – SPR and conventional pressure driven flow SPR indicating that this approach is viable and does not affect SPR measurements. This successful demonstration of an electrically controlled sample transport system directly coupled to SPR imaging may be important for SPR miniaturization and for scaling systems to

accept larger numbers of different samples. However, there were a couple of issues which needed immediate attention to move in the direction of multi-ligand/multi-analyte detection. One of the issues was that high electrical current in the interaction chamber leads to electrochemical reactions around the gold sensing islands. Another point was mixing of samples will increase the risk of cross contamination of analytes and the flow rate should be sufficient and of a constant value to avoid other effects, such as mass transport limitations.

Chapter 7: Considering all the points mentioned above, the second chip was designed with parallel microchannels instead of a single interaction chamber and each channel is used for a single sample. Hence the number of samples that needs to be used should have the same number of channels. We have successfully demonstrated various possibilities of biosensing including multi-ligand/multi-analyte detection with the new device using electrokinetic fluid transport. The demonstration of the multi-ligand/multi-analyte concept using electrokinetics shows a new direction for biosensing chips when large numbers of reagents are simultaneously measured. For that situation, we propose to increase the number of channels further for optimizing the throughput and multiplexing the assay and implement the chip for drug screening application.

Chapter 8: Finally, we have developed a biochip with 12 channels where each channel has 12 sensing locations leading to the measurement of more than 100 sensing areas simultaneously. This should be within the dimensions of the CCD camera of iSPR system. However, in the end we have demonstrated 90 simultaneous measurements with this chip using nine well-known interactant pairs on the iSPR platform. We also propose to improve the chip for drug screening applications.

In most of the chip based approaches, the dissociation phase of the sensorgrams shows more deviations, and in some cases, there is hardly any dissociation. This might be due to the fact that there is a rebinding effect (desorbing molecules binds to the surface again). This might arise due to the lower flow rate used in the measurements. This variation in dissociation phase has a direct impact on the error calculated in the dissociation rate which directly adding up the error values in affinity values calculated. The exact reason for the same is not known and it needs

more experimental work with various biomolecules. The recommendation for improvement is discussed in the following section.

9.2 Recommendations for future work

The proposed drug screening assay could be implemented on this chip only after certain problems are addressed. The problems include the corrected chip design as per the CCD camera dimensions, sensitivity issues in the corners, replacement of the PDMS with glass chips, for which the low temperature bonding problem must be addressed. Apart from these problems, there are also a couple of issues that need to be solved when electrokinetics has to be used for operating such a chip. The major issues and possible recommendation are listed here.

9.2.1 Lab-on-a-Chip

Metal Adhesion: The first problem is flow rate. In order to increase the flow rate, a high voltage should be applied across the containers, which in the end leads to a higher electric field and current flow over the sensing area. A buffer with high salt concentration is important for many complex biomolecular interaction measurements and in combination with a high electric field along the channel it may generate undesirable high currents. If currents are higher then a certain critical value, Joule heating will take place with many biochemical and physical consequences. It not only may affect the protein binding/denaturation, but also will affect the SPR resonance angle, conductivity of the buffer etc. Higher currents over the gold might lead to electrochemical reactions and etching of the gold surface. In our experiments, we have protected the gold layer to a certain extent by coating the gold with dextran/functionalized hydrogel, as well as by using a low conductivity buffer such as 10 mM HEPES buffer with low ionic strength background electrolytes. Both are effective strategies, but only to some extent. A solution is that the adhesion layer is replaced from titanium to tantalum, which withstands higher currents without forming bubbles over the metal surface or lift-off of the gold layer from the glass substrate.

Because proteins in complex matrices will stick to the walls of the channels, the electro osmotic flow will be affected resulting in a reduced flow at equal electric fields. Kinetics of biomolecular interactions are dramatically affected by non-constant flow over time. A static or dynamic precoating, which shows very low levels of non specific binding in combination with samples at very low diluted complex matrices could overcome this. However during the 4 years time period it did not allow me to work on this subject and should be transferred to future work. For SPR measurements, the gold layer should be homogeneous and without trace metals in order to achieve a good response. In the present situation, it is not possible to achieve a pure tantalum/gold layer in our cleanroom. Professional chips should be obtained from the chip manufacturers who rely on high quality SPR gold. (eg. IBIS Technologies B.v.)

Glass/Glass Chip: We have used chips made of PDMS as a top layer in our experiments. However, there were some problems which we have noticed while working on the hybrid PDMS/glass chips, e.g. stability of the bond over a certain period of time; adsorption of proteins to the PDMS walls leading to change in electro osmotic mobility and; improper dicing and punching of holes (manual) leading to alignment problems. We decided to shift to full glass chips instead of the hybrid PDMS/Glass. However, there is a bonding problem for this combination which is yet to be solved. Normally, glass/glass bonding is done at a high temperature which in our case is problematic due to faster oxidation of titanium layer which is used as the adhesion layer for gold. It is possible that the titanium diffuses into the gold and changes the property of the surface which is no longer suitable for SPR measurements. If e.g. spotting of different ligands to the SPR surface is desirable the chips cannot be closed using high temperature bonding. Biological ligands will not survive elevated temperatures. So there is a need for low temperature bonding which still should be developed for such applications.

9.2.2 Surface Plasmon Resonance Imaging System

CCD camera: The pixel noise of the camera has to be improved to make the assay

more sensitive. With the present configuration of the iSPR system, it is not possible to detect small molecules < 2000 Daltons even when high capacity chips are applied.

Software: At present, the electrokinetics has to be controlled using a separate custom built labview or C++ interface to control the flow in chips which is not integrated with the software of the iSPR instrument provided by the company (IBIS technologies b.v., Hengelo, the Netherlands). It is desirable to integrate the SPR data acquisition with the control of the fluidics using the electrokinetic control unit. The recorded sensorgram data are stored in the database and can only be exported to Excel or in text data format for further characterization. Besides the determination of the dissociation rate constants with SPRint software, the value of the affinity constant must be separately analyzed using another commercial software package "scrubber2". There is a need for integrated software packages, which controls both the electrokinetics the iSPR measurements and the data analysis.

9.2.3 Drug Screening Assay

When the above mentioned issues are solved we could implement the proposed drug screening assay (Chapter 8) directly which would lead to the successful realization of the goal of the proposed project. There are different ways by which the analyte screening experiments can be performed using the new lab-on-a-chip device.

1. Various small ligand molecules (drugs) can be immobilized in various channels. This can be followed by the injection of HSA in order to measure the drug-protein interactions in real-time.[1]

2. The method mentioned in "1" can also be extended to perform experiments to record serial kinetic interaction (also known as "kinetic titration") data for which regeneration steps can be completely avoided.[2]

3. Another possible approach could be to immobilize the same ligand in multiple channels and various concentrations of analyte are injected (one analyte per channel) in microchannels and to extract the kinetics and affinity constant of the interactant sets. This can be done similar to the conventional approach where various concentrations of

analyte are injected one after the other. Since it is done with a single step, it is termed "one shot kinetics".[3]

4. Various drug molecules can be immobilized on each gold sensing island (could also be different molecules in single channel) using a commercially available spotter.[4] Injecting the HSA in all the channels leads to data recording of all the drug-protein interactant sets. Since, we can measure up to 90 interactions simultaneously with the present chip design, it is possible to screen 80-90 drugs in a single experiment.

In all the cases, the recorded iSPR data can be directly fitted to its model functions to extract the kinetics and affinity parameters, which are of main importance in the screening of drugs for a specific purpose. It could be of very high advantage for the drug discovery community to have such a high-throughput multiplex biochip which makes the drug discovery faster when compared to the present existing systems which take weeks to screen the potential drug candidates and extract the kinetics, and affinity parameters.

9.3 Reference

(1) Krishnamoorthy G., Carlen ET., deBoer HL., van den Berg A., and Schasfoort RBM.; (Manuscript submitted).
(2) Karlsson R., Katsamba PS., Nordin H., Pol E., and Myszka DG.; Anal. Biochem., 349 (2006) 136-147.
(3) Bravman T., Bronner V., Lavie K., Notcovich A., Papalia GA., and Myszka DG.; Anal. Biochem. 358 (2006) 281-288.
(4) Raz SR., Bremer MG., Haasnoot W., and Norde W.; Anal Chem., 81 (2009) 7743-7749.

List of Abbreviations

SPR	Surface plasmon resonance
iSPR	Surface plasmon resonance imaging
LSPR	Localized surface plasmon resonance
SPP	Surface plasmon polaritons
PDMS	Poly di-methyl silaxone
PMMA	Poly (methyl methacrylate)
PET	Polyethylene terephthalate
ROI	Regions of interest
LOC	Lab-on-a-chip
EKF	Electrokinetic focusing
EOF	Electro osmotic flow
EKLB	Electrokinetic lab-on-a-biochip
pI	Isoelectric point
SAM	Self assembled monolayer
DNA	Deoxyribonucleic acid
RNA	Ribonucleic acid
mRNA	Micro ribonucleic acid
IgG	Immunoglobulin G
IgA	Immunoglobulin A
IgD	Immunoglobulin D
IgE	Immunoglobulin E
IgM	Immunoglobulin M
h-IgG	Human immunoglobulin G
a-IgG	Anti-immunoglobulin G
BSA	Bovine serum albumin
HSA	Human serum albumin
β2M	β2-microglobulin
a-β2M	Anti-β2-microglobulin
Fab	Fab fragment
CMD	Carboxy methyl dextran
Noa	Norland optical adhesives
mAb	Monoclonal antibody
NHS	N-hydroxy-succinimide
EDC	1-ethyl-3-(3-dimethylaminopropyl) carbodiimide
HCl	Hydrochloric acid
MES	2-(N-morpholino) ethanesulfonic acid
HBS-EP	10mM Hepes, 150mM NaCl, 3mM EDTA, 0.005% Tween-20
RU	Response unit
ELISA	Enzyme-linked immunosorbent assay
CFM	Continuous flow microfluidics
CCD	Charge coupled device
ATR	Attenuated total reflectance
EWOD	Electrowetting on Dielectrics

Summary

This thesis titled “Lab-on-a-Chip Surface Plasmon Resonance Biosensor for Multiplex Bioassays” describes new developments in the integration of an SPR imaging based biosensor and electrokinetic lab-on-a-chip. This research was aimed to develop a strategy to multiplex a bioassays in combination with high-throughput, which not only saves a huge amount of time, but also reduces the cost of such assays while performing multiple assays simultaneously. The major advantage of using electrokinetic driven fluidics instead of conventional pressure driven flow is to avoid complex plumbing network, valves and pumps, especially when large number of microchannels ($n > 10$) are used. This thesis describes a successful operation of a newly developed integrated biosensor system which needs a single voltage supply only. This thesis also explores the possibilities of measuring (multiple) biomolecular interaction kinetics in a different way compared to the conventional approaches, taking the advantage of the microarray integrated SPR imaging system.

The initial focus was on the development of a microfluidic lab-on-a-chip with the goal to demonstrate the feasibility of integrating both the biosensor microarray and applying electrokinetic pumping in a single device. After the demonstration of such an integrated biosensor, some of the observed practical and technical problems were addressed. Eg. higher current flow in the interaction chamber leads to electrolysis reactions near the gold metal layer giving additional unwanted effects as bubble formation, etching of the gold, pH shifts etc. A solution was found to protect the gold film by a hydrogel/dextran coating as well as usage of low conductivity buffers. In a new design of the chip the large interaction chamber was changed to individual microchannels (four microchannels operated in parallel) for guiding the sample flow. The modified chip (electrokinetic lab-on-a-biochip) was demonstrated with various types of biomolecular interaction experiments which includes multi-ligand/multi-analyte detection which is the core of the thesis. Kinetics and affinity of the model

biomolecular interactant pair (human IgG – a-IgG) was extracted from the integrated biosensor and compared with the conventional approaches. Both were in very good agreement with each other.

The device was further scaled-up to 12 channels in combination with up to 9 times multiplexing per channel, which were demonstrated with well known interactant pairs. A recommendation for future work prior to the implementation of this newly developed chip for biological applications (for eg. drug screening) is firstly changing the titanium adhesion layer for the gold film to tantalum which withstands higher currents and secondly replacing the PDMS/glass hybrid chips with full glass chips although a low temperature bonding technique has still to be developed. With the modifications as suggested, it should be possible to screen ~ 80-90 drugs simultaneously with the extraction of its kinetics parameters straightaway from the measured SPR responses. The new device could be of further interest for not only drug discovery applications, but it also opens up a new dimension in the development of analytical tools in various application areas to measure many biomolecular interactions in multiplex format and at high throughput.

Samenvatting

Dit proefschrift met de titel “Lab-on-a-Chip Surface Plasmon Resonance Biosensor for Multiplex Bioassays” beschrijft recente ontwikkelingen bij het integreren van een biosensor gebaseerd op SPR imaging en een lab-on-a-chip. Het doel van dit onderzoek was het ontwikkelen van een strategie om bioassays te multiplexen, om in combinatie met een hoge monster doorvoer, de benodigde tijd en kosten van assays te verminderen indien meerdere assays simultaan worden uitgevoerd. Het grote voordeel van het gebruik van elektrokinetisch gedreven vloeistofstromen in plaats van conventionele, drukgedreven vloeistofstroom is het voorkomen van een complex netwerk van slangen, kleppen en pompen. Dit is vooral van belang indien een groot aantal microkanalen ($n > 10$) wordt gebruikt. Dit proefschrift beschrijft de succesvolle werking van een nieuw ontwikkeld, geïntegreerd biosensor systeem, dat gebruik maakt van slechts één enkele spanningsbron voor het verpompen van de vloeistoffen in de chip. Tevens wordt in dit proefschrift de mogelijkheid onderzocht om bindingssterktes van biomoleculen aan liganden op een niet-conventionele manier te meten, waarbij het voordeel van de geïntegreerde SPR microarray optimaal wordt benut.

De oorspronkelijke focus lag bij het ontwikkelen van een micofluidisch lab-on-a-chip met het doel om de haalbaarheid van een geïntegreerde biosensor microarray en elektrokinetisch pompen in één enkel device te demonstreren. Na demonstratie van het bovengenoemde device zijn een aantal van de geobserveerde praktische en technische problemen aangepakt. Een hogere electrische stroom bij het sensoroppervlak leidt bijvoorbeeld tot electrolyse bij de gouden dunne film elektrode, wat resulteert in ongewenste effecten zoals gasbelformatie, het weg-etsen van de elektrode en verschuivingen in de pH. De oplossing van deze problemen is gevonden in een beschermende hydrogel coating over de goudfilm, samen met het gebruik van een buffer met lage geleidbaarheid. In een verbeterde versie van de microchip is de grote interactiekamer opgesplitst in individuele microkanalen (vier microkanalen opereren in parallel) om de meetvloeistof in de juiste baan te leiden. Met behulp van

deze verbeterde chip (elektrokinetic lab-on-a-biochip) zijn verschillende types biomoleculaire interactie experimenten in multiplex (meerdere interacties tegelijkertijd) uitgevoerd en gedemonstreerd, wat de kern vormt van dit proefschrift. De kinetiek en de affiniteit (bindingssterkte) van een bekend paar antilichamen (humaan IgG en anti-humaan IgG) is bepaald met behulp van de geïntegreerde biosensor en vergeleken met de conventionele aanpak. De resultaten waren in goede overeenstemming.

Het device is opgeschaald naar 12 kanalen in combinatie met een 9-voudige multiplexing per kanaal, waarvan de werking is gedemonstreerd met bekende interactie paren. Voordat dit opgeschaalde device kan worden geimplementeerd in biologische toepassingen, is het raadzaam om eerst de titanium hechtlaag onder de goudfilm te vervangen voor tantaal, omdat tantaal beter bestand is tegen grote stromen. Daarnaast is het aan te bevelen om de hybride PDMS/glas chip te vervangen door een volledig glazen chip, alhoewel lage-temperatuur bonding nog niet goed is ontwikkeld. Met de voorgestelde verbeteringen zou het mogelijk moeten zijn om ~80-90 verschillende stoffen tegelijkertijd rechtstreeeks uit de SPR respons te onderzoeken op de kinetiek-parameters. Dit nieuwe device zou niet alleen interessant zijn in medicijnonderzoek, maar het opent ook een nieuwe weg in de richting van het ontwikkelen van analytische gereedschappen in diverse onderzoeksgebieden waarbij vele monsters tegelijkertijd en in gemultiplexte vorm gemeten kunnen worden.

Acknowledgements

In 2006, I started working in the Biochip group which was then a part of the Biophysical Engineering group headed by Prof. Vinod Subramanian. As a process engineer and having a little research experience in downstream processing and modeling and simulation of surfaces, I made up my mind to work in the biosensor project offered to me, which turned out to be more challenging than expected. At the end of my project, I would definitely say that my decision was for the right research area and work place.

During my research work in the past 4 years, I have come across an enormous number of people who encouraged, helped and supported me in making this project a success. I do not have words to express my gratitude for these persons, but I would like to mention a few of them here to whom I would like to express my sincere and heart felt acknowledgements. Thank you very much to you all and I wish to dedicate this entire section to you people.

Even though I started as a Biochipper, I spent most of my time as a BIOSer. I learned a lot in the BIOS Lab-on-a-Chip group, such as, planning the experiments properly with respect to timings, organizing chemicals in the right place, collaboration of projects, gathering very useful technical information through technical discussion meetings and so on, which I was not used to earlier.

First, my deepest gratitude and thanks to *Dr. Edwin Carlen*, without whom it would not have been possible to successfully finish my PhD. As we befriended each other in the Dutch language course, it was a little hard for me to accept you as my supervisor. But, in the end, you turned out to be more than a supervisor to me; you have been a well-wisher, a friend and an advisor altogether. I am awestruck at the way you discuss not only scientific stuff, but also a lot of off-subject matter. You are really helpful to your students and I am very lucky to be a part of your subgroup "nanosensing". Of late, we have also been having pleasant nanosensing gatherings, which gave us a nice opportunity to socialize with others. I learned a lot during our face-to-face discussions as well as from our late-night email conversations. Till date, if somebody were to ask me who has sent me the most number of emails, I would reply without a second thought that it is you, Edwin. At one particular time, if I did not get an email from you, I felt that the day was incomplete and I have even enquired after your health that day. Of late, it has gradually decreased and I can understand that it is because of the fact that you have more students now. I have improved a lot in writing papers, letters and emails in the right way, speaking more politely, handling problems in the best possible way, and many more positive things are just because of you, Edwin. I can write more about you, but I am stopping here and express my sincere thanks once again to you.

I hardly have words to express my thanks to you, *Dr. Richard Schasfoort*. You offered me this project with full confidence even though I had a different background. I thoroughly enjoyed the freedom that you gave me as well as your trust in me. None of

the supervisors will give so much freedom to his students not only in projects but also when it comes to participating in conferences. I have met almost all the famous researchers in SPR field and I am still in contact with almost all of them, just because of you. You allowed me to go to the most expensive biosensor workshop in USA, as well as on a week-long visit to the world famous research lab, the National Institute of Health, USA, all of which are heavenly gifts to me in my career. I should not forget the fun times we had in the biochip group, such as while canoeing during the "biochip uitje", several dinner gatherings and parties in excellent restaurants, car trips to various meetings in the Netherlands and our funny discussions during those times. I always admire the way you come up with new ideas during our discussions almost instantaneously. Richard, I am really grateful to you for giving me such a wonderful opportunity.

My special thanks to *Prof. Albert van den Berg* for agreeing to be my promoter as well as giving me room to be a part of the BIOS group. Even though I was an outsider, you put the situation in such a way that I felt as though I was also a BIOSer. We had very nice and fruitful discussions during our work meetings. While Richard was responsible for introducing me to high level contacts in the SPR field, it was you who made it possible for me to have high level contacts in the microfluidics research field. I am much obliged to you for allowing me to attend very high level conferences such as MicroTAS and Gordon Research conferences twice; this gave me a good opportunity to meet many important people. These meetings also triggered and enhanced the final outcome of my research. Meeting with Prof. George Whitesides is the best moment and I feel privileged to have got such a wonderful opportunity. When it comes to fun-related things, there is a lot to mention, such as Bios Christmas outings, the summer barbecue at Nijverdal, and the Sinterklaas evening; they impressed me a lot and I really enjoyed them very much.

Before I move on to other persons, it is highly important to thank the technical engineers behind the successful completion of such a complex and challenging project. *Johan, Daniel* and *Stefan*, without you guys, it is not possible for me to have very nice biochips. Three cheers to you guys for shielding my life by risking your own with hazardous chemicals in cleanroom fabrication procedures. *Stefan*, thank you very much making the nice photos of my chips and chip holders. *Hans*, it is you who made my chip a holder, especially in a very short time and these were the talk of the people who discussed my research posters in conferences. Thanks a lot for all your extensive technical help which is the best of the best in the BIOS chair.

I would like to thank all the former biochip group members for their extreme support during various stages of my PhD project. *Bianca*, I really enjoyed almost 1 year as your officemate even though we had a very tough fight about certain things, as well as lots of very funny things, including the correlation of my English word "kool" to the Dutch word "kool" for which the meaning is "cabbage", about which you teased me a lot. A special thanks to you for boosting me with lots of positive words and hearing a lot of my complaints patiently. Thanks to *Geert* and *Anna* for extensive support during my start-up time as well as for various scientific discussions we had to set the project in the right direction, to *Dietrich* and *Dawid* for sharing the office room

for the first few months as well as for providing me the software for use with my EOF power supply which worked well and saved my time. I cannot forget our frequent faculty club gatherings and gatherings for dinner (specifically at the Thai restaurant in Enschede city center). *Verena,* thanks a lot for working on my project as an intern. I should not forget to say my thanks to other former biochip students like *Bjorn* and *Remco* as well as visitors like *Angelique* and *Lou-ella*.

Hermine and *Sylvia*, a special salute to you both for making my life easier in this new country. Without you both, it might have been terrible to complete not only the burocratic procedures, but also other necessary things with respect to arranging everything regarding my thesis defense. *Iris,* thanks a lot for sharing my office for the last 1.5 years and hearing everything that I say patiently and calming me down with your simple words. I am very much impressed with your cool attitude even though you have a lot of tension about deadlines, meetings, paper submission and presentations. I wish you the best of luck for your forthcoming thesis. *Severine*, you are the one who teased me a lot and you are the person to receive a lot of teasing from me, which, if it had gone to the extreme of hurting you, I wish to say that I did not intend to say. I learned some positive things from you and lately I also stopped teasing you for good. We had very useful scientific discussions regarding cells (for me, the word "cell" comes from another planet). You gave me very nice explanations about the things that I did not understand quite easily. I really enjoyed the time we worked together in the lab for PDMS bonding. *Rerngchai* and *Arpita*, thanks a lot for sharing my office for the last few months. *Lingling*, thanks for helping me during the finishing of my thesis and hinting me about what I should do next with respect to the other formalities. I would like to thank the remaining BIOS group colleagues for the good time I had, either individually or in group with them, as well as for their help: *Jan E* (especially, trip to Italy with you and inspiring stories that you told me about the Italian sculptures and paintings), *Wouter O, Georgette, Wouter S, Justyna, Floor & Loes* (both for arranging fun-filled BIOS events), *Egbert* (COMSOL introduction), *Ad, Anja, Rogier, Eddy* (the way you organize TDMs), *Songyue, Mingliang, Evelien* (the friendly way you talk with people), *Eric, Masood* (fruitful surface chemistry and protein biosensing discussion), *Maarten, Mathieu* (timely help in translation of my thesis summary to Dutch), *Fleur, Yanbo, Paul* (timely ordering of all my orders), *Jan N* (for all my computer problems, both hardware and software).

Another very important person behind the successful completion of my thesis is *Prof. Vinod Subramanian*. I am very grateful to you, Vinod, for your timely help and advice during problematic times as well as the steps you took to transfer smoothly from BPE group to BIOS group, for the newly-built modern chemistry as well as other labs which are really exceptional and which I still miss in BIOS. I would also like to thank your research group whose members are also my former colleagues. I really enjoyed the time that I spent in the BPE group as well as all the outings we had and also the coffee breaks we had in the newly-developed olive garden in Zuidhorst.

I would like to thankfully acknowledge the very valuable scientific inputs given by all my project user committee members, especially *Prof. Willem Norde*, *Sabina* and *Monique* from RIKILT, Wageningen and the Dutch technology foundation

STW for financially supporting my project. My special thanks to *Mr. Hans-Karl Engeldinger* of tesa AG, Hamburg, Germany for supporting me from the beginning of my career in Europe as well as for sending me lots of different double-sided tapes for my research as a gift. I would like to thank *Mr. Erk Gedig* of XanTec Bioanalytics GmbH, Germany for sending me the sensor disks even before he received the order to save my time. My heart felt gratitude to *Dr. Peter Schuck*, for giving me valuable scientific tips and suggestions, inviting me to NIH for one full week and gave me training in the operation of Biacore SPR systems, teaching me new affinity distribution analysis software (Evilfit) and also initiating the project to collaborate with me. I am very grateful to *Prof. David Myszka*, for giving me a wonderful training in SPR kinetics as well as for the inclusion of my name in author list for the benchmark study paper which was published last year.

I would like to thank all my Indian friends here who made me feel at home here in the Netherlands. I would like to mention about few of them here. *Vishnu*, a special thanks to you for hearing everything that I say (almost all the evenings). Special thanks to wireless circle at this moment, which lets us talk for free. If we do not have wireless circle, we both will be in debts by now due to our very high phone bill. *Raghav, Anand-Subhashini, Anand-Renuka, Vikram-Asmita*, *Pramod-Vishaka, Ashvin, Rajagopal, Arpita, Sandeep, Jittu, Srivatsa, Chandra and Chakki*, for the wonderful gatherings that we had from time to time.

My very special thanks and gratitude of acknowledgement go to *my parents* who always supported me in each and every phase of my life to reach greater heights. Same goes to my *sister Sathyapriya* and her *husband Ramchander* as well as my *brother Hariharan*, for supporting me in all aspects, whatever decision I make. I should not forget my father-in-law's extensive support during this time and also for asking me critical questions after reading my papers before I submit them to journals. I would like to give my whole-hearted gratitude to my lovable uncle *Mr. M. V. Venkatraman*, for his support and help, starting from my school days. Thanks a lot uncle. Finally my special gratitude to my *wife Karthika* (who also read my whole thesis and spent huge amount of time in formatting and creating a database of all the references that I have used) and my *daughter Nirupa* for being the best, understanding, supportive and affectionate daughter in my life.

Ganeshram Krishnamoorthy.
March 2010.

List of Publications

Journal articles

1) Ganeshram Krishnamoorthy, Edwin T. Carlen, Johan G. Bomer, Daniël Wijnperlé, Hans L. deBoer, Albert van den Berg and Richard B. M. Schasfoort; Electrokinetic Label Free Screening Chip: A Marriage of multiplexing and high through-put analysis using Surface Plasmon Resonance imaging, **Lab Chip,** DOI:10.1039/C000705F (2010) – Chapter 8.
2) Ganeshram Krishnamoorthy, Edwin T. Carlen, J. Bianca Beusink, Richard B. M. Schasfoort and Albert van den Berg; Single Injection Microarray-based Biosensor Kinetics, **Analytical Methods**, 1 (3), 162-167 (2009) – Chapter 4.
3) Ganeshram Krishnamoorthy, Edwin T. Carlen, Dietrich Kohlheyer, Richard B. M. Schasfoort and Albert van den Berg; Integrated Electrokinetic Sample Focusing and Surface Plasmon Resonance Imaging System for Measuring Biomolecular Interactions, **Analytical Chemistry**, 81 (5), 1957-1963 (2009) – Chapter 6.
4) Rebecca L. Rich, Giuseppe A. Papalia, Ganeshram Krishnamoorthy, Bianca Beusink, David G. Myszka, et al..; A Global Benchmark Study using Affinity-based Biosensors, **Analytical Biochemistry**, 386(2):194-216 (2009).
5) Ganeshram Krishnamoorthy, Edwin T. Carlen, Albert van den Berg and Richard B. M. Schasfoort; High-Throughput Multiplex Bioassays – Where Are We Now?, Manuscript submitted (Review in Process) – Chapter 2.
6) Ganeshram Krishnamoorthy, Edwin T. Carlen, Albert van den Berg and Richard B. M. Schasfoort; Multiplexed Biosensor: Parallel Kinetics Screening Assay for Multiple Biomolecular Interactions, Manuscript submitted (Review in Process) – Chapter 5.
7) Ganeshram Krishnamoorthy, Edwin T. Carlen, Hans L. deBoer, Albert van den Berg and Richard B. M. Schasfoort; Electrokinetic Lab-on-a-BioChip for Multi-Ligand/Multi-Analyte Biosensing, Manuscript submitted (Review in Process) – Chapter 7.

Conference contributions

1) Ganeshram Krishnamoorthy, Edwin T. Carlen, Hans de Boer, Richard Schasfoort and Albert van den Berg; Multi-Analyte Label-Free Detection System with Electrokinetic Transport, Gordon Research Conference – Physics and Chemistry of Microfluidics, 28th June – 03rd July 2009, Ciocco, Italy.
2) Ganeshram Krishnamoorthy, Edwin T. Carlen, Dietrich Kohlheyer, Richard Schasfoort and Albert van den Berg; On-chip electrokinetic sample focusing for microarray-based biomolecular interaction assays, October 2008, MicroTAS 2008, SanDiego, USA. Pp 311-313.

3) Ganeshram Krishnamoorthy, Bianca J. Beusink, Edwin T. Carlen, Stefan Schlautmann, Hans L. deBoer, Albert van den Berg and Richard B. M. Schasfoort; Combined Lab-on-a-Chip and microarray approach for biomolecular interaction sensing using surface plasmon resonance imaging, The proceedings of MicroTAS 2007 Conference, 7-11 October 2007, Paris. pp. 676-678.
4) Ganeshram Krishnamoorthy, E.T. Carlen, S. Schlautmann, H.L. de Boer, A. Van den Berg and R. B. M. Schasfoort; Lab-on-a-chip biomolecular interaction measurement system with integrated microfluidics and surface plasmon resonance imaging, Gordon Research Conference – Physics and Chemistry of Microfluidics, 15 – 20 July 2007, Waterville Valley Resorts, Waterville Valley, U.S.A.
5) Ganeshram Krishnamoorthy, Stefan Schlautmann, Hans L. de Boer and Richard B.M. Schasfoort; Lab on a Chip Approach for Biomolecular Interaction Sensing Using Surface Plasmon Resonance Imaging, Lab on a Chip World Congress 2007, 15 – 16 May 2007, Edinburgh, Scotland.

Lectures

1) Ganeshram Krishnamoorthy, Electrokinetic Lab-on-a-BioChip for Multi-Ligand/Multi-Analyte Biosensing, 28 September 2009, Joanneum Research, Austria.
2) Ganeshram Krishnamoorthy, Electrokinetic Focusing based Biomolecular Interaction Measurement and Microarray based Kinetics Evaluation, 24 October 2008, National Institute of Health, Bethesda, USA.
3) Ganeshram Krishnamoorthy, Stefan Schlautmann and Richard B.M. Schasfoort; Biosensing : A New Lab on a Chip Approach based on Surface Plasmon Resonance Imaging, Frontiers Research Meeting, 9-11 May 2007, Toulouse, France.
4) Ganeshram Krishnamoorthy and Richard B.M. Schasfoort; Microarray Approach and Multi-kinetic Evaluation of Biomolecular Interactions Based On Surface Plasmon Resonance Imaging, Bio/Nano Frontiers Meeting, 18-21 March 2007, Zermatt, Switzerland.
5) Ganeshram Krishnamoorthy; Multikinetics Evaluation: A Miniaturized Approach Based on Biosensor Imaging, Biosensortools 2007, 17-23 February 2007, Salt Lake City, USA.